ANL-6687

Argonne National Laboratory

CHEMICAL ENGINEERING DIVISION

SUMMARY REPORT

January, February, March, 1963

ANL-6687
Chemical Separations Processes
for Plutonium and Uranium
(TID-4500, 22nd Ed.)
AEC Research and
Development Report

ARGONNE NATIONAL LABORATORY
9700 South Cass Avenue
Argonne, Illinois 60440

CHEMICAL ENGINEERING DIVISION

January, February, March, 1963

S. Lawroski, Division Director
R. C. Vogel, Associate Division Director
Milton Levenson, Associate Division Director
V. H. Munnecke, Assistant Division Director

Preceding Quarterly Reports:

ANL-6648	October, November, December, 1962
ANL-6596	July, August, September, 1962
ANL-6569	April, May, June, 1962

Operated by The University of Chicago
under
Contract W-31-109-eng-38
with the
U. S. Atomic Energy Commission

TABLE OF CONTENTS

TABLE OF CONTENTS

LIST OF TABLES

LIST OF TABLES

LIST OF TABLES

LIST OF FIGURES

LIST OF FIGURES

LIST OF FIGURES

LIST OF FIGURES

SUMMARY

CHEMICAL ENGINEERING DIVISION SUMMARY REPORT

I. Chemical-Metallurgical Processing (pages 27 to 85)

Development work on the melt refining process to be used for the recovery of enriched uranium from the first core loading of EBR-II is essentially complete, and plant equipment has been installed at the EBR-II site in Idaho.

Complementary to the melt refining process is the skull reclamation process, which is under development for the recovery of skull material which remains in a zirconia crucible after melt refining. Two small-scale demonstration runs (each starting with about 150 g of skull oxide) were completed during the last quarter. These demonstration runs showed that the process is capable of providing adequate uranium recovery (at least 95 percent). Adequate separation from uranium of fission product elements (with the possible exception of zirconium) was also demonstrated. Zirconium removal will be a problem if an excessive amount of zirconia from melt refining crucible fragments is introduced into the skull oxide. Concentrations of zirconia crucible fragments of up to about three percent (considered an abnormally large introduction of crucible fragments) can be handled in the process.

Preliminary experimentation has been started with the large-scale integrated equipment for the skull reclamation process. This has included transfers of flux and metal, determination of heating and cooling rates in the furnaces, and measurements of equilibrium temperatures in various parts of the equipment.

Beryllia crucibles made by a thixotropic casting process are being evaluated for use in the final three steps of the skull reclamation process (two uranium precipitation steps and a retorting step). One crucible (of 4-in. OD and 9 in. high) which had been in use for a considerable period of time failed after 465 hr of process use. This is equivalent to about 23 plant uses (about 20 hr of use per processing batch) and is regarded as satisfactory performance.

Work has continued on separations processes for fast reactor fuels containing uranium and plutonium. One procedure involves an equilibration of the fuel constituents between liquid magnesium-zinc solutions and molten halides. Distribution data for curium and preliminary information on the distribution of neptunium between liquid zinc-magnesium and magnesium chloride at 800 C have been obtained. The distribution coefficients (ratio of w/o in flux to w/o in metal) for neptunium

and curium are similar to those for uranium and plutonium, reaching a minimum value of about 10^{-2} at a magnesium concentration of approximately 10 w/o in the metal phase. In contrast, americium resembles the rare earth elements in its behavior, with a minimum distribution coefficient of about 0.3 at 5 to 10 w/o magnesium in the zinc phase. Thus, separations of americium from plutonium and curium can be effected by this method. Separation factors for americium and curium at 800 C vary from 15 to 40 as the magnesium concentration in the metal phase is increased from 5 to 100 w/o.

The solubility of uranium in calcium-zinc solutions was determined at 700, 750, and 800 C to provide supporting data for a separations process in which uranium and plutonium are coprecipitated, leaving the rare earth fission products in the liquid metal solution. Uranium solubility at 750 C varied from 2.89 to 0.046 w/o as the calcium concentration was increased from 0 to 23.7 w/o.

An alternative blanket process for separating plutonium from uranium was investigated briefly during the past quarter. In this process, uranium and plutonium are first oxidized into a molten halide flux by zinc chloride at 800 C and subsequently reduced at 800 C from the flux phase with magnesium metal. The reduced plutonium dissolves in excess magnesium reductant, while uranium, which has a very low solubility in magnesium, precipitates and should settle out of the magnesium phase. All reactions went as expected, but the separation of precipitated uranium from the magnesium supernatant solution was poor. Although consideration will be given to this phase separation, work will be devoted principally to scale-up of the already-demonstrated blanket process.

In order to take advantage of the good mechanical properties of porous, coarse-grained crucibles (of alumina, beryllia, and possibly magnesia) for use in liquid metal-salt processes, an attempt is being made to seal the pores of these crucibles by coating or impregnating the inner surfaces with slurries containing finely divided mixtures of low-melting oxides. After each of two applications of a coating, the crucible is fired at an elevated temperature to fuse the coating. Porous alumina crucibles have been made impervious to water by a coating consisting of a mixture of alumina, calcia, magnesia, and baria. The coated crucibles have not yet been tested for the containment of molten metal and halide salt systems.

Additional spectrophotometric studies indicate that the soluble uranium (V) species formed on the addition of higher uranium oxides to molten chloride media is similar in some respects but not identical to uranium oxytrichloride, $UOCl_3$. This result tends to support earlier indications that the species in solution is UO_2^+ ion.

Work has been started to obtain experimental measurements of natural convection heat transfer rates in liquid metal. Experimental equipment is currently being constructed and assembled.

Construction of equipment for the preparation of uranium and plutonium carbides in high-purity inert atmospheres has continued. The reaction of methane with uranium-zinc intermetallic phases at 655 to 870 C has been shown to produce uranium monocarbide. The product is non-homogeneous, however, and requires a homogenization treatment. Preliminary experiments on the preparation of uranium monosulfide by the reaction of hydrogen sulfide with hydrided-dehydrided uranium metal has resulted in a product containing less than 0.5 percent oxide and oxysulfide impurities.

Further results have been obtained on the reduction of thorium dioxide by zinc-magnesium alloy at 800 C in the presence of halide fluxes. The use of a flux containing only magnesium cation has extended the range of magnesium concentrations in the zinc phase over which complete reduction of the thorium dioxide occurs. The maximum practical thorium loading in the metal phase appears to be about 10 w/o.

Further information on the preparation of uranium metal by the direct reduction of ore concentrates in the presence of a flux indicates that about 90 percent of the silicon can be removed from the ore concentrate by a simple pretreatment with ammonium bifluoride or uranium tetrafluoride. However, relatively large amounts of these reagents are required (fluoride: ore concentrate weight ratios of about 0.2 to 0.3). In a laboratory-scale demonstration experiment, an arc-melted uranium ingot was prepared from a typical ore concentrate by this method.

Study of factors affecting nonturbulent vaporization (vaporization from liquid-vapor interface) of mercury was continued. When the level of the mercury pool was increased from 1 to 2 or 3 in., a slight increase in the nonturbulent vaporization rate was realized, i.e., from 105,000 to 115,000 Btu/(hr)(sq ft) heat flux at the surface. Changes in the induction heater coil configuration were necessary as the liquid metal depth was increased.

Work is continuing on the installation, testing and correcting of equipment in the EBR-II Fuel Cycle Facility.

A series of tests have determined the in-leakage rate of air into the Argon Cell. In the last test of the series, the Argon Cell was purged with nitrogen, and most of the remaining oxygen removed by means of the cell atmosphere-purification system. The air in-leakage rate, determined by measuring the rate of increase in the oxygen level in the Argon Cell, was 0.006 cfm at a pressure in the cell of -4 in. of water.

A portable luminaire, mirror, and stand have been developed to provide brilliant lighting for local areas in the process cells.

A radiation-resistant clutch has been developed for use with the drive motors that move the shielding window shutters.

One interbuilding fuel-transfer coffin has been delivered to Idaho. A second is under construction. Mercury is being considered as an emergency heat transfer medium to remove fission product heat from these coffins.

A process has been developed for the in situ removal of sodium from fuel subassemblies in the interbuilding transfer coffin. The scheme consists of converting the sodium to the oxide at low gas-phase concentrations of oxygen, converting the oxide to the hydroxide with humidified air, and washing the hydroxide from the subassembly with water. A sodium-removal station has been designed and procurement of equipment items has begun.

A purification system, which was designed to remove water vapor and oxygen from the inert atmosphere of a glovebox, was tested and sent to Idaho.

An offgas-filter assembly has been designed for use with the melt refining furnace and similar equipment. The filter assembly utilizes glass filter media for removing radioactive particulate material and a charcoal bed for adsorbing fission product iodine vapors.

An oxygen feed-control system for the skull-oxidation furnace has been tested. A maximum rate of 1.5 g uranium/min was achieved in the oxidation of the uranium in the skull material to uranium oxide (U_3O_8). The skull was oxidized to a fine powder.

The first model of the skull reclamation furnace is undergoing preliminary tests.

New equipment has been installed which will permit the testing of inductive heating and mixing at higher power inputs.

Experiments to develop a satisfactory metal-vapor condenser and collector for use with the melt refining furnace are continuing. A new condenser and collector have been designed and built which can be used with the enclosure and the base plate of the melt refining furnace. The new design can accommodate a larger charge of uranium-magnesium-zinc than that which could be accommodated in the melt refining furnace. A test run with the new apparatus gave encouraging results.

The solubility of barium in liquid zinc between 560 and 710 C may be represented by the empirical equation

$$\log (\text{w/o barium}) = 10{,}464 - 10640\ T^{-1}.$$

The solubility of neodymium over the temperature range 525 to 753 C may be best represented by two empirical equations:

$$(525\text{-}700\ \text{C})\ \log (\text{w/o Nd}) = 10.227 - 12310\ T^{-1} + 2.340 \cdot 10^{6}\ T^{-2} \quad ;$$

$$(700\text{-}753\ \text{C})\ \log (\text{w/o Nd}) = 22.843 - 39810\ T^{-1} + 17.152 \cdot 10^{6}\ T^{-2} \quad .$$

The thermodynamics of the plutonium-zinc system have been studied by a high-temperature galvanic cell method. The free energy of formation of the zinc-rich phase ("Pu_2Zn_{17}") in equilibrium with the saturated solution may be represented by the following empirical equation:

$$\Delta Gf^{\circ}\ (\text{kcal/g-atom Pu}) = -66.36 + 25.35 \times 10^{-3}\ T + 11.66 \times 10^{-6}\ T^{2} \quad .$$

The yttrium-zinc system has been studied by the effusion method. The following phases have been found: YZn_{12}, Y_2Zn_{17}, YZn_5, Y_2Zn_9, YZn_3, and YZn_2. The effusion studies did not extend below YZn_2 and, hence, the existence of YZn was not confirmed.

X-ray diffraction powder photographs of V_4Zn_5 could be indexed on the basis of a body-centered tetragonal cell. Both X-ray and neutron diffraction patterns were used to establish the cell parameters: $a_0 = 8.910$ Å and $c_0 = 3.227$ Å.

II. Fuel Cycle Applications of Volatility and Fluidization Techniques (pages 86 to 152)

The development of a Direct Fluorination Process for the recovery of uranium and plutonium from irradiated nuclear fuels is continuing. In this process, uranium and plutonium dioxides are fluorinated to produce hexafluoride products, which are then decontaminated and separated by volatility techniques.

Experimental work has been carried out on the oxidation of uranium dioxide as a means of "decladding" chopped fuel elements in the Direct Fluorination Volatility Process; this is not decladding as the term is normally used. The uranium dioxide, on being oxidized to uranosic oxide, increases in volume and is also transformed into a very fine powder which separates from the metallic cladding. Preliminary results with uranium dioxide pellets clad in Type 304 stainless steel indicate that this is a feasible process and that slower oxidation rates (air oxidation rather than oxidation in pure oxygen) result in greater removal of uranium dioxide as uranosic oxide from the cladding.

It is desirable to know to what extent uranium dioxide reacts with chlorine at 600 to 650 C, if chlorine is to be used as a reactant with stainless steel in the decladding step of fluoride volatility processes for uranium dioxide reactor fuels. Dry chlorine was reacted with a $\frac{1}{2}$-in.-diameter, $\frac{1}{2}$-in.-long uranium dioxide pellet at 650 C for 3 hr, resulting in a conversion of 48 percent of the uranium dioxide to uranyl chloride. When the same reaction was carried out with an equimolar mixture of chlorine and nitrogen at 600 C, two percent of the uranium dioxide was converted to uranyl chloride.

The reaction of uranium hexafluoride vapor and hydrogen sulfide vapor takes place readily at 25 C to produce uranium tetrafluoride, sulfur tetrafluoride, and hydrogen fluoride. The hydrogen sulfide is fluorinated quantitatively to hydrogen fluoride. The reaction can probably be expressed by the equation

$$3\ UF_6(g) + H_2S(g) = 3\ UF_4 + SF_4 + 2\ HF(g) \quad .$$

In an experiment at 300 C (with a temperature excursion to 480 C), free sulfur was also formed.

Uranium hexafluoride vapor reacts readily with carbon disulfide vapor at room temperature. When excess uranium hexafluoride is used, the solid product is diuranium enneafluoride (U_2F_9). When excess carbon disulfide is used, the solid product is uranium tetrafluoride. When the temperature of the reaction mixture is 100 to 200 C, with excess carbon disulfide, the gaseous products are sulfur tetrafluoride, sulfur hexafluoride, tetrafluoromethane, and bistrifluoromethyl disulfide, and possibly bistrifluoromethyl trisulfide. When the reaction with excess carbon disulfide proceeds to completion at room temperature, the main gaseous products are bistrifluoromethyl disulfide and bistrifluoromethyl trisulfide, with traces of sulfur tetrafluoride. When the reactants are diluted with helium gas and the reaction is carried out at room temperature with excess carbon disulfide, the only organic gaseous product is bistrifluoromethyl disulfide.

Plutonium hexafluoride reacts vigorously with carbon disulfide at room temperature. The solid product of the reaction is PuF_4. The gaseous products are SF_4, SF_6, and CF_4.

Corrosion of an alloy containing 98 percent nickel and two percent thoria by fluorine was tested at 600 C. Coupons of the alloy and of A-nickel were fluorinated simultaneously in a static system at 600 C for four days in order to obtain a direct comparison of the rates of fluorination. The rate of fluorination of the nickel-thoria alloy is about an order of magnitude greater than that of A-nickel. Also, the fluoride film formed on the nickel-thoria alloy tended to spall and fall away. The alloy is therefore not suitable as a material for construction to contain fluorine at elevated temperatures.

The absorption spectra of gaseous plutonium hexafluoride in the ultraviolet, visible, and near infrared regions have been determined. The results indicate a rather complicated spectrum with bands of sharp lines at 9583-10,684 cm^{-1}, two band groups at approximately 12,000 cm^{-1} and 12,700 cm^{-1}, and several other bands before the very strong absorption in the 50,000 cm^{-1}-30,000 cm^{-1} region.

When the use of plutonium hexafluoride is proposed as in the Direct Fluorination Process, the decomposition to plutonium tetrafluoride and fluorine caused by alpha particles emitted by the plutonium must be considered. A kinetic study of the decomposition of plutonium hexafluoride by alpha radiation is being made. The results indicate that the rate of decomposition of gaseous plutonium hexafluoride increases when the initial pressure of plutonium hexafluoride is raised from 50 mm to 100 mm. The rate decreases, however, when the time of decomposition is extended from 5.6 or 12.6 days to 158 or 176 days. Decomposition rates for gaseous plutonium hexafluoride at an initial pressure of 50 mm were 0.30 ± 0.04 percent per day for 12.6 days and 0.14 ± 0.01 for 158 days. At 100 mm initial pressure, the rate for 5.6 and 12.6 days was 0.37 ± 0.02 percent per day and for 158 and 176 days was 0.20 ± 0.04 percent per day.

Additional experiments on the decomposition of gaseous plutonium hexafluoride by gamma radiation have corroborated earlier results. The combined results give a G value of 7.5 ± 0.7. Experiments carried out on the decomposition of mixtures of helium and plutonium hexafluoride by gamma radiation have affirmed that helium has a slight effect on the decomposition of plutonium hexafluoride by gamma radiation. An average G value of 6.0 has been obtained for these experiments. Addition of krypton to plutonium hexafluoride reduces the extent of the decomposition by gamma radiation, and a G value of approximately 3.8 is obtained for krypton pressures up to one atmosphere and total energy absorption of less than approximately 5×10^{21} ev. At a pressure of krypton greater than one atmosphere or an energy absorption of 1×10^{22} ev, a G value of 1 is obtained for the decomposition. Further work will be done with krypton as an additive. Addition of fluorine or oxygen to plutonium hexafluoride apparently reduces the extent of decomposition of plutonium hexafluoride by gamma radiation.

An attempt was made to react PuF_6 and CaF_2 by contacting them at room temperature for one hour. Results indicate that no stable complex (i.e., no complex having a low decomposition pressure) is formed under these conditions.

Engineering-scale development studies are being carried out on the direct fluorination of uranium dioxide pellet fuel with the aim of optimizing batch-processing time and fluorine efficiency in single-vessel operation. In these studies, fluidization of inert, refractory alumina above

the uranium dioxide pellet bed and in the voids of the pellet bed is used as an aid to heat removal. Heat removal is also improved by use of a two-zone oxidation-fluorination technique which involves oxidation of the uranium dioxide to uranosic oxide fines in a lower zone (pellet bed), and fluorination of the fines in an upper, unhindered fluidized bed of alumina. In a current series of runs, further tests of thermal gradients in the pellet bed were made and evaluation of a gas-pulsing technique was begun. These techniques are intended to improve fines transport from the lower to the upper zone. In three runs, excessive rates of fines production and transport led to formation of intermediate uranium fluorides or plugging of fluorine inlet lines to the reactor. These results indicated that high oxygen concentrations (about 20 percent) and thermal gradients in the pellet bed were not necessary to produce uranium hexafluoride at practical rates, since a significant improvement in fines transport was obtained by use of the gas-pulsing apparatus. Accordingly, with gas pulsing and with both the oxidation and fluorination zones at about 500 C, two 12-in. batches of pellet bed charges of 8.8 kg uranium dioxide were completely fluorinated with 4.5 and 6.0 percent oxygen in nitrogen in total processing times of 15 and 12.5 hr, respectively. These processing times included a period of alumina bed cleanup and established the shortest processing times for 12-in. beds of pellets yet achieved in these fluorination studies. These runs were without operational difficulty. Sustained periods of high hexafluoride production rates were obtained in the runs, and a maximum rate of 107 lb UF_6/(hr)(sq ft of reactor cross section) was demonstrated. Overall fluorine efficiencies of about 70 percent were achieved in both runs.

One possible method of separating uranium dioxide reactor fuel from its cladding is to shear the fuel elements into short lengths and carry out an oxidation to produce uranosic oxide (U_3O_8) powder. This powder may then be separated from the cladding pieces by mechanical means. Studies have been undertaken on the removal of uranium dioxide pellets from stainless steel cladding by oxidation in a packed-fluidized bed. This process may then be incorporated into the two-zone oxidation-fluorination scheme for producing uranium hexafluoride. Preliminary experiments have shown that a high reaction temperature (up to 500 C) and gas pulses improve the rate of separation of uranium oxide from stainless steel cladding in a bed of $1\frac{1}{8}$-in.-long simulated fuel element segments. Rates of removal are nearly constant with time for removals of up to about 80 percent of the uranium dioxide (80 percent in 10 hr at 450 C). Tests are continuing.

Supporting studies were also undertaken to obtain heat transfer and elutriation data for mixtures of uranosic oxide in fluidized Alundum in the particular equipment configurations used in the Direct Fluorination Process.

When gas is passed through a bed of pure uranosic oxide fines (mean diameter of 4 μ), channeling of the bed takes place and there is no fluidization. By visual observation, this gas channeling appeared to be

eliminated by gas pulsing of the fluidizing gas; thus, more uniform agitation was established throughout the bed. Although gas pulsing of the fluidizing gas improved heat transfer coefficients at fluidization gas velocities above 0.2 ft/sec, the rate of gas pulsing did not have a significant effect on the coefficient of heat transfer from the surface of an internal heater to the bed. At superficial fluidizing gas velocities below 0.6 ft/sec, high gas-pulse rates provided better heat transfer.

For mixtures of the uranosic oxide fines and 50 to 170 mesh Alundum at gas-pulse rates of about 25 pulses/min, small increases in the heat transfer coefficient were observed upon increasing the Alundum content from 0 to 100 w/o (balance U_3O_8) and upon increasing the superficial gas velocity from 0.1 to 0.9 ft/sec. The effect of the superficial gas velocity on the heat transfer coefficient was less at the higher Alundum compositions in the U_3O_8-Alundum mixtures. The data indicate a maximum value for the heat transfer coefficient of 200 Btu/(hr)(sq ft)(F) at about 15 w/o U_3O_8-85 w/o Alundum and a superficial gas velocity of 0.6 ft/sec.

In heat transfer studies made without gas pulsing, the heat transfer coefficients of mixtures of 65 to 100 w/o Alundum and 35 to zero w/o U_3O_8 did not differ significantly from the coefficients obtained with similar mixtures which were subjected to gas pulsing. However, at the lowest superficial fluidizing gas velocity (0.2 ft/sec), which is slightly above the minimum fluidization point for Alundum, the maximum heat transfer coefficient value was somewhat more pronounced.

Studies were made of the elutriation rates of U_3O_8 fines (average diameter: 4 μ) from fluidized mixtures containing about 6 w/o U_3O_8 fines in Alundum (-40, +170 mesh). A strong effect of superficial velocity of the fluidizing gas (air) on the elutriation rate was noted. Gas pulsing superimposed on the fluidizing gas increased the elutriation rate slightly, with higher rates being observed at higher frequencies of pulsing. In general, the fines were elutriated initially at a constant rate, expressed in terms of percent of fines elutriated per unit time. At the point at which about 75 percent of the original charge of fines had been elutriated, the elutriation rate decreased. In the constant-rate period, elutriation rates of 3.7 percent/min, 1.8 percent/min, and 0.42 percent/min were measured for fluidizing gas velocities of 1.0 ft/sec, 0.67 ft/sec, and 0.33 ft/sec, respectively, in the absence of pulsing. At a gas rate of 0.67 ft/sec and a pulse frequency of 20 pulses/min, the elutriation rate was 2.3 percent/min.

The presence of a uranium dioxide pellet bed which is submerged in the fluidized bed had the effect of lowering the elutriation rate of U_3O_8 fines. However, elutriation in this case can be increased with high pulse gas manifold pressures and/or high gas pulse rates. Without

pulsing of the fluidizing gas and with the packed bed extending above the fluid bed, the elutriation rates were reduced to very low values (about 0.1 percent/min).

An effect of size of the fluidized Alundum particles on the elutriation rates for U_3O_8 fines was demonstrated. Elutriation rates for U_3O_8 fines were higher in mixtures of U_3O_8 and Alundum which contained 60 or 90 mesh Alundum than for mixtures which contained 120 mesh or -40 +170 mesh Alundum. In 60 min, about 85 percent of the fines was elutriated from the 60 and 90 mesh Alundum, whereas about 70 percent of the fines was elutriated from the 120 mesh and the 40 to 170 mesh Alundum.

Development work on a fluid bed-volatility process scheme for the recovery of enriched uranium from low uranium-zirconium alloy fuel is in progress. This process involves a chlorination of the alloy while it is submerged in an inert fluidized bed (currently Norton Company Alundum), and a subsequent fluorination step. The zirconium is separated from the alloy as the volatile tetrachloride during the chlorination step. The uranium is recovered as the volatile hexafluoride during the fluorination step.

Current studies involve the hydrogen chloride-fluorine cycle and the modified procedure whereby several batches of fuel are hydrochlorinated in succession, followed by a single fluorination to recover the uranium. In these studies, three equal-weight batches (total of 720 g) of five w/o uranium-Zircaloy alloy were processed.

Data on the progress of the hydrochlorination reaction was obtained by continuous analysis of the off-gas streams with in-line thermal conductivity cells. The data indicated that about 70 percent of the first batch of alloy had been reacted when the second batch was charged and that a total of 79 percent of the first two batches had been reacted when the final batch was charged. During the period of constant reaction rate, the alloy was reacted at a rate of about 70 g/hr; peak rates were about 90 g/hr, as compared with previous peak rates of about 50 g/hr.

Overall results showed that this two-reactant cycle gave uranium losses comparable with those sustained previously from a more lengthy, four-reactant cycle which involved reactions with hydrogen chloride, a hydrogen chloride-phosgene mixture, hydrogen fluoride, and finally fluorine. The quantity of uranium lost through the static bed filter during the entire hydrochlorination period (20.5 hr) was about 0.1 percent of the total uranium charged, as compared with a previous loss of about 0.25 percent in the four-reaction run; the quantity of uranium retained by the Alundum beds after the fluorination was about 0.5 percent of the total uranium charged, as compared with a previous value of 0.4 percent. The final uranium concentration in the Alundum was about 0.05 w/o. Data obtained from the analysis of samples taken from the fluid bed at half-hour intervals

during fluorination tend to confirm the previous results which showed that only one hour of fluorination at 350 C followed by one hour of fluorination at a higher temperature (~500 C) are required to achieve these acceptable residual uranium values.

Data obtained during the fluorination step from the thermal conductivity cells indicated that about 90 percent of the uranium was recovered from the reactor assembly during the first 30 min of the low-temperature (350 C) fluorination period.

Studies were continued on a fluid bed-pyrohydrolysis reaction scheme for converting the waste zirconium tetrachloride produced during the hydrochlorination of uranium-zirconium alloy fuels to zirconium dioxide for more convenient storage. Current efforts are concerned with demonstrating the operability of the 6-in.-diameter reactor system with feed rates that are significantly higher than those used previously, typical values being 4.1 to 5.1 kg/hr of zirconium tetrachloride as compared with previous rates of 2 to 3 kg/hr.

In two of the four experiments carried out during this period at these higher rates, the starting beds were relatively fine mesh sand (96.5 percent passing 100 mesh, 78 percent passing 200 mesh). These beds were intended to simulate the possible condition of extended-length operation wherein excessive amounts of fines would have accumulated in the bed. The overall results of the experiments, which were of $2\frac{1}{4}$ to $5\frac{3}{4}$-hour duration, were considered satisfactory, the criteria being:

a) no pressure increase across the exit gas filters;

b) complete conversion of the zirconium tetrachloride vapor to the solid oxide (indicated by the absence of zirconium in the off-gas condensate stream);

c) no caking of the bed, even when the bed consisted primarily of fines (less than 200 mesh material);

d) reasonably good material balances obtained in each run.

Installation of the pilot plant facility intended for demonstration of the fluidization-volatility process scheme for the recovery of uranium from uranium-zirconium alloy fuels is now about 75 percent complete. Leak-testing and instrument calibration is proceeding concurrently with installation. Current plans call for operation of this facility with only nonirradiated fuel material (up to 30 kg of alloy per charge). A study at high radiation levels is planned for a bench-scale ($1\frac{1}{2}$-in.-diameter) unit now in preliminary design stages.

A pulsed-bed method of loading large fuel elements into a bed of solids has been developed. This method offers a solution to the problem of loading the fuel assemblies in the fluidization-volatility pilot plant.

Fluid-bed studies of a simple process scheme for producing high-density spheroidal uranium dioxide particles directly from uranium hexafluoride were continued in a 3-in.-diameter Monel column. The scheme involves reaction of the uranium hexafluoride vapor with a mixture of steam and hydrogen in the presence of a product oxide bed at temperatures of 650 to 700 C. The reaction occurs preferentially on the surface of the bed particles, and the solid reaction products (uranium dioxide plus a relatively small amount of fluoride-bearing material) are deposited as a dense, adhering layer. The residual fluoride is removed by further reaction (with steam and hydrogen only).

Current work was concerned with further demonstrating the feasibility of preparing relatively specific size fractions, which might be needed in particulate fuel applications. Material, primarily of 80 to 100 mesh size and having a particle density of 9.4 g/cc (as measured by mercury displacement), was prepared from a starting bed of 100 to 140 mesh particles. The product contained about 62 percent +100 mesh material and less than one percent +80 mesh material.

Preparation of relatively coarse (+20 mesh) particles from a starting bed of 20 to 40 mesh material was attempted also. In the current experiment, a gas pulse-fixed bed technique was employed instead of the regular fluid-bed method, in order to avoid using the high flow rates of gas essential for fluidizing beds of coarse material. However, this procedure does not appear presently to be feasible. Attrition of the particles occurred such that there was only a slight overall increase in particle size; also, many fragmented sections of the coating were found in the product.

III. Calorimetry (pages 153 to 166)

The combustion techniques developed for the low-melting metals have been used to determine the heat of formation of zinc difluoride: ΔHf°_{298} (ZnF_2,c) = -183.0 ± 0.4 kcal/mole.

Two series of combustions of tantalum in fluorine have been run. By the same techniques and in a concurrent study, a series of combustions of niobium in fluorine has been partially completed. Final data have not been obtained; however, the precision obtained for the preliminary data, 0.01 percent, is excellent.

Calorimetric combustions of ruthenium in fluorine have been completed. Preliminary but incomplete calculations indicate that the energy of

combustion of ruthenium in fluorine is approximately 2097.8 cal/g and that the precision of six determinations is 1.3 cal/g or 0.06 percent.

Preliminary exploratory experiments are being carried out to develop techniques for the determination of the heats of formation of tetrafluoromethane and silicon carbide by fluorine bomb calorimetry. Preliminary exploratory experiments are also being carried out to develop techniques for the determination of the heat of formation of uranium monosulfide by fluorine bomb calorimetry.

Testing of the 1500 C drop calorimeter furnace is continuing. A dummy platinum capsule with thermocouples on the top and bottom was used to probe the hot zone of the furnace for temperature gradients. A maximum temperature gradient of 0.18 C was observed with the furnace operating at 1004 C. Design of the 2500 C furnace is continuing.

IV. Reactor Safety (pages 167 to 187)

The air oxidation of uranium at temperatures above 500 C is being investigated in order to determine the nature and degree of protectiveness of oxide films formed. Previous studies of ignition behavior have indicated that protective oxides may be formed at these high temperatures. An important part of the study is an assessment of the role of nitrogen in the oxidation reaction.

In this current study, uranium specimens were heated by induction in a flowing stream of an argon-air mixture. It was possible to compensate for heat generated by the air-uranium reaction by manual adjustment of the induction generator power. Depletion of oxygen and nitrogen in the gas stream was determined by mass spectrometric determinations at 2-min intervals. Results showed that the reaction followed a linear rate law at 500, 600, 700, and 800 C, and was initially parabolic at 900 and 1000 C, but subsequently became linear. Mass spectrometric analyses indicated that there was no significant uptake of nitrogen at any temperature studied.

Isothermal studies of the oxidation of plutonium are continuing. Research is being carried out in new glovebox facilities. Isothermal oxidations are performed with plutonium cubes containing less than 1000 ppm of analyzed metallic impurities. An automatically loaded analytical balance equipped with a temperature transducer is used. Oxidations were found to be initially parabolic over the entire temperature range studied, i.e., from 140 to 480 C. A consistent parabolic rate law is followed over the range of stability of the beta and gamma phases, namely, 120 to 320 C. A decrease with temperatures in the parabolic rate constant occurs in the delta phase between 320 and 450 C. The initially parabolic rates become linear after a period of time. The activation energy for the parabolic rate law is

about 32 kcal/mole over the temperature range from 140 to 320 C, whereas the subsequent linear rates have an activation energy of 16 kcal/mole over the same temperature range. The rates and activation energies were consistent with a mechanism based on the diffusion of oxygen ions through an oxide film composed either of PuO or Pu_2O_3. The second-stage linear rates might then result from failure of the protective oxide film. A third stage occurred in the reaction between 140 and 220 C (region of stability of beta-phase plutonium) in which a temperature-independent linear reaction occurred. The complex paralinear reaction in the region of the delta phase of plutonium (320 to 450 C) may be influenced by changes (recently determined to occur at 300 C) in the crystal structure of plutonium oxides.

The experimental program to determine rates of reaction of molten reactor fuel and cladding metals with water is continuing. One method involves the rapid melting and dispersion of metal wires in a water environment by a surge current from a bank of condensers. A series of runs with stainless steel-302 samples in the form of wires has been performed in order to compare results with those of previous studies with stainless steel-316. Runs with the 302 alloy were made in water at room temperature and at 200 C. The extents of metal-water reaction, as measured by the quantity of hydrogen generated, were identical for the two alloys except in the region of high initial metal temperature in heated water, for which greater reaction occurred with the 302 alloy. The somewhat greater reaction may have resulted from the formation of smaller particles by the 302 alloy. If the increase had resulted from a difference in reaction kinetics for the 302 alloys, greater reaction in room temperature water also would be expected.

Studies of metal-water reactions initiated by a nuclear transient are continuing. In these studies, small fuel specimens were submerged in water in high-pressure autoclaves which were placed in the center of TREAT and subjected to severe nuclear transients. Eleven unclad 81 w/o aluminum-17 w/o fully enriched uranium-2 w/o nickel fuel plates (SL-1 type) were subjected to destructive transients. One additional transient was performed with clad SPERT 1-D fuel material to complete the previously reported series of experiments (see ANL-6648, page 201). The appearance of the samples after irradiation showed the effects of increasingly destructive reactor energies. Degree of fragmentation as judged by the particle size and porosity of individual fragments increased regularly as the energy was increased beyond the melting energy. Slab-like crystals in the fragments were characteristic of material which received nuclear energy inputs between 530 and 800 cal/g during reactor periods of 40 to 80 msec.

The extent of metal-water reaction increased with energy input in three regions. Reaction was slight below an energy input of 530 cal/g, reaching seven percent. Reaction increased uniformly with increasing

energy input to about 27 percent at 880 cal/g. The appearance of the residue from runs at still higher energies suggested that vapor-phase burning had occurred which resulted in extensive damage to internal parts of the autoclave. Reaction was as high as 54 percent in this high-energy region.

V. Energy Conversion (pages 188 to 202)

Temperature-emf-composition data for the lithium-bismuth bimetallic cell have been obtained. Reproducibility and reliability of the data are satisfactory for the calculation of thermodynamic quantities, but analysis of the data is incomplete. Instability of the cell voltage caused by the reduction of potassium chloride in the electrolyte by the lithium anode and voltage drop due to irreversible transfer of lithium from the anode to the cathode were eliminated. It is suggested that the liquid metal alloy which serves as the cathode of a regenerative emf cell might also operate as a liquid fuel element in a reactor. This would allow the direct deposition of heat in the liquid metal system to be regenerated. In a single experiment, the cell voltage was not seriously affected by the addition of a small amount of normal uranium to the lithium-bismuth alloy serving as the cathode in a bimetallic cell with a pure lithium anode. Spontaneous thermal regeneration of the lithium-bismuth cell at 1000 C appears to be questionable with a calculated lithium vapor pressure of 0.8 mm.

The phase diagram of the lithium chloride-lithium hydride system is presented in final form with the analysis of the thermodynamic data for lithium hydride and lithium chloride.

Data on the permeation rates of hydrogen through iron-molybdenum alloys and pure vanadium metal are reported. The iron-molybdenum alloys do not show a significantly greater permeation rate than pure iron in spite of the reported greater solubility of hydrogen in the iron-molybdenum alloys. Vanadium shows very high permeation rates. However, the metal surface is very sensitive to trace impurities, and some method of stabilizing the metal-gas interface needs to be devised to make the operation of the diaphragm reliable.

The results of thermoelectric parameter measurements made on sintered specimens of uranium monosulfide (US)-thorium monosulfide (ThS) solid solutions having compositions (expressed in mole percent) of 75 US-25 ThS and 25 US-75 ThS are consistent with previous observations, namely, that (1) the Seebeck coefficient decreases with increasing ThS content, (2) the thermoelectric power shows a weak dependence on temperature, and (3) the resistivity decreases with increasing ThS content.

Equipment planning and equipment acquisition is in progress for effusion and mass spectrometric studies of the gaseous decomposition products of refractory nuclear reactor fuel materials.

VI. Routine Operations (page 203)

The operation of the radioactive waste-processing facility and the gamma-irradiation facility continued without incident.

CHEMICAL ENGINEERING DIVISION
SUMMARY REPORT

January, February and March, 1963

I. CHEMICAL-METALLURGICAL PROCESSING*

Pyrometallurgical processes for the recovery of fissionable material from discharged reactor fuels offer promise of achieving a reduction in the reprocessing costs associated with nuclear power. The principal characteristics of pyrometallurgical processes which are likely to result in reduced costs are their simplicity, compactness, low-volume dry wastes, and capability for handling short-cooled fuels, with an attendant reduction in fuel inventories. Since pyrometallurgical processes are at present low-decontamination processes their use in a fuel cycle requires remote refabrication of the fuel. This problem for plutonium-bearing fuels of high burnup is present to some extent because of the radiation problem associated with the higher plutonium isotopes and is not unique for pyrometallurgical processes. Among the pyrometallurgical processes under development are melt refining (a simple melting procedure for metallic fuels) and various processes for core and blanket materials which utilize liquid metal solvents as processing media. Pyrometallurgical techniques also show promise for the preparation of various reactor-fuel materials, including metals and carbides. The melt refining process is presently in the most advanced state of development and will be used for recovery of enriched uranium from the first core loading of the second Experimental Breeder Reactor (EBR-II).

A. Pyrometallurgical Development

1. Melt Refining

(R. K. Steunenberg, L. Burris, Jr.)

The fuel charge to the melt refining process consists of approximately 50 percent enriched uranium alloyed with about 5 w/o noble metal fission product elements. The fuel pins are clad with stainless steel, thermally bonded by a small amount of sodium. The pins are declad mechanically, chopped, and charged to a lime-stabilized zirconia crucible in which they are melted and maintained in a liquid state at 1400 C for a period of 3 to 4 hr. Approximately two-thirds of the fission products are removed in this procedure through volatilization and selective oxidation. The purified metal product is poured to form an ingot from which new pins are prepared by injection casting. A mixture of oxidized and unpoured metal remaining in the crucible as a skull is recovered by a separate process employing liquid metal solvents.

*A summary of this section is given on pages 11 to 15.

Development of the melt refining process is essentially complete, and plant equipment is currently being installed in the Fuel Cycle Facility at the EBR-II site in Idaho.

2. Processes Utilizing Liquid Metal Solvents
(L. Burris, Jr., R. K. Steunenberg)

The development of several processes which employ liquid metals and salts as media has continued. The skull reclamation process for recovering the fissionable material remaining in the crucible residue (skull) after a melt refining operation has been investigated further in pilot-plant runs with unirradiated material. Equipment-development studies and demonstration experiments on a larger scale are also being conducted in essentially full-scale integrated process equipment. Demonstrations of a liquid metal process for the extraction of plutonium from EBR-II blanket material have continued. Laboratory development work is continuing on processes for the recovery of uranium and plutonium from future fast breeder reactor cores by means of pyrometallurgical procedures.

Supporting fundamental studies of liquid metals and molten salts of process interest are in progress. These studies include investigation of the chemical reactions involved in process steps and accumulation of information of engineering importance, i.e., on distillation, heat transfer, and mixing characteristics of liquid metals and salts.

a. Demonstration of the Skull Reclamation Process
(R. D. Pierce and K. R. Tobias)

The skull reclamation process is being developed as an auxiliary to melt refining for processing the first fuel loading of the EBR-II reactor. The skull process has two purposes: (1) recovery of fissionable materials from melt refining crucible scoria and (2) separation of fission products from uranium. The recovered and purified uranium will be returned to the main processing line of the EBR-II fuel cycle. The skull recovery process provides the necessary separation of all nonvolatile fission products from uranium.

Small-scale demonstrations of the skull reclamation process (involving 100 to 150 g of uranium) are in progress in equipment located inside an argon glovebox as discussed in Chemical Engineering Division Summary Report for January, February, March 1962, ANL-6543, pp. 32 to 35. These demonstration runs are being made to expose and rectify any process difficulties, and to establish permissible ranges of process variations. The determination of optimum flowsheet conditions in these small-scale runs will permit emphasis to be given to process mechanics and equipment performance in large, integrated process equipment, construction of which is now essentially complete (see Section C).

A material-balance flowsheet for two demonstration runs is presented in Figure I-1. The skull oxide employed in the runs was from a common batch of material prepared from a melt refining skull containing ruthenium-rhodium-106 tracer, since the ruthenium concentration was too low for analysis by methods other than radiochemical. The fraction of fine crucible fragments in this skull oxide was unusually large - 10 percent instead of more typical percentages of one to three. (Zirconium is also introduced into the feed material of the skull reclamation process as a fission product.) By use of this material, the maximum capability of the process for zirconium removal could be determined.

The salt flux charge in both runs had the following composition (in mole percent): 46.8 calcium chloride, 46.8 magnesium chloride, 4.9 magnesium fluoride, and 1.5 zinc chloride. Zinc chloride was present in the flux phase to insure oxidation of any uranium metal present. On oxidation, uranium transfers into the flux phase. On reduction of the zinc chloride, which occurs in the reduction step (Step B of Figure I-1) and may partially occur in the noble metal extraction step (Step A), the flux composition becomes 47.5 magnesium chloride, 47.5 calcium chloride, and 5.0 magnesium fluoride.

The overall process performance obtained in the demonstration runs is given in Table I-1. The cerium removal of over 90 percent is considered good. Because the required removals of ruthenium and molybdenum are modest (a minimum of 50 to 60 percent), their removals are also adequate. The somewhat low overall ruthenium removal of 53 percent experienced in Run BJ-16 was the result of deliberate process variation, as will be explained later, and would normally be considerably higher (as in Run BJ-17). The zirconium removal is adequate for normal skull oxide which contains less than three percent zirconia crucible fragments. Although the removal is not adequate for skull oxide of high zirconia content such as that used in these runs, occasional products containing a higher zirconium concentration will not be objectionable because fuel performance is not impaired by high concentrations of zirconium.

Since the percentage of EBR-II fuel material processed in the skull reclamation process will be about ten percent of the total fuel material, the required uranium recovery is only about 95 percent. It should be easier to achieve high uranium recoveries in large-scale runs than in the present small-scale demonstration runs. A uranium yield of 95 percent was realized in Run BJ-17.

The lower yield of 85 percent in Run BJ-16 is attributed to the following: First, in Run BJ-16 the uranium in the reduction heel solution was not compensated for by an incoming reduction heel as in Run BJ-17 (see Figure I-1). In the calculation of the yield, the uranium in the heel solution was treated as being lost, although, in repetitive runs,

Figure I-1

SUMMARIES OF SKULL RECLAMATION PROCESS DEMONSTRATION RUNS BJ-16 AND BJ-17

(The skull oxide employed was from a common batch of skull oxide - Batch No. 50-73. Figures in parentheses are estimates based on previous experimental evidences.)

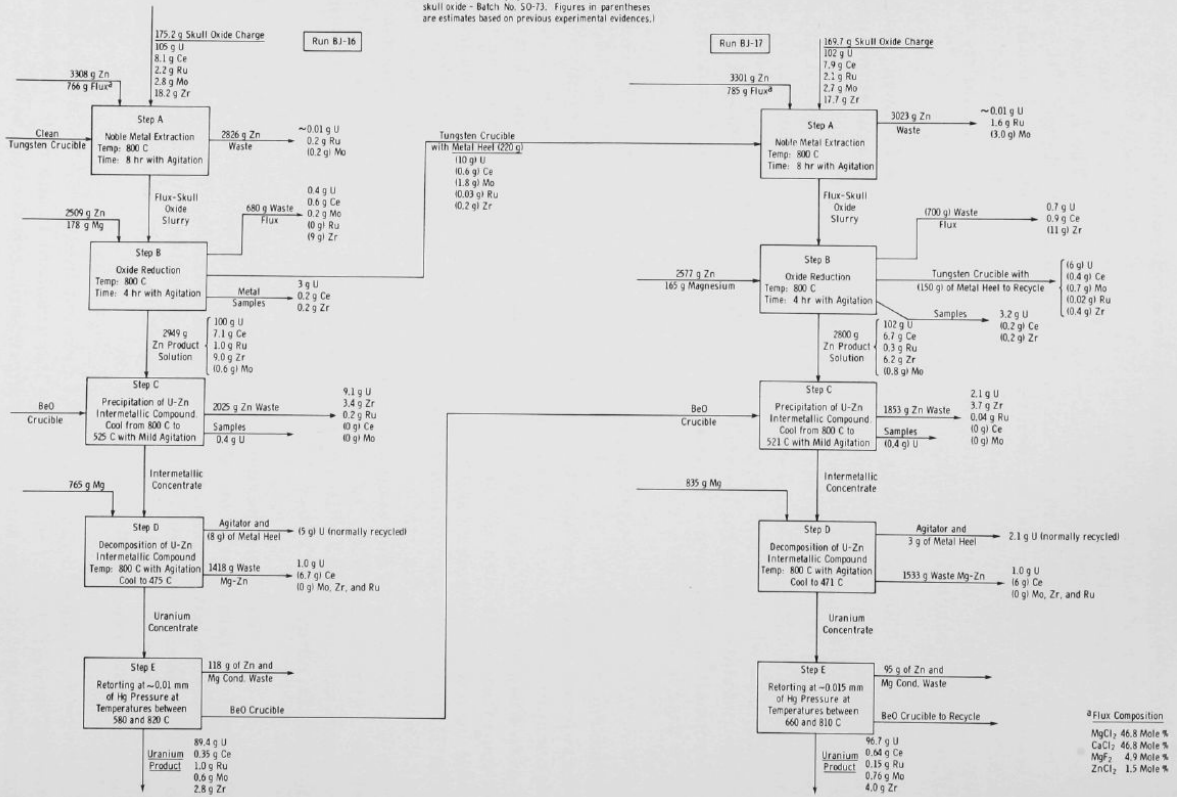

108-6504

Table I-1

PERFORMANCE OF SKULL RECLAMATION PROCESS IN TWO SMALL-SCALE DEMONSTRATION RUNS (BJ-16 AND BJ-17)

(see conditions in Figure I-1)

Constituent	Charge Composition - Oxygen-free Basis (w/o)	Run BJ-16			Run BJ-17		
		Uranium Yield (%)	Fission Product Removal (%)	Product Composition (w/o)	Uranium Yield (%)	Fission Product Removal (%)	Product Composition (w/o)
Uranium	77	85	-	94.9	95	-	94.5
Cerium	5.9	-	96	0.37	-	92	0.63
Molybdenum	2.0	-	80	0.60	-	72	0.74
Ruthenium	1.6	-	53	1.1	-	93	0.15
Zirconium	13.3	-	85	3.0	-	87	3.9

the heel solutions are recycled to succeeding runs. If the uranium in the reduction heel solution is credited, the uranium yield in Run BJ-16 is over 90 percent. The second reason for the lower yield in Run BJ-16 is that an unusually high uranium loss was experienced in the supernatant waste solution of the intermetallic precipitation step. Since this loss is greatly in excess of that represented by the solubility of uranium in this phase, physical carryover of precipitated uranium is indicated. If this problem recurs in future runs, it will be given special attention.

Other factors in these two demonstration runs which merit special consideration are discussed below.

(1) Noble Metal Extraction

The noble metal extraction steps of Runs BJ-16 and BJ-17 differed in two respects: the agitator position was closer to the metal-salt interface in Run BJ-17, and the waste zinc phase was agitated during the transfer in BJ-17 but not in BJ-16.

The extraction of ruthenium into zinc in Run BJ-16 was only 50 percent after 4 hr at 800 C as compared with extraction of 85 to 100 percent in Run BJ-17 and in Runs BJ-13, BJ-14, and BJ-15, previously reported in ANL-6648, p. 40. The same downward-deflecting agitator operating at 1000 rpm was employed in all five runs, but in the three earlier runs a small zinc charge was employed. This resulted in placing the flux-salt interface just above the agitator, whereas in Run BJ-16 made with a larger zinc charge the interface was $1\frac{1}{2}$ in. above the top of the agitator blade. In an attempt to evaluate the effect of agitator position, the blade was positioned $\frac{1}{4}$ in. below the interface in Run BJ-17, which otherwise was identical with Run BJ-16. Since these results emphasize the importance of the agitation, additional attention will be given to mixing variables in future runs.

In Runs BJ-16 and BJ-17, the flux phase was frozen before the zinc phase was transferred (by pressure through a dip tube). At the temperature (525 C) at which the zinc phase was transferred, the bulk

of the ruthenium precipitated since its solubility at this temperature is only about 0.02 w/o. In Run BJ-17, the zinc phase was stirred at 300 rpm during transfer, whereas in Run BJ-16 it was not. Chemical analysis of the zinc phase in Run BJ-16 prior to cooling from 800 to 525 C for the transfer showed that 50 percent of the total ruthenium had been extracted from the skull oxide. However, only about 10 percent of the total ruthenium was found in the transferred zinc. In Run BJ-17, the ruthenium transferred (85 percent) corresponded to that found in solution at 800 C. Mild agitation of the zinc extract is evidently necessary to keep noble metals in suspension during transfer of the zinc to waste. The loss of uranium in the waste zinc phase was negligible - less than 0.01 percent.

(2) Oxide Reduction

Reduction of uranium to metal was 99.6 percent complete in Run BJ-16 and 99.3 percent complete in Run BJ-17. After completion of the oxide reductions, the metal and flux phases were transferred together into a mold by pressure siphoning and separated after solidification. A semi-automatic procedure of separating flux and metal phases, which has been developed for use in the plant equipment (see Chemical Engineering Division Summary for January, February, March 1962, ANL-6543, pp. 39 to 42), cannot be conveniently employed with the small-scale demonstration equipment.

By material balances, it was determined that the zirconium oxide reductions were about 50 percent in Run BJ-16 and 35 percent in Run BJ-17. These low reductions were advantageous and provided removal in the flux wastes of much of the zirconium present in the skull oxide charges.

(3) Uranium-Zinc Intermetallic Compound Precipitation

Uranium is precipitated from zinc solution as zinc intermetallic compounds by cooling to about 525 C. The uranium solubility at this temperature is about 0.03 w/o. In both runs, the uranium loss in the supernatant solution was higher than the solubility value, particularly in Run BJ-16. The solubility of uranium at 525 C corresponds to a uranium loss of only 0.55 g in the zinc supernatant solution as compared with measured losses of 9.1 g sustained in Run BJ-16 and of 2.1 g in Run BJ-17. The difference is the result of precipitate entrainment. If necessary, this entrainment could be avoided by use of a filter in the transfer tube at the point of solution entry. Runs on a larger scale may result in a better evaluation of this problem.

Zirconium Removal

Zirconium is introduced into the skull reclamation process from two sources: (1) the fuel material itself, i.e., through the

fission process (which results in the introduction of 0.25 w/o zirconium for a fuel burnup of 2 percent), and (2) fragments or particles of the zirconia crucible which may slough off into the skull oxide. Since it is believed that the major mechanism for zirconium removal is its removal in the supernatant waste metal solution of the zinc-uranium intermetallic compound precipitation step, it is necessary to determine the maximum zirconium-removal capability of the process. The concentrations of zirconium found in the zinc phase before and after intermetallic compound precipitation were:

Run	Initial Zirconium Concentration[a] (w/o)	Transfer Temp (C)	Concentrations (w/o) in Transferred Zinc Solution	
			Magnesium	Zirconium
BJ-16	0.31	521	5.7	0.19
BJ-17	0.22	525	5.4	0.20

[a]Present in zinc solution of reduction step.

Since zirconium does not coprecipitate with the uranium-zinc intermetallic compound (see Chemical Engineering Division Summary Report for July, August, September, 1958, ANL-5924, p. 136), the above values are probably values of the zirconium solubility in a zinc-5.5 w/o magnesium solution at 525 C. Because zirconium was present in concentrations greater than its solubility value, the excess zirconium precipitated along with the uranium-zinc intermetallic compounds in these runs.

Because uranium loss (as a result of uranium solubility in the supernatant solution) becomes excessive at temperatures much above 525 C, this latter temperature is the maximum practical temperature of operation. The zirconium solubility of 0.2 percent and the weight of supernatant solution are such that with the expected 85 percent removal of the supernatant solution satisfactory zirconium removal can be achieved with skull oxide containing up to about 2 percent zirconium. This is more than adequate for the removal of zirconium whose source is the fuel material itself, which will contain well under 1 percent zirconium. Generally, the concentration of crucible fragments in skull oxides is about 1 percent, and results in a total zirconium concentration that can be readily accommodated in the process. However, concentrations of crucible fragments of up to 3 percent may be occasionally encountered. This is not of real concern because occasional high concentrations of zirconium in the fuel will not impair the performance of the fuel, and because the zirconium concentration will be lowered in the course of future processing cycles.

A process change is now being considered whereby the skull material would be oxidized to an extent just sufficient to permit release

of the skull from a melt refining crucible. This procedure may result in less introduction of crucible fragments than does complete oxidation of the skull material.

Two procedures for effecting additional zirconium removal have been tried in succeeding demonstration runs. In one of these, iron was added in the oxide-reduction step in an effort to precipitate $ZrFe_2Zn_x$; in the other, carbon was added in this same step in the hope of precipitating zirconium carbide and subsequently removing it in the waste-flux phase. Although analyses of these experiments are not complete, it appears that neither procedure was successful in effecting removal of zirconium.

(4) Decomposition of Uranium-Zinc Intermetallic Compound

By the addition of sufficient magnesium to produce a 50-50 zinc-to-magnesium weight ratio in the resulting supernatant solution, the uranium-zinc intermetallic compound is decomposed (see Step D of Figure I-1), leaving a precipitate of uranium metal. The decomposition is performed at 800 C; then the solution is cooled to below 475 C to reduce the solubility of uranium in the supernatant solution before removal of this solution. Rare earths, which were represented in the demonstration runs by cerium and which coprecipitate with uranium in the intermetallic compound precipitation step, are released upon decomposition of the intermetallic compounds and dissolve in the supernatant solution. About 90 to 95 percent of the supernatant solution was removed by pressure siphoning, leaving a uranium metal cake wetted with the residual solution.

Uranium concentrations in the transferred supernatant solutions were the same as the solubility values at the transfer temperature of about 470 C (0.07 w/o uranium), indicating no entrainment of precipitated uranium.

(5) Retorting

The uranium concentrates from the decomposition steps were retorted under vacuum (less than 0.05 mm Hg at 600 to 800 C) to vaporize the adhering zinc and magnesium. The product obtained was a uranium metal sponge. Normally, this material would be returned to the melt refining step of the main process line of the EBR-II fuel cycle. However, in order to facilitate sampling, the sponge products of the demonstration runs were weighed and then oxidized. The compositions of the products as metal are given in Table I-1.

(6) Summary

The two demonstration runs indicate the following:

(i) The skull reclamation process is capable of providing adequate uranium recovery (at least 95 percent) as a process complementary to the melt refining process in the EBR-II fuel cycle.

(ii) Adequate purification from fission products can be achieved from all fission product elements with the possible exception of zirconium.

(iii) A capability for adequate zirconium removal exists if the concentration of zirconia crucible fragments in the skull oxide does not, for reasons given previously, exceed about three percent. However, occasional batches containing more than three percent zirconium would not be objectionable.

(iv) Loss of uranium by entrainment of precipitated uranium in supernatant waste solutions may be a problem which bears watching and possibly further study.

b. Construction of Large-scale Integrated Equipment for the Skull Reclamation Process
(I. O. Winsch, D. E. Grosvenor, G. L. Rogers)

Construction of the integrated equipment for large-scale (2.5 kg of skull oxide) demonstrations of the skull reclamation process has been completed, and equipment shakedown testing has begun. The equipment consists essentially of two large furnaces covered with bell jars and containing stationary processing crucibles. Figure I-2 is a photograph of the glovebox, furnaces, and panelboard. Figure I-3 shows the furnaces with bell jar covers in place. A transfer line is shown in position for the transfer of molten metal from one furnace to the other. Figure I-4 shows one of the furnaces with the bell jar cover removed and the large tungsten crucible (of 12-in. OD by 20 in. high) in position within the induction heating coil. A somewhat similar large beryllia crucible will be used in the other furnace but has not yet been received.

Operation of these furnaces has been started by making transfers of flux and metal simulating the process flux and metal systems. Individual transfers were made of 15 kg cadmium (a stand-in for the actual magnesium-zinc process alloy) and 13 kg Dow-230 flux (a substitute for the actual process flux). Next, the automatic separation of Dow-230 flux from liquid cadmium was demonstrated. Very good phase separations were achieved by controlling the transfer rate of metal at about 4 lb/min. Metal

transfer at the desired rate was achieved by use of an orifice in the metal transfer line and by employing a pressure only slightly in excess of that required to transfer metal. Both of these measures are practical. At high rates of metal transfer effected by use of high pressures, phase separations were poor.

Figure I-2

GLOVEBOX, FURNACES, AND PANELBOARD FOR LARGE-SCALE DEMONSTRATION OF SKULL RECLAMATION PROCESS

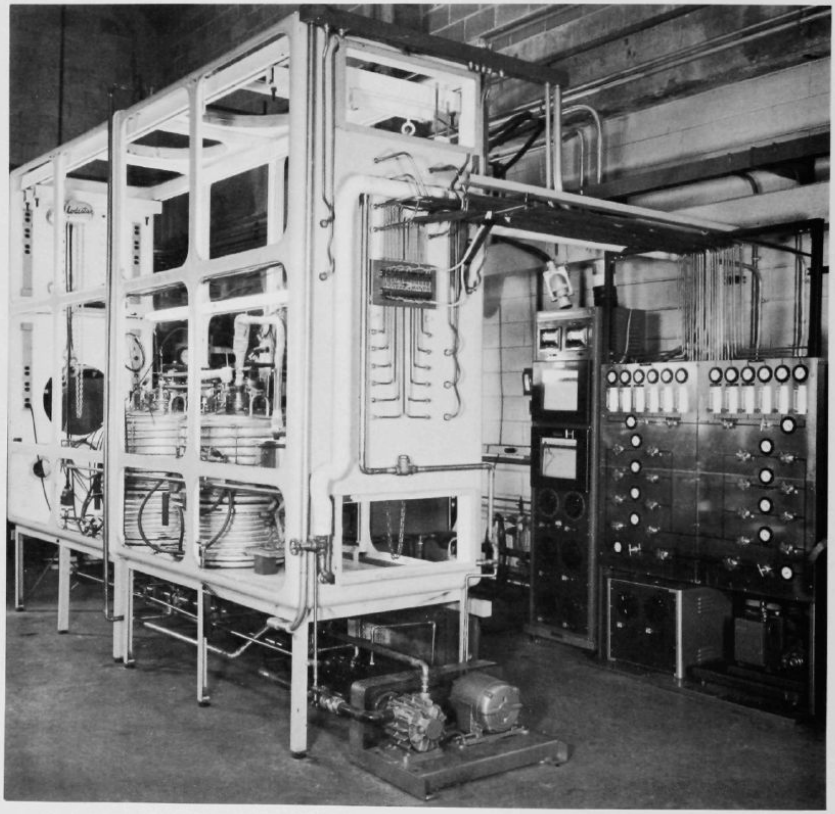

108-5968

The furnace containing the tungsten crucible is heated to 400 C in about one hour. The beryllia crucible is heated to 400 C in one hour and 20 min. The gross power input required to maintain the melt

at a temperature of 600 C is 5.2 kw. The static cooling rate, which was about 100 C/hr between 600 and 500 C, dropped gradually to 40 C/hr at 400 C. Between 200 C and 100 C, a cooling rate of 150 C/hr was obtained by circulating air initially at 40 C at a rate of about 26 cfm. Argon will be employed as the cooling gas when process operations begin.

Figure I-3

LARGE-SCALE RECLAMATION FURNACES WITH BELL JARS IN PLACE

Transfer line (with insulation partially removed) connects furnace for uranium precipitations (left) with furnace for noble metal extraction (right)

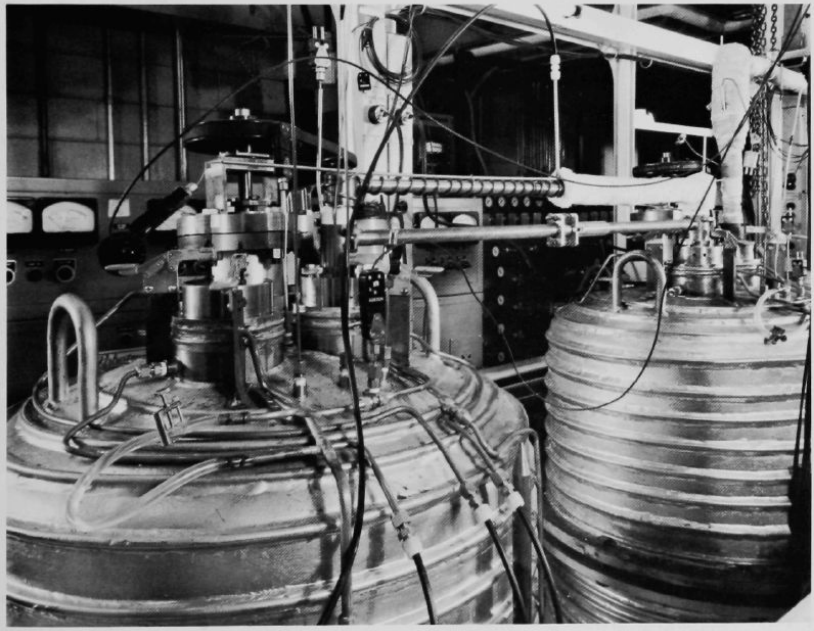

108-5972

Surface temperatures of the furnace bell jar and ring were maintained at satisfactory levels with water-cooled coils; temperatures of the rubber gaskets were near 40 C, which is well below the maximum allowed (150 C).

The solid copper induction coil is cooled only by radiation and convection. The surface temperature of the coil reached 300 C while the flux-metal temperature was being increased from 20 to 600 C at a

power input of 15 kw. The coil temperature then dropped to 175 C while a 600 C melt temperature was maintained at a power input of 5.2 kw. Temperatures of the furnace components are satisfactorily low.

Figure I-4

LARGE-SCALE SKULL RECLAMATION FURNACE WITH BELL JAR REMOVED

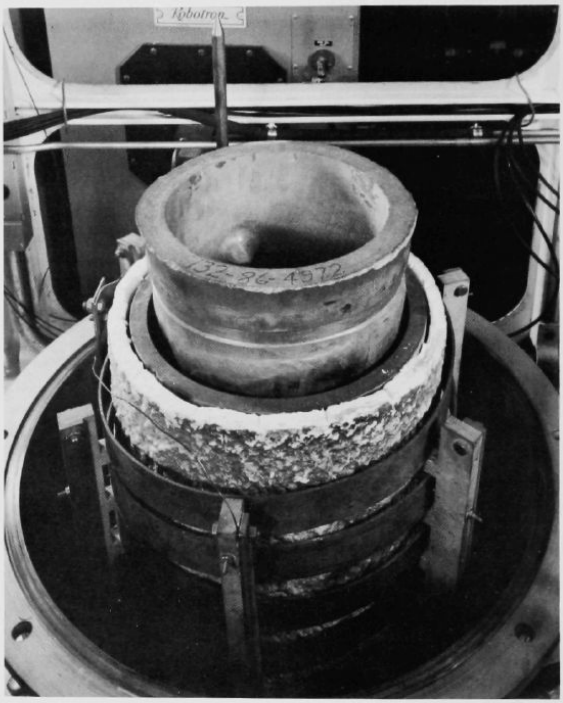

108-5965

It is anticipated that a number of process runs with skull oxide will be completed in this equipment during the next three months.

c. Retorting of Uranium Concentrates
(J. F. Lenc, M. A. Bowden, P. Mack, M. Deerwester)

In one of the steps of the skull reclamation process, uranium metal is precipitated by decomposition of the "epsilon" uranium-zinc intermetallic compound (approximate composition: U_2Zn_{23}) by the addition of sufficient magnesium to raise the magnesium concentration to 50 w/o.

Following removal of the supernatant liquid metal, the uranium precipitate remains enveloped in residual zinc and magnesium. The aim of current experimental work is to achieve easy removal of the uranium, both prior to retorting (to vaporize the residual zinc and magnesium) and after retorting. Removal of the uranium as a concentrate (i.e., enveloped in residual zinc and magnesium) prior to retorting is necessary (1) if retorting is to be conducted in a crucible other than the decomposition crucible or (2) if the uranium concentrate is considered the end product of the skull reclamation process and is to be recycled directly to the melt-refining operation. Uranium isolated in the final retorting step also must be easily removable in a form suitable for remote recycle to the melt-refining process.

Previous experiments have shown that only ceramic crucibles permit easy removal of the uranium in the crucible either as a concentrate after decomposition of the intermetallic compound or as an isolated product after retorting. Because beryllia has a high thermal conductivity (and, consequently, a low susceptibility to thermal shock) and a high chemical stability, beryllia has been investigated more extensively than other ceramics for use as a crucible material in the precipitation and final retorting steps of the process. However, other less-expensive ceramics (such as alumina and magnesia) may prove to be equally suitable.

Performance of an Unjacketed, Thixotropically Cast Beryllia Crucible

Beryllia crucibles are being subjected to repetitive process operations in order to determine their probable lifetime in plant use. During the last quarter, five additional 150-g uranium-scale runs (Runs 8 through 12) were conducted in an unjacketed, thixotropically cast beryllia crucible (4 in. in OD by 9 in. high with a $\frac{3}{8}$-in.-thick wall). The previous runs, reported in ANL-6596, p. 54, and ANL-6648, p. 44, were conducted in general accord with the "three-step" procedure.* Two of the runs were long-term tests (similar to the run shown schematically in ANL-6596, p. 53) in which the melts in the first two steps were subjected repeatedly to thermal cycling between approximately 450 and 800 C.

In the eighth and ninth runs, the precipitated uranium concentrate (enveloped in residual zinc and magnesium) was readily removed from the beryllia crucible after the intermetallic-decomposition step. However, in the tenth and eleventh runs, the uranium concentrate adhered to

*The three steps, all of which are conducted in the same crucible, simulate the last three steps of the skull reclamation process, namely, (1) precipitation of the uranium-zinc intermetallic compound and removal of supernatant liquid metal, (2) decomposition of this compound with magnesium to precipitate the uranium, and, following removal of the supernatant liquid metal, (3) retorting to drive off the residual zinc and magnesium.

the bottom of the crucible after the decomposition step. In addition, some erosion of the bottom of the crucible was detected after the latter two experiments. To determine whether the useful life of the thixotropically cast beryllia crucible had been expended, a twelfth run was performed in the same crucible. The uranium concentrate from the decomposition step did not adhere to the crucible in this last run, but circumferential cracks were clearly visible in the bottom 2 in. of the crucible. The crucible was therefore judged to be too unsound for further service.

In ten of the twelve runs, a final retorting step was conducted in which isolation of the uranium metal was accomplished by vacuum evaporation of the residual zinc and magnesium. Essentially 100 percent of the isolated uranium product was easily recovered from the crucible in each of these runs.

In the course of the twelve runs, the thixotropically cast beryllia crucible was subjected to process conditions simulating 24 intermetallic precipitation steps, 25 intermetallic-decomposition steps, and 10 final retorting steps. During the precipitation steps in these runs, the crucible successfully contained zinc-magnesium solutions at temperatures above 450 C for about 465 hr. For comparison, it is estimated that a crucible will be exposed to similar conditions for approximately 20 hr in processing a single batch of material on a plant scale.

Two additional thixotropically cast beryllia crucibles are being purchased for further evaluation of the performance of this type of crucible. Large-size (12-in. OD by 20 in. high), thixotropically cast beryllia crucibles are also being obtained for use and evaluation in a pilot plant for the skull reclamation process. Evaluation of other less-expensive ceramic crucibles (such as alumina and magnesia) is also planned.

d. Processes for Plutonium Reactor Fuels
(R. K. Steunenberg)

Plutonium-uranium alloys containing fissium elements or other metals are receiving consideration as fuels for fast power breeder reactors. A critical separation in processing irradiated fuels of this type by pyrometallurgical methods is the removal of rare earth fission products from the plutonium. Two promising methods for effecting this, as well as other separations, are under study. One utilizes a selective extraction of the rare earths from a zinc-magnesium solution of uranium and plutonium by means of a molten halide flux. The other method involves coprecipitation of the uranium and plutonium from a zinc-calcium solution in which the rare earths are soluble.

(1) Extraction Studies with Molten Salts
(J. B. Knighton, J. D. Schilb, J. W. Walsh)

The purpose of this program is to investigate the separation of constituents in irradiated reactor fuels by equilibration between liquid magnesium-zinc alloys and molten halide fluxes. Distribution coefficients, K_d = (w/o in flux)/(w/o in metal), for a magnesium chloride flux and a magnesium-zinc phase of varying composition have been reported previously for thorium, uranium, plutonium, americium, barium, yttrium, cerium, praseodymium, neodymium, zirconium, vanadium, and iron (see ANL-6569, p. 39; ANL-6596, p. 59; and ANL-6648, pp. 50-53). The effects of other variables, such as temperature, concentration, and composition of the flux and metal phases, have also been described (ANL-6596, p. 59, and ANL-6648, p. 46). Work during the past quarter has been concerned with the distribution behavior of curium and neptunium, and the possible separation of curium from americium by this method.

Distribution of Curium between Zinc-Magnesium Alloy and Magnesium Chloride

The distribution of curium between zinc-magnesium alloy and magnesium chloride at 800 C has been investigated with a magnesium chloride flux and a zinc-magnesium metal phase of varying composition. The separation of curium from other transuranium elements, and from americium in particular, is of importance in the preparation of curium and the heavier actinide elements.

Approximately 0.1 mg of curium-244 coprecipitated with 100 mg of lanthanum fluoride was used in each experiment. All of the metal samples were filtered through porous tantalum frits into tantalum tubes. Flux samples were withdrawn into open-end tantalum tubes. The relative amounts of curium in the flux and metal samples were determined by alpha counting. The equilibrium points were approached from both the zinc-rich side and the magnesium-rich side of the zinc-magnesium metal phase.

The results are presented in Figure I-5. The data show the same general type of dependence on magnesium concentration in the metal phase that has been observed with other elements. The curium distribution curve falls very close to that for plutonium (see Figure I-6).

Possible Separation of Americium from Curium and the Other Actinide Elements

Distribution coefficients at 800 C for thorium, uranium, plutonium, americium, and curium are shown as a function of magnesium concentration in the metal phase in Figure I-6. In all cases, the

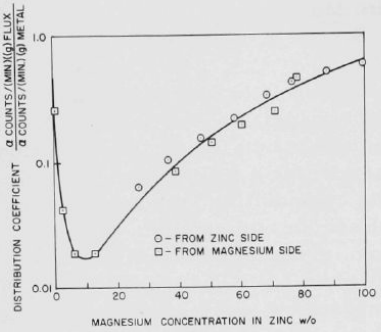

108-6505

Figure I-5

DISTRIBUTION OF CURIUM BETWEEN ZINC-MAGNESIUM ALLOY AND MAGNESIUM CHLORIDE

Conditions

Temp:	800 C
Mixing Rate:	300 rpm
Crucible:	Tantalum
Atmosphere:	Argon

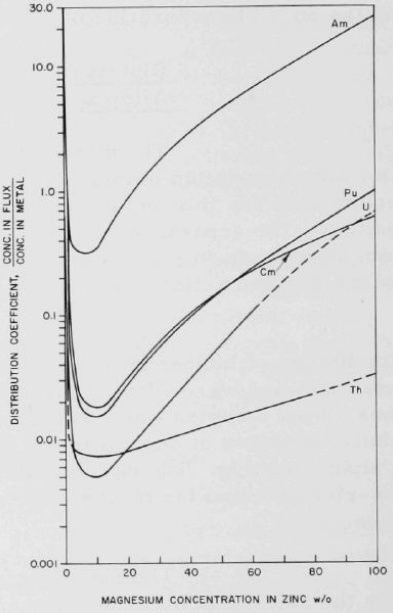

108-6506

Figure I-6

DISTRIBUTION OF THE ACTINIDE ELEMENTS BETWEEN ZINC-MAGNESIUM ALLOY AND MAGNESIUM CHLORIDE

Conditions

Temp:	800 C
Mixing Rate:	300 rpm
Crucible:	Tantalum
Atmosphere:	Argon

flux phase was magnesium chloride. Americium is the only actinide element investigated thus far which has the relatively large distribution coefficients characteristic of the rare earth elements. It is apparent from these data that a separation of americium from the other actinide elements can be effected by equilibration between molten salt and liquid metal phases. For example, a curium-americium separation could be based on the

tendency of americium to appear in the flux and curium in the metal. Some separation factors for curium and americium are given in Table I-2 for a magnesium chloride flux and a zinc-magnesium alloy of varying magnesium content.

Table I-2

AMERICIUM-CURIUM SEPARATION FACTORS FOR A MAGNESIUM CHLORIDE FLUX AND A ZINC-MAGNESIUM METAL PHASE

Conditions

Temperature:	800 C
Mixing Rate:	300 rpm
Apparatus:	Tantalum
Atmosphere:	Argon
Flux/metal Weight Ratio:	0.5-1.5
Minimum Equilibration Time:	~1 hr

Magnesium Concentration in Zinc-Magnesium Phase (w/o)	Separation Factor $[K_d(Am)/K_d(Cm)]^a$	Magnesium Concentration in Zinc-Magnesium Phase (w/o)	Separation Factor $[K_d(Am)/K_d(Cm)]^a$
5	15	60	30
10	19	70	31
20	27	80	34
30	29	90	37
40	28	100	40
50	29		

[a] Distribution coefficient, $K_d = \frac{\text{w/o in flux}}{\text{w/o in metal}}$.

On the basis of the temperature effect on the praseodymium-plutonium separation factors (see ANL-6596, p. 63), it is expected that a considerable increase in the americium-curium separation factor could be achieved by reducing the temperature.

Distribution of Neptunium between Zinc-Magnesium Alloy and Magnesium Chloride

A preliminary experiment has been completed in which the distribution behavior of neptunium between zinc-magnesium alloy and magnesium chloride was investigated. Tracer-level neptunium-239 used in the experiment was prepared by neutron irradiation of highly depleted uranium-238. The uranium was not removed prior to the experiment. Samples of the metal phase were filtered through porous tantalum frits into tantalum tubes, and flux samples were withdrawn into open-end tantalum tubes. The neptunium in the flux and metal samples was determined by using a gamma-ray spectrometer.

The results of the preliminary experiment indicate that neptunium exhibits the same distribution behavior as plutonium and curium. Additional experiments are in progress to complete the study of neptunium.

(2) Extraction Studies with Calcium: Solubility of Uranium in Zinc-Calcium Solutions
(M. Ader, J. T. Feeney)

The solubilities and cosolubilities of uranium and plutonium in zinc-calcium solutions are being determined in connection with processes for fast reactor fuels. The solubility of uranium in zinc-calcium solutions containing 0 to about 25 w/o calcium has been redetermined at 800 C and 750 C, with a few additional data at 700 C. Previous measurements, reported in Chemical Engineering Division Summary Report for April, May, June 1961, ANL-6379, p. 66, were suspect because of the use of porous graphite filters in obtaining samples of the saturated melt. Tantalum filter frits were used in the present experiment (MA-Ca-14), and appreciably different results were obtained.

A charge consisting of 50 g of uranium and 1000 g of zinc was placed in a tantalum crucible, heated, and stirred with a tantalum paddle at about 460 C for about $7\frac{1}{2}$ hr in an argon atmosphere. The charge was cooled overnight to room temperature and was then reheated with stirring to 750 C. The melt was stirred at this temperature for 3 hr, allowed to settle, and then sampled. Calcium was added next and the procedure of equilibration at temperature, settling, and sampling was repeated. Continued stepwise additions of calcium were made, and samples were taken at 800 and 750 C, and in a few cases at 700 C. The order of equilibrations, i.e., with rising or falling temperature, was varied and equilibrations of at least $1\frac{1}{2}$ hr at temperature were employed. An additional 7.8 g of uranium was added to the melt during the solubility determination at 13 w/o calcium to ensure uranium saturation. Samples were taken by pressurizing the melt through tantalum frits press-fitted into $\frac{1}{4}$-in.-diameter tantalum tubes. The samples were subsequently dissolved in a nitric acid-hydrochloric acid solution and analyzed for (a) calcium, by an EDTA procedure, and (b) uranium, either colorimetrically (>0.2 w/o) or fluorophotometrically (<0.2 w/o).

The analytical data from Experiment MA-Ca-14 are arranged in Table I-3 so that each horizontal line represents the results after a particular calcium addition. These data are plotted in Figure I-7 as weight percent uranium solubility versus weight percent calcium concentration.

The general shape of the uranium solubility curves is similar to that found previously (see ANL-6379, p. 68). However, the uranium solubilities in the present experiment are appreciably higher than in the earlier experiments over the entire range of calcium concentration.

The solubility values differ by about 10 to 40 percent between 0 and 16 w/o calcium and by factors of 15 to 50 beyond 20 w/o calcium. The low results obtained in the earlier experiments are attributed to the use of graphite filter frits which reacted with and removed dissolved uranium during sampling. The effect was more pronounced at the higher calcium concentrations because of the much smaller uranium content of the samples and increased uranium activity coefficients.

Table I-3

SOLUBILITY OF URANIUM IN ZINC-CALCIUM SOLUTIONS

Experiment:	MA-Ca-14
Charge:	50 g uranium, 1000 g zinc; calcium added incrementally
Equipment:	Tantalum
Atmosphere:	Argon
Equilibration:	1.5 hr minimum
Sampling:	Melt pressurized through tantalum filters into tantalum tubes

800 ± 2 C		750 ± 2 C		700 ± 1 C	
Calcium (w/o)	Uranium (w/o)	Calcium (w/o)	Uranium (w/o)	Calcium (w/o)	Uranium (w/o)
(0)	(5.36)[a]	0	2.89	-	-
		2.04	1.63	-	-
3.42	2.51	3.61	1.03	-	-
4.95	1.95	5.26	0.79	-	-
6.10	1.93	6.31	0.67	-	-
7.27	2.09	7.64	0.71	-	-
8.43	2.38	9.03	0.97	-	-
9.73	3.33	10.7	1.45	-	-
10.6	4.29	11.6	2.03	-	-
11.7	4.24	12.3	3.04	-	-
12.9[b]	2.67	12.7	2.50	-	-
14.8	1.28	14.9	1.12	-	-
16.3	0.75	16.4	0.55	16.5	0.45
20.6	0.17	20.3	0.14	20.4	0.094
23.1	0.091	23.7	0.046	23.2	0.040
28.5	0.021				

[a] Solubility calculated from the equation: log (w/o U) = 7.101 - (6837/T) (from A. E. Martin, private communication).

[b] 7.8 g uranium added before equilibration to ensure saturation.

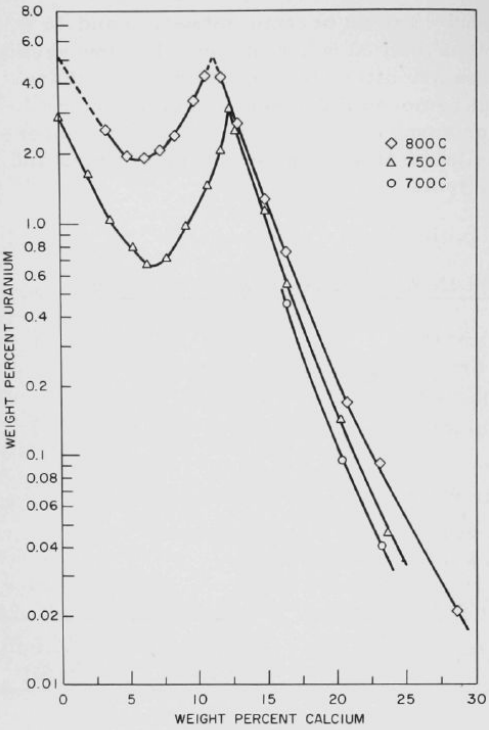

108-6507

Figure I-7

SOLUBILITY OF URANIUM IN ZINC-CALCIUM SOLUTIONS

(Experiment MA-Ca-14)

Similarities between the solubility curves of uranium in zinc-calcium and zinc-magnesium alloys (see Chemical Engineering Division Summary Reports ANL-6477, p. 93; ANL-6101, p. 67; ANL-6569, p. 83) have been noted previously, namely: the solubility curves exhibit minima followed by cusped maxima, followed by a sharp drop. However, both on a weight percent basis and on an atom percent basis, calcium is more effective than magnesium in depressing the solubility of uranium in zinc. At calcium concentrations above about 30 w/o, the uranium solubility becomes sufficiently low that the amount in solution is negligible for process purposes.

Further experiments at higher calcium concentrations and over a wider temperature range are in progress.

e. Recovery of Plutonium from EBR-II Blanket Material
(I. O. Winsch, T. F. Cannon, P. J. Mack)

Plutonium will be generated in the depleted uranium blanket material of the EBR-II reactor to a concentration of about one percent

before the blanket material is discharged for the separation of plutonium from uranium by a pyrometallurgical method. The blanket processes under investigation are based on the high solubility of plutonium in magnesium-rich zinc alloys and the contrasting low solubility of uranium in these alloys.

(1) Processing of Irradiated Uranium Blanket Material

A blanket process demonstration run has been completed with irradiated blanket uranium rods. The purpose of this run was to determine the behavior of iodine and fission products* in the blanket process presently being developed (see flowsheet in Chemical Engineering Division Summary Report for October, November, December 1961, ANL-6477, p. 47). Analytical results for this run are not available at the present time.

(2) Investigation of an Alternative Blanket Process

A possible alternative or flux blanket process has been studied. Both this process and the one that is under development are based on the preferential solubility of plutonium in magnesium for the separation of plutonium from uranium, but the alternative process utilizes a sequence of oxidation-reduction reactions in metal and molten flux phases. A schematic flowsheet of the process is shown in Figure I-8.

In the first or oxidation step, uranium-1 w/o plutonium alloy is dissolved with agitation in a zinc chloride-containing flux at 800 C to produce a flux solution of plutonium and uranium chlorides. The resulting zinc phase collects below the flux phase, and separation of the metal phase from the flux is required after this step. Reduction of the uranium and plutonium chlorides is accomplished in the second step by the addition of magnesium metal at 800 C with suitable agitation. The uranium, although wetted by magnesium, precipitates from both the metal and the flux phases while the plutonium dissolves in the magnesium phase. A fairly high-density flux would be required to cause the plutonium-bearing magnesium phase to float and thereby effect a separation from the precipitated uranium. If, as an alternative, the zinc phase were not removed after the first step in the process, a magnesium-zinc alloy having a density of about 5 g/cc would result from reduction of the uranium and plutonium chlorides. This alloy would settle, together with the precipitated uranium, to the bottom of the vessel. Subsequent separation of the plutonium-bearing magnesium phase from the magnesium-zinc-uranium mixture would be difficult. If such a separation could be performed, the final step in the process would be the distillation of magnesium from the magnesium-plutonium phase to recover the plutonium product. Such a distillation step

*Inactive fission product elements were also added to bring the concentrations of fission product elements up to expected process levels.

would be unnecessary if the amount of magnesium added in the reduction step provided a concentrated plutonium product solution. This concentrated plutonium solution could be fed directly into the process used for core material.

Figure I-8

ALTERNATIVE BLANKET PROCESS BASED ON OXIDATION-REDUCTION REACTIONS IN METAL AND FLUX PHASES

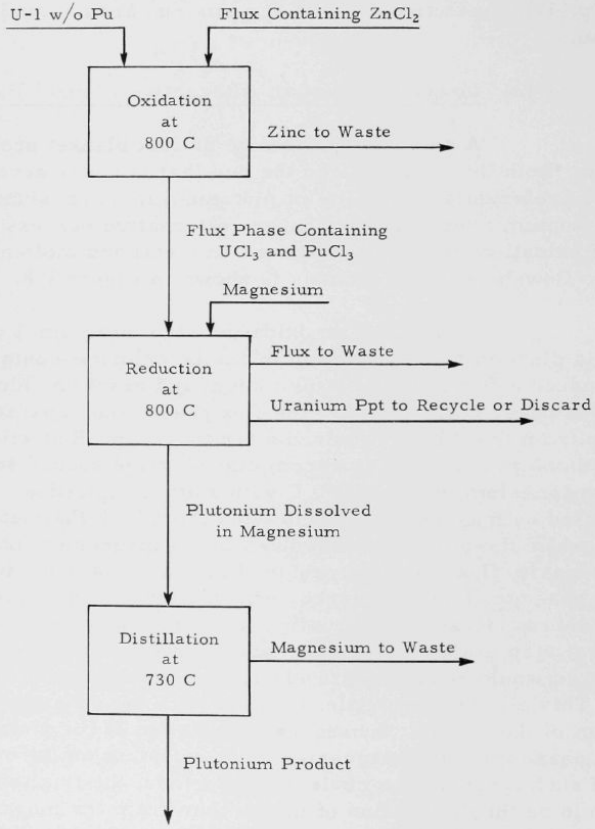

108-6508

The principal advantage of this scheme over the present blanket process (see ANL-6477, p. 47) would be the smaller volumes of reactant materials required. In processing 10 kg of blanket material, it is estimated that the volume of the magnesium-plutonium solution would be about 2.5 liters, which is about one-tenth the volume of the plutonium product solution that would be obtained in the present blanket process.

Three scouting runs were made to investigate the alternative flowsheet. Uranium-1 w/o plutonium alloy was dissolved in a flux whose initial composition (in weight percent) was: 67.5 barium chloride, 20.6 potassium chloride, 2.0 lithium fluoride, and 9.9 zinc chloride. This flux was chosen because its relatively high density (about 2.9 g/cc) would promote separation of the magnesium and uranium phases after the reduction step. In the oxidation step of two of the runs, the uranium and plutonium were completely dissolved in the flux with only trace amounts (~0.01 percent) of uranium and plutonium found in the zinc phase. In the third run, magnesium oxide (to the extent of 5 w/o) was added to the flux to increase the density of the flux and to improve thereby the separation of the plutonium-bearing magnesium phase. However, the presence of the magnesium oxide apparently hindered the oxidation of the uranium and plutonium, for analyses showed that the flux phase contained only 75 percent of the uranium and plutonium charged.

The reduction steps in all three runs were successful in that the uranium chloride and plutonium chloride were reduced essentially completely by the magnesium and were removed from the flux phase. Uranium in a finely divided state precipitated from the magnesium upon the reduction of uranium trichloride. In none of the three runs was good separation of the magnesium phase from the precipitated uranium obtained. The reason for this poor separation is believed to be poor coalescence of finely divided uranium in the magnesium phase. This uranium was well wetted by the magnesium, but its very low solubility in the magnesium phase hindered its coalescence. Because of the suspended uranium, the magnesium phase had an average density sufficiently high to cause it to settle in the flux rather than float.

This alternative or flux blanket process would be very attractive if the difficulties encountered in the various phase separations could be overcome. Since the solution of the problem may be difficult, the main emphasis will be placed on the development of the original blanket process.

f. Materials and Equipment Evaluation
(P. A. Nelson)

Studies are in progress to evaluate the compatibility of various materials of construction with liquid metal and salt systems of the types which may be employed in processes of fuel recovery. The selection

of materials for EBR-II processing equipment is the major objective, but data of more general interest are also being accumulated. Corrosion tests and performance tests under processing conditions are being used to evaluate materials. Methods of fabricating materials into items of process equipment are also being evaluated. Considerable attention was given during the past quarter to the fabrication of vessels from ceramic materials.

Fabrication of Ceramic Containers

(P. A. Nelson, Z. D. Jastrzebski,* W. Pehl, and M. Deerwester)

A need for large ceramic vessels is envisioned for future large-scale liquid metal processes. Beryllia, alumina, and magnesia are among the ceramic materials which are sufficiently inert to process systems (magnesium-zinc and halide salt systems) to be considered as container materials. A commercial source of large crucibles of these materials having good resistance to thermal and mechanical shock and having low permeability to halide salts has not been found. Crucibles formed by ramming or casting and containing large prefired aggregate have good mechanical properties, but, unfortunately, also have high porosity. On the other hand, low-porosity crucibles formed by slip casting or isostatic pressing from very fine, highly reactive powders have low thermal and mechanical shock resistances.

In order to take advantage of the good mechanical properties of porous, coarse-grained crucibles, an attempt is being made to seal the pores of these crucibles by coating or impregnating the inner surfaces with a slurry or thin paste containing a finely divided solid solution of low-melting oxides. Subsequent firing of the crucible fuses the coating or impregnating material, thereby sealing the pores.

Screening Tests of Coating Materials

In preliminary studies (see ANL-6596, p. 76) various coating materials were applied to fragments of alumina crucibles (Norton Alundum-213, 99 percent aluminum oxide) and fragments of magnesia crucibles (Norton Magnesite-473, 97 percent magnesium oxide). Each fragment, about 4 sq in. in area, was coated on its concave surface with a thin paste containing a low-melting mixture of oxides. The coated fragments were fired at 1400 to 1500 C in air. The thicknesses of the as-fired coatings were usually between 5 and 10 mils.

The results of the preliminary studies are given in Table I-4. Coatings 1 through 5 were each composed of a mixture of oxides which on melting (at 1345 C) and refreezing forms a eutectic containing equimolar

*Consultant from Lafayette College, Pennsylvania.

quantities of magnesia, pentacalcium trialuminate, and monocalcium aluminate.[1] Coatings 7 and 8 contained alumina in excess of the eutectic composition; Coatings 9, 10, and 11 contained magnesia in excess of the eutectic composition. The composition of Coating 6 was 52 w/o calcia-48 w/o alumina.

Table I-4

COMPOSITION AND PERFORMANCE OF LOW-MELTING OXIDE COATINGS FOR SEALING POROUS CERAMIC BODIES

Coatings were applied in the form of a thin paste with a brush to crucible fragments about 4 sq in. in area. Two tests were run with each coating material.

Coating No.	Coating Composition (w/o)[a] Al_2O_3	CaO	MgO	BaO	Melting Point or Melting Point Range (C)	Suspending Medium[b]	Firing Temp (C)	Remarks
			Part 1 - Application of Coatings on Norton Alundum-213 Crucible Fragments					
1	52	41	7	0	1345	Ethyl alcohol	1500	Shiny, impervious coating formed from a low-viscosity liquid.
2	52	41[c]	7[c]	0	1345	Ethyl alcohol	1400	Similar in appearance to Coating 1.
3	52	41	7	0	1345	Water	1400	Similar to Coating 1 except coating was rough and did not cover substrate.
4	52	41[c]	7[c]	0	1345	Water	1500	Similar in appearance to Coating 1.
5	52[d]	41[c,d]	7[c,d]	0	1345	Ethyl alcohol	1500	Dull, impervious coating formed by reaction and partial liquefaction.
6	48	52[c]	0	0	1400	Ethyl alcohol	1400	Similar in appearance to Coating 1.
7	60	34	6	0	(1345-1575)	Ethyl alcohol	1400	Similar in appearance to Coating 1.
8	67	28[c]	5[c]	0	(1345-1575)	Ethyl alcohol	1400	Coating was porous and crumbly.
9	43	34	23	0	(1345-2000)	Ethyl alcohol	1400	Rough, impervious coating formed by partial liquefaction.
10	43[e]	34[e]	23[e]	0	(1345-2000)	Ethyl alcohol	Not fired	Coating flaked off when the alcohol evaporated.
11	36	28	36	0	(1345-> 2000)	Ethyl alcohol	1400	Coating did not appear to wet the surface; droplets formed, leaving large uncovered areas.
12	Calcium Aluminate Cement				No data	Water	1400	Cracked, porous surface.
			Part 2 - Application of Coatings on Norton Magnesite-473 Crucible Fragments					
6	48	52[c]	0	0	1400	Ethyl alcohol	1400	Coating melted and soaked in; the surface remained porous.
8	67	28[c]	5[c]	0	(1345-1575)	Ethyl alcohol	1400	Coating partially liquefied; liquid soaked in. Excess Al_2O_3 produced a crumbly surface.
9	43	34	23	0	(1345-2000)	Ethyl alcohol	1400	Most of the coating was absorbed; the surface remained porous.
12	Calcium Aluminate Cement				No data	Water	1400	Cracked, porous surface.
13	0	0	15	85	1500	Ethyl alcohol	1400	Green coloration to a depth 1/8 in.; surface was checked and porous.
14	0	8[c]	12[c]	80[c]	-	Ethyl alcohol	1400	Same as Coating 13.

[a]All materials were finely ground, chemically pure materials except the Al_2O_3, which was 240 mesh Norton-38 alumina grain.

[b]The ethyl alcohol was denatured ethyl alcohol; the water was distilled water.

[c]Added in the form of the corresponding carbonates.

[d]Coating materials were melted together at 1500 C in an alumina crucible and then ground in denatured alcohol in a porcelain ball mill with alumina balls for 48 hr.

[e]Ground in a ball mill in denatured ethyl alcohol for 24 hr.

Coatings 1 through 4 formed a low-viscosity liquid on melting, which in the amounts employed (10- to 15-mil-thick coating) did not react extensively with the alumina substrate but flowed to the bottom of the concave samples. Although of the same composition, Coating 5

[1]Levin, E. M., McMurdie, H. F. and Hall, F. P., Phase Diagrams for Ceramists, The American Ceramics Society, Inc., Columbus, Ohio (1956) p. 114.

reacted differently and fused into a smooth adherent coating even though fired at 1500 C, 155 C above its melting point. Presumably, Coating 5 behaved differently as a result of the premelting and grinding procedure used in its preparation (see Table I-4, footnote d). It is believed that Coating 5 reacted with the alumina substrate of the sample before melting. Figure I-9 is a macrograph of Coating 5 on the alumina substrate and shows the high-density, glass-like structure of the coating.

Figure I-9

REFRACTORY OXIDE COATING NO. 5 ON ALUMINA CRUCIBLE FRAGMENT

The surface in the plane of the picture is broken and unpolished.

Coating Composition: 52% Al_2O_3, 41% CaO, and 7% MgO

Fragment Thickness: $\frac{3}{8}$ in.

Coating Thickness: 10 to 15 mils

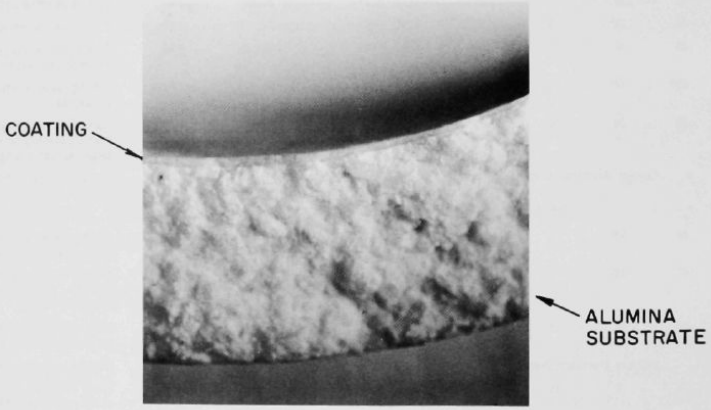

108-6509

The use of alumina in excess of the eutectic amount (Coatings 7 and 8) was not beneficial. However, the addition of excess magnesia (as compared with the eutectic) in Coating 9 prevented the coating material from running off the alumina substrate on melting. At the melting point of the eutectic mixture, sufficient excess magnesia was present to form a slurry containing 17 percent solids (MgO). This apparently prevented the coating material from slumping and produced an adherent coating similar to that obtained with the Coating 5 material. When the

combined constituents of Coating 9 were ballmilled in ethyl alcohol for 24 hr and this coating (No. 10) was applied to the alumina substrate, the coating material flaked off when the alcohol evaporated. A large excess of magnesia (Coating 11) resulted in the formation of beads rather than a continuous coating.

Coating 6, which has the lowest melting (about 1400 C) eutectic composition in the calcia-alumina system,[2] was similar in appearance to Coatings 1 through 4. Calcium aluminate cement (Coating 12) cracked and did not melt and fill the pores.

All of the coated alumina specimens were tested for porosity with a penetrant dye. This test showed that Coatings 1, 2, 4, 5, 6, 7, and 9 were impervious to the dye.

When applied to a magnesia substrate, all of the coatings which were tested failed (see Table I-4). In all cases, the liquid phase that was formed during firing was absorbed into the substrate leaving a porous surface.

Performance of Coating Materials on Crucibles

Some of the coating materials were applied to Norton Alundum-213 crucibles, which have a fairly coarse, porous structure with good thermal shock resistance. Alundum-213 (99 percent alumina) was used in the screening tests. Two methods of application were tested. In the first, the coating was applied to the inside surface of the crucible by pouring an ethyl alcohol slurry containing the coating material into the crucible and drawing a vacuum on the outside of the crucible by means of an apparatus built for this purpose. It was hoped that this technique would cause the finely ground material in the slurry to impregnate the crucible to a depth of 1-2 mm. However, examination of crucibles after firing indicated that little, if any, penetration had occurred, although, as noted below, an impervious coating had formed on the surface. In the second method of application, the coating was applied as a thin paste with a brush to the inside surface. Coatings 2 and 5 of Table I-4 were used in these experiments. The results were as follows:

1) Coating 2, applied by both techniques, ran into the bottom of the crucible when melted.

2) Coating 5 worked very well when applied in two applications (and firings) inside two alumina crucibles, of 4-in. OD by 8 in. high. One application was not enough to close all of the pores. One crucible was coated by the vacuum impregnation technique. The first application was fired at 1500 C, the second at 1300 C. The other crucible was coated by brushing on a thin paste, both applications being fired at 1400 C. Both crucibles were rendered impervious to water as indicated by the ability to

[2] op. cit., p. 46.

draw a 30-in. mercury vacuum on the outside of the crucibles filled with water. The water level dropped less than 2 mm in several hours. Further evidence of the imperviousness to water of the coated crucibles was indicated by the fact that the level of water held in one crucible for one week dropped only imperceptibly. However, the surface was roughened after this exposure, possibly indicating slight hydration.

Coating 9, which also showed promise in the screening tests and which does not require premelting of the constituents, has not yet been properly tested on a crucible.

In summary, Coating 5, applied to porous alumina crucibles, renders them impervious to water. The coating material must be premelted, ground, and applied in two applications with firing at 1400 C after each coating. It is believed that a fired thickness of 10 mils is sufficient to obtain an impermeable coating. Coating 9, which does not require premelting and grinding, is also promising but has not been tested as extensively. The coating materials might work equally well on crucibles made from a castable alumina which could be used to form crucibles up to several feet in diameter. This possibility is under investigation.

The utility of the coatings described above for containing skull reclamation systems depends largely on the inertness of the coatings to magnesium in zinc solution. Several crucibles are being made for corrosion testing with halide salts and zinc-magnesium solutions.

g. Supporting Chemical Investigations
(R. K. Steunenberg)

Liquid metals and molten salts are used as process media and reagents in the development of pyrometallurgical processes for EBR-II fuels. Fundamental chemical studies of these materials are needed to supply data for process use and to gain a fuller understanding of the principles involved. Work on this program during the quarter has been confined to further spectrophotometric studies of uranium oxides in molten salt media.

Reactions of Uranium Oxides in Molten Chloride Media
(D. A. Wenz, M. D. Adams, J. S. Tait)

A soluble uranium (V) species, believed to be UO_2^+ ion, is formed on the addition of the higher uranium oxides to molten chloride salts (see ANL-6569, p. 54). A characteristic absorption spectrum attributed to this species has been determined in the visible and near-infrared regions (see ANL-6648, p. 77).

Since the chemical behavior of this species suggests that it is an oxygen-bearing uranium (V) compound, the most likely possibilities are that it is UO_2Cl or $UOCl_3$. To obtain a comparison with a known material by spectrophotometric methods, a sample of the latter compound, uranium oxytrichloride, was prepared by the reaction of uranium tetrachloride with uranyl chloride at 370 C:

$$UCl_4 + UO_2Cl_2 \rightarrow 2\ UOCl_3 \quad .$$

The uranium and chlorine contents obtained by chemical analyses of the brown product resulting from the reaction corresponded to theoretical values for uranium oxytrichloride. The X-ray powder pattern for uranium oxytrichloride is not catalogued, and the pattern for the brown product obtained in the preparation did not correspond to any known pattern of uranium oxides, chlorides, or oxychlorides.

Decomposition of the product made it impossible to obtain a spectrum in molten salt solutions at 400 C. However, a spectrum of the solid material in a petrolatum mull was obtained at room temperature (see Figure I-10). Some of the absorption peaks occurred at wavelengths

Figure I-10

COMPARISON OF SPECTRA OF URANIUM OXYTRICHLORIDE AND PREVIOUSLY OBSERVED URANIUM (IV), (V), AND (VI) SPECIES

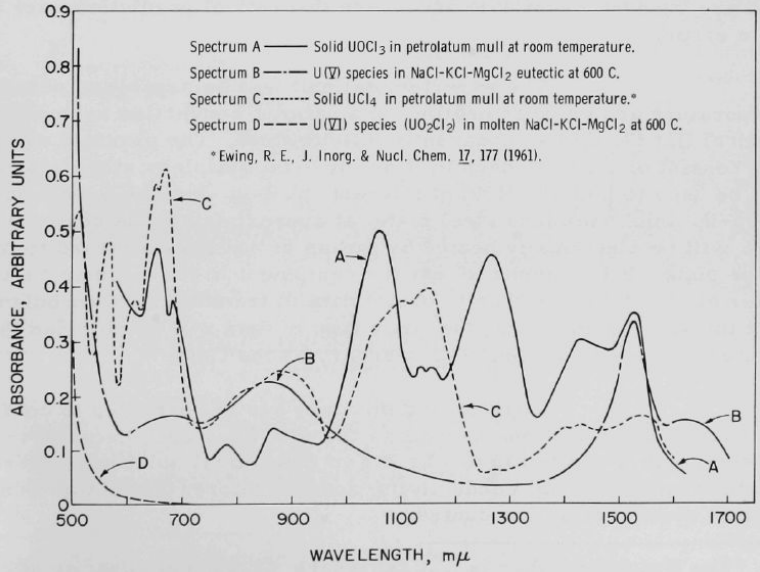

108-6510

corresponding to those for the previously determined uranium (V) spectrum in molten salt solution. Also present were several additional absorption peaks that did not occur in the previously observed uranium (V) spectrum, nor in the spectra of known uranium (III), (IV), or (VI) compounds. Thus, it appears that the uranium (V) species observed in molten salt solutions has some characteristics in common with uranium oxytrichloride, but is a different compound. This conclusion tends to support the assignment of the uranium (V) spectrum in molten salt solutions to UO_2^+ ion, although it is not conclusive evidence.

h. Supporting Engineering Studies

(1) Natural Convection Heat Transfer in Liquid Metals (R. Akins, P. Nelson)

Work has been started to obtain experimental measurements of natural convection heat transfer rates in liquid metals. The data obtained will be compared with values calculated by the use of available theories. Theoretical calculations seem to be on very firm ground in the area of laminar-flow natural convection for fluids whose Prandtl numbers* are of the order of one. However, outside of this area (for example, in the transition zone or turbulent flow zone or with fluids like liquid metals whose Prandtl numbers are much different from one), there are practically no analytical results or experimental data. Therefore, experimental equipment is being built to obtain data in those areas where no data are currently available and where theoretical predictions are likely to be in error.

The experimental unit will be capable of obtaining temperature and velocity profiles in a natural-convection system having a vertical flat plate in an apparently infinite fluid. The physical equipment will consist of a 12-in.-deep by 7-in. by 9-in. stainless steel tank which will be used to hold the fluid of interest. A 2-in.-high by 4-in.-wide by 0.006-in.-thick stainless steel plate, at approximately the center of the tank, will be electrically heated by means of bus bars attached to the ends of the plate. It is planned to test the equipment in the laminar region, with water as the fluid, and then to obtain data in transition and turbulent flow with the same fluid. Next, the same type of data will be obtained in the natural-convection system with mercury as the fluid.

The data for mercury are not expected to conform to the analytical predictions as well as the data for water, because vertical conduction is neglected in all the known theoretical solutions. Mercury has a rather large thermal conductivity, and, therefore, conduction in any direction should not be discounted.

---

*The Prandtl number is $C_p\mu/k$, where C_p is heat capacity at constant pressure, μ is viscosity, and k is thermal conductivity.

Calculations are also underway to solve the differential equations for this system by means of a variation of the perturbation theory with the vertical conduction as the first-order perturbation. If this scheme is successful, new analytical results will be available for comparison with the experimental data.

Figure I-11

CALIBRATION OF PITOT TUBE FOR NATURAL-CONVECTION HEAT TRANSFER STUDIES IN LIQUID METALS

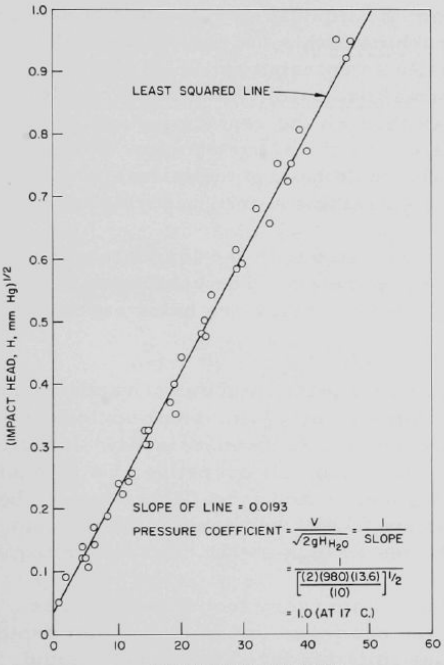

108-6511

The major pieces of the experimental apparatus are under construction, and some of the associated equipment has been tested. At present, the temperature-measuring instruments are being calibrated. Calibration of the velocity-measuring Pitot tube has been completed with flowing water in a tube; the results are shown in Figure I-11. The calibration is in accord with theory, namely, that the velocity is proportional to the square root of the impact pressure. The calibration line shows that flow measurements can be measured to speeds as small as one cm/sec with an accuracy of ±0.5 cm/sec. The equipment is capable of measuring flow velocities as small as about 0.3 cm/sec, but extraneous mechanical vibrations prevent accurate measurements below one cm/sec. Attempts will be made to eliminate mechanical vibrations in the experimental setup, but the range over which measurements can now be made is sufficient to cover many of the areas of interest. Although other, more sensitive instruments are available for measuring average flow rates, the present equipment has the advantage of indicating rapid fluctuations in flow, such as occur in turbulent flow. The pressures of the Pitot tube probe were measured by means of a pressure transducer and were recorded on a Sanborn, Model 350, dual-channel recorder* which will be used to record the temperatures. The impact part of the Pitot tube is a "fish mouth"-shaped opening of the type used in boundary-layer work. The maximum dimension of the impact head is 0.33 in., with a 0.005-in. by 0.019-in. opening.

*Sanborn Co., 175 Wyman St., Waltham 54, Mass.

The work in the immediate future will consist of further calibrations, completion and assembling of the equipment, and test runs to check the operation. Attempts are being made to improve the mathematical analyses of natural-convection heat transfer in liquid metals.

(2) Study of Mechanisms of Liquid Metal Boiling and Entrainment
(J. Wolkoff, L. F. Dorsey)

Vaporization from the liquid-vapor surface of a liquid pool without the formation of vapor bubbles within the pool (here called nonturbulent vaporization) is essentially an entrainment-free method of accomplishing the phase change. In normal nucleate, transition, and film boiling, the vapor bubbles which break through the surface generally create droplets of liquid which may be entrained by the vapor stream. Nonturbulent vaporization rates of liquid metals would have potential usefulness if high enough for applications requiring entrainment-free vaporization.

The phenomena associated with the liquid-to-vapor phase change are being studied with liquid metals. The conditions necessary to achieve high nonturbulent vaporization rates are being examined with pure mercury in glass equipment.

It was found previously that nonturbulent vaporization rates from a shallow pool ($2\frac{5}{8}$ in. in diameter by $1\frac{1}{8}$ in. deep) could be increased by active stirring of the mercury (see ANL-6648, p. 84). Induction heating, by means of a flat, four-turn induction coil operating at a frequency of 10 kc, provided both heat and mixing power, and a heat flux through the vaporizing surface of 103,000 Btu/(hr)(sq ft) was achieved. More recent runs under similar conditions gave fluxes as high as 115,000 Btu/(hr)(sq ft).

With the same boiling mercury loop under similar conditions, the effect of liquid level was examined for mercury pool depths of 2 and 3 in. The previously used flat coils produced inadequate liquid circulation in these pools. Therefore, a number of cylindrical coil shapes were tested to improve the circulation. Maximum heat fluxes at the vaporizing surface of 115,000 and 109,000 Btu/(hr)(sq ft) were achieved for the 2-in. and 3-in. levels with four-turn and seven-turn cylindrical coils, respectively.

The 3-in.-deep pool was also heated by an external cylindrical resistance heater. The maximum heat flux obtainable with nonturbulent vaporization was 77,000 Btu/(hr)(sq ft).

The circulation within the pool was poorer at greater pool depths. The pronounced center rise with accompanying active circulation, which was prominent in the 1-in.-deep pool, changed to a random

surface pattern with increased depth. There was a tendency toward rocking and splashing in the 3-in.-deep pool at the higher vaporization rates. To achieve greater electrical current penetration and improved circulation in the pool, induction heating with 60-cycle power will be tried.

3. Reactor Materials
(R. K. Steunenberg)

Pyrometallurgical techniques offer considerable promise as simple, economical methods for producing nuclear fuels. Metallic fuel materials, such as uranium, plutonium and thorium, can be prepared in high purity and with essentially no losses through the direct reduction of oxides, fluorides, and chlorides by liquid metal solutions containing magnesium. Refractory compounds of interest as high-performance reactor fuels, such as carbides and sulfides of uranium and plutonium, can also be prepared by various pyrometallurgical methods. During the past quarter work has been devoted to (1) construction of equipment suitable for the preparation of uranium and plutonium carbides and of uranium sulfide, (2) the direct reduction of thorium dioxide to thorium metal, and (3) the preparation of uranium metal from ore concentrates by pyrometallurgical methods.

a. Equipment for the Preparation of Uranium and Plutonium Carbides
(T. R. Johnson, J. F. Lenc, M. A. Bowden, J. R. Pavlik, J. S. Tait)

In order to minimize impurities in the product, preparations of uranium monocarbide will be conducted in a vacuum-inert gas glovebox. The glovebox is designed in such a way that various types of furnaces can be attached and removed without exposure of the furnace or glovebox contents to air. Completion of this facility within the next quarter is expected.

An alpha glovebox facility to be used for the preparation of plutonium carbides in high-purity inert gas atmospheres has been completed. Operation of this facility, in which highly alpha-active materials can be handled, is currently being tested by performing several operations with uranium as a stand-in for plutonium.

b. Reduction of Thorium Dioxide
(W. H. Hauschildt,* J. B. Knighton)

The effects of variables such as flux composition, temperature, thorium loadings, and agitation on the reduction of thorium dioxide by zinc-magnesium solutions have been reported previously (see ANL-6596, p. 91; ANL-6648, p. 90). Additional work has been done to explore further

*Dow Chemical Co.

the effect of magnesium concentration in the metal phase on the reduction reaction. In a series of experiments, 68.3-g charges of thorium dioxide were reduced for 4 hr at 800 C under an argon atmosphere. The metal phase consisted of 612.5 g of zinc-magnesium alloy of various compositions, and the flux was 300 g of 90 m/o magnesium chloride-10 m/o magnesium fluoride. The results are compared in Figure I-12 with earlier data obtained with other fluxes (see ANL-6648, p. 93).

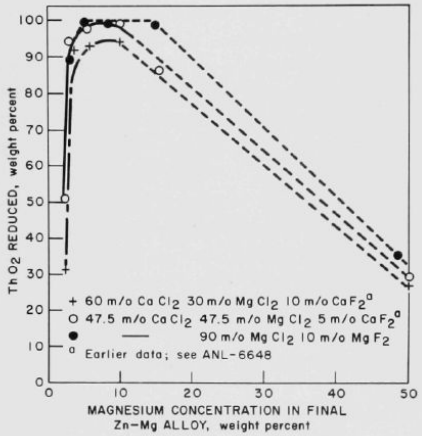

108-6512

Figure I-12

EFFECT OF MAGNESIUM CONCENTRATION IN ZINC ON REDUCTION OF THORIUM DIOXIDE

Experimental Conditions

612.5 g of Mg-Zn Alloy
300 g of Flux
68.3 g of ThO_2 Charge
800 C for 4 hr
Heat to 850 C, sample, and pour
Argon atmosphere

The use of this flux, which contained 100 percent magnesium cation, yielded nearly complete reduction of thorium dioxide over a range of magnesium concentrations in the metal phase from about 5 to 15 w/o. In these experiments, the theoretical thorium content of the final metal phase was 9.1 w/o.

Preliminary studies have been made to determine the thorium loadings that can be accommodated by this system. Over a range of 8 to 14 w/o magnesium and 6 to 24 w/o thorium in the metal phase, incomplete reduction (98 percent or less) was obtained at thorium loadings above 10 w/o. It appears that this value may be a practical limit on the capacity of the system for thorium dioxide reduction.

c. Direct Reduction of Uranium Ore Concentrates

(R. B. Subramanyam,* J. B. Knighton)

The successful reduction of uranium oxides to the metal by zinc-magnesium solutions in the skull recovery process has led to consideration of this technique for the direct production of

*Affiliate, International Institute of Nuclear Science and Engineering.

uranium metal from ore concentrates. Production of reactor-grade uranium by this technique, if successful, would eliminate a series of purification and chemical conversion steps currently in use.

Previous studies have shown that silicon is the principal impurity found in uranium metal produced in the laboratory by the method described in ANL-6648, p. 95. In a series of exploratory studies with beach sand, silicon was volatilized as the fluoride upon treatment with ammonium bifluoride, uranium tetrafluoride, or fused mixtures of sodium carbonate with calcium fluoride or magnesium fluoride (see ANL-6648, p. 95).

Further work has been completed with a typical uranium ore concentrate (Anaconda resin-in-pulp ion exchange type) to determine the minimum quantities of reagents required for effective silica removal. Figure I-13 gives the results of 4-hr treatments of the ore concentrate with varying amounts of ammonium bifluoride at 145 C. An ammonium bifluoride:ore concentrate weight ratio of about 0.15 to 0.20 appears to be required for removal of 85 to 90 percent of the silicon. This removal would result in about 1000 ppm silicon in the uranium metal product, assuming that all of the unvolatilized silicon would remain with the uranium.

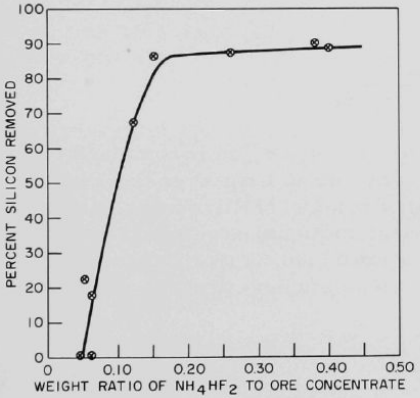

108-6513

Figure I-13

REMOVAL OF SILICA FROM URANIUM ORE CONCENTRATE BY FUSION WITH AMMONIUM BIFLUORIDE

Conditions	
Temperature:	145 C
Time:	4 hr
Crucible:	Platinum
Atmosphere:	Air
Ore Concentrate:	~2 g (Anaconda resin-in-pulp ion exchange type)
Ratio of NH_4HF_2 to ore concentrate:	As indicated

In the treatment of ore concentrate with uranium tetrafluoride, a weight ratio of about 0.35 was needed to remove 95 percent of the silicon after 3 hr at 900 C (see Figure I-14).

A demonstration experiment has been completed in which a typical ore concentrate (Anaconda ion exchange resin-in-pulp type) was (1) pretreated with ammonium bifluoride to remove silica (2) chlorinated to remove certain other gangue elements (chlorine was generated by exposure of the magnesium chloride-magnesium fluoride flux to air), (3) reduced

by zinc-5 w/o magnesium alloy under argon atmosphere, (4) retorted under vacuum to remove zinc and magnesium, and (5) arc-melted to form a button. Although final results are not yet available on the yield and purity of the product, the uranium concentrate apparently was completely reduced to metal.

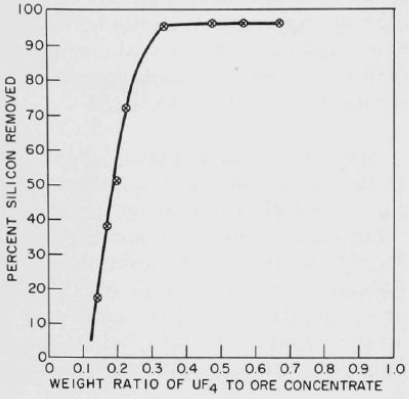

108-6514

Figure I-14

REMOVAL OF SILICA FROM URANIUM ORE CONCENTRATE BY FUSION WITH URANIUM TETRAFLUORIDE

Conditions

Temperature:	900 C
Time:	3 hr
Crucible:	Platinum
Ore Concentrate:	~2 g (Anaconda resin-in-pulp ion exchange type)
Weight ratio of UF_4 to ore concentrate used:	As indicated
Atmosphere:	Air

B. Fuel Processing Facilities for EBR-II
(L. F. Coleman, M. Levenson, J. H. Schraidt)

A direct-cycle fuel-reprocessing plant based on pyrometallurgical procedures was designed and is being constructed as part of the Experimental Breeder Reactor No. II (EBR-II) Project. Melt refining, liquid metal extraction, and processes involving fractional crystallization from liquid metal systems are methods being examined for the recovery and purification of EBR-II fuels. Based on these studies, process equipment is being designed and tested.

1. Status of Fuel Cycle Facility

a. Building and Building Services
(E. J. Petkus, J. O. Ludlow)

(1) Equipment Installation

Work is continuing on the installation and testing of equipment in the EBR-II Fuel Cycle Facility. Corrective work is also being carried out.

Leaks which were found in the shield plug of the 7-ft-square hatch in the roof of the Argon Cell (see ANL-6648, p. 98) have been

repaired by welding a steel cover plate on the plug. This hatch is to be used for the emergency removal of equipment that is too large to be moved through the large transfer lock.

(2) Air In-leakage Tests of Argon Cell

Tests have been conducted to determine the in-leakage rate of air into the Argon Cell. The design specification leak rate for the Argon Cell is 0.01 cfm (see Chemical Engineering Division Summary Report for July, August, September 1957, ANL-5789, p. 125) at a cell pressure of -2 in. H_2O. This leak rate is equivalent to 0.02 percent of cell volume per day. The volume of the Argon Cell and associated gas-handling, cooling, and purifying equipment is approximately 66,000 cu ft. For the first two tests, the pressure inside the Argon Cell was lowered slightly below atmospheric pressure, and the rate of in-leakage of air was determined by measuring the increase in pressure inside the cell. Periodically, during the testing period, an inventory of the amount of gas in the cell was determined from the differential pressure, the barometric pressure, and the temperature of the cell gas. A change of one degree F in the temperature of the cell gas is equivalent to an inventory change of about 120 cu ft of gas, and a change in the pressure of the cell gas of one inch of water is equivalent to an inventory change of about 200 cu ft of cell gas. These values vary slightly as a function of cell temperature and absolute pressure.

The results of the first test, based on data obtained over a 65-hr testing period, indicated a leak rate of the order of 0.1 cfm at a pressure in the Argon Cell of -10 in. H_2O. Freon leak testing of cell penetrations disclosed a number of small leaks which were repaired. The results of a second test, based on data obtained over a 90-hr period, showed an in-leakage rate of about 0.05 cfm at a cell pressure of -6 in. H_2O. The leak rate of 0.05 cfm is considered to be the lower limit of detection for this type of measurement.

In the third test, the in-leakage rate of air into the Argon Cell was determined by a leak test method which involved replacing the air in the Argon Cell with nitrogen and measuring the increase in oxygen content of the nitrogen in the cell. A total volume of 160,000 cu ft of nitrogen was added to the cell, which reduced the oxygen concentration in the cell to about one percent. The oxygen level was further reduced by operating the argon-purification system. Initial test measurements indicated high in-leakage of air into the cell. Leaks were found in several valves and flanges, which were then repaired; the subsequent increase in the oxygen level indicated an air in-leakage rate of less than 0.006 cfm at a pressure in the Argon Cell of -4 in. H_2O. The air in-leakage determinations were made at oxygen levels in the Argon Cell of 8 to 30 ppm and at a water level of about 5 ppm. The results of this test indicate that the Argon Cell is adequately air tight.

Operation of the pressure-control system for the Argon Cell has shown that the control valves for the refrigerant flow are oversized. It will be necessary to replace these valves, which were installed by the original construction contractor, before satisfactory operational control can be achieved.

b. Cell Viewing and Lighting
(T. W. Eckels, J. Graae)

(1) Auxiliary Local Lighting

It is anticipated that on occasion brilliant lighting of an area in the process cells may be needed. For this purpose a portable lamp (see Figure I-15) using a 500-w Quartzline* lamp bulb has been built. The luminaire unit, which is about 20 in. long by 10 $\frac{1}{2}$-in. maximum width and which weighs 7 $\frac{1}{2}$ lb, can be mounted at two heights (3 or 5 ft) on a portable lamp pole. (The mounting fitting at the 3-ft height is not shown in Figure I-15.)

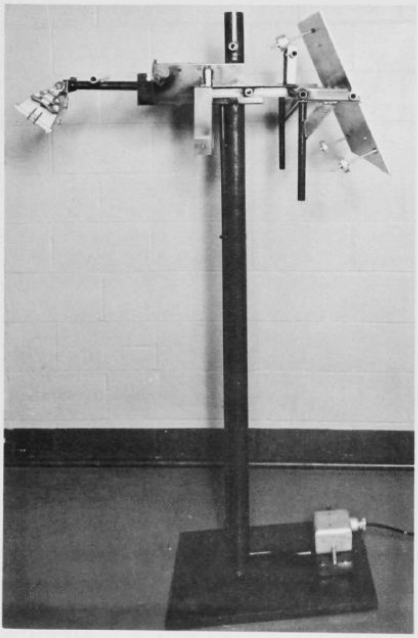

Figure I-15

PORTABLE LAMP AND MIRROR FOR USE IN PROCESS CELLS

108-5946

*An incandescent, filament-type, quartz-envelope lamp which contains iodine. The iodine prevents the tungsten that is evaporated from the filament from accumulating on the lamp walls. The lamp is a product of the General Electric Company.

The portable pole stand is designed to serve as a lamp pole and as a mirror standard. It is made of 2-in.-diameter, 6-ft-long steel pipe which is mounted on a 1-in.-thick x 16-in. x 24-in. steel base plate. The pole assembly weighs about 150 lb. Electric power for the luminaire will be supplied by a portable, flexible, metal-covered, electric cable. The cable is remotely connected to receptacle terminations on the base of the pole stand and the electrical feed-through.

The mirror assembly, which carries a front surface-coated glass mirror (20 in. high x 24 in. wide), will weigh about 50 lb. The mirror will be adjustable about a horizontal axis.

The in-cell service life expectancy of the luminaire unit and the electric cable is about 2000 hr. The portable pole stand with its mounting brackets and fixed wiring has an in-cell service life expectancy of at least 25,000 hr. The mirror and its frame can be replaced as required.

(2) Shielding Window Shutters

Shielding window shutters will be used to protect the process cell windows from radiation damage when the windows are not in use. The high stalling torque of the motor used for moving the shutter causes chattering of the drive gear when the shutter reaches the end of its travel. To overcome this high stalling torque, a slip clutch has been designed and successfully tested on one of the window shutters. This clutch can stand slipping for long periods of time without overheating when operated at the required speed and torque. Clutches of the type successfully tested have been ordered for all of the shutter drive units.

2. Development of Service Equipment

a. Interbuilding Fuel-transfer Coffins
(G. J. Bernstein, A. A. Chilenskas)

Fuel subassemblies containing spent or reconstituted fuel will be transported between the Reactor Building and the Air Cell of the Fuel Cycle Facility in 20-ton interbuilding fuel-transfer coffins. Two types of interbuilding coffins are being fabricated (see ANL-6569, p. 71). One of the coffins was designed by Argonne National Laboratory personnel and is being built at Argonne. In this coffin, the fission product heat from the subassembly will be removed by a circulating argon stream and will then be transferred to the lead body of the coffin through an internal heat exchanger. The body of the coffin has been fabricated and filled with lead. Performance tests of the blower for recirculating the argon in the coffin were conducted at Argonne National Laboratory and at the manufacturer's plant. Results of the tests showed that the drive motor initially supplied was too small. This motor is being replaced with a motor of greater horsepower.

An emergency cooling system for removing fission product heat has been incorporated in the design of the coffin. This system involves gravity flooding of the cavity of the coffin with mercury from a reservoir attached to the coffin. The fission product heat will be removed from the spent fuel subassembly by conduction through the mercury to the lead in the coffin body.

It has been estimated that a spent fuel subassembly will be coated with less than 100 g of sodium at the time when it is placed in the coffin. Since the sodium will be brought into contact with mercury in the event that emergency cooling is necessary, the study of the reaction between sodium and mercury was undertaken.

A 4-in.-long section of an EBR-II stainless steel fuel pin can (of 0.174-in. OD) was dipped into molten sodium. The resulting sodium coating on the fuel pin can weighed 0.8 g. The sodium-coated fuel pin can section was then immersed in 220 g of mercury. The sodium-to-mercury mass ratio was equal to the estimated mass ratio that will exist in the core portion of the fuel subassembly if the fuel subassembly is flooded with mercury. The average sodium film thickness in the experiment was about twelve times the average sodium film thickness expected on the fuel subassembly. The reaction was inhibited initially (probably owing to a thin layer of sodium oxide) but, once begun, it was completed in about one second. The temperature rise of the system was 35 C.

By means of the result obtained in this experiment, it has been calculated that if a subassembly (with a fission product decay heat of 1 kw) reaches 430 C owing to a failure of the normal gas-cooling system and is then flooded with mercury initially at room temperature, the temperature of the subassembly will be reduced rapidly to about 200 C. Further cooling of the subassembly by heat transfer through the mercury to the shielding lead of the coffin will occur until the subassembly reaches an equilibrium temperature of about 100 C.

A coffin has also been designed and built by O. G. Kelley and Company of Boston, Massachusetts, and has been delivered to Idaho. This coffin is more complex than the Argonne coffin, since it includes an external argon-to-air heat exchanger to remove the fission product heat from the primary circulating argon stream. The secondary air stream is delivered to the heat exchanger by means of a vaneaxial-type blower. If the results of the heat-removal performance tests are successful with the coffin that is being built at Argonne National Laboratory, the cooling system of the coffin furnished by O. G. Kelley and Company will be replaced by one of Argonne design. The commercially fabricated coffin is undergoing leak testing and dimensional checking. Several leaks have been corrected, and some corrective machining will be necessary.

Since irradiated fuel subassemblies on discharge from the EBR-II reactor will be coated with a thin film of sodium, a sodium-removal station, which will be located between the Reactor Building and the Fuel Cycle Facility, has been designed. At this station, the sodium will be removed while the fuel subassembly is contained within the transfer coffin. The proposed procedure allows the sodium film to be removed without causing an excessive rise in the temperature* of the subassembly and precludes the occurrence of an explosion by minimizing the reaction in which hydrogen is generated. The proposed sodium-removal scheme consists of the following reaction steps:

(1) $Na + 1/4\ O_2 = 1/2\ Na_2O$; $\Delta H_f = -49.72 \times 10^3$ cal/mole ;

(2) $1/2\ Na_2O + 1/2\ H_2O = NaOH$; $\Delta H_f = -52.24 \times 10^3$ cal/mole ;

(3) $NaOH(s) + H_2O = NaOH\ (sol)$; $\Delta H_s = -10.18 \times 10^3$ cal/mole .

In Step (1), the sodium will be converted to sodium oxide by the addition of a small amount of humidified air to the recirculating argon atmosphere of the coffin. The required humidity will be determined by experiments at the EBR-II site. The quantity of air added will be just sufficient to permit the slow conversion of the sodium to the oxide. The progress of the reaction will be followed by monitoring the temperature of the recirculating gas leaving the fuel subassembly. The rate of the reaction will be controlled by increasing or decreasing the rate of addition of humidified air to the recirculating argon. The fission product heat of a fuel subassembly irradiated to a burnup of 2 percent and cooled for 15 days has been estimated to be 1 kw. Based upon a 100-g holdup of sodium in the fuel subassembly, the sodium-to-sodium oxide conversion reaction must be allowed to proceed over a 15-min period if an average total heat generation (fission product plus chemical) of about 2 kw is to be maintained. The heat-removal systems proposed for the two interbuilding fuel-transfer coffins will readily remove this amount of heat without an excessive rise in the temperature of the fuel subassembly.

In Step (2), the sodium oxide will be converted to sodium hydroxide by increasing the concentration of humidified air within the coffin until sufficient water vapor has passed over the sodium oxide to convert it to sodium hydroxide. As in Step (1), the temperature of the gas leaving the subassembly will be monitored to follow the progress of the reaction. About 15 min should be sufficient time for the completion of this reaction. During this reaction time, the total heat load should not exceed 2 kw.

In Step (3), the solid sodium hydroxide is removed by a water wash. About 25 gal of water at a rate of about 5 gpm will be passed through the cavity in the coffin. Prior to the water wash, argon at 30 cfm

*600 F has been chosen as a design criterion.

will be passed through the cavity and through the subassembly in order to cool the subassembly and to replace the air in the coffin with argon. This step reduces the possibility of hydrogen explosion at the water-gas interface should some of the sodium remain in the metallic form.

The wash solution containing the sodium will be flushed out of the coffin and collected in a 45-gal tank. The solution will be sampled and monitored for gross radiation. If the activity level is low (as would be expected in normal operation), the waste will be pumped from the 45-gal tank into a waste storage tank located in the Fuel Cycle Facility. If the activity level should be too high for routine disposal, the waste will be transferred into a shielded pot and handled as a low-volume, high-activity waste. The gases which have been used for purging the coffin and contacting the subassembly will be passed through a venturi-scrubber and a high-efficiency filter before being exhausted to the suspect stack.

Two small-scale laboratory experiments have been performed to test the three steps. The results indicate that the reaction rates are rapid and will go essentially to completion. A small amount of hydrogen was produced in the first experiment but only trace amounts in the second. The results indicate that the proposed procedure should be satisfactory. Additional work on this procedure will be done at the EBR-II site with a sodium-coated, unirradiated, full-scale subassembly in an interbuilding fuel-transfer coffin.

b. Materials Testing
(G. J. Bernstein, A. A. Chilenskas, J. Graae)

Insulators* and insulating laminates* molded from a polyester compound reinforced with glass fibers were evaluated as possible substitutes for the ceramic insulators now being used for the crane bus bar collectors in the Air Cell. After an exposure of 1×10^9 rad, the insulators and insulating laminates exhibited some loss (about 20 percent) in physical strength. The electrical insulation resistance of both items was essentially unaffected. The machining properties of the laminates were good and threads were strong. Unlike ceramics, the materials were not brittle. The test results of the mechanical, physical, and electrical properties of these two items were considered satisfactory. Therefore, insulators molded of this glass fiber-reinforced plastic will replace the ceramic insulators now in use for the bus bar collectors on the crane in the Air Cell.

c. Miscellaneous Service Equipment Development
(W. E. Miller, M. A. Slawecki, H. L. Stethers)

(1) Purification System for Inert-atmosphere Gloveboxes

Two purification systems for removing water vapor and oxygen in order to maintain the purity of inert atmospheres in gloveboxes

*Product of the Glastic Corporation of Cleveland, Ohio.

are needed for use with two glovebox systems installed in the EBR-II facilities. One purification system has been tested and shipped to Idaho. The second, a duplicate of the first, is being constructed at Argonne.

Each purification system is portable, and consists of a gas blower installed in a gas-tight enclosure, a purifier containing a palladium catalyst, a dryer containing Molecular Sieves,* and a control panel. The system is designed so that, when it is attached to a glovebox, gas from the glovebox is moved (in succession) through the purifier, the blower, and the dryer, and returned to the glovebox. Hydrogen is added at a stoichiometric or lower than stoichiometric rate to the circulating gas upstream of the purifier and reacts on the palladium catalyst with the oxygen in the circulating gas to form water. The water formed on the catalyst and any other water in the circulating gas stream is then sorbed on the desiccant in the dryer. Periodically, the desiccant in the dryer becomes saturated and requires regeneration. This is accomplished by heating the desiccant by electric heaters installed in the dryer, and passing a dry (dew point of -40 C or less) gas through the dryer. During the regeneration, the dryer is isolated from the glovebox and the rest of the purification system.

After the purification system had been assembled, it was leak tested using a helium mass spectrometer. No leaks were found. The purification system was then connected to a glovebox containing an argon atmosphere and the gas in the glovebox circulated through the purification system for a total of 55 days. (As no oxygen analyses were made, hydrogen was not added during this test period.) The glovebox had a volume of 80 cu ft and had sixteen gloves. During the 55-day test, these gloves were covered with gasketed covers. The water concentrations of the gas in the glovebox and of the gas leaving the dryer were periodically determined by means of a water analyzer containing a phosphorus pentoxide electrolytic cell. The concentration of water in the glovebox, initially greater than 100 ppm, was continually reduced. After eleven days, the concentration of water in the glovebox was 20 ppm; after sixteen days, it was 13 ppm. The concentration of water in the gas leaving the dryer was about 0.5 ppm for 27 days and then rose to 2 ppm. At this time, the concentration of water in the glovebox was 13 ppm. The dryer was then regenerated. After regeneration of the dryer, a recirculation time of 12 hr was required before the water content in the glovebox was reduced to 13 ppm and the concentration of water in the gas leaving the dryer was reduced to about 0.5 ppm. The water concentrations remained at approximately these values for the remainder of the 55-day test.

(2) Off-Gas Filter Unit

A filter unit has been designed for use in a vacuum system and will be fabricated by a commercial filter manufacturer. The

*Product of the Linde Air Products Company.

filter, made of radiation-resistant components, will be suitable for use with the melt refining furnace, the skull oxidation equipment, and the skull oxide processing equipment. The filter unit will utilize glass filter media and will contain charcoal for trapping any fission product iodine which may be released during processing operations. The filter units will be attached to equipment vacuum lines by means of low-melting alloy seals. After removal of a filter from a vacuum line, the filter will be capped to prevent spread of radioactive particulate material.

3. Development of Process Equipment

a. Skull Oxidation Equipment
(W. E. Miller, M. A. Slawecki, H. Stethers)

After the melt refining step is carried out, a skull remains in the zirconia crucible. The skull will be oxidized in order to convert it into a powder form for ease of removal of the material from the crucible. Equipment for the skull oxidation step and for the transfer of the oxide powder is being developed.

An oxygen feed-control system (see ANL-6596, p. 102) which is associated with the skull-oxidation furnace has been installed in the EBR-II mockup area at Argonne and tested in a preliminary skull-oxidation run. The oxygen feed-control system is being provided to regulate the rate of the oxidation of the skull in the furnace for the skull oxidation step. The gas-control system feeds oxygen to the furnace in such a manner that a nearly constant rate of oxidation is maintained. It is also suitable for oxidizing skulls which are nitrided. The use of the control system will overcome the difficulty of excessive oxidation rates which result in the production of undesirable sintered agglomerates of the oxides and cause fragmentation of the zirconia crucible. The control system furnishes process control information and shuts off the supply of oxygen when the oxidation of the skull is complete. If desired, partial oxidation of the skull can be achieved by stopping the reaction at any given time.

The operation of the oxygen feed-control system is best described by reference to the pressure-time plot shown in Figure I-16. This plot is based on data obtained by means of the pressure recorder for the skull oxidation furnace during the "normal run" portion of the overall skull oxidation cycle. This part of the cycle starts after the skull in the zirconia crucible has been heated to 700-750 C in an argon atmosphere. When the selector switch on the panelboard is set at the "normal run" position, a valve opens in the gas discharge of the furnace and the pressure in the furnace is reduced to P_3. The reduction in pressure closes the valve in the gas discharge of the furnace and opens the oxygen feed valve. When the furnace pressure rises to P_1, the oxygen feed valve closes. When the furnace pressure falls to P_2 because of depletion of the oxygen, the gas-discharge valve on the furnace opens and the furnace pressure falls to P_3.

This cycle is repeated until the pressure no longer drops from P_1 to P_2, thereby indicating that the skull is essentially completely oxidized. While the oxygen feed valve is open, oxygen is being fed at a constant rate into the furnace. During this period, the pressure in the furnace will rise, remain constant, or fall (after the first cycle), depending on whether the oxygen feed rate is greater than, equal to, or less than the rate of oxidation at any particular instant. In the run in which the data shown in Figure I-16 were obtained, the oxygen was fed at a rate equivalent to 1.4 g of uranium converted to U_3O_8 per minute assuming 100 percent utilization of oxygen.

Figure I-16

PRESSURE CHANGE IN SKULL OXIDATION FURNACE DURING SKULL OXIDATION USING OXYGEN-CONTROL SYSTEM

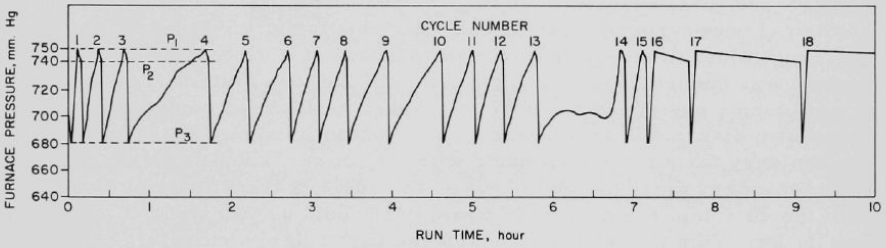

108-6515

The pressure-time data given in Figure I-16 allow the calculation at any time during the run of: (1) the instantaneous oxidation rate, (2) the concentration of oxygen in the skull-oxidation furnace, (3) the total amount of oxygen consumed by the skull, and (4) the amount of oxygen discharged from the furnace. After initiation of the oxidation reaction in the first cycle (see Figure I-16), the minimum instantaneous oxidation rate during the following 7-hr period was 1.0 g/min. At the end of the 16th cycle, the oxidation reaction was essentially completed, and the rate of conversion of the skull to the oxide had decreased to 0.01 g/min. The maximum oxidation rate, which occurred during the 14th cycle, was 1.5 g/min. The concentration of oxygen in argon at the end of the 16th cycle was calculated to be 77 m/o. About 70 percent of the oxygen fed to the furnace was utilized in the oxidation reaction. The skull was oxidized to a fine powder.

b. Inductive Heating and Mixing
(A. A. Chilenskas, M. A. Slawecki)

The skull reclamation process requires the heating and mixing of molten metal-molten salt systems at temperatures up to about 800 C. Because a high radiation field is associated with this process, it is

necessary to carry out the process steps remotely. Appreciable simplification and greater reliability of plant equipment is anticipated if inductive mixing can be used instead of mechanical mixing.

Preliminary work has demonstrated that vigorous mixing of molten metal charges can be obtained by 60-cycle power (see ANL-6596, pp. 104-105). The skull oxide reduction step of the skull reclamation process was chosen to demonstrate the feasibility of inductive mixing. In this reduction step, skull oxide (mainly U_3O_8), magnesium, zinc, and salt flux are mixed for several hours at 800 C. The reduction of the uranium oxide to uranium and its dissolution in the metal phase are used as a measure of the effectiveness of the mixing.

In several reduction runs, which have been described previously (see ANL-6596, pp. 106 to 107; ANL-6648, pp. 178 to 182), the electrical power-supply system could not supply sufficient power for adequate agitation. Consequently, the installation of a larger power supply system was undertaken. The installation of the new system, a 60-cycle power-supply system of about 37-kw capacity, has been completed. A schematic diagram of this power supply system is shown on Figure I-17. Preliminary tests have been made with this power-supply system using both secondary taps (40- and 60-v) on the 100-kva transformer. In a test with the 40-v tap, the maximum power that could be transferred to the load was 11 kw. This test was not considered particularly successful, since the saturable core reactor and the load were not properly matched for maximum reactor control and power transfer. In a test using the 60-v tap, which resulted in a better match between the saturable core reactor and the load, the maximum power delivered to the load was 20 kw. Higher levels of power to the load will be possible because of additional power factor corrections that are being provided by the capacitor bank in the power-supply system (see Figure I-17).

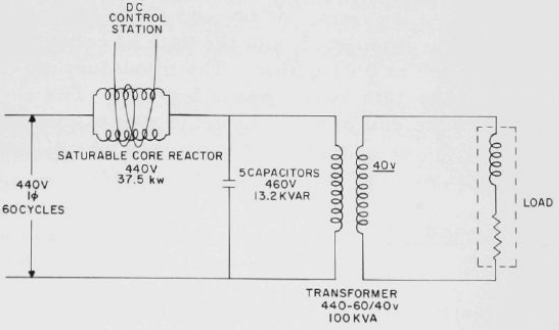

Figure I-17

INDUCTIVE MIXING: 60-CYCLE POWER-SUPPLY SYSTEM

108-6516

c. Collection of Metal Vapors
(W. E. Miller)

The product from the precipitation step of the skull reclamation process is uranium coated with magnesium-zinc. Distillation is a convenient means of removing the magnesium-zinc coating from the uranium. Originally, it had been planned to distill off the magnesium-zinc in the melt refining furnace (see ANL-6648, p. 110). However, because of the small size of the crucible that could be used in the melt refining furnace, a severe limitation was placed upon the quantity of magnesium-zinc-coated uranium that could be charged. To increase the uranium-magnesium-zinc capacity of the furnace for these distillations, a distillation heater, crucible, condenser, and collector are to be designed as an integrated operating unit to replace the crucible coil and frame assembly of the melt refining furnace. However, the baseplate and the bell jar enclosure of the melt refining furnace will be utilized as a part of the new distillation unit.

The development of a condenser and collector to collect the metal vapor distillate is continuing. A new condenser design, which was incorporated in the apparatus shown in Figure I-18, was tested in a single run in which 1000 g of 50 w/o magnesium-zinc was charged to the crucible. The test run with the new condenser and collector gave encouraging results as follows:

Percent of Charge Distilled	>99
Magnesium-Zinc Distillate Balance	
Percent in collector	91.5
Percent in condenser	3.0
Percent in crucible cap	0.8
Percent in insulator gasket	1.1
Total percent contained within condenser assembly	96.4
Percent in condenser insulator	1.3
Percent unaccounted for	2.3

After the run, the equipment components could be easily taken apart by lifting each component. The new condenser and collector design differs from the one previously tested (see ANL-6648, p. 111) in many features. The metal vapor condenser and collector are insulated from the heat source. This eliminates the tendency of the condensate in the collector to reboil. An insulation-type gasket is used between the distillate collector and the crucible cap. This gasket consists of Fiberfrax felt sandwiched between two layers of graphite felt. Although graphite felt is not as good an insulator as Fiberfrax felt, the graphite felt does not react with the magnesium-zinc vapor, whereas Fiberfrax felt does. Thus, the graphite felt serves to prevent bonding of the gasket to the collector and cap.

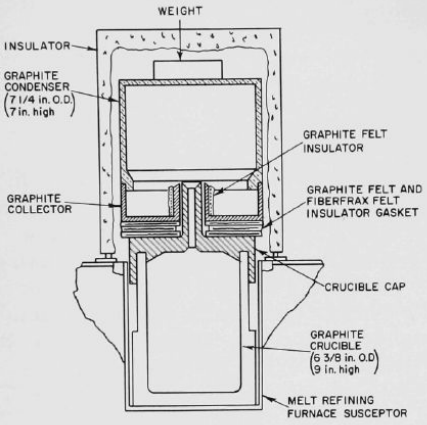

108-6517

Figure I-18

MAGNESIUM-ZINC-DISTILLATION APPARATUS

The new collector also differs from the previous collector tested (see ANL-6648, p. 111) in that no enclosure surrounds the outer circumference of the collector. In the previous condenser and collector design, under certain experimental conditions, some of the metal vapor condensed between the outside wall of the distillate collector and the inside wall of the condenser. In these instances, there was a tendency of the distillate collector to bond to the condenser.

Since the results obtained with the present apparatus are encouraging, work will be continued with it to check the consistency of the results and to improve the performance of the unit.

C. Chemistry of Liquid Metals
(I. Johnson and H. M. Feder)

The chemistry of liquid metal systems is being investigated to provide basic concepts and data for the design of methods for the reprocessing of nuclear fuels as well as to provide a basis for the development of the technology of liquid alkali metals. The results of these studies also provide ideas and data for the formulation and testing of theories of liquid metal solutions.

1. Solubilities in Liquid Metals

Of prime importance in the practical designs of fuel-reprocessing methods are the solubilities of the metals whose separations are being attempted. These solubilities need to be known as a function of both temperature and solvent composition. Since the solubility and temperature coefficient of solubility of a metallic phase in a liquid metal

solvent are dependent on the interatomic forces operative in the solution, systematic studies may lead to a greater insight into the nature of these forces and their variation with the basic properties of the solute and solvent atoms. For such fundamental applications, it is necessary to know the constitution and the thermodynamic properties of the solid phase in equilibrium with the saturated liquid phase.

Solubility of Barium in Liquid Zinc

(I. Johnson, K. E. Anderson, and J. Bartos*)

The solubility of barium in liquid zinc has been measured by analyzing filtered samples of the equilibrium liquid phase. Barium metal containing tracer quantities of 12-day barium-131 was used. The specific activity was determined by analyzing the most concentrated solutions by a flame photometric method. The data obtained in this study are shown on Figure I-19, along with the earlier data reported by Knighton, Burris, and

Figure I-19

SOLUBILITY OF BARIUM IN LIQUID ZINC

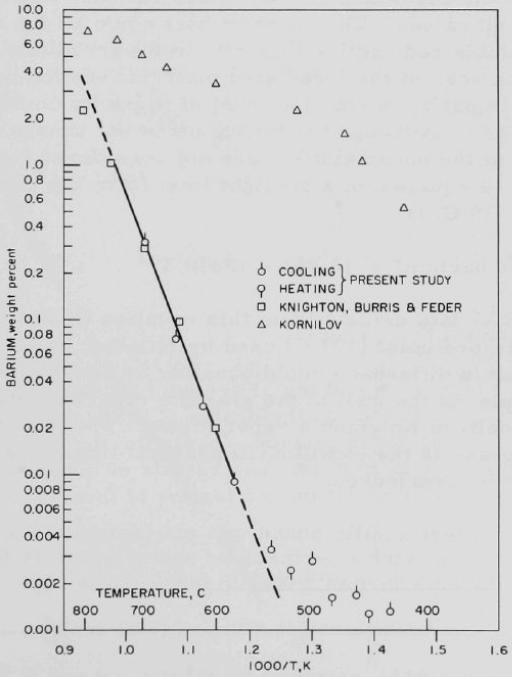

108-6518

*Co-op Student.

Feder (Purification of Reactor Fuels Using Liquid Zinc, ANL-6223, p. 16) as well as the data reported by Kornilov.[3] The results of the present study agree with those reported by Knighton. An attempt to extend Knighton's data to lower temperatures was not entirely successful for reasons given later. The results of both studies from this Laboratory, however, are in marked disagreement with Kornilov's data, which we suggest are grossly in error. It is obvious that the low solubilities indicated for this system make the thermal analysis method used by Kornilov totally unsuitable.

The tailing off of the observed data below about 560 C has several probable causes. First, since the data obtained on approaching the sampling temperature from above are significantly higher than the data obtained by approaching from below, this suggests that either supersaturation occurs or that some of the fine crystals, which are formed when minute amounts of intermetallic precipitate, pass through the filters into the sample. Although both of these factors could occur together, it is thought that supersaturation may be more important in the present case. The tailing off could also result from a constant bias in the analytical method. Thus, a constant error, equivalent to about 10 ppm of barium, would almost completely remove the curvature at low concentrations, while not significantly affecting the high values. The constant bias could be the result of a small amount of a soluble radioactive impurity in the irradiated barium. Although a gamma scan of the irradiated material showed no significant amount of radioactive impurity, a small amount of impurity could have concentrated in the liquid phase. Although the tailing off is not unusual, the data below 560 C, in view of the uncertainties, are not considered to be equilibrium solubilities. The equation of a straight line, fit to the combined data between 560 and 710 C, is

$$\log (\text{w/o barium}) = 10.464 - 10640\ T^{-1} \quad .$$

The experimental data deviate from this equation by ±16 percent. The highest temperature point (797 C) used by Knighton deviates from the line by about 17 C; this difference could possibly be caused by the location of the thermocouple, in the wall of the graphite crucible between the heating coils and the melt, in Knighton's experiments. The possibility that a second intermetallic phase is the equilibrium phase at this higher temperature should also not be overlooked.

The intermetallic phase was not isolated from the solubility ingot. The most zinc-rich intermetallic phase known is $BaZn_{13}$, which is assumed to be the equilibrium phase in the present case.

---

[3] Kornilov, I. I. (1935), reported by M. Hansen and K. Anderko, Constitution of Binary Alloys, McGraw-Hill Book Co., Inc., New York (1958), p. 277.

Solubility of Neodymium in Liquid Zinc
(I. Johnson and K. E. Anderson)

The solubility of neodymium in liquid zinc has been measured by analyzing filtered samples of the equilibrium liquid phase. Tantalum sampling tubes fitted with porous tantalum filters were used. The samples containing more than about 0.1 w/o neodymium were analyzed by a volumetric EDTA method, whereas those below 0.1 w/o were analyzed by a radiochemical method. The radiochemical method involved the use of 11.3-day Nd^{147} prepared by neutron irradiation of neodymium metal. The specific activity was determined by chemical analysis (EDTA) of samples containing about 0.5 w/o neodymium.

The data obtained in three experiments, which together covered the temperature range from 426 to 753 C, are shown on Figure I-20. Separate lines have been drawn through the data points above and below about 660 C to suggest that different equilibrium solid phases are involved. The

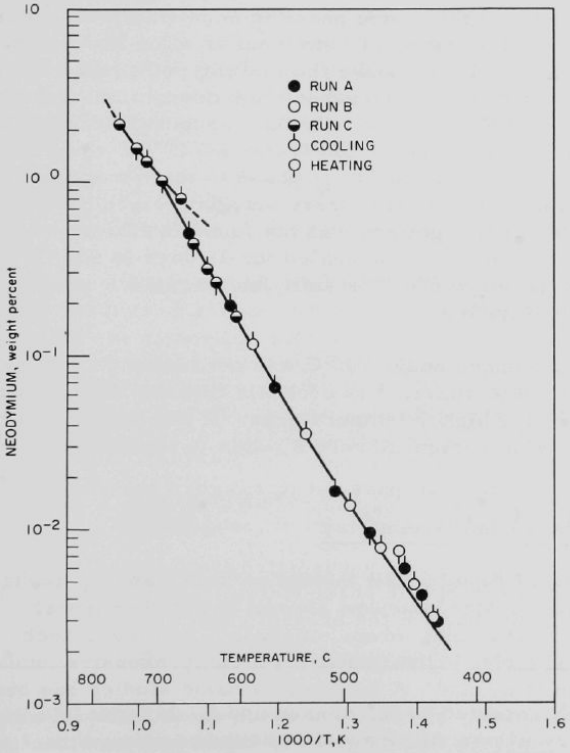

Figure I-20

SOLUBILITY OF NEODYMIUM IN LIQUID ZINC

108-6519

solubility data, in the present system, do not permit an accurate determination of the peritectic temperature between the two equilibrium phases. The data may be represented by the equations:

$$(700\text{-}753\ \text{C})\ \log\ (\text{w/o Nd}) = 22.843 - 39.810\ \frac{10^3}{T} + 17.152\ \frac{10^6}{T^2}\ ;$$

$$(525\text{-}700\ \text{C})\ \log\ (\text{w/o Nd}) = 10.227 - 12.310\ \frac{10^3}{T} + 2.340\ \frac{10^6}{T^2}\ .$$

These two equations intersect at 700 C. The 668 C datum point (~0.8 w/o) may represent the solubility of the high-temperature phase in the temperature region where it is not the most stable phase.

The intermetallic compound present in the ingot formed by slow cooling from 658 C was isolated by preferential dissolution of the zinc matrix. X-ray diffraction analysis indicated a pattern similar to that found for the epsilon zinc-rich uranium-zinc intermetallic ($UZn_{\sim 12}$). Veleckis (see ANL-6648, p. 120) reported this same phase in neodymium-zinc samples prepared by controlled evaporation of zinc from an alloy that had been made by reacting neodymium and zinc above the melting point (1024 C) of neodymium. On the other hand, alloys prepared from neodymium and zinc which were not heated above 500 C showed only the tetragonal $NdZn_{11}$ phase. Thus, at some temperature between about 700 C and 500 C, the equilibrium phase should change from the epsilon $NdZn_{\sim 12}$ phase to the tetragonal $NdZn_{11}$ phase. The transformation must be very sluggish, since $NdZn_{11}$ was not detected in the solubility ingot and was not found in alloys prepared at high temperatures even though annealed for 14 days at 500 C. The scatter of the solubility data below 550 C is sufficient to mask a small change in slope of the solubility line.

The equilibrium phase above 700 C was not isolated. In view of the phase studies referred to above, it is probable that the $NdZn_{8.5}$ phase is the equilibrium phase at the higher temperatures. If this is found to be true, then the neodymium-zinc system is very similar to the uranium-zinc system.

2. Liquid Sodium Coolant Chemistry

The utilization of liquid alkali metals as heat transfer media in high-power-density fast nuclear reactors as well as in other power sources makes essential a continuing advancement in alkali metal technology. To insure a sound technological advance, a comprehensive fundamental research program is needed. A program of basic studies has been started to elucidate the chemistry of reactions which occur in liquid alkali metal solutions; special emphasis will be given to liquid sodium since its practical importance is greatest.

Definition of problem areas has been undertaken, and construction of suitable experimental facilities for the studies has been started. The first chemical reaction to be studied involves the carburization and decarburization of ferrous alloys in liquid sodium. The first step will involve a study of the carbon-sodium-oxygen system. The experimental part of this problem will involve the preparation of high-purity sodium, the equilibration with carbon under controlled conditions, and the analysis of the liquid sodium phase. Experimental apparatus has been designed and construction is underway.

3. Thermodynamic Studies

Thermodynamic functions for key elements in liquid metal solvents and for the more important solid intermetallic phases are being measured. Several methods are being used. Galvanic cells have proved to be especially useful for the measurement of activities in liquid metal solutions as well as for the determination of the free energy of formation of the equilibrium solid phase in solid-liquid two-phase alloys. For systems composed of several well-defined intermetallic phases, measurement of the decomposition pressure by the effusion method is proving to be very useful. Systems in which only a small difference in the electrochemical potential of the components exists and in which both components have comparable vapor pressures are not conveniently studied by either the galvanic cell or effusion method. For such systems, a vapor-phase optical-absorption method is being developed. In this method, the optical absorptivity of the equilibrium vapor phase for the strongest atomic spectral line will be related to the partial pressure, from which activities are readily computed.

The galvanic cell method is being used to study systematically binary plutonium alloys with the low-melting B-subgroup metals. The results for the plutonium-zinc system are presented below. The effusion method is being used to study the light rare earth-zinc and light rare earth metal-cadmium systems. The results for the yttrium-zinc system are presented below. The optical method is under development and will be used to study the binary alkali metal systems.

Thermodynamics of the Plutonium-Zinc System
(I. Johnson, M. G. Chasanov and R. Yonco)

The thermodynamic quantities for the plutonium-zinc system are being determined by emf measurements made with the galvanic cell

$$\text{Pu} \mid \text{PuCl}_3\text{-KCl-LiCl (eutectic)} \mid \text{Pu-Zn (2-phase alloy)} \quad .$$

The cell reaction consists of the dissolution of plutonium into the fused salt at the pure plutonium electrode and the deposition of plutonium into the saturated liquid zinc-plutonium phase at the alloy electrode. Since

the equilibrium solid phase in the two-phase alloy is reported[4] to be the plutonium-zinc intermetallic compound Pu_2Zn_{17}, the overall cell reaction is

$$Pu + 8.5\ Zn\ (liq,\ satd) \rightarrow 1/2\ Pu_2Zn_{17}(s) \quad .$$

The cell assembly used for these studies is shown in Figure I-21. The stainless steel furnace tube was heated by means of a clam-shell furnace around the tube. The apparatus was operated in a glovebox. The details of the preparation of the KCl-LiCl eutectic and general operation of the cell were similar to that previously reported for the uranium systems.[5] Two types of plutonium electrodes were used. In Cell I the plutonium (high purity, prepared by electrorefining, and furnished by M. B. Brodsky and G. B. O'Keeffe of the Metallurgy Division of Argonne National Laboratory) was contained in a small thoria crucible. A tungsten lead wire was used. In Cell II a small cylinder of plutonium was welded to a tungsten lead wire. The alloy electrodes were prepared by premelting an 8 w/o plutonium-zinc mixture in a thoria crucible. Tungsten leads were also used for the alloy electrodes, thus avoiding thermal emf's.

Figure I-21

HIGH-TEMPERATURE GALVANIC CELL

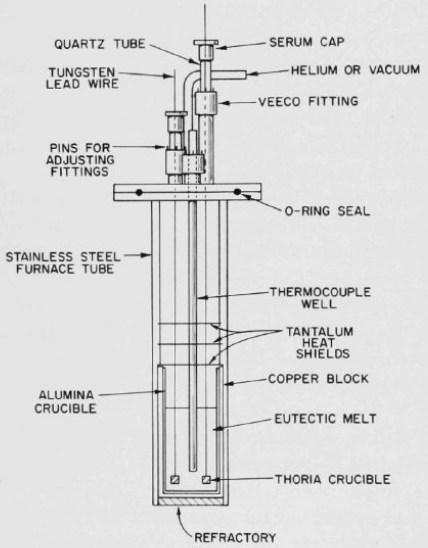

108-6520

The plutonium chloride, prepared by the method reported by Bjorklund et al.,[6] was melted, sparged with HCl and helium, and filtered before being added to the purified eutectic mixture. X-ray examination of the purified $PuCl_3$ showed no contamination by PuOCl or SiO_2. The electrolyte contained 3 w/o $PuCl_3$ in Cell I and 0.3 w/o $PuCl_3$ in Cell II.

---

[4]Cramer, E. M., Ellinger, F. H., and Lord, C. C., Extractive Metallurgy of Plutonium and Its Alloys, Interscience Publishers, New York (1960) p. 169.

[5]Johnson, I., and Feder, H. M., Trans. Met. Soc. AIME 224, 468 (1962).

[6]Bjorklund, C. W., Reavis, J. G., Leary, J. A., and Walsh, K. A., J. Phys. Chem. 63, 1774 (1959).

Figure I-22

EMF OF GALVANIC CELL

Pu | $PuCl_3$, KCl-LiCl (eutectic) | Pu-Zn (2-phase alloy)

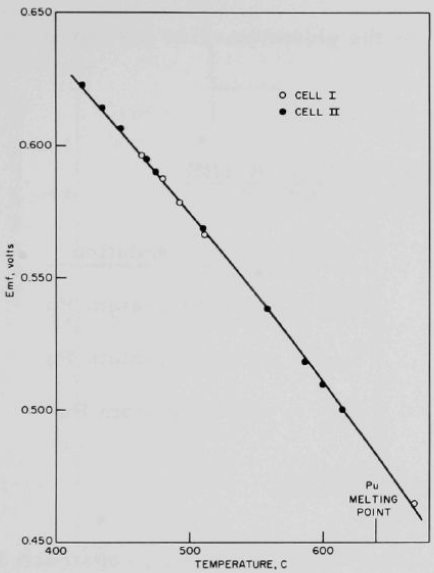

108-6521

The data for the emf as a function of temperature of the cells are shown in Figure I-22. The emf at any temperature was constant (± 0.1 mv) for at least 15 min. The same emf values were observed after the concentration effects, which were caused by polarizing the cell by passage of a current first in one direction and then in the opposite direction, had been allowed to disappear. Stirring the two-phase alloy with the tungsten lead wire did not significantly affect the emf. The same emf's were obtained with cells containing 3 and 0.3 w/o $PuCl_3$ in the electrolyte. All of the data were obtained within a 4-day period. Only one measurement was obtained on Cell I after the plutonium was melted.

Succeeding attempts to measure emf's at temperatures at which the plutonium was liquid indicated that the emf's were very erratic. Some irreversible change occurred at the liquid plutonium electrodes which is not understood. Data obtained at these higher temperatures have not been used for the computation of thermodynamic quantities because of questions concerning the reversibility of the electrode reaction.

The emf, over the range from 420 to 670 C, may be represented by the quadratic equation

$$E(v) = 0.9591 - 0.3664 \times 10^{-3} T - 0.1684 \times 10^{-6} T^2 \quad ,$$

with a standard deviation of 0.6 mv. If a three-electron change is assumed for the cell reaction, the free energy of formation of Pu_2Zn_{17} from pure plutonium and liquid zinc (saturated with plutonium) is given by

$$\Delta Gf^\circ \text{ (kcal/g-atom Pu)} = -66.36 + 25.35 \times 10^{-3} T + 11.66 \times 10^{-6} T^2 \quad .$$

The solubility of plutonium in liquid zinc (see ANL-5789, p. 89) does not exceed 0.4 a/o over the temperature range of these measurements and, consequently, the correction to the free energy of formation for the deviation of the zinc activity from unity is not significant.

The activity of plutonium in saturated zinc solutions over the temperature range from 420 to 670 C is given by the equation

$$\log a_{Pu} = 5.541 + 2.547 \times 10^{-3}\, T - 14.50 \times 10^{3}\, T^{-1} \quad .$$

Thermodynamic functions for the plutonium-zinc system at 450 C are given in Table I-5.

Table I-5

THERMODYNAMIC FUNCTIONS FOR THE PLUTONIUM-ZINC SYSTEM AT 450 C

$1/2\ Pu_2Zn_{17}$	Saturated Zinc Solution
$\Delta Gf° = -42.0$ kcal/g-atom Pu	$\bar{G}^{xs}_{Pu} = -28$ kcal/g-atom Pu
$\Delta Hf° = -72.5$ kcal/g-atom Pu	$\bar{L}_{Pu} = -46$ kcal/g-atom Pu
$\Delta Sf° = -42.2$ cal/deg g-atom Pu	$\bar{S}^{xs}_{Pu} = -25$ cal/g-atom Pu

Zinc-Yttrium System (Effusion Studies)
(E. Veleckis and E. VanDeventer)

The yttrium-zinc phase diagram has been recently constructed by Chiotti et al.[7] on the basis of thermal and metallographic evidence. According to that study, seven intermediate phases exist in the system: YZn, YZn_2, YZn_3, YZn_4, YZn_5, Y_2Zn_{17}, and YZn_{11}. Of these phases, YZn, YZn_2 and Y_2Zn_{17} were found to melt congruently, whereas the remaining phases are believed to undergo peritectic reactions.

The similarity of yttrium to the rare earth metals prompted us to include the system yttrium-zinc in the current study of the phase relationships in the systems of zinc with the light rare earths employing the recording effusion balance.

The starting alloy (of approximate composition YZn_{15}) was prepared by reacting the pure components in a rocking furnace at 650 C in an inert atmosphere. The effusion isotherm obtained at 540 C (Figure I-23) gave indications of the following intermetallic phases: YZn_{12}, Y_2Zn_{17}, YZn_5, Y_2Zn_9, YZn_3, and YZn_2. Because of the unfavorable evaporation rates below 66.6 a/o Zn, the experiment was terminated before YZn could be identified.

---

[7] P. Chiotti, J. T. Mason, and K. J. Gill, to be published, Trans AIME.

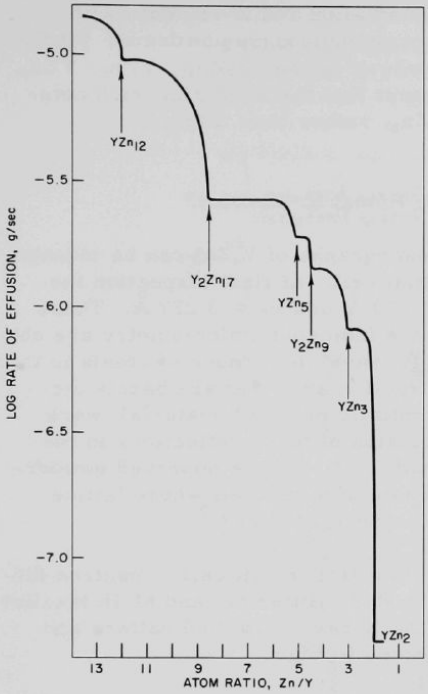

108-6522

Figure I-23

EFFUSION ISOTHERM OF YTTRIUM-ZINC SYSTEM AT 540 C

Ten effusion experiments were terminated at preselected intermediate compositions. The results of X-ray powder diffraction analysis of the residual alloys, shown in Table I-6, give good agreement between the effusion and X-ray data.

Table I-6

YTTRIUM-ZINC SYSTEM. RESULTS OF X-RAY ANALYSIS[a]

Sample No.	Composition, Zn/Y	Results	Sample No.	Composition, Zn/Y	Results
G-55	15.0	A[b] + Zn	J-11	5.0	C
J-4	11.9	A	J-6	4.4	D[d,e]
J-8	10.1	A + B[c]	J-9	3.1	E[d]
J-3	8.6	B	J-10	2.5	F[d] + E
J-7	6.0	B + C[d]	J-2	2.0	F

[a]Analysis performed by R. Schablaske and B. Tani.

[b]Patterns can be indexed on the basis of the tetragonal $ThMn_{12}$ type, with a = 8.879 Å; c = 5.201 Å.

[c]Probably U_2Zn_{17} type, with a = 8.969 Å; c = 8.761 Å.

[d]Symbols C, D, E, and F correspond to very complex diffraction patterns believed to represent single phases.

[e]Patterns bear resemblance to those found in the rare earth-cadmium systems at composition Cd/rare earth = 4.5.

From the comparison of the effusion and X-ray data with Chiotti's phase diagram,[7] the following conclusions may be drawn: (1) the results of this study confirm the existence of phases Y_2Zn_{17}, YZn_5, YZn_3, and YZn_2; (2) the results strongly suggest that the most zinc-rich compound in the system corresponds to YZn_{12} rather than YZn_{11}.

Zinc-Vanadium System
(R. Schablaske, B. Tani, M. Homa, R. Larsen)*

X-ray diffraction powder photographs of V_4Zn_5 can be indexed on the basis of a body-centered tetragonal cell. At first inspection the lattice parameters appear to be a_0 = 2.970 Å and c_0 = 3.227 Å. These parameters, the observed density, and the indicated stoichiometry are not compatible, however, with any seemingly plausible number of atoms in the unit cell. A few very low-intensity diffraction arcs that are barely discernible, or discernible only in preferentially oriented material, were disregarded in the initial indexing. Inclusion of these reflections in the indexing indicates a need for a larger unit cell. All the observed powder-diffraction arcs can be indexed on the basis of a unit cell whose lattice dimensions are a_0 = 8.910 (3 x 2.970) Å and c_0 = 3.227 Å.

To substantiate the choice of the larger unit cell, a neutron diffraction pattern of the alloy was made by R. L. Hitterman and M. H. Mueller of the ANL Metallurgy Division. Both the X-ray diffraction pattern and the neutron diffraction pattern are recorded in Figure I-24.

It should be noted that the prominent reflections in the X-ray pattern can be indexed with either set of lattice parameters. Reflections in the X-ray pattern that are not discernible, or at best barely discernible, are quite prominent in the neutron diffraction pattern, e.g., 110, 200, 220, 211, 411, and 510. Thus, the neutron diffraction pattern provides the necessary evidence for the choice of the larger cell parameters: a_0 = 8.910 Å and c_0 = 3.227 Å.

*Members of the X-ray Diffraction and Spectroscopy Group.

Figure I-24

X-RAY DIFFRACTION PATTERN AND
NEUTRON DIFFRACTION PATTERN
OF V_4Zn_5

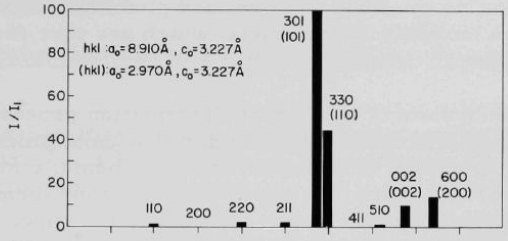

(a) X-ray Diffraction Pattern

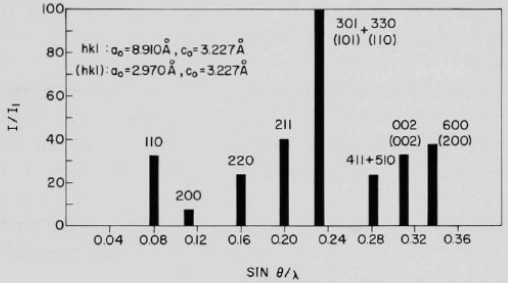

(b) Neutron Diffraction Pattern

108-6523

II. FUEL CYCLE APPLICATIONS OF VOLATILITY AND FLUIDIZATION TECHNIQUES*

The development of a Direct Fluorination Volatility Process for the recovery of uranium and plutonium from irradiated nuclear reactor fuels was continued. In this process, uranium and plutonium dioxides are fluorinated to produce hexafluoride products, which are then decontaminated by volatility techniques.

In the development of the Direct Fluorination process, current emphasis has been placed on the evaluation of a two-zone process technique as a means of avoiding caking tendencies. In this scheme, a mixture of oxygen and nitrogen is introduced into the lower reaction zone formed by a uranium dioxide pellet bed, and fluorine is introduced into the upper zone, which consists of a fluidized bed of alumina grain. The alumina, which also fills the voids of the pellet bed, is fluidized by the mixture of oxygen and nitrogen. This mixture is introduced into the system at the bottom of the pellet zone, while fluorine is introduced at the top of the pellet zone. Uranium oxide fines (U_3O_8) are formed in the lower zone and transported into the upper zone where they are removed by fluorination.

Additional studies on a fluidization-volatility scheme for reprocessing enriched uranium-zirconium alloy fuels were carried out. This processing scheme involves, first, a direct hydrochlorination (or chlorination) reaction while the alloy is submerged in an inert fluid-bed medium (currently Norton Type RR Alundum). This step produces volatile zirconium tetrachloride and permits ready separation of the uranium from the bulk of the alloying material. The uranium is recovered as the volatile hexafluoride by means of a subsequent fluorination step.

Studies were continued on a fluid-bed pyrohydrolysis reaction of zirconium tetrachloride with steam. The tetrachloride, which is produced during the chlorination of uranium-zirconium alloy fuels, is converted to the solid dioxide, a form which is more convenient for ultimate waste disposal.

Additional studies were made of the conversion of uranium hexafluoride to high-density uranium dioxide by the simultaneous reaction of the hexafluoride with steam and hydrogen.

Studies were made to determine the possibility of "decladding" stainless steel-clad uranium dioxide pellets by converting the uranium dioxide to uranosic oxide. In this reaction, the uranium dioxide pellets are transformed to a fine powder that is removed from the cladding.

---

*A summary of this section is given on pages 15 to 22.

The study of the decomposition of plutonium hexafluoride by alpha radiation was continued.

The reactions of uranium hexafluoride with hydrogen sulfide and carbon disulfide and the reaction of plutonium hexafluoride with carbon disulfide have been studied.

A. Laboratory Investigations of Fluoride Volatility Processes
(J. Fischer)

1. Fluid-bed Fluorination of Plutonium-Uranium Dioxide
(G. Manevy,* R. L. Jarry, A. V. Hariharan,** J. Riha, and J. Stockbar)

Laboratory development work has been started in which fluorinations will be carried out in a fluidized bed. A $1\frac{1}{2}$-in.-diameter fluid-bed fluorination reactor will be employed in these experiments. Initially, all experiments will be made with uranium dioxide. The procedure will consist of oxidizing the uranium dioxide to convert it to powdered uranosic oxide. The powder will then be fed into the fluidized bed of the fluorination reactor, either by gas transport or by a mechanical feeding device. Based on the results obtained in this work, a two-zone oxidation-fluorination reactor may be designed for studies of the overall process. Experiments with materials containing plutonium will begin after the apparatus has been tested and the experimental conditions have been defined.

2. Oxidative Decladding of Stainless Steel-clad Uranium Dioxide Pellets
(A. V. Hariharan, R. L. Jarry)

Oxidation and simultaneous "decladding"† of uranium dioxide pellets is being considered as a head-end step preceding fluid-bed fluorination of the uranosic oxide (U_3O_8) to uranium hexafluoride in the Direct Fluorination Volatility Process. Experiments are being carried out to determine the extent of oxidation and decladding of uranium dioxide pellets clad in type 304 stainless steel and in Zircaloy. Oxidation of uranium dioxide-plutonium dioxide solid solution, which may result in a breakdown of the oxide lattice, has been shown by results previously obtained (see ANL-6648, p. 125) to render the plutonium more vulnerable to fluorination.

---

*Appointee from Atomic Energy Commission, France.

**Affiliate, International Institute of Nuclear Engineering.

†This is not decladding as the term is normally used. The uranium dioxide, on being oxidized to uranosic oxide, increases in volume and is also transformed into a very fine powder which separates from the metallic cladding.

Preliminary experiments were carried out to determine the rate and extent of oxidation of uranium dioxide powder at different temperatures in a flowing stream of air. The reactions were carried out in a conventional, horizontal tube reactor. The uranium dioxide powder used was prepared by the fluid-bed reduction of uranium hexafluoride and consisted of small spherical particles. The extent of oxidation was determined by the weight change of the uranium dioxide with time. Within the temperature range from 300 to 500 C, 95 percent conversion of uranium dioxide to uranosic oxide was obtained in one hour. This extent of conversion was not increased with an increase in reaction time to 2 or 3 hr. The uranosic oxide product was uniformly black in color and fluffy in physical appearance.

Experiments with uranium dioxide pellets inserted into open-end stainless steel tubing to simulate chopped stainless steel-clad fuel elements have been started. Uranium dioxide pellets (0.423 in. in diameter and $\frac{3}{8}$ in. long) were inserted into $\frac{1}{2}$-in. lengths of type 304 stainless steel tubing (of 0.4655-in. OD and 0.4275-in. ID). Oxidations were carried out in a horizontal tube furnace which had connections to nitrogen, air, and oxygen supplies.

In a typical experiment, four of these stainless steel sections (each containing about 10 g of uranium dioxide) were laid on their sides in a shallow nickel boat and charged into the furnace. Either air or oxygen was used as the oxidizing gas at temperatures of 450 and 550 C. At the end of one-hour intervals, the boat and its contents were weighed to determine the extent of oxidation and, after the loose powder was removed, each pellet-stainless steel tubing unit was individually weighed to determine the extent of removal of the oxidized material from the cladding. Results are given in Table II-1.

Table II-1

OXIDATION OF URANIUM DIOXIDE PELLETS CONTAINED IN STAINLESS STEEL TUBING

Weight of UO_2 in a single experiment: 40 g (4 pellets, each separately clad in an open-end, $\frac{5}{8}$-in. length of type 304 stainless steel tubing, $\frac{1}{2}$-in. OD, 0.065-in.-thick wall).

Oxidizing Gas Flow Rate: 2 liters/min

Temp (C)	Oxidizing Gas	Percent Conversion to U_3O_8				Percent Removal of Oxidized Material from Tubing
		1 hour	2 hour	3 hour	4 hour	
450	Air	44.1	79.6	100.0	100.0	68.8
450	Oxygen	100.0	-	-	-	38.7
550	Air	49.8	85.1	100.0	-	50.8
550	Oxygen	96.8	100.0	-	-	31.4

The oxidized material was a loose, black powder. No swelling or distortion of the cladding was observed when air was used as the oxidizing gas. The material remaining in the cladding at the end of the reaction could be easily removed by shaking or tapping the tube. However, when oxygen was used as the oxidizing gas, slight swelling of the cladding tube occurred and caking of the oxidized material was observed. In addition, the material remaining in the cladding at the end of the oxidation period was more adherent than the material remaining after experiments in which air was used. This greater adherence contributed to the lower removal of the oxidized material in the experiments in which oxygen was used.

Future work will be concerned with oxidative decladding of uranium dioxide pellets placed in stainless steel and Zircaloy tubes having a series of holes punched along their long dimension. This procedure, which was developed by Atomics International,[1] is expected to result in rupture of the tubing, allowing greater access of the oxidizing gas to the uranium dioxide pellet. Experiments will also be performed to carry out simultaneous oxidation and decladding in a fluidized bed of alumina. This small-scale work is being carried out in conjunction with the work of the engineering group.

3. Chlorination of Uranium Dioxide
(H. A. Porte)

An understanding of the reaction of chlorine with uranium dioxide is important if chlorine is to be considered for use in the decladding of stainless steel-clad uranium dioxide fuels. Holmes and Raue (see Chemical Engineering Division Summary for April, May, June, 1961, ANL-6379, pp. 175 to 177) have reported that the chlorination of uranium dioxide at 650 C produced as the main product UO_2Cl_2, which is a liquid at the temperature of the reaction. The objective of the study reported here was to investigate the extent of this reaction under anhydrous experimental conditions.

The experimental procedure for the first experiment was as follows: A uranium dioxide pellet (manufactured by Numec Corp.), $\frac{1}{2}$ in. in diameter and $\frac{1}{2}$ in. long, was placed in a fused silica boat and evacuated overnight (to a pressure $< 1\mu$) in a quartz reaction tube. The system was heated to 650 C while under vacuum. Then chlorine which had been dried by passing it through a Linde Molecular Sieve No. AW 500 was flowed over the uranium dioxide pellet for 3 hr. During this time, the uranium dioxide reacted with the chlorine to form a brown liquid. The contents of the reaction tube were cooled in a stream of helium, and the liquid solidified to a shiny, yellow crystalline material.

---

[1] Guon, J., et al., Low Decontamination Reprocessing Studies on Irradiated Uranium Dioxide Reactor Fuels, NAA-SR-7136 (Dec 15, 1961).

The reactor was evacuated at room temperature and then transferred to a dry box where samples of the yellow solid were taken for X-ray diffraction and chemical analyses. X-ray analysis identified the substance as UO_2Cl_2; the results of chemical analysis were: U, 71.5 percent; Cl, 22.2 percent (UO_2Cl_2 theoretical: U, 69.8 percent, Cl, 20.8 percent). The contents of the reaction tube were weighed and, on the basis that the only product formed was UO_2Cl_2, it was calculated that 48 percent of the uranium dioxide had been converted to UO_2Cl_2.

A second experiment was conducted at 600 C with a mixture of 50 v/o chlorine and 50 v/o nitrogen as the reacting gas. Under these conditions, considerably less reaction took place, as is indicated by the fact that only two percent of the UO_2 was converted to UO_2Cl_2. The dilution of the chlorine either slowed up the reaction rate or decreased the surface temperature.

The fact that UO_2Cl_2 is formed is in itself not detrimental to the decladding step or to a further fluorination step. However, since the UO_2Cl_2 is a liquid at the temperature (600-650 C) at which the stainless steel is reacted with chlorine, it may interfere with the proper operation of a fluidized bed during the decladding procedure.

This concludes the work with chlorine on a laboratory scale.

4. Investigations of Reactions of Uranium Hexafluoride and Plutonium Hexafluoride

There is need for information on the chemical reactions in which plutonium and uranium hexafluorides act as fluorinating agents. In particular, a study of the reactions of these materials with hydrogen sulfide and carbon disulfide is interesting since differences in the fluorinating behavior of the two hexafluorides can be studied through the determination and identification of the several reaction products.

a. Reaction of Uranium Hexafluoride with Carbon Disulfide (L. Trevorrow, W. Gunther)

Ruff and Heinzelmann[2] reported that uranium hexafluoride reacted slowly with dry carbon disulfide and rapidly with wet carbon disulfide. They stated that the products of the reaction were uranium tetrafluoride and a gas which was identical to that produced by the reaction of uranium hexafluoride with elemental sulfur. Although this product was not identified, the melting and boiling points indicate that it probably was sulfur

[2]Ruff, O., and Heinzelmann, A., Z. Anorg. Chem. 72, 63-84 (1911).

tetrafluoride. The reaction between uranium hexafluoride and carbon disulfide has been investigated in more detail in our laboratory recently, and the observations are reported below.

An experiment was carried out in glass equipment to allow visual observation of the reaction. Uranium hexafluoride and carbon disulfide, which had been previously dried over phosphorus pentoxide, were mixed in the gas phase at room temperature. Both gases were initially at a partial pressure of about 100 mm in glass bulbs. The uranium hexafluoride was in a 500-ml bulb and the carbon disulfide was in a 100-ml bulb. The reaction started immediately after the gases were allowed to mix, with the production of a yellowish smoke, and proceeded readily but not with violence. The solid which accumulated on the walls of the vessel was initially bright green in color, but turned to dark brown or black after standing a few hours. An X-ray analysis showed that the major solid phase was diuranium enneafluoride, U_2F_9, with minor phases of β-uranium pentafluoride and uranium tetrafluoride. The initial solid product probably was uranium tetrafluoride which reacted with the excess uranium hexafluoride vapor to produce the intermediate uranium fluorides.

A second experiment, similar to the first, was carried out to produce a larger quantity of the solid, which was also found to be diuranium enneafluoride with both β-uranium pentafluoride and uranium tetrafluoride probably present as minor phases. Chemical analysis of this solid showed that it contained 1.7 percent total sulfur and < 0.3 percent free sulfur.

Additional experiments in which an excess of carbon disulfide was mixed with uranium hexafluoride were carried out in nickel bulbs of 500-ml volume. In one set of experiments, quantities of up to 100 g of uranium hexafluoride were used. The reactants were condensed successively into the vessel at a temperature of -196 C. The vessel and contents were then allowed to warm to room temperature. The heat released by reaction of the relatively large quantities of materials eventually caused the temperature of the vessel to rise to an estimated temperature of 100 to 200 C. These reactions produced solid uranium tetrafluoride and rather complex gaseous mixtures. The constituents identified by infrared spectral analysis were sulfur hexafluoride, tetrafluoromethane, sulfur tetrafluoride, and thionyl fluoride (SOF_2), a compound that usually accompanies sulfur tetrafluoride as a result of the reaction of the tetrafluoride with traces of moisture. Also present was bistrifluoromethyl disulfide, $(CF_3)_2S_2$. The infrared absorption spectra of bistrifluoromethyl disulfide and bistrifluoromethyl trisulfide have maxima attributed to a C-F stretching vibration at 1176 and 1105 cm^{-1} for the trisulfide,[3] and at 1095, 1133,

---

[3]Hazeldine, R. N., and Kidd, J. M., J. Chem. Soc., 1953, 3219.

1190, and 1205 cm^{-1} for the disulfide.[4] Because of the proximity of these maxima, it is possible that a relatively large quantity of one compound could mask the presence of the other when the infrared spectra are used for identification. The positions of the absorption maxima of the two compounds in the ultraviolet region are also quite similar,[3] 426 x 10^2 cm^{-1} for the disulfide and 424 x 10^2 cm^{-1} for the trisulfide, and are therefore not useful for the detection of one compound in the presence of the other. The ultraviolet spectra of the product gases showed a peak at 424 x 10^2 cm^{-1}.

In a second set of experiments in which an excess of carbon disulfide was used, the reagents were mixed in smaller quantities (about 1 g of uranium hexafluoride) as gases at room temperature. The reactants were contained at room temperature in separate 500-ml nickel bulbs. A valve joining the two bulbs was opened to mix the reactants. This technique allowed the reaction to proceed to completion at room temperature. The solid compounds produced in these experiments were analyzed by X-ray powder techniques. The solids were almost amorphous in nature, but the pattern obtained strongly resembled that of uranium tetrafluoride. The reactions between uranium hexafluoride and carbon disulfide which proceeded to completion at room temperature produced a much simpler mixture of gases. The principal absorption maxima of the gaseous products in the infrared region were those of the trifluoromethyl sulfides. Sulfur tetrafluoride and thionyl fluoride, which are strong absorbers in the infrared region, were barely detectable. There is a significant difference in the volatilities of the two trifluoromethyl sulfides. The boiling points are 34.6 C for bistrifluoromethyl disulfide and 86.4 C for bistrifluoromethyl trisulfide.[3] Simple distillation of the reaction products provided partial separation, which was enough to demonstrate that both compounds were present. The fraction of gaseous products which was volatile at -78 C had the absorption spectrum of bistrifluoromethyl disulfide. In the fraction of gaseous products which was nonvolatile at -78 C, the absorption spectrum of bistrifluoromethyl trisulfide was predominant.

A reaction was carried out in nickel bulbs at room temperature with helium as a diluent. A 530-ml mixture of uranium hexafluoride (pressure of 100 mm) and helium (pressure of 500 mm) was mixed by diffusion with a 525-ml mixture of carbon disulfide (pressure of 200 mm) and helium (pressure of 300 mm). The infrared spectra of the gas phase of this reaction mixture and also the fraction of the mixture which was volatile at -78 C showed the presence of only carbon disulfide, bistrifluoromethyl trisulfide, and traces of thionyl fluoride. Small amounts of sulfur tetrafluoride were probably formed and were hydrolyzed to thionyl fluoride by traces of moisture present in either the reaction system or the spectrometer cell.

---

[4]Nabi, S. N., and Sheppard, N., J. Chem. Soc. 1959, 3439.

The chemical literature indicates that carbon disulfide reacts with fluorinating agents to produce a wide variety of compounds of carbon, sulfur, and fluorine. The nature of the fluorinating agent and the conditions under which it is used determine which compounds are produced. Mercury difluoride reacts with carbon disulfide at 250 C to produce bis-(trifluoromethylthio)-mercury, $Hg(SCF_3)_2$, but above 300 C the main product is bistrifluoromethyl disulfide, $(CF_3)_2S_2$.[5] In the electrochemical fluorination of carbon disulfide in anhydrous hydrogen fluoride, the main product was trifluoromethyl sulfur pentafluoride, CF_3SF_5, and small amounts of difluoromethylenebis-(sulfur pentafluoride), $CF_2(SF_5)_2$, and difluoromethylenebis-(sulfur trifluoride), $CF_2(SF_3)_2$, were also produced.[6] Fluorine gas at 40 C reacts with carbon disulfide to produce a complex mixture of tetrafluoromethane, CF_4, sulfur hexafluoride, SF_6, thiocarbonyl fluoride, CSF_2, sulfur tetrafluoride, SF_4, trifluoromethyl sulfur pentafluoride, CF_3SF_5, trifluoromethyl sulfur trifluoride, CF_3SF_3, disulfur decafluoride, S_2F_{10}, difluoromethylene sulfur trifluoride sulfur pentafluoride, $SF_3CF_2SF_5$, and difluoromethylenebis-(sulfur pentafluoride), $CF_2(SF_5)_2$.[7] Cobalt trifluoride reacts with carbon disulfide at 200 to 250 C to produce trifluoromethyl sulfur pentafluoride, sulfur hexafluoride, and sulfur tetrafluoride.[8] Iodine pentafluoride reacts with carbon disulfide at temperatures between 60 and 200 C to produce bistrifluoromethyl disulfide and bistrifluoromethyl trisulfide, and at the higher temperatures this reaction also produces sulfur tetrafluoride and tetrafluoromethane.[2] If uranium hexafluoride is compared with the fluorinating agents listed above, it is found to be most similar to iodine pentafluoride with respect to the type of sulfur and carbon compounds produced in the reaction with carbon disulfide.

Table II-2 summarizes the results of the reaction of carbon disulfide with uranium hexafluoride and the results listed in the literature for the reaction of carbon disulfide with other fluorinating agents.

The products formed by the reaction of covalent fluorides with carbon disulfide can be used to compare the covalent fluorides as fluorinating agents. Uranium hexafluoride, mercury difluoride, and iodine pentafluoride are all considered to be weak fluorinating agents, since they react with carbon disulfide to break only one carbon-sulfur bond per carbon disulfide molecule, and to form products with the sulfur-sulfur bond intact. Cobalt trifluoride is considered to be a stronger fluorinating agent; it breaks one carbon-sulfur bond per molecule, but the products do not contain sulfur-sulfur bonds which are susceptible to fission and

[5] Man, E. H., Coffman, D. D., and Muetterties, E. L., J. Am. Chem. Soc. 81, 3575 (1959).

[6] Clifford, A. F., El-Shamy, H. K., Emeleus, H. J., and Hazeldine, R. N., J. Chem. Soc., 1953 2372.

[7] Tyckzkowski, E. A., and Bigelow, L. A., J. Am. Chem. Soc. 75, 3523 (1953).

[8] Silvey, G. A. and Cady, G. H., J. Am. Chem. Soc. 72, 3624 (1950).

fluorination by cobalt trifluoride.[9] Plutonium hexafluoride is then considered to be the strongest fluorinating agent amongst those which have been reacted with carbon disulfide (see Section b); the only carbon-containing product of the reaction, tetrafluoromethane, results from the breaking of both carbon-sulfur bonds per molecule.

Table II-2

REACTIONS OF URANIUM HEXAFLUORIDE, PLUTONIUM HEXAFLUORIDE, AND OTHER FLUORINATING AGENTS WITH SULFIDES

No.	Reactants	Reaction Temp (C)	Products	Reference
1	UF_6(g)(excess) + CS_2(g)	25	U_2F_9(s), CF_4(g), SF_4(g), $(CF_3)_2S_2$(g) $(CF_3)_2S_3$(g)(?)	This work
2	UF_6(g) + CS_2(g)(excess)	100-200 estimated	UF_4(s), SF_6(g), CF_4(g), SF_4(g), $(CF_3)_2S_2$(g), $(CF_3)_2S_3$(g)(?)	This work
3	UF_6(g) + CS_2(g)(excess)	25	UF_4(s), $(CF_3)_2S_2$(g), $(CF_3)_2S_3$(g), trace SF_4(g)	This work
4	UF_6(g) + CS_2(g)(excess) He diluent	25	UF_4(s), $(CF_3)_2S_3$(g), trace SF_4(g)	This work
5	HgF_2(s) + CS_2(g)	<250	Hg $(SCF_3)_2$(g)	5
6	HgF_2(s) + CS_2(g)	>300	$(CF_3)_2S_2$(g)	5
7	F_2 (electrochemical fluorination in anhydrous HF) + CS_2	~0	CF_3SF_5(g), $CF_2(SF_5)_2$(g) $CF_2(SF_3)_2$(g)	6
8	F_2(g) + CS_2(g)	40	CF_4(g), SF_6(g), CSF_2(g), SF_4(g) CF_3SF_5(g), CF_3SF_3(g), S_2F_{10}(g), $SF_3CF_2SF_5$(g), $CF_2(SF_5)_2$(g)	7
9	CoF_3(s) + CS_2(g)	200-250	CF_3SF_5(g), SF_6(g), SF_4(g)	8
10	IF_5 + CS_2(g)	80-200	$(CF_3)_2S_2$(g), $(CF_3)_2S_3$(g), SF_4(g), also CF_4(g) at the higher temperatures	3
11	PuF_6(g) + CS_2(g)	25	PuF_4(s), SF_4(g), SF_6(g), CF_4(g)	This work
12	UF_6(g) + H_2S(g)	25	UF_4(s), SF_4(g), HF(g)	This work
13	UF_6(g) + H_2S(g)	300[a]	UF_4(s), S(s), SF_4(g), HF(g)	This work

[a] An excursion to 480 C occurred during the reaction.

b. The Reaction of Plutonium Hexafluoride with Carbon Disulfide

(R. Wagner, W. Shinn, W. Gunther)

Uranium hexafluoride is known to react with carbon disulfide (see the preceding section of this report) to produce bistrifluoromethyl di- and trisulfides. Cobalt trifluoride, a stronger fluorinating agent than

[9] Brandt, G. A. R., Emeleus, H. J., and Hazeldine, R. N., J. Chem. Soc., 1952, 2198.

uranium hexafluoride, is known to produce trifluoromethyl sulfur pentafluoride when reacted with carbon disulfide.[10] An exploratory experiment was undertaken to determine if plutonium hexafluoride would also form trifluoromethyl sulfur pentafluoride from carbon disulfide.

The reaction was carried out in two 500-ml Pyrex spheres connected in a vertical arrangement by a vacuum stopcock. The spheres were dried and then treated with 500 mm of fluorine at room temperature for 20 hr. The lower sphere was filled with 6.56 millimoles of carbon disulfide which had been dried over phosphorus pentoxide; the upper sphere contained 2.71 millimoles of plutonium hexafluoride. Both gases were at 25 C. When the stopcock between the carbon disulfide and plutonium hexafluoride gases was opened slightly, the carbon disulfide (being at a higher pressure) entered the upper sphere and reacted with the plutonium hexafluoride immediately above the stopcock bore. The reaction was rapid and simultaneously gave a finely divided light-tan solid and a rose-colored glow which extended almost across the diameter of the upper sphere.

Infrared scans of the gaseous products were made. The scans were taken from one to 24 μ. The following products were found: sulfur tetrafluoride, sulfur hexafluoride, thionyl fluoride, tetrafluoromethane, silicon tetrafluoride, and carbon disulfide. The thionyl fluoride is apparently a side reaction product formed from a trace of moisture and the sulfur tetrafluoride. The silicon tetrafluoride is apparently a product of reaction with the Pyrex container. Based on the absence of more than one important peak, plutonium hexafluoride, trifluoromethyl sulfur pentafluoride, bistrifluoromethyl disulfide, and bis-trifluoromethyl trisulfide were not present. Silvey and Cady,[10] however, reported the decomposition of trifluoromethyl sulfur pentafluoride to tetrafluoromethane and sulfur tetrafluoride in an electric spark. Any trifluoromethyl sulfur pentafluoride formed in the carbon disulfide-plutonium hexafluoride reaction may have likewise decomposed in the glow.

Chemical analysis of the solid product showed it to have a fluorine to plutonium ratio of 4.1 to 1. An X-ray diffraction pattern for the solid showed it to be plutonium tetrafluoride.

The products of the fluorination of carbon disulfide using plutonium hexafluoride are compared in Table II-2 with products formed using uranium hexafluoride and other fluorinating agents.

---

[10] Silvey, G. A., and Cady, G. H., J. Am. Chem. Soc., 72, 3624 (1950)

c. The Reaction of Uranium Hexafluoride with Hydrogen Sulfide
(L. Trevorrow, W. Gunther)

The reaction between uranium hexafluoride and hydrogen sulfide has been carried out under a variety of conditions. In all experiments, the reactants were brought together by vacuum techniques under anhydrous conditions. The hydrogen sulfide was the purified grade obtained from the Matheson Company.

A reaction was carried out first in glass vacuum equipment so that the progress of the reaction could be followed visually. A 111-ml volume of hydrogen sulfide at a pressure of 101 mm and a 105-ml volume of uranium hexafluoride at a pressure of 100 mm were allowed to mix by diffusion in the gas phase at 25 C. The reaction started immediately on mixing, and a finely divided, yellowish-green powder was produced. X-ray analysis of the powder showed it to be amorphous; however, a pattern suggestive of uranium tetrafluoride was obtained. In another experiment, the hydrogen sulfide was condensed onto solid uranium hexafluoride in nickel equipment, and the reactants were warmed to room temperature. This technique yielded a crystalline, solid reaction product which was identified definitely by X-ray analysis as uranium tetrafluoride.

A flow experiment was also carried out in which streams of uranium hexafluoride and hydrogen sulfide were mixed in a tubular, nickel reactor heated in a furnace. The temperature of the reactor was 300 C except for a brief excursion up to 480 C which occurred during the course of the reaction. A yellowish-green powder and dark-green chunks of solid were produced in the reaction. X-ray analysis showed that the major phase in the yellowish-green powder was uranium tetrafluoride and that a minor phase present was orthorhombic sulfur. Chemical analysis showed that 7.0 percent of the yellowish-green powder was sulfur. X-ray analysis showed that the dark-green pieces were uranium tetrafluoride, and a chemical analysis showed that they contained 0.76 percent sulfur.

The infrared spectra of the gaseous products of the reactions carried out both at room temperature and at 300 C showed that sulfur tetrafluoride was present. In all cases thionyl fluoride was also present. The presence of this compound is ascribed to the hydrolysis of sulfur tetrafluoride by moisture. It is normally very difficult to obtain an infrared spectrum of sulfur tetrafluoride which does not show traces of thionyl fluoride. In experiments in which extreme precautions were taken to exclude moisture from the equipment, the absorption peaks of thionyl fluoride were quite small compared with the peaks of sulfur tetrafluoride.

At 500 C sulfur tetrafluoride disproportionates to sulfur hexafluoride and sulfur.[11] Thus, in the experiment in which the temperature rose to 480 C, disproportionation of sulfur tetrafluoride formed in the reaction between uranium hexafluoride and hydrogen sulfide would explain the presence of sulfur in the solid products.

It was suspected that hydrogen fluoride was formed from the hydrogen contained in hydrogen sulfide. The fate of the hydrogen was determined (as described below) by separating from the reaction mixture the hydrogen fluoride formed in the reaction of a known quantity of hydrogen sulfide with an excess of uranium hexafluoride and then weighing the hydrogen fluoride. A sample of 32.6 g (92.6 millimoles) of uranium hexafluoride was reacted with 0.882 g (25.9 millimoles) of hydrogen sulfide. The excess uranium hexafluoride was apparently absorbed by the uranium tetrafluoride formed in the reaction to yield uranium enneafluoride, U_2F_9. An X-ray analysis of the solid products showed the major phase to be uranium tetrafluoride, and the minor phase to be diuranium enneafluoride. No uranium hexafluoride could be condensed from the gaseous reaction mixture.

The gas phase was then transferred by vacuum distillation back and forth several times through a bed of sodium fluoride pellets contained in a tubular nickel reactor at 100 C. The hydrogen fluoride in the reaction mixture was absorbed by the sodium fluoride to form sodium bifluoride, $NaHF_2$. The hydrogen fluoride was released subsequently by increasing the temperature of the reactor to 400 C. The hydrogen fluoride was then condensed and weighed. It had been established previously that a sample of hydrogen fluoride could be absorbed by the sodium fluoride bed and quantitatively recovered. It had been established also that a sample of sulfur tetrafluoride could be transferred by vacuum distillation back and forth through the bed without loss. This proved to be an efficient technique for separating the hydrogen fluoride from the sulfur tetrafluoride formed in the reaction between uranium hexafluoride and hydrogen sulfide. The 0.882 g (25.9 millimoles) of hydrogen sulfide produced 1.02 g (51.1 millimoles) of hydrogen fluoride. These data allow it to be concluded that a mole of hydrogen sulfide reacts quantitatively with an excess of uranium hexafluoride to produce 2 moles of hydrogen fluoride. The stoichiometry of the gas phase reaction between uranium hexafluoride and hydrogen sulfide has not been definitely established, but it can probably be represented by the equation

$$3\ UF_6(g) + H_2S(g) = 3\ UF_4(s) + SF_4(g) + 2\ HF(g) \quad .$$

---

[11] Muetterties, E. L. (to E. I. duPont de Nemours and Company), U. S. Patent 2,883,267, April 21, 1959.

The results of the reaction of uranium hexafluoride with hydrogen sulfide have also been summarized in Table II-2.

5. Fluorine Corrosion Test of Nickel-Thoria Material
(L. E. Trevorrow, W. H. Gunther)

Samples of a material consisting of 98 percent nickel and 2 percent thorium dioxide have been tested to determine if this is a suitable material of construction for the containment of fluorine gas at 600 C. Since it is known that above 600 C the rate of corrosion of nickel by fluorine increases rapidly, 600 C was selected for these studies because it represents the practical upper limit at which nickel can be used for the containment of fluorine. In order to compare A-nickel and the nickel-thoria alloy directly, the corrosion of both of the materials was studied under the same experimental conditions.

Discs of both the nickel-thoria material and A-nickel were prepared; each disc had a thickness of $\frac{1}{16}$ in. and a diameter of $\frac{1}{2}$ in. A $\frac{1}{8}$-in.-diameter central hole was drilled in each disc so that it could be supported on an Alundum rod. Each disc was polished with a series of emery papers through the 3/0 grade, degreased in trichloroethylene, weighed, and measured.

The reaction vessel was a $1\frac{1}{4}$-in.-diameter nickel tube, positioned horizontally in a furnace, and connected to a vacuum line.

Figure II-1

SAMPLE ASSEMBLY USED IN COMPARISON OF FLUORINE CORROSION OF A-NICKEL AND NICKEL-THORIA MATERIAL

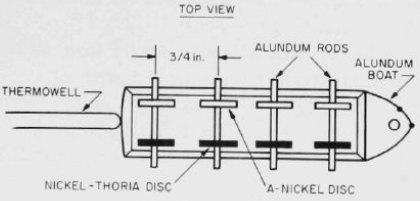

108-6524

The discs were positioned on Alundum rods with faces parallel to the longitudinal axis of the vessel. Nickel-thoria discs and A-nickel discs were placed opposite each other, about $\frac{1}{2}$ in. apart, as shown in Figure II-1. Thus, corrosion of four pairs of discs was compared at a temperature of 600 ± 10 C, as measured by a thermocouple in a well in the reaction vessel.

The fluorination procedure was as follows: Discs were mounted on the Alundum holder and inserted into the reaction vessel, which was closed, evacuated, and heated to 600 C. Fluorine gas was then admitted to the reaction vessel, and the pressure was maintained at 700 ± 25 mm for 4 days. Following this, the reaction vessel was evacuated, filled with helium, and allowed to cool slowly to room temperature.

Nickel fluoride was formed on the A-nickel discs as a uniform and adherent film, but the nickel fluoride on the nickel-thoria discs was nonadherent and fell away from the discs. Consequently, the amount of nickel fluoride on the nickel-thoria discs was determined by completely removing the nickel fluoride and weighing the clean disc to determine the weight loss. The amount of nickel fluoride on the A-nickel discs was measured by leaving the adherent films intact, and reweighing them to determine the weight gain.

The results are summarized in Table II-3. The extent of fluorination is recorded as milligrams of fluorine consumed per square centimeter of disc surface. Pair No. 1 was located closest to the center of the furnace, where the temperature would be expected to be highest. The distances of the pairs from the center of the furnace increased with increasing pair number, and apparently the temperature decreased with increasing pair number. The data in Table II-3 indicated that the extent of fluorination decreased for pairs farthest from the furnace center.

Table II-3

FLUORINE CORROSION OF NICKEL-THORIA AND A-NICKEL

Nominal Temperature:	600 ± 10 C at center of furnace[a]
Time:	4 days
F_2 Pressure:	700 ± 25 mm
Materials:	98% nickel-2% thoria alloy discs; A-nickel discs; commercial grade fluorine

Pair No.	Material	Surface Area (sq cm)	Calc Fluorine Consumed (mg)[b]	Calc Fluorine Consumed per Unit Surface (mg/sq cm)	Ratio of Fluorine Consumption (nickel-thoria/nickel)
1	Nickel-Thoria	3.21	184	57.3	12
	Nickel	2.93	14	4.7	
2	Nickel-Thoria	3.21	78	24	8
	Nickel	3.45	10	2.9	
3	Nickel-Thoria	3.21	61	19	12
	Nickel	3.13	5	2	
4	Nickel-Thoria	3.21	36	11	9
	Nickel	3.33	4	1	

[a]The temperature decreased along the length of the furnace from a maximum at the center. Pair No. 1 was nearest to the center, and the distance of the pairs from the center increased with the number of the pair.

[b]The weight of fluorine consumed was calculated from the weight of nickel fluoride formed.

It is assumed, however, that because of the way in which the discs were positioned, a valid comparison of the two materials was obtained.

The ratios of fluorine consumption by the two materials are also presented in the table. The extent of fluorination for the alloy was 8 to 12 times higher than that for A-nickel. In view of the extent of fluorination and the spallation of the fluoride coating from nickel-thoria samples, it is concluded that the nickel-thoria is of no value as a material for construction of equipment which is intended for containment of fluorine at 600 C.

The Absorption Spectrum of Gaseous Plutonium Hexafluoride
(M. Steindler, D. V. Steidl)

The process of energy absorption by plutonium hexafluoride is of fundamental interest to the study of the decomposition of plutonium hexafluoride by radiation. An understanding of the photodecomposition of plutonium hexafluoride may shed some light on the mechanism of the decomposition of plutonium hexafluoride by radiation. The absorption spectrum of plutonium hexafluoride in the ultraviolet, visible, and near-infrared spectral region was determined in anticipation of experiments which may be carried out on the photolysis of plutonium hexafluoride and also in support of a search for instrumental methods of analysis for plutonium hexafluoride. A search of the literature failed to reveal other than brief mention of the spectrum of plutonium hexafluoride. Jorgensen[12] indicated by reference to unpublished work of Weinstock and Fred that plutonium hexafluoride has a very complicated absorption spectrum with a weak band group at 3780-6604 K,* six very sharp lines at 9583-10678 K, two band groups at 12260 K and 12720 K, and finally three bands at 17260 K, 17817 K, and 18448 K before the strong electron transfer band. Our results are in substantial agreement with these generalizations, and we have extended the data to 50,000 K (2000 Å).

Samples of plutonium hexafluoride used in the current study were prepared by fluorination of plutonium tetrafluoride by elemental fluorine at elevated temperatures.[13] Samples of the hexafluoride were purified by trap-to-trap distillation under vacuum until the vapor pressure of the plutonium hexafluoride at the ice point agreed with the value quoted in the literature.[14]

---

*K = cm^{-1}.

[12]Jorgensen, C. K., Mol. Phys. 2, 96 (1959).

[13]Steindler, M. J., Steidl, D. V., and Steunenberg, R. K., Nucl. Sci. Eng. 6, 333 (1959).

[14]Weinstock, B., Weaver, E. E., and Malm, J., J. Inorg. Nucl. Chem. 11, 104 (1959).

The nickel cell used for this work had a 5-cm light path and was constructed as described by Steunenberg and Vogel.[15] The cell was equipped with 3-mm-thick quartz windows, and was pretreated first with elemental fluorine and then by exposure to plutonium hexafluoride. After pretreatment, the cell was evacuated and filled with purified plutonium hexafluoride to the desired pressure.

The spectra of plutonium hexafluoride were obtained on a Cary Recording Spectrophotometer, Model 14, which recorded values of the absorbance. In order to utilize the recorded data directly, the empty cell was scanned over the entire spectral region before each experiment and suitable adjustments were made on the instrument to produce a zero base line. The data obtained from the spectrophotometer were used, together with the pressure (2.5 mm to 93 mm Hg) and temperature (24 C) of the gas to calculate (by means of the perfect gas laws) the molar absorbancy index for gaseous plutonium hexafluoride at the various wavelengths. These data are shown in Figure II-2, and the locations and molar absorbancy indices of principal peaks are given in Table II-4.

Figure II-2

ABSORPTION SPECTRUM OF GASEOUS PLUTONIUM HEXAFLUORIDE

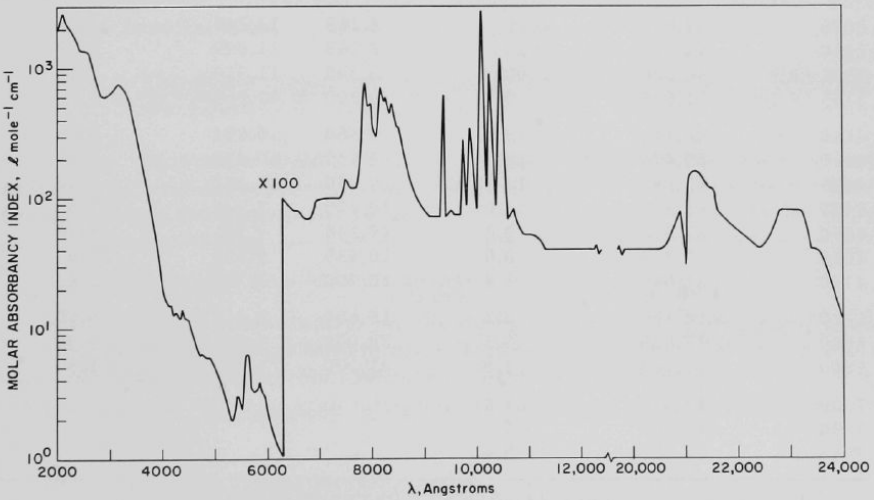

108-6525

The spectrum of plutonium hexafluoride in the region 2000-4000 Å shows relatively strong absorption, particularly at 2090, 2250, 2500, and 3155 Å. In contrast, UF_6 shows very little absorption at

---

[15] Steunenberg, R. K. and Vogel, R. C., J. Am. Chem. Soc. 78, 901 (1956).

wavelengths greater than 3200 Å in this region (ANL-5254, p. 49). At 3400 Å, the ratio of molar extinction coefficients of gaseous plutonium hexafluoride to that of gaseous uranium hexafluoride is approximately 600. The magnitude of this ratio should permit the determination of plutonium hexafluoride in mixtures of uranium hexafluoride and plutonium hexafluoride by absorption spectrophotometry. The observed brown color of gaseous plutonium hexafluoride results in absorption peaks in the visible region of the spectrum, particularly in the green, the blue, and the violet.

Table II-4

PRINCIPAL PEAKS IN THE ABSORPTION SPECTRUM OF GASEOUS PLUTONIUM HEXAFLUORIDE

Cell Length: 5 cm
Window: Quartz
Temperature: 24 C
Instrument: Cary, Model 14
Pressures: Various (2.5 mm to 93 mm)

λ (Å)	ν (cm^{-1})	Molar Absorbancy Index (ℓ $mole^{-1}$ cm^{-1})	λ (Å)	ν (cm^{-1})	Molar Absorbancy Index (ℓ $mole^{-1}$ cm^{-1})
2090	47,846	2670	8,165	12,247	7.08
2250	44,444	1930	8,265	12,099	5.97
2500 (B)[a]	40,000	1300	8,390	11,919	5.25
3155 (VB)[a]	31,695	760	8,500	11,764	3.50
4142	24,143	15.2	9,360	10,684	6.29
4260	23,474	13.4	9,735	10,272	2.82
4376	22,852	14.1	9,870	10,132	3.42
4480	22,321	12.0	10,075	9,925	27.3
4550	21,978	9.3	10,245	9,761	8.96
4600	21,739	8.0	10,435	9,583	12.0
4750	21,053	6.4	10,700	9,346	0.83
5420	18,450	3.2	15,600	6,410	0.60
5610	17,825	6.5	20,900	4,785	0.80
5840	17,123	3.9	21,100	4,739	1.59
7500	13,333	1.4			
7870	12,706	7.76			
7960	12,563	5.41			

[a]B = Broad; VB = Very Broad.

Examination of the fine structure of the bands at 5610, at approximately 8160, and at 10075 Å reveals a band separation which may be correlated with the infrared spectrum of PuF_6.[16] Peak separations in the

[16]Malm, J., Weinstock, B., and Claasen, M., J. Chem. Phys. 23, 2192 (1955).

sequence 5420, 5610, and 5840 Å are 625 cm^{-1} and 702 cm^{-1}. A fundamental vibration frequency of 628 cm^{-1} (ν_1) has been observed for PuF_6.[16] A similar correlation has been made with a series of bands observed in the spectrum of UF_6 at approximately 3670 Å.[17]

In the near-infrared region, the band structure of the first band (8160 Å) shows peak separations of 627 cm^{-1}, 143 cm^{-1}, 316 cm^{-1}, 148 cm^{-1}, and 180 cm^{-1}. With the exception of the 316 cm^{-1} separation, all of these may be correlated with fundamental frequencies of PuF_6 (ν_1 = 628 cm^{-1}; ν_6 = 171 cm^{-1}). A peak at 320 cm^{-1} ($\nu_2 - \nu_4$) has been calculated but not observed for PuF_6.* The second observed band of PuF_6 in the near-infrared, the 10075 Å band, consisting of six sharp peaks, shows separations of 412 cm^{-1}, 140 cm^{-1}, 207 cm^{-1}, 164 cm^{-1}, 178 cm^{-1}, and 237 cm^{-1}. The fundamental frequencies which are applicable include ν_6 = 171 cm^{-1} and ν_4 = 203 cm^{-1}. Further, a weak band at 414 cm^{-1}, observed for PuF_6, has been assigned as $\nu_4 + \nu_5$.

While the application of ligand field theory to gaseous hexafluorides has been reported for the transition metals rhenium, osmium, iridium, and platinum,[18] no such data have been reported in the literature for plutonium hexafluoride, although the problems related to such a calculation have been discussed by Goodman.[19] It is not possible, therefore, to present assignments for the several absorption bands observed in the spectrum of plutonium hexafluoride.

The Alpha-radiation Decomposition of Plutonium Hexafluoride
(R. Wagner, W. Shinn)

Plutonium hexafluoride decomposes under the influence of alpha radiation to plutonium tetrafluoride and fluorine.[20,21,22] Reported values for the rate of decomposition range from 0.6 to 2 percent per day for solid

---

*A similar peak has been observed[17] for NpF_6 at 323 cm^{-1}.

17 Dieke, G. H., and Duncan, A. B. F., Spectroscopic Properties of Uranium Compounds, National Nuclear Energy Series, Division III, Vol. 2, McGraw-Hill Book Co., Inc., New York (1949), p. 120.

18 Moffitt, W., Goodman, G. L., Fred, M., and Weinstock, B., Mol. Phys. 2, 109 (1959).

19 Goodman, G., Metal Hexafluorides: Some Applications of Ligand Field Theory to Octahedral Molecules, Ph.D. thesis, Harvard University (1959).

20 Mandleberg, C. J., Rae, H. K., Hurst, R., Long, G., Davies, D., and Francis, K. E., J. Inorg. Nucl. Chem., 2, 358 (1956).

21 Florin, A. E., Tannenbaum, I. R., and Lemons, J. F., J. Inorg. Nucl. Chem., 2, 368 (1956).

22 Weinstock, B. and Malm, J., J. Inorg. Nucl. Chem., 2, 380 (1956).

plutonium hexafluoride and from 0.060 to 0.35 percent per day for plutonium hexafluoride in the vapor phase. A study was initiated to correlate the extent of alpha decomposition of plutonium hexafluoride with such variables as time, plutonium hexafluoride pressure, container material, vessel volume, presence of foreign gases, and intensity of radiation. The decomposition of plutonium hexafluoride by gamma radiation is being studied (ANL-6477, p. 118; ANL-6596, p. 125; this report, the following section) by Steindler and Steidl. Corrections for alpha decomposition are also necessary in the gamma-radiation studies.

The vessels used in the alpha-decomposition studies are nickel and aluminum spheres having 6.35-cm outside diameters and wall thicknesses of 0.0635 cm. Pyrex and quartz vessels having 6.36- and 6.08-cm outside diameters are also used. The vessels were equipped with a small bellows valve (Hoke number 1479) and were attached to a gas manifold with standard flare fittings. Before use, the vessels were pretreated with 400 mm of fluorine at room temperature for 2 days. The volumes of the vessels ranged from 125 to 128 ml, depending on the internal volume of the valve.

The Pyrex and quartz spheres used had small bellows valves attached to them by means of Kovar graded seals. The Pyrex spheres had diameters of 6.36 cm and total volumes of 137 ml and 141 ml. The diameters of the quartz spheres were 6.08 cm, and their total volumes were 119 ml and 122 ml. The glass vessels were pretreated with one atmosphere of fluorine for two days at room temperature.

All of the vessels were weighed through use of a tare constructed of the same material and similar in size and shape to the vessel being weighed in order to eliminate the need for buoyancy corrections. Plutonium hexafluoride which had been purified by vacuum fractionation was used. Groups of 10 to 16 vessels were filled simultaneously from a common source of plutonium hexafluoride. The pressures were measured with a Booth-Cromer pressure transmitter and a mercury manometer. They were then attached to the vacuum system, and the volatile fluorine and undecomposed plutonium hexafluoride were removed. The vessels were again weighed. The difference in weights of the vessels was equal to the amount of plutonium tetrafluoride deposited in each vessel.

The results are reported in Table II-5. The rates are expressed as average daily rates of decomposition in terms of percentages of the initial plutonium hexafluoride weight.

Results obtained in nickel spheres containing an initial pressure of 50 mm of plutonium hexafluoride show that decomposition was not a linear function of time. The average rate for 12.6 days was 0.30 ± 0.04 percent per day, whereas for 157.7 days the decomposition rate decreased to

0.14 ± 0.01 percent per day. A nonlinear relationship between decomposition rate and time is also observed for data obtained with the initial plutonium hexafluoride pressure at 100 mm. The average decomposition rate for this system over a period of 5.6 or 12.6 days was 0.37 ± 0.02 percent per day, whereas the average rate over a period of 156.7 or 175.9 days was 0.20 ± 0.04 percent per day.

Table II-5

DECOMPOSITION OF PLUTONIUM HEXAFLUORIDE BY ITS ALPHA RADIATION

Spherical Vessels	Radius (cm)	Volume (ml)
Aluminum and Nickel	3.175	125.128
Pyrex	3.18	137.141
Quartz	3.04	119.122

Vessel Material	Test Temperature (C)	PuF_6 Pressure (mm Hg)	Initial Weight of PuF_6 (mg)	PuF_6 Decomposed (mg)	Decomposition (percent per day) (No. of days) 5.6	12.6	21.9	157.7	175.9
Nickel	26	50	115.6	4.8	-	0.33	-	-	-
Nickel	26	50	116.4	3.8	-	0.26	-	-	-
Nickel	27	50	116.7	23.8	-	-	-	0.13	-
Nickel	27	50	118.6	25.4	-	-	-	0.14	-
Nickel	27	80	194.0	49.1	-	-	1.15[a]	-	-
Nickel	26	100	233.3	4.8	0.37	-	-	-	-
Nickel	26	100	232.9	5.0	0.38	-	-	-	-
Nickel	26	100	234.8	9.6	-	0.32	-	-	-
Nickel	26	100	236.3	12.2	-	0.41	-	-	-
Nickel	27	100	236.4	49.5	-	-	-	0.13[b]	-
Nickel	26	100	229.4	99.2	-	-	-	-	0.25
Nickel	26	100	226.9	84.5	-	-	-	-	0.21
Nickel	82	94	192.6	39.2	-	-	0.97[c]	-	-
Nickel	82	797	1635.7	391.3	-	-	1.10[d]	-	-
Pyrex	26	100	260.9	156.3	-	-	-	-	0.34
Pyrex	26	100	253.6	153.6	-	-	-	-	0.34
Quartz	26	100	221.4	87.9	-	-	-	-	0.23
Quartz	26	100	216.4	88.0	-	-	-	-	0.23
Aluminum	27	75	181.7	47.5	-	-	1.19[a]	-	-
Aluminum	82	87	178.3	28.2	-	-	0.72	-	-
Aluminum	82	88	181.4	33.4	-	-	0.84	-	-
Aluminum	82	787	1615.7	287.0	-	-	0.81	-	-

[a] These anomalous results are unexplained at present.

[b] 156.7 days instead of 157.7 days.

[c] 21.0 days instead of 21.9 days.

[d] 21.8 days instead of 21.9 days.

The data also show that for nearly equal times the rate of decomposition was slightly higher for an initial plutonium hexafluoride pressure of 100 mm than for one of 50 mm. This was shown in the short-duration experiments in which the decomposition was 0.37 ± 0.02 percent per day for 100 mm and 0.30 ± 0.04 for 50 mm. The longer experiments, lasting 156.7 or 175.9 days, show a slight rate decrease from 0.20 ± 0.04 percent per day with 100 mm to 0.14 ± 0.01 percent per day for 50 mm initial plutonium hexafluoride pressure.

Decomposition occurred in quartz spheres (0.23 percent per day) at about the same rate as in nickel spheres (0.25 and 0.21 percent per day). Decomposition proceeded in Pyrex spheres at a higher rate (0.34 percent per day); this can be attributed to reaction of plutonium hexafluoride with Pyrex. Etching of the Pyrex, which indicates chemical reaction, was observed.

At 82 C the decomposition of gaseous plutonium hexafluoride in nickel vessels was faster (0.97 and 1.10 percent per day) than in aluminum vessels (0.72, 0.84, and 0.81 percent per day). Except for two anomalous results obtained at room temperature, the rates obtained at 82 C were higher than those obtained at room temperature. Decomposition in one nickel sphere and one aluminum sphere (which had been heated to 82 C and filled simultaneously from a common source of plutonium hexafluoride) amounted to 1.15 and 1.19 percent per day, respectively, at room temperature.

Unexpectedly, no dependence of decomposition rate on the initial plutonium hexafluoride pressure was observed at 82 C. This anomaly and the increase in decomposition rates which occurred upon raising the temperature to 82 C can be explained if thermal decomposition of the plutonium hexafluoride (which is independent of initial pressure) occurs in addition to radiation decomposition.

Future experiments will be designed to investigate the effect on decomposition rate of temperatures up to 120 C. Rates of thermal decomposition of plutonium hexafluoride have been investigated by Fischer, Trevorrow, and Shinn[23] at 140, 161, and 173 C. Experiments are being carried out to investigate the effects of the presence of foreign gases such as fluorine, oxygen, nitrogen, krypton, and helium on the rate of alpha decomposition of gaseous plutonium hexafluoride.

Decomposition of Plutonium Hexafluoride by Gamma Radiation
(M. J. Steindler and D. V. Steidl)

The volatility of plutonium hexafluoride is utilized in fluoride volatility processes to separate plutonium from most of the fission products. During the fluorination step and in subsequent operations, plutonium hexafluoride is exposed to radiation from fission products. A study of the decomposition of plutonium hexafluoride by gamma radiation has been undertaken to obtain information concerning the extent of decomposition, the products of decomposition, and the fundamental processes involved in the radiation chemistry of plutonium hexafluoride. The effect of various added gases on the decomposition is also being investigated. The available literature, the experimental procedures, and early results have been presented previously (see ANL-6477, p. 118; ANL-6596, p. 125). The decomposition of plutonium hexafluoride by gamma radiation likely to be encountered in a separation process is, on the basis of present data, unlikely to cause a serious practical problem.

Three additional experiments have been done on irradiation of plutonium hexafluoride without additives. These results, as well as those previously reported, are given in Table II-6 and are presented graphically

[23] Fischer, J., Trevorrow, L., and Shinn, W., J. Phys. Chem. 55, 1843 (1961).

in Figure II-3. An average G value* of 7.5 molecules of plutonium hexafluoride decomposed for each 100 ev of absorbed energy, in the range from zero to 3.73 x 10^{21} ev, appears to be well established by these data. The value of one standard deviation for G is 0.7.

Table II-6

DECOMPOSITION OF PLUTONIUM HEXAFLUORIDE BY GAMMA RADIATION

Average Gamma Energy:	0.75 Mev
Dose Rate:	1 x 10^4 to 4 x 10^4 rad/min
Temperature:	60 to 70 C
Plutonium Hexafluoride Pressure:	80 to 100 mm Hg at 25 C

Experiment	Initial PuF_6 (millimoles)	Absorbed Dose[a] (ev x 10^{-20})	PuF_4 Formed[b] (millimoles)	PuF_6 Lost[c] (millimoles)	G[d]
848F-177-13	0.279[e]	1.48	0.017	0.024	8.1
848F-177-14	0.323[e]	1.59	0.032	0.028	11
848F-187-15	0.302[e]	4.88	0.031	0.058	5.6
848F-187-13	0.315[e]	6.34	0.038	0.050	4.2
1199F-74	0.977	14.7	0.230	0.196	8.7
1026F-183	1.057[e]	18.8	0.285	0.275	9.0
1026F-157	1.113[e]	23.9	0.282	0.270	7.0
1026F-191	2.076[e]	31.2	0.372	0.333	6.8
1199F-51	0.992	35.6	0.490	0.505	8.4
1199F-59	0.953	37.3	0.370	0.404	6.2

[a] Determined from the Fricke dose and the ratio of electron densities of plutonium hexafluoride and water.

[b] By chemical analysis of the solid residue.

[c] By tensiometric methods.

[d] G value calculated by averaging the values for PuF_4 formed and PuF_6 decomposed.

[e] Presented previously (see ANL-6596, Table 23).

Figure II-3

DECOMPOSITION OF PLUTONIUM HEXAFLUORIDE BY GAMMA RADIATION

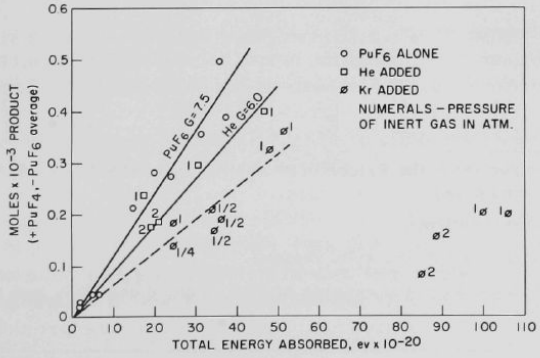

108-6526

*Molecules decomposed per 100 ev of absorbed energy.

Results of two further experiments on irradiation of mixtures of plutonium hexafluoride and helium have affirmed the expected slight effect (see ANL-6596, p. 127) of helium on the extent of decomposition of plutonium hexafluoride. The decomposition rate with two atmospheres of helium added (see Table II-7) is substantially the same as the rate with one atmosphere of helium added, when energy absorption in the helium is included in the calculation of G. An average G value of 6.0 has been obtained for plutonium hexafluoride decomposition in the presence of helium from zero to 4.67×10^{21} ev of absorbed energy (see Table II-7 and Figure II-3).

Table II-7

DECOMPOSITION OF PLUTONIUM HEXAFLUORIDE BY GAMMA RADIATION IN THE PRESENCE OF INERT GASES

Average Gamma Energy: 0.75 Mev
Dose Rate: 1×10^4 to 4×10^4 rad/min
Temperature: 60 to 70 C
Plutonium Hexafluoride Pressure: 80 to 100 mm Hg at 25 C

Experiment	Initial PuF_6 (millimoles)	Inert Gas (millimoles)	Absorbed Dose[a] (ev x 10^{-20}) In PuF_6	In Inert Gas	Total	PuF_6[b] Lost (millimoles)	PuF_4[c] Formed (millimoles)	G[d]
1199F-7	1.073[e]	8.132 He	15.6	1.8	17.4	0.252	0.222	8.2
1199F-40	0.964	8.133 He	26.7	3.7	30.4	0.299	0.291	5.9
1199F-49	0.935	8.298 He	40.5	6.2	46.7	0.361	0.436	5.1
1199F-10	1.097[e]	17.29 He	16.8	4.0	20.8	0.184	0.183	5.3
1199F-34	1.035[e]	17.16 He	15.6	3.7	19.3	0.150	0.203	5.5
1199F-101	1.000	2.376 Kr	15.1	9.4	24.5	0.138	f	3.4
1199F-99	1.011	4.782 Kr	14.9	19.2	34.1	0.210	f	3.7
1199F-70	0.984	4.753 Kr	14.8	19.7	34.5	0.195	0.141	2.9
1199F-94	1.042	5.408 Kr	15.0	21.1	36.1	0.190	f	3.2
1199F-97	0.999	8.402 Kr	7.5	17.0	24.5	0.181	f	4.5
1199F-15	1.074[e]	8.146 Kr	15.1	32.9	48.0	0.315	0.332	4.0
1199F-30	1.006[e]	9.238 Kr	13.8	37.5	51.3	0.346	0.352	5.0
1199F-90	1.008	8.635 Kr	29.7	70.4	100	0.219	0.185	1.2
1199F-103	1.023	8.429 Kr	32.8	73.5	106	0.198	f	1.1
1199F-42	1.026	16.86 Kr	16.8	68.5	85.1	0.039	0.124	0.6
1199F-62	0.998	17.64 Kr	15.4	73.1	88.5	0.163	0.144	1.0

[a] Dose determined from the Fricke dose and the ratio of electron densities of plutonium hexafluoride and water.

[b] By tensiometric methods.

[c] By chemical analysis of the solid residue.

[d] G value calculated from the average of PuF_4 formed and PuF_6 lost and the total absorbed energy.

[e] Presented previously (see ANL-6596, Table 24).

[f] Analytical results not available. G calculated from PuF_6 loss only.

When mixtures of krypton and plutonium hexafluoride are irradiated, the relationship of decomposition to absorbed dose is again linear ($G \cong 3.8$) up to approximately 5×10^{21} ev absorbed dose and krypton pressures to one atmosphere (see Table II-7 and Figure II-3). In two experiments with one atmosphere of krypton added, absorbed energies of approximately 1×10^{22} ev gave G values of approximately 1. In two experiments with two atmospheres of krypton added, an absorbed dose of approximately 8.5×10^{21} ev also gave G values close to 1. At present, the results may be explained on the basis of several competing excitation and quenching reactions which are to be defined and evaluated in future experiments to be performed with intermediate values of both krypton pressure and total dose.

The behavior of plutonium hexafluoride with added fluorine or oxygen is important since both fluorine and oxygen will be present in the gas stream from the fluorinator in the Direct Fluorination Process. Three experiments with fluorine added to plutonium hexafluoride and three additional experiments with oxygen added to plutonium hexafluoride have been performed. The results are reported in Table II-8. The experiments with fluorine added to plutonium hexafluoride, in which the total absorbed dose was 6.86×10^{21} ev, resulted in no significant increase in decomposition compared with two experiments in which similar samples were not irradiated but were held at the temperature of irradiation (60-70 C) for 7 or 10 days. The experiments with oxygen added showed the same lack of effect of irradiation when a comparison was made with experiments in which the samples were not irradiated. In view of the possible chemical reactions of oxygen with plutonium hexafluoride and the reaction of fluorine with the plutonium tetrafluoride product of the decomposition (whose rate is likely increased by radiation), these experiments are not directly comparable with those with plutonium hexafluoride alone. The results do, however, demonstrate that increased stability can be expected of plutonium hexafluoride in process gas streams containing fluorine or oxygen. The discrepancies observed between the amount of plutonium hexafluoride lost and the amount of plutonium tetrafluoride formed are believed to be due to experimental error although, in the case of experiments with oxygen, the nature of the solid compound has not been established.

The Reaction of Plutonium Hexafluoride and Calcium Fluoride

(M. J. Steindler and D. V. Steidl)

Owing to the importance of the chemistry of plutonium hexafluoride to the development of fluoride volatility processes, a brief investigation of the reaction of plutonium hexafluoride and calcium fluoride is reported. The purpose of the experiment was to determine if calcium

fluoride readily forms a stable complex with plutonium hexafluoride. Cathers and Jolley[24] have indicated that plutonium hexafluoride, unlike uranium hexafluoride, forms a complex with calcium fluoride.

Table II-8

DECOMPOSITION OF PLUTONIUM HEXAFLUORIDE BY GAMMA RADIATION IN THE PRESENCE OF OXYGEN OR FLUORINE

Average Gamma Energy: 0.75 Mev
Dose Rate: 1×10^4 to 4×10^4 rad/min
Temperature: 60-70 C
Plutonium Hexafluoride Pressure: 80-100 mm Hg at 25 C

Experiment	PuF_6 Initial (millimoles)	Inert Gas (millimoles)	Absorbed Dose[a] (ev x 10^{-20}) In PuF_6	In Inert Gas	Total	PuF_6[b] Lost (millimoles)	PuF_4[c] Formed (millimoles)
1199F-38[d]	0.972	7.870 O_2	-	-	-	0.156	0.114
1199F-47[d]	0.961	8.311 O_2	-	-	-	0.079	0.035
1199F-36	1.020[e]	7.958 O_2	15.9	14.3	30.2	0.075	0.039
1199F-20	1.088[e]	8.676 O_2	16.7	15.7	32.4	0.154	0.063
1199F-68	1.113	17.32 O_2	33.0	62.1	95.1	0.186	0.123
1199F-88[d]	1.012	8.191 F_2	-	-	-	0.105	0.079
1199F-92[f]	1.000	7.780 F_2	-	-	-	0.097	g
1199F-83	1.039	8.983 F_2	32.2	36.4	68.6	0.107	0.040

[a]Dose determined from Fricke dose and the ratio of electron densities of plutonium hexafluoride and water.

[b]By tensiometric methods.

[c]By chemical analysis of solid residue.

[d]Held for 7 days at 60-70 C without irradiation.

[e]Presented previously (see ANL-6596, Table 24).

[f]Held for 10 days at 60-70 C without irradiation.

[g]Analytical results not available.

A 0.3937-g sample of powdered, reagent-grade calcium fluoride was prefluorinated at 80 C for 17 hr in the presence of fluorine at 1000 mm Hg. (A sample of CaF_2 dried at 120 C overnight in helium had a specific surface area of 12.7 m^2/g.) The fluorine was pumped off at room temperature, and 0.4194 g plutonium hexafluoride was distilled onto the calcium fluoride. Plutonium hexafluoride was in contact with calcium fluoride at room temperature in a 20-ml nickel test tube for one hour, during which

[24]Cathers, G. I., and Jolley, R. L., Recovery of PuF_6 by Fluorination of Fused Fluoride Salts, ORNL-3298 (1962).

time the mixture was shaken at intervals. Both solid and gaseous plutonium hexafluoride were present. After one hour, the plutonium hexafluoride was pumped off at room temperature (to a pressure of $\sim 2.5 \times 10^{-4}$ mm) and the calcium fluoride was removed from the tube and assayed for its plutonium content.

Owing to the anticipated difficulty in dissolving calcium fluoride, a scan of the entire solid sample was made for gamma activity. Results indicated intense activity at 17 kev, the gamma energy usually used for plutonium determination in solid samples. Further investigation indicated that most of the gamma activity should be assigned to U^{237}, although some 17-kev activity was not accounted for by this procedure. Further analysis by aqueous chemical means revealed that a small amount of plutonium (equivalent to 3 mg PuF_6) was present in the sample.

A number of interesting observations were made in this experiment. The amount of plutonium hexafluoride (0.7 percent of the initial material or 3 mg) which remained in the calcium fluoride was small, indicating that no stable complex between calcium fluoride and plutonium hexafluoride under the conditions of the experiment was formed. However, it is possible that a compound can be formed whose decomposition pressure is high. Further, the hazard of using gamma counting to assay a sample of this type is indicated by the fact that, as in this instance, the 17-kev gamma activity could also be assigned to U^{237} as well as to Pu^{239}. The quantity of U^{237} was very small ($\sim 10^{-10}$ g), indicating that, although uranium hexafluoride does not form a complex with calcium fluoride, adsorption of uranium hexafluoride on calcium fluoride takes place readily. This fact suggests that it might easily be possible for trace quantities of plutonium hexafluoride to be adsorbed on calcium fluoride without formation of a complex.

Examination of the data of Cathers and Jolley[24] indicates that the surface area of the calcium fluoride used by them could easily accommodate the plutonium hexafluoride available in their experiments by an adsorption mechanism. The total quantity of plutonium hexafluoride (0.1 mg) was small. Calculations indicate that all of the available plutonium hexafluoride could be accommodated on 0.6 percent of the available surface area of the calcium fluoride as adsorbed plutonium hexafluoride, and thus complex formation need not be postulated. However, it is also true that if the decomposition pressure of a plutonium hexafluoride-calcium fluoride complex were high at room temperature, the complex might possibly have been dissociated in our experiment by evacuation at room temperature.

B. Engineering-scale Investigation of Fluoride Volatility Process
(A. A. Jonke)

1. Direct Fluorination of Uranium Dioxide Fuel
(W. J. Mecham, L. Anastasia, J. D. Gabor, R. Kinzler, A. Rashinskas, and J. Wehrle)

In the Direct Fluorination Process, uranium and plutonium dioxides from discharged reactor fuel are reacted with fluorine to produce the hexafluorides, which are then decontaminated by volatility techniques. The fluorination is carried out in a packed fluidized-bed reactor, in which the packed section is formed by uranium dioxide pellets. Alumina grain is used to fill the voids in the uranium dioxide pellet bed and to form a fluidized bed above the pellets. Development studies on an engineering scale have thus far been directed toward process optimization of the primary fluorination of uranium dioxide pellets. The major objectives of these studies have been to demonstrate short-time batch fluorination (less than 20 hr) and satisfactory fluorine utilization efficiencies (greater than 75 percent). Currently, emphasis has been placed on the evaluation of a two-zone oxidation-fluorination technique that is carried out in a single vessel.

In the two-zone method of operation, a mixture of oxygen and nitrogen is used to oxidize the pellets to uranosic oxide (U_3O_8) fines (~20μ in diameter) which have a high specific surface area. The fines are formed in the uranium dioxide pellet zone (oxidation zone) and are carried to the upper fluidized bed of alumina (fluorination zone), where they react with fluorine to produce uranium hexafluoride. The fluorine is admitted to the upper fluidized zone at a point which is just above the pellet bed. The two-zone method of operation offers several advantages over the single-zone method. One advantage is that caking due to solids formation by the reaction of uranium hexafluoride with uranium oxides is minimized. Another advantage is that the quality of fluidization in the upper (fluorination) zone is improved by the absence of uranium dioxide pellets. Thus, fluorination of U_3O_8 fines (ΔH = -231 kcal/mole uranium at 25 C) takes place in the upper, unhindered fluidized bed where high rates of heat removal are more easily achieved, and the oxidation reaction (ΔH = -25 kcal/mole uranium at 25 C) takes place in the pellet zone where lower rates of heat removal are obtained.

In the initial two-zone run (UOF-61), a 12-in. bed of pellets was fluorinated at an average production rate of 33 lb UF_6/(hr)(sq ft) (see ANL-6596, p. 142). A second run, UOF-62, was made under generally similar conditions, but the superficial gas velocity was lowered. The lower gas velocity caused an accumulation of fines in the pellet zone (see ANL-6596, p. 145). Attention, therefore, was directed toward methods of reducing oxidation rates and improving fines transport from the pellet

zone. Lowering of the temperature in the pellet oxidation zone reduced the oxidation rate in runs UOF-63 and UOF-64 (see ANL-6648, p. 137). In these runs the upper part of the reactor was heated and the bottom flange of the reactor was cooled by ambient air so that a longitudinal temperature gradient was established in the pellet bed. The (upper) fluorination zone was maintained at 525 to 550 C, while the (lower) oxidation zone ranged from 400 C near the top of the pellet bed to 140 C at the bottom. These temperatures were measured by means of thermocouples located at various levels in a vertical thermowell which passed through the pellet bed. Previous tests have shown that pellet temperature is not substantially different from the temperature of the fluidized material in the voids when good fluidization is maintained.

With this technique higher oxygen concentrations (18 to 31 percent in nitrogen as compared with 4 to 8 percent) could be used to produce most of the oxide fines near the top of the oxidation zone. It is believed that oxidation of the pellets near the top of the oxidation zone facilitated the transport of uranium oxide (U_3O_8) fines to the upper (fluorination) zone. In Runs UOF-63 and -64, overall production rates of about 34 lb UF_6/(hr)(sq ft reactor cross section) and overall fluorine efficiencies of about 51 percent were obtained. Higher rates and efficiencies were achieved in major portions of each of these batch runs. These results and the generally satisfactory operational performance indicated that short processing time with satisfactory fluorine efficiency and freedom from caking could be achieved with the two-zone scheme of operation.

Two-zone Operation with Temperature Gradients and Gas Pulsing

During this quarter, a series of two-zone oxidation-fluorination runs (UOF-65, UOF-66, and UOF-67) have been made to evaluate the effects of gas pulsing and longitudinal temperature gradients in the pellet-bed (oxidation) zone as methods of improving rapid transport of fines from the oxidation zone to the fluorination zone. A schematic diagram of the gas-pulsing apparatus and of the fluid bed reactor arrangement for two-zone operation is shown in Figure II-4.

Operational difficulties were encountered in these runs because of the formation of an excessive quantity of uranium oxide fines. This led to a termination of the runs before their completion. In Run UOF-66, the production of an excessive amount of fines resulted in the formation of intermediate fluoride compounds and in the accumulation of fines on the cone of the disengaging section of the fluid-bed reactor. In Runs UOF-65 and UOF-67, the accumulation of fines at the fluorine inlet resulted in the formation of a plug in the fluorine inlet line. The three runs differed from previous thermal-gradient fluorination runs in two respects: (a) Blue

Label Alundum* (a high-purity grade), rather than the Type 38 Alundum used formerly, was used in Run UOF-65 and subsequent runs, and (b) pulsing was used in Run UOF-66 and subsequent runs. The operating conditions and the results of Runs UOF-65, UOF-66, and UOF-67 are given in Table II-9.

Figure II-4

SCHEMATIC DIAGRAM OF APPARATUS FOR PULSING OF GAS TO FLUORINATOR IN TWO-ZONE OPERATION

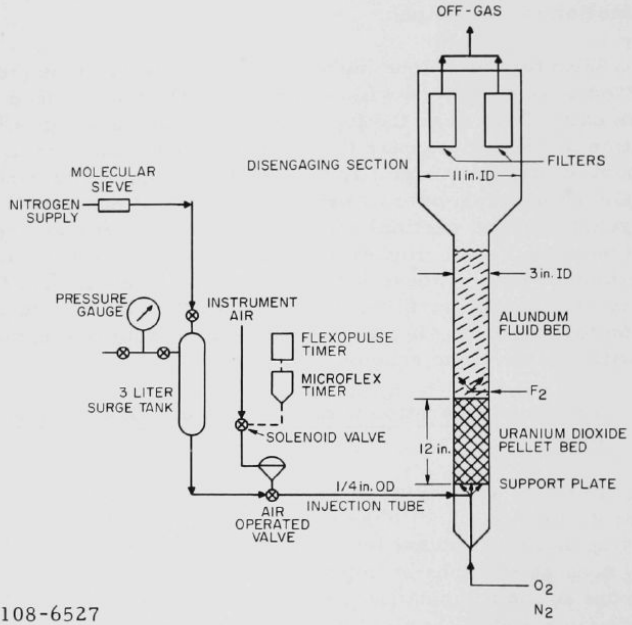

For Run UOF-65, with the fluid bed at 500 C, a temperature gradient was established in the pellet bed such that the top layer of pellets was at 390 C and the bottom of the pellet bed was at 310 C. This thermal gradient was poor when compared with gradients obtained in previous runs (see ANL-6648, p. 137), in which the temperature of the upper layer was about 400 C and that of the bottom was about 140 C. The major significance of the difference in these temperature gradients is that in Run UOF-65 the average temperature of the oxidation zone was higher, and this higher temperature caused more rapid oxidation and higher rates of production of U_3O_8 fines. High concentrations of these fines tend to lower the rates of heat transfer, and thus may have been responsible for the failure to achieve

*A product of the Norton Company, Worcester, Mass.

the desired temperature gradients of the bed in the longitudinal direction. The large-size Alundum used in this run is also less favorable for high-quality fluidization in a bed with a high concentration of fines. The poor gradient may have been caused by the larger size Alundum grains present in the as-purchased Blue Label Alundum. Particle size distributions for the mixtures of Alundum used in these two-zone oxidation-fluorination runs are shown in Figure II-5. Thus, in Run UOF-65, the excessive production of fines is attributed to the use of 23 percent oxygen in nitrogen combined with the rather high initial temperatures of the pellets. The plugging of the fluorine inlet is attributed to the introduction of fluorine in an undiluted stream and to the high concentration of fines present in the fluid bed.

Table II-9

OPERATING CONDITIONS AND RESULTS FOR TWO-ZONE OXIDATION-FLUORINATION OF URANIUM DIOXIDE PELLETS WITH A THERMAL GRADIENT THROUGH THE PELLET BED

Weight of Pellets: 8.8 kg
Pellet Bed Height: 12 in.

	UOF-65	UOF-66	UOF-67
Blue Label Alundum Charge:			
Weight (kg)	8.1	8.1	6.1
Static Height above Pellets (in.)	24	24	16
Size Limit (US mesh)	-40 +120	-40 +170	-40 +170
Pulsing Conditions			
Pressure (psig)	-	20	20
Duration (sec)	-	0.3	0.04
Frequency (pulses/min)	-	1, 2, and 6	2
Oxidation Zone			
Pellet Bed Thermal Gradient (C)	390-310	395-260[a]	400-260
Comments	Poor; Temperature too high	Satisfactory without pulsing	Satisfactory with pulsing
Gas Flow (cfm at 25 C and 1 atm)	1.3	1.3	1.0
Oxygen Concentration in Nitrogen (percent)	23	22	20
Fluorination Zone			
Temperature (C)	500	500[a]	500
Total Gas Flow (cfm at 25 C and 1 atm)	1.4	1.4	1.1
Fluorine Concentration (percent)	12	6.8	11
Superficial Velocity at 500 C (ft/sec)	1.2	1.2	1.0
Run Duration (hr)	7.5	13.5	1.5
Maximum UF_6 Production Rate lb/(hr)(sq ft)	30	31	13
Operational Difficulty	F_2 inlet plugged	Intermediate fluoride compound formation	F_2 inlet plugged
Cause of Run Stoppage	Excessive U_3O_8 Fines	Fines accumulation in disengaging section	Excessive U_3O_8 Fines

[a]Temperature of fluorination zone decreased to 450 C and thermal gradient changed to 440 to 380 C when pulsing was started.

For Run UOF-66, the Blue Label Alundum mixture was formulated to approximate the particle size distribution of Type 38 Alundum (see Figure II-5). A satisfactory temperature gradient of 395 to 260 C was established in the pellet bed at the beginning of the run. However, the starting of the gas pulsing appeared to disrupt the temperature gradient and the desired gradient was not re-established. Also, the temperature in

the fluorination zone decreased from 500 C to 450 C as a result of the gas pulsing. The combination of a reduced fluorination temperature and an increased oxidation temperature (see Table II-9) resulted in increased formation and accumulation of oxide fines in the pellet-bed zone and the formation of intermediate uranium fluorides (mostly UO_2F_2) in the fluorination zone. The entire pellet bed was oxidized during the run, but about 40 percent of the initial charge had accumulated on the cone of the disengaging section in the form of uranyl fluoride and uranosic oxide fines. This rather high accumulation of fines is attributed in part to the introduction of relatively large quantities of pulse gas (about 0.04 cu ft of nitrogen with each 0.3-sec pulse). The temperature of 200 C in this portion of the disengaging section was too low to allow removal of this material by fluorination. External vibration of the column was not used to return the uranium fines to the reactor proper.

Figure II-5

PARTICLE SIZE DISTRIBUTION OF NORTON ALUNDUM MIXTURES USED IN URANIUM DIOXIDE PELLET OXIDATION-FLUORINATION RUNS

Symbol	Alundum Grade	Composition (w/o)	Nominal Particle Size (U. S. Mesh)	Maximum Size Range (U. S. Mesh)	Used in Runs
○	Type 38	100	54-100	-40 +170	Prior to UOF-65
□	Blue Label	50 50	60 90	-40 +120	UOF-65
◇	Blue Label	32 56 22	60 90 120	-40 +170	UOF-66 to UOF-69

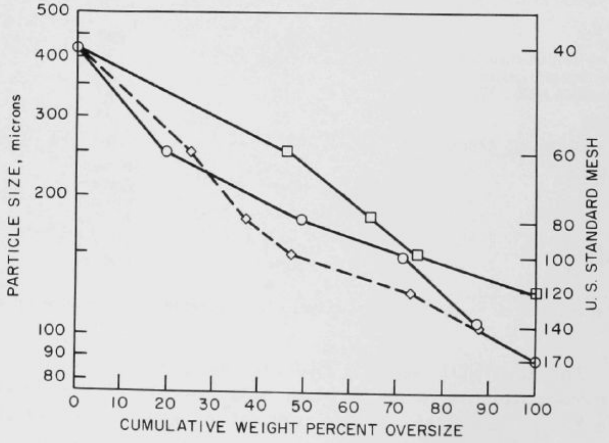

108-6528

In Run UOF-67, the pulse duration was reduced from 0.3 to 0.04 sec (through use of a Microflex* reset timer). Pulsing of the pellets was started before the reactor reached operating temperatures, and no difficulties were encountered with the thermal gradient through the pellet bed. The Alundum bed height was decreased from 24 to 16 in. to increase the freeboard above the fluid bed in an effort to reduce fines elutriation to the fluorinator disengaging section. The use of 20 percent oxygen in nitrogen, which produced uranosic oxide fines at a rapid rate, and the improved fines transport from the pellet bed, which was brought about by the pulsing operation, resulted in an accumulation of an excessive amount of oxide fines in the fluorination zone and caused the fluorine inlet to plug after 1.5 hr of operation.

Although Runs UOF-65, -66, and -67 were not carried to completion, they served to provide information on operating conditions:

1. In these runs oxidation rates were too high, leading to excessive concentrations of fines. In Runs UOF-65 and -66 this was shown by poor temperature control resulting from poor quality of fluidization.

2. Pulse gas rate was too high in Run UOF-66, resulting in excessive lowering of the temperature for the fluorination. However, the pulse gas rate appeared satisfactory in Run UOF-67.

3. The introduction of undiluted fluorine into the upper (fluorination) zone in these runs (with high concentrations of uranium fines) led to plugging of the inlet line. Plugging is circumvented by dilution of the fluorine with nitrogen or oxygen prior to admission of the gas to the fluorination zone.

Two-zone Reactor Operation with Gas Pulsing and Dilution of Inlet Fluorine

On the basis of the experience gained in the runs described in the previous section, two runs (UOF-68 and UOF-69) were made in which relatively low concentrations of oxygen (4.5 and 6.0 percent in nitrogen) were used in the oxidation zone. In these runs, no attempt was made to establish or to maintain a definite temperature gradient in the pellet bed. In addition, the fluorine admitted to the reactor was diluted by partial recycle of the process off-gas at a constant recycle rate of 0.25 cfm. Off-gas recycle was used in this instance primarily to maintain adequate gas velocity in the fluorine-injection tube to the reactor and not as a means of increasing fluorine efficiency, since less than 20 percent of the off-gas was recycled.

*Product of Eagle Signal Company, Moline, Illinois.

In Run UOF-68, the effect of fluorine input rate, gas pulse pressure and external column vibration was determined by the response in the production rate for uranium hexafluoride. External vibration of the column was used to return fines from the disengaging section to the fluorination zone. The fluidizing gas in the oxidation zone contained 4.5 percent oxygen in nitrogen. The operating conditions and the production rates for uranium hexafluoride for Run UOF-68 are given in Table II-10 and Figure II-6. As these data indicate, the fluorination of the 12-in. bed of pellets was carried to completion with very promising results.

Table II-10

OPERATING CONDITIONS AND RESULTS FOR RUN UOF-68, A TWO-ZONE OXIDATION-FLUORINATION OF URANIUM DIOXIDE PELLETS WITH GAS PULSING

UO_2 Pellet Charge:	Weight: 8.8 kg Bed height: 12 in.
Alundum Charge:	Weight: 7.1 kg Static height above pellets: 20 in. Size limits (U. S. mesh): -40 +170
Temperatures:	Fluorination zone (Alundum): 500 C Oxidation zone (pellets): $310 \leqslant T \leqslant 490$ C
Pulsing Conditions:	Duration: 0.04 sec Frequency: 2 pulses/min
Oxygen Diluent:	Nitrogen
Fluorine Diluent:	Process off-gas (0.25 cfm)
Run Time:	15 hr
Overall Fluorine Efficiency:	64.5%

Major Periods[a] (hr)	Gas Flow: Oxidation Zone Total (cfm)	Gas Flow: Oxidation Zone O_2 (%)	Gas Flow: Fluorination Zone Total (cfm)	Gas Flow: Fluorination Zone Average F_2 in Reactor (%)	Average F_2 in Off-gas (%)	Gas Pulse Pressure (psig)	External Column Vibration	Average Fluorine Utilization Efficiency[b] (%)	Average UF_6 Production Rate [lb/(hr)(sq ft)]
3-8.5	0.9	4.5	1.3	12.6	3.0	15	No	60.5	35
9.5-11	0.9	4.5	1.3	14.3	0	20	No	100	73
12-13	0.9	4.5	1.4	14.3	0	20	Yes	>100[c]	97

[a]These are the major periods of stable operating conditions. Start-up and transition periods are not shown because they do not describe typical behavior.

[b]Fluorine efficiency $= 100\left[\frac{3\ (\text{mole } UF_6 \text{ produced/hr})}{(\text{mole } F_2 \text{ fed/hr})}\right]$

[c]The greater than 100% efficiency is attributed to the accumulation of intermediate fluoride compounds in the preceding period.

The initial period of fluorination proceeded smoothly with a gas-pulse manifold pressure of 15 psig, and resulted in an average uranium hexafluoride production rate of 35 lb UF_6/(hr)(sq ft) and an average fluorine utilization efficiency of 60.5 percent. When the gas-pulse pressure was increased to 20 psig after 8.5 hr of operation (see Figure II-6), the uranium hexafluoride production rate increased to 73 lb UF_6/(hr)(sq ft) at a fluorine utilization efficiency of 100 percent. When external column vibration was begun after 12 hr of operation, a further increase in the uranium hexafluoride production rate, to 97 lb UF_6/(hr)(sq ft), was obtained. Since external vibration of the column is effective in returning accumulated fines from the disengaging section to the fluorination zone, it was concluded that fines had been elutriated from the fluid bed. The fluorine efficiency to form uranium hexafluoride was greater than 100 percent during the

first hour of column vibration, according to the overall reaction $U_3O_8 + 9\ F_2 \rightarrow 3\ UF_6 + 4\ O_2$. This was an indication that the accumulated fines contained significant quantities of intermediate uranium fluoride compounds. Since the average production rate for uranium hexafluoride doubled in response to an increase in the manifold pulse pressure (from 15 to 20 psig), this was also an indication that the transport of oxide fines from the oxidation zone had increased.

Figure II-6

FLUORINE INPUT RATES AND URANIUM HEXAFLUORIDE PRODUCTION RATES DURING RUN UOF-68, A TWO-ZONE OXIDATION-FLUORINATION OF URANIUM DIOXIDE PELLETS WITH GAS PULSING

Pulse Duration: 0.04 sec
Pulse Frequency: 2/min

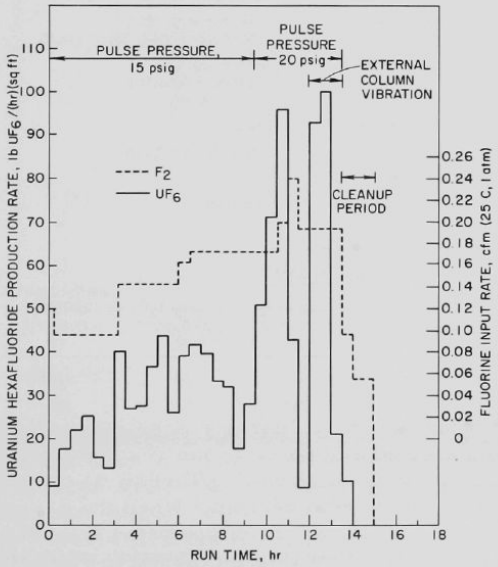

108-6529

The entire batch of uranium dioxide pellets (8.8 kg) was fluorinated in 15 hr. The initial 13.5 hr of operation were carried out with fluorine which was diluted by means of partial recycle of the process off-gas (0.25 cfm). During this period of operation, the average fluorine utilization efficiency to form uranium hexafluoride was 66.5 percent. During

the final 1.5 hr of operation, the Alundum fluid bed was cleaned up with fluorine (enriched to nearly 100 percent fluorine). Total off-gas recycle was used to conserve fluorine losses; however, the cleanup step reduced the overall fluorine efficiency for the run (UOF-68) to 64.5 percent.

In Run UOF-69 the operating conditions (see Table II-11) were similar to those for Run UOF-68. However, the oxygen concentration was increased from 4.5 to 6 percent in nitrogen and the manifold pulse pressure was 20 psig. The operating conditions and the uranium hexafluoride production rates for Run UOF-69 are shown in Table II-11 and Figure II-7.

Table II-11

OPERATING CONDITIONS AND RESULTS FOR RUN UOF-69, A TWO-ZONE OXIDATION-FLUORINATION OF URANIUM DIOXIDE PELLETS WITH GAS PULSING

UO_2 Pellet Charge:	Weight: 8.8 kg Bed height: 12 in.
Alundum Charge:	Weight: 7.1 kg Static height above pellets: 20 in. Size limits (U. S. mesh): -40 +170
Temperatures:	Fluorination zone: 500 C Oxidation zone (pellets): 340 ≤ T ≤ 480 C
Pulsing Conditions:	Duration: 0.04 sec Frequency: 2 pulses/min Pressure: 20 psig
Oxygen Diluent:	Nitrogen
Fluorine Diluent:	Process Off-gas (0.25 cfm)
Run Duration:	12.5 hr
Overall Fluorine Efficiency:	72.5 percent

	Gas Flow						
	Oxidation Zone		Fluorination Zone				
Major Periods[a] (hr)	Total (cfm)	O_2 (%)	Total (cfm)	Average F_2 to Reactor (%)	Average F_2 in Off-gas (%)	Average Fluorine Utilization Efficiency[b] (%)	Average UF_6 Production Rate [lb/(hr)(sq ft)]
1-4.5	0.9	6.0	1.3	12.0	2.4	59.8	33
5.5-9	0.9	6.0	1.4	16.6	0	100	86

[a]These are the major periods of stable operating conditions. Start-up and transition periods are not shown because they do not describe typical behavior.

[b]Fluorine efficiency $= 100\left[\frac{3 \text{ (mole } UF_6 \text{ produced/hr)}}{\text{(mole } F_2 \text{ fed/hr)}}\right]$

The use of external column vibration early in the run (in the period from 4.0 to 5.5 hr; see Figure II-7) increased the production rate for uranium hexafluoride from 35 to 45 lb UF_6/(hr)(sq ft) for a period of one hour, which indicated that little or no accumulation of fines occurred in the disengaging section of the column. The use of external column vibration after the period (from 5.5 to 9.0 hr) of very high production rate [86 lb UF_6/(hr)(sq ft)] again indicated no accumulation of fines.

Figure II-7

FLUORINE INPUT RATES AND URANIUM HEXAFLUORIDE PRODUCTION RATES DURING RUN UOF-69, A TWO-ZONE OXIDATION-FLUORINATION OF URANIUM DIOXIDE PELLETS WITH GAS PULSING

Pulse Pressure: 20 psig
Pulse Duration: 0.04 sec
Pulse Frequency: 2/min

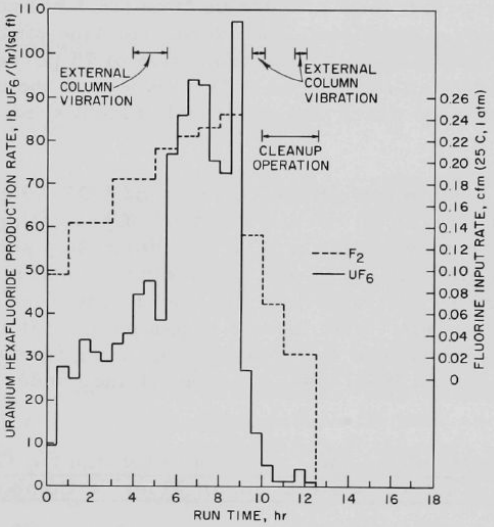

108-6530

During the period of 1 to 4.5 hr of operation in Run UOF-69, both the production rate for uranium hexafluoride [33 lb UF_6/(hr)(sq ft)] and the average fluorine utilization efficiency to form uranium hexafluoride (59.8 percent) was slightly higher than that for a similar period in Run UOF-68 (see Figures II-6 and II-7). However, in Run UOF-69, during the period from 5.5 to 9.0 hr, very high production rates for uranium hexafluoride were achieved, which averaged 86 lb UF_6/(hr)(sq ft) and reached a maximum of 107 lb UF_6/(hr)(sq ft) during the eighth hour of operation. These rates were accomplished without the use of external column vibration and at 100 percent average fluorine utilization efficiency to form uranium hexafluoride. Fluorine input to the reactor was not increased during this period because of brief (5-min) periods of local temperature rise (and return) at a thermowell located just above the fluid bed. Five of these temperature pulses, which reached a maximum temperature of 690 C, were recorded during the period from 6.5 to 7.5 hr.

In this run (UOF-69), the overall processing time for the 12-in. bed of pellets (8.8 kg) was 12.5 hr. The reaction was essentially complete in 10 hr of operation. During this period, an average fluorine utilization efficiency to form uranium hexafluoride of 74.9 percent was achieved with once-through gas flow and with dilution of the inlet fluorine by a partial off-gas recycle (0.25 cfm). During the additional 2.5 hr of operation, the Alundum bed was cleaned up with fluorine (enriched to nearly 100 percent fluorine) by means of total off-gas recycle. This cleanup step reduced the overall fluorine efficiency for Run UOF-69 to 72.5 percent.

For complete fluorination of a 12-in. bed of pellets, Run UOF-69 established the shortest total processing time (12.5 hr) yet achieved in these fluorination studies. In addition, the overall fluorine efficiency of 72.5 percent approached the current process objective of 75 percent, and uranium hexafluoride production rates were well in excess of the nominal objective of 50 lb UF_6/(hr)(sq ft) which was previously established with a 6-in. bed of pellets.

The results from Runs UOF-68 and UOF-69 give further evidence that gas pulsing is an effective method of promoting fines transport from the oxidation zone (pellet bed) to the fluorination zone. The simplicity of a gas-pulsing method also makes this method of obtaining satisfactory fines transport more desirable than the use of controlled temperature gradients in the reactor. With the use of gas pulsing, it appears that the major process objectives of short batch processing time with high fluorine efficiency and freedom from caking can be attained under practical operating conditions.

Analysis of the Two-zone Operation and the Control of Formation of Intermediate Uranium Fluoride Compounds

In the fluorination of uranium dioxide pellets by the two-zone method of oxidation-fluorination, uranium hexafluoride is produced from uranosic oxide fines which are formed in the pellet bed (oxidation zone). The fines are transported from this zone to the upper fluidized zone where they are reacted with fluorine. It is evident, therefore, that the rate of uranium hexafluoride production is dependent upon the rates of oxidation and fines transport from the pellet bed. If the rate of fines transport remains constant, sufficient fluorine can be introduced to the fluorination zone to prevent an accumulation of intermediate fluoride compounds of uranium. However, if the quantity of uranosic oxide fines in the fluorination zone is suddenly increased, fluorine input must also be increased to prevent formation of the intermediate fluorides which may be formed by the following reactions:

$$U_3O_8(s) + 3\ F_2(g) \rightarrow 3\ UO_2F_2(s) + O_2(g) \qquad (1)$$

and

$$U_3O_8(s) + 2\ UF_6(g) \rightarrow 4\ UO_2F_2(s) + UF_4(s) \qquad (2)$$

The formation of solid fines by these reactions may increase the quantity of fines in the fluid bed to the point of lowered fluidization quality (see ANL-6596, p. 100) and higher elutriation of fines to the disengaging section of the reactor column. When sufficient amounts of fluorine are present in the fluid bed, fines accumulation is prevented by reaction of the intermediate fluoride compounds of uranium to uranium hexafluoride according to the following equations:

$$UF_4(s) + F_2(g) \rightarrow UF_6(g) \quad (3)$$

$$UO_2F_2(s) + 2\ F_2(g) \rightarrow UF_6(g) + O_2(g) \quad . \quad (4)$$

The overall fluorination reaction represented by Equations (1) through (4) is given by

$$U_3O_8(s) + 9\ F_2(g) \rightarrow 3\ UF_6(g) + 4\ O_2(g) \quad . \quad (5)$$

Operationally, several alternative means are available to test whether formation of intermediate fluoride compounds is taking place. The rate of uranium hexafluoride production at constant fluorine input can provide an indication of net buildup of intermediate fluoride compounds in two ways: (a) If the rates of formation of intermediate compounds are relatively high, and fluorine input is the rate-controlling step for the overall process, an increase in the fluorine input will provide an increase in uranium hexafluoride production rate according to Equations (3) and (4). (b) However, if the amount of intermediate fluorides formed is relatively small and the formation of these compounds is the rate-controlling step, the rate of uranium hexafluoride production will increase slightly or not at all in response to the increased fluorine input. A second method of following the reaction is by comparison of the fluorine efficiency to form the hexafluoride and the overall fluorine efficiency (total fluorine consumption in the reactor). Net intermediate fluoride formation would be indicated by an excess of the overall fluorine efficiency over the efficiency to form uranium hexafluoride.

These operational analyses were carried out in the operation of Runs UOF-68 and -69, and the actual program of increased fluorine input for these runs is shown in Figures II-6 and II-7. In general, the fluorine rate increases and the fluorine efficiencies indicated that formation of intermediate fluoride compounds was not significant during the early portions of the runs. This condition was maintained during the batch runs by providing higher fluorine-input rates whenever the above tests gave positive indications of intermediate fluoride formation or whenever uranium hexafluoride production showed a sudden increase.

With the present equipment, continuous weights of the collected uranium hexafluoride product are obtained, and measurement of fluorine efficiency to the hexafluoride is available fairly quickly. However, the

efficiency of overall fluorine utilization is determined by fluorine analysis of the process off-gas, and this analysis involves a time lag of $\frac{1}{2}$ to $\frac{3}{4}$ hr. While an analysis is in progress, intermediate fluoride formation can increase significantly and no indication of this condition can be obtained at the reactor control panel. Hence, there is a need to improve this feature of process control. Further instrumentation is planned to provide continuous monitoring of unreacted fluorine in the process off-gas.

2. Oxidative Separation of Uranium Dioxide Fuel from Stainless Steel Cladding
(M. Baerns, J. Wehrle, and L. Marek)

Studies have been started to determine the feasibility of removing uranium dioxide pellets from stainless steel cladding by converting the uranium dioxide to uranosic oxide in a packed, fluidized bed. The conversion of the dioxide to U_3O_8 creates large internal stresses because of the differences in the densities of the two oxides and may result in the fragmentation of the pellets. The U_3O_8 fines formed during the oxidation can be elutriated from the oxidation zone to a fluorination zone by the oxidizing gas stream. Thus, if this separation step is feasible, it could be incorporated into the two-zone oxidation-fluorination process for the production of uranium hexafluoride.

A preliminary series of five runs has been completed in which the batch charge for each run consisted of 40 one-in. lengths of simulated fuel segments. These were randomly packed in a 2-in.-diameter fluidized-bed reactor. The simulated fuel segments were made by placing two dense uranium dioxide pellets (0.42 in. in diameter and in length) in each of the close-fitting stainless steel (Type 304) tubes ($1\frac{1}{8}$ in. long by 0.5 in. OD by 0.035 in. wall thickness). The ends of the cladding were open to simulate sheared fuel elements. Each of the runs was made with an 8-in.-deep (static condition) bed charge of simulated fuel segments and Alundum (740 g; -40 + 170 mesh). The height of the packed bed of fuel segments alone was about 6 in. In these runs, air was used to oxidize the uranium dioxide pellets, and the oxidation temperatures ranged from 350 to 450 C. Gas pulsing was investigated in two of the runs.

A schematic diagram of the apparatus used in the runs is shown in Figure II-8. A 2-in.-diameter column was used to carry out these studies. A perforated plate, which also served as a gas distributor, was used to support the packed fluidized bed. The inlet air which was used for the oxidation of the uranium dioxide pellets and the fluid-bed reactor column were heated to establish the desired reaction temperature. The temperature inside the bed was measured and automatically controlled. The elutriated uranosic oxide fines that were formed during the reaction were separated from the off-gas in a filter system. The filtered fines were not returned to the fluid-bed reactor. Gas pulses were introduced into the column by means of a timed valve system.

Figure II-8

EQUIPMENT FOR STUDYING OXIDATION OF STAINLESS STEEL-CLAD URANIUM DIOXIDE PELLETS

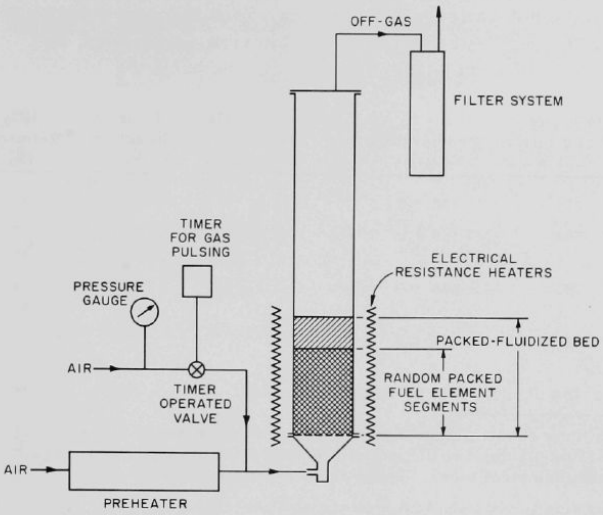

108-6531

The experimental conditions and the results of the runs are shown in Table II-12. In Run X02, which was carried out at about 350 C, the removal of 44 percent of the uranium dioxide from the cladding was achieved in 18.6 hr, a very low removal rate. A higher removal rate (52 percent) was obtained at 400 C (Run X01) and at 450 C (Run X03); however, this rate of removal is also considered to be inadequate.

In order to increase the rate of removal, gas pulsing was applied in Runs X04 and X05. During pulsing the fluidizing gas (air) was turned off, since previous studies showed that under these conditions the tubes were lifted and agitated by the gas pulses. Ten gas pulses of nitrogen in Run X04 and of air in Run X05 were introduced into the reaction column (below the distribution plate) every 15 min at a frequency of 10 pulses/min and a pulse duration of 1 sec. The oxidation temperature in both runs was about 450 C.

In Run X04, one hole, $\frac{7}{64}$ in. in diameter, was drilled through the cladding of each of twenty simulated fuel segments in order to test whether perforation would affect the rate of oxide removal. The cladding of the remaining twenty of the simulated fuel segments in the batch charge was not perforated. Thus, the removal of uranium dioxide from both perforated and unperforated cladding was tested in the same oxidation experiment.

Table II-12

OPERATING CONDITIONS AND RESULTS OF OXIDATION RUNS FOR REMOVAL OF URANIUM DIOXIDE FROM STAINLESS STEEL CLADDING

Equipment: 2-in.-diameter column

Inert Bed Charge: 740 g of Alundum, -40 +170 mesh

Oxidizing Gas: Air

Run No.	Weight of UO_2 Pellets[a] (g)	Temperature (C)	Superficial Gas Velocity[b] (ft/sec)	Time of Reaction (hr)	UO_2 Removed (%)	Elutriated Fines (%)
X01	775	400 ± 8	1.0	5.45	52	18
X02	784	350 ± 5	0.95	7.10	17	0.3
				18.6	44	8
X03	793	445 ± 5	1.1	7.00	52	-
				12.5	80	44.5
X04[c]	792	445 ± 5	1.1	6.00	67[d], 72.5[e]	32
X05[c]	796	445 ± 10	1.1	9.00	86	53

[a]Added as forty random-packed pieces of simulated sheared fuel segments which were made by placing two UO_2 pellets (of 0.42-inch diameter and length) in close-fitting stainless steel tubes. These tubes were open at both ends.

[b]Corresponding to reaction temperature and pressure.

[c]Gas pulses introduced into bottom of reactor column. Ten gas pulses of nitrogen in Run X04 and of air in Run X05 every 15 min at a frequency of 10 pulses/min and a pulse duration of 1 sec.

[d]Removal from tubes in which a hole, $\frac{7}{64}$ in. in diameter, was drilled through the cladding wall.

[e]Removal from tubes in which no hole was drilled through the cladding wall.

In Run X04, about 70 percent of the uranium dioxide was removed from the cladding in a reaction time of 6 hr. The perforation in the cladding did not affect the rate of removal of uranium dioxide. The amount of uranium dioxide removed was about equal for both the perforated and non-perforated cladding. In Run X05, a removal of 86 percent of the uranium dioxide was achieved in 9 hr. The uranium oxides were completely removed from one-third of the stainless steel tubes, while the remaining two-thirds of the tubes still contained solid residues of uranium oxides.

The results of Runs X04 and X05 indicate that gas pulsing increases the rate of removal of uranium oxide from the cladding; however, further experiments are necessary to establish optimum reaction conditions.

The relatively uniform rate of removal of uranium oxide from cladding (see Figure II-9) may be used advantageously to feed the uranium oxide at a uniform rate to the fluorination zone of the two-zone reactor.

Further experiments are planned to investigate the feasibility of combining the oxidative decladding process with the fluorination process.

Figure II-9

EFFECT OF TEMPERATURE AND GAS PULSING ON REMOVAL OF URANIUM DIOXIDE FROM STAINLESS STEEL CLADDING

Symbol	Run No.	Reaction Temp (C)	Gas-Pulsing
○	X04,5	445	Yes
□	X02	350	No
△	X03	445	No

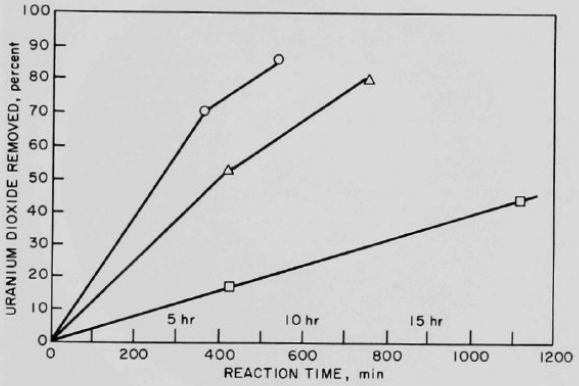

108-6532

Some observations concerning the mechanism of removal of uranium dioxide from the cladding are of interest. In some of the tubes, after partial removal of uranium dioxide there remained a solid, disk-shaped layer of oxide residue which had the same diameter as the tube. In other tubes, there remained portions of uranium oxide residues which adhered to the tubing walls. These residues had an annular shape across the whole diameter, similar to that shown in Figure II-10. The oxygen content of uranium oxide solid residue was determined by chemical analysis.

In Runs X01, X02, and X03, the oxygen:uranium ratios determined for the residues were 2.30, 2.40, and 2.53, respectively. For complete conversion to U_3O_8, the ratio is 2.67. Under the conditions of oxygen partial pressure and temperature used in these runs, rapid conversion of

UO_2 to U_3O_8 was expected; therefore, the possibility exists that U_3O_8 is formed on the outer surface of the dense oxide residue in the cladding and is capable of preventing further oxidation of the residue. In this case the cladding may hold in and compress the U_3O_8 product. Further experiments will be made to find conditions for complete removal of the oxide from the cladding and to determine whether chemical reaction or mechanical confinement of the product is limiting the extent of removal.

Figure II-10

OXIDE RESIDUE REMAINING IN SOME CLADDING SECTIONS AFTER AN OXIDATIVE SEPARATION RUN

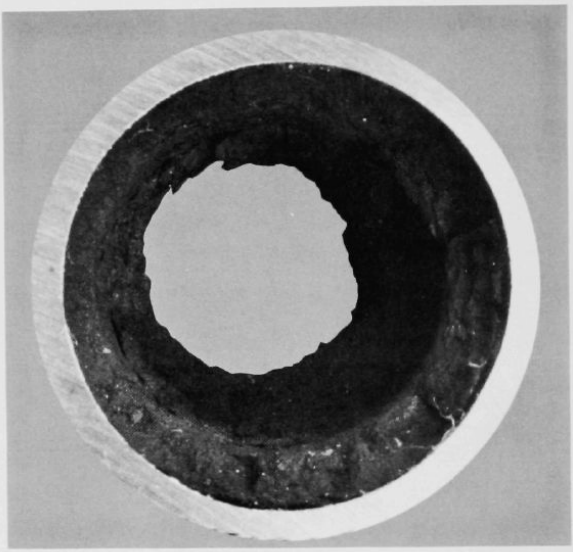

108-5891 Rev.

3. Heat Transfer and Elutriation Characteristics of Uranosic Oxide Fines in Fluidized Packed Beds
(J. D. Gabor, D. L. Benzing,* E. D. Johanson,** and C. F. Lehmann)

In the recovery of uranium from uranium dioxide pellets in the Direct Fluorination Process, intermediate uranium compounds, U_3O_8 and UO_2F_2, are formed which appear mostly as fine particles (~4 to 20μ in mean diameter). The behavior of these fines requires careful consideration

*Co-op student from the University of Detroit.

**Co-op student from Northwestern Technological Institute.

because (1) they tend to be elutriated from the fluid bed fluorinator and (2) their presence tends to reduce heat transfer in the bed. Because of the high angle of internal friction of a fine powder, there is less tendency for the fine particles to flow. Specifically, a fluidized bed containing too high a proportion of fines may not flow together to fill the void behind a bubble rising through the bed. This creates a path of low resistance which lends itself to gas channeling and poor fluidization quality. However, because of the greater specific surface area of the fines, reaction rates are increased, and fines, therefore, may be an asset to processing. In order to obtain additional information about the behavior of uranosic oxide (U_3O_8) fines under process operating conditions, a study of the heat transfer and elutriation characteristics of the fines was made. These supporting studies were carried out with fluidized-bed reactor configurations similar to those used in the Direct Fluorination Process.

The fines used in these studies were produced in four runs by oxidation of uranium dioxide pellets with mixtures of air and nitrogen in a reactor which consisted of a 2-in.-diameter nickel pipe heated by external calrods. The elutriated fines were collected in a filter chamber in the process off-gas line. The filter was a bayonet type made of sintered nickel. The operating conditions and the results of these runs are described in Table II-13. Although the major objective of these runs was the preparation of uranosic oxide powder, the following observations concerning the general processing behavior during the oxidation of a bed of uranium dioxide pellets were noted:

1. The absence of fluidizing material resulted in a heterogeneous system with poor temperature control.
2. The formation of a cake first occurred at the bottom of the pellet bed. This appears to be the result of rapid production of fines which fill the voids between the pellets. The difficulty stems from the efficient removal of produced fines from the surface of the pellets.
3. The use of lower oxygen concentrations, higher gas velocities, and a fluidizing material as bed diluent improved fines removal and counteracted the caking tendency.

The size distribution of the uranium oxide fines was measured by a Coulter Counter,* and the average particle diameter was shown to be approximately 4 μ. Alundum (-40 +170 mesh; 85% +100 mesh) was used as the inert fluidizing material for the bed diluent.

*Product of Coulter Electronics, Inc., Chicago, Illinois.

Table II-13

OPERATING CONDITIONS AND RESULTS OF URANIUM DIOXIDE PELLET OXIDATION RUNS TO PRODUCE URANOSIC OXIDE

Equipment: 2-in.-diameter nickel column
Inert Material: Alundum, Type 38, -40 +170 mesh (85% +100 mesh)
Temperature: 500 C

Run No.	Duration (hr)	UO_2 Bed Material	UO_2 Bed Height (in.)	Alundum Bed Height (in.)	Fluidizing Gas Composition		Superficial Fluidization Velocity (ft/sec)	U_3O_8 Fines Elutriated[a] (g)	Comments
					Air (v/o)	Nitrogen (v/o)			
UX1	1	Fines to whole 1/2-in. pellets	59	0	100	0	1	1	Rapid caking.
UX2	5.5	Pellet fragments +3/16 in.	24	0	50	50	1.5	84	Caking after 2 hr. Good production.
UX3	3.5	1/2-in. pellets	4	16	50	50	1.5	70	No caking. 20% conversion of UO_2 charge.
UX4	3.5	pellet fragments, +1/8 in.	13	23	50	50	1.5	188	Caking. Good production.

[a]The elutriated material was part of the U_3O_8 product; the balance of the product was obtained by screening out the unreacted material in the bed.

Heat Transfer

The characteristically high rates of heat transfer from a heater surface to a well-fluidized bed have been previously established (see Chemical Engineering Division Summary for July, August, September, 1960, ANL-6231, pp. 111-116). In the present study, such film coefficients were determined and taken as criteria for evaluating the fluidization quality for fluidized beds containing uranosic oxide fines of about 4-μ mean diameter.

The heat transfer coefficients for the heater were studied as a function of the fluidizing air velocity and of the composition of the fluidized materials (uranosic oxide and alumina). Values of the heat transfer coefficients were calculated by the usual formula

$$q/A = h\,\Delta T \quad ,$$

where

q/A = average heat flux of the heater;

ΔT = temperature difference between the heater surface and the fluid bed;

h = heat transfer coefficient, Btu/(hr)(sq ft)(F) .

A 3-in.-diameter by 6-ft-long glass column was used for both the heat transfer and the elutriation studies of the uranosic oxide fines. For the heat transfer studies, a sintered metal filter with a blowback system was mounted in the column to prevent loss of fines from the system. A cylindrical heater, 2 in. long and $\frac{1}{2}$ in. in diameter, was operated at 50 w. The heater wall temperature was measured by a thermocouple soldered in place on the side of the heater. The heater was positioned at the radial center of the column, and the bed temperature was measured by a bare-wire thermocouple which was located $\frac{1}{2}$ in. from the heater surface. The heat transfer coefficients were calculated from the power and surface area of the heater, and the difference in temperature between the heater wall and the bed. Fluidization was accomplished by means of a metered gas flow distributed through a perforated bed support plate and a 3-in. layer of $\frac{1}{4}$-in. steel balls. Since pulsed gas flow of fluidizing gases has been shown to be effective in reducing channeling and improving solids agitation, a timer and solenoid-valve system were installed on the column to cause a pulsed gas flow to be superimposed upon a steady flow of fluidizing gas. Both the fluidizing gas and the pulsing gas were air.

For the first of the tests, a 9-in.-deep bed of uranosic oxide fines alone (no Alundum present in bed) was used. The fluidization of the bed of fines, with and without gas pulsing, was observed visually. Without pulsing, the following conditions resulted:

1. Agitation occurred only in the upper portion of the bed of fines; even at a fluidizing gas rate of 1.0 ft/sec the bottom of the bed remained stagnant.
2. The inlet fluidizing gas was not evenly distributed, as indicated by the channeling that occurred along several paths at the column wall.
3. Channeling along the heater or column wall for gas velocities below 0.6 ft/sec was observed.

With pulsing, the following conditions resulted:

1. Agitation of the fines extended throughout the bed; in particular, the fines at the interface of the steel balls and fines were in constant motion.
2. Channeling was substantially eliminated by pulsing, as indicated by visual observation.
3. Although pulsing improved heat transfer at gas velocities above 0.2 ft/sec, the rate of pulsing did not have a significant effect on the coefficient of heat transfer from the surface of an internal heater to the bed of fines. At gas velocities below 0.2 ft/sec, high pulse rates provided better heat transfer.

It was also found that, because of the severe channeling which occurred when the fluidizing gas was not pulsed, reproducible heat transfer coefficients were not obtained for a bed of pure uranosic oxide fines. Alundum (-40 +170 mesh) was then added to the bed of uranosic oxide fines in order to determine the amount of Alundum necessary to insure good fluidization. The proportion of Alundum was increased until it attained a concentration of 40 w/o. The heat transfer coefficients for a heater surface in a pulsed bed of uranosic oxide have been determined as a function of bed composition and superficial air velocity. These results are shown in Table II-14. The data in Table II-14 show that the heat transfer coefficients increase slightly with increases in Alundum content and with increases in superficial gas velocity.

Table II-14

HEAT TRANSFER COEFFICIENTS FOR HEATER SURFACE IN A PULSED BED OF URANOSIC OXIDE FINES. EFFECT OF ALUNDUM CONCENTRATION AND SUPERFICIAL GAS VELOCITY

Bed Material: U_3O_8 fines (~4-μ diameter)
Alundum (-40 +170 mesh)
Fluidizing Gas: Air
Heat Transfer Coefficient, h, Btu/(hr)(sq ft)(F)

Superficial Gas Velocity (ft/sec)	Fluid Bed Composition[a] (w/o Al_2O_3)[b]					
	0	5	10	20	30	40
0.1	34.9	38.5	39.1	39.1	46.1	44.4
0.3	45.0	45.0	48.6	48.6	56.2	56.2
0.5	49.2	49.1	52.6	56.0	58.7	58.7
0.7	-	52.6	56.0	58.7	58.7	61.4
0.9	-	56.0	56.0	70.4	67.9	67.9

[a]Pulse rate for 0 w/o Alundum was 18 pulses/min. For all other concentrations it was 22 pulses/min.

[b]Remainder - Uranosic oxide.

No optimum values of the heat transfer coefficient h were measured over the range of conditions studied (0 to 40 w/o Alundum and superficial gas velocities of 0.1 to 0.9 ft/sec). Channeling of the bed was observed over the entire range of conditions, but apparently the pulsing was sufficient to promote heat transfer to an extent that variations of h with bed composition and gas velocity (considered to be the usual determinants of h) were insignificant.

In a subsequent series of tests, the experimental procedure was modified. The initial bed consisted only of Alundum, and the proportion of uranosic oxide fines was increased in successive runs. The placement of thermocouples on the heater was also changed in that two thermocouples were welded to the heater surface, one at the top of the heater and one at the midpoint; a third thermocouple was positioned in the bed $\frac{1}{2}$ in. from the heater.

The heat transfer coefficients for a heater to a fluidized bed were determined as a function of fluid bed composition, gas pulsing of the fluidizing gas, and superficial gas velocity of the fluidizing gas. The calculated values of the heat transfer coefficient are summarized in Tables II-15 and II-16 for the midpoint and the top thermocouple locations on the heater surface, respectively. Although the temperatures of the heater at the two thermocouple locations could be reproducibly measured, systematic differences in the measured temperature levels at the two thermocouple locations were obtained. These differences are reflected in the

Table II-15

HEAT TRANSFER COEFFICIENTS FOR HEATER SURFACE (MIDPOINT) IN FLUIDIZED BED MIXTURE OF U_3O_8 AND ALUNDUM. EFFECT OF FLUID BED COMPOSITION, SUPERFICIAL VELOCITY, AND GAS PULSING

Fluidizing and Pulsing Gas: Air

Bed Material: U_3O_8 fines (~4-μ diameter)
Alundum: -40 +170

Heater: 1/2-in. diameter by 2 in. long

Heat Transfer Coefficient h, Btu/(hr)(sq ft)(F)

Without Pulsing

Superficial Gas Velocity (ft/sec)	Fluid Bed Composition (w/o U_3O_8)[a] 0	5	10	15	20	25	30	35	Avg.
0.2	58	70	70	67	61	53	49	42	59
0.4	82	82	82	77	70	66	60	54	72
0.6	77	79	82	79	74	72	64	54	73
0.8	75	75	75	77	75	72	66	54	71
1.0	72	72	72	74	74	70	64	57	69
1.2	68	70	70	74	70	68	64	58	68
1.4	67	68	67	72	68	67	64	60	67
Avg.	71	74	74	74	70	67	62	54	

With Pulsing

(25 pulses/min at pulse gas manifold pressure of 10 psig; pulse duration, 0.3 sec)

Superficial Gas Velocity (ft/sec)	Fluid Bed Composition (w/o U_3O_8)[a] 0	5	10	15	20	25	30	35	Avg.
0.2	75	77	74	75	70	66	59	54	69
0.4	77	79	75	75	74	70	64	58	72
0.6	75	75	74	75	74	72	66	54	71
0.8	74	74	70	72	74	72	67	54	70
1.0	70	70	67	70	70	68	66	54	67
1.2	66	67	68	68	70	68	64	53	66
1.8	64	67	67	66	67	70	64	51	65
Avg.	72	73	71	72	71	69	64	54	

[a]Remainder - Alundum.

Table II-16

HEAT TRANSFER COEFFICIENTS FOR HEATER SURFACE (TOP) IN FLUIDIZED BED MIXTURE OF U_3O_8 AND ALUNDUM. EFFECT OF FLUID BED COMPOSITION, SUPERFICIAL VELOCITY, AND GAS PULSING

Fluidizing and Pulsing Gas: Air

Bed Material: U_3O_8 fines (~4-μ diameter)
Alundum: -40 +170

Heater: 1/2-in. diameter by 2 in. long

Heat Transfer Coefficient h, Btu/(hr)(sq ft)(F)

Without Pulsing

Superficial Gas Velocity (ft/sec)	Fluid Bed Composition (w/o U_3O_8)[a]								
	0	5	10	15	20	25	30	35	Avg.
0.2	95	146	146	138	120	98	84	68	112
0.4	192	192	192	159	138	120	120	100	161
0.6	168	180	192	200	180	159	132	117	166
0.8	159	159	180	192	192	168	138	120	164
1.0	150	150	159	180	192	168	146	125	159
1.2	146	150	159	192	192	159	150	132	160
1.4	138	146	159	180	180	168	130	132	157
Avg.	150	160	170	182	174	151	131	114	

With Pulsing

(25 pulses/min at a pulse gas manifold pressure of 25 psig; pulse duration, 0.3 sec)

Superficial Gas Velocity (ft/sec)	Fluid Bed Composition (w/o U_3O_8)[a]								
	0	5	10	15	20	25	30	35	Avg.
0.2	159	168	180	180	168	146	98	104	150
0.4	168	180	180	192	180	159	132	117	164
0.6	168	168	180	192	192	168	138	117	165
0.8	159	159	168	180	192	168	146	120	164
1.0	150	146	159	180	180	168	146	120	156
1.2	146	146	159	180	192	168	138	120	156
1.4	146	146	150	168	168	168	146	120	152
Avg.	157	159	168	182	182	164	133	117	

[a]Remainder - Alundum.

values of the heat transfer coefficients and are attributed to the particular orientation of the heater and its mount. Accordingly, evaluation of the effect of fines concentration on the values of the heat transfer coefficient should be made separately for each thermocouple location.

In Tables II-15 and II-16, the heat transfer coefficients h show a general tendency (at all superficial gas velocities, both with and without pulsing) to decrease as the fines concentration increases above about 20 w/o. The usual effect of the heat transfer coefficient increasing with superficial gas velocity in the range from the incipient fluidization velocity (approx 0.2 ft/sec) to velocities several times higher is also seen. The data show that at low velocities the heat transfer coefficient is increased by the presence of fines and/or by pulsing. There appears to be little effect of pulsing on the value of the heat transfer coefficient for the range of 0 to 35 w/o U_3O_8 fines in Alundum. Although large variations of the heat

transfer coefficient with fines concentration and superficial gas velocity are not shown, some of the data suggest that a maximum value of h occurs at a superficial gas velocity of about 0.6 ft/sec and at about 15 w/o U_3O_8 fines in Alundum. The addition of U_3O_8 fines to the Alundum bed increases the spread in the size distribution of the fluidized material, which results in better fluidization quality. However, with excessive amounts of the fines, heat transfer decreases because of greater internal flow resistance of the particulate solid being fluidized.

Elutriation Studies

In this study the elutriation rates for U_3O_8 from a mixture of U_3O_8 fines and Alundum particles were studied as a function of fluidization gas velocity, gas pulsing, and the presence (or absence) of a packed bed of $\frac{1}{2}$-in.-diameter by $\frac{1}{2}$-in.-long uranium dioxide pellets. All runs in this study utilized a standard measure of 3100 g of Type 38 Alundum (-40 +170 mesh) and 200 g of uranosic oxide fines (average diameter of 4 μ).

The apparatus used for the study of the elutriation rates consisted of the same 3-in.-diameter glass column which was used in the heat transfer studies. It was modified by removing the internal filter and placing it in a separate chamber in the process off-gas line. This filter chamber could be disconnected and weighed to determine the rates of U_3O_8 fines collection. The bed height (static) for all the runs was about 18 in., and the initial reactor column freeboard (static) was 54 in. Humidified air was the gas used for pulsing and fluidizing.

Experimental conditions were chosen for these runs which would be in the range encountered in the fluorination step of the Direct Fluorination Process. In Figure II-11, an increase in the elutriation of U_3O_8 is shown for increasing fluidization gas velocity (from $\frac{1}{3}$ to 1 ft/sec). In Figure II-12, the elutriation rate for U_3O_8 fines as a function of pulse rate is shown. The gas-pulse manifold pressure was 10 psig, and the fluidization gas velocity was $\frac{2}{3}$ ft/sec in these experiments. The elutriation rate of U_3O_8 fines doubled as the gas-pulse rate was increased from 0 to 20 pulses/min. The duration of the pulse was kept constant at 0.3 sec. In Figure II-13, an increase in elutriation of U_3O_8 is shown for increasing gas manifold pulse pressure (from 10 to 30 psig) at a constant gas-pulse frequency (10 pulses of 0.3-sec duration/min).

The elutriation rate of U_3O_8 fines from a fluidized packed bed was also studied as a function of the uranium dioxide pellet-bed height, gas-pulse frequency, pulse gas manifold pressure, and Alundum particle size. Uranium dioxide pellets, of $\frac{1}{2}$-in. diameter by $\frac{1}{2}$ in. long, were used for packing, and the fluidized material was composed of a mixture of U_3O_8 fines (~4-μ diameter) and Type 38 Alundum (+50 -170 mesh). Air, at a

superficial fluidization velocity of $\frac{2}{3}$ ft/sec, was used as the fluidizing gas in these studies. The results of these studies are shown in Figures II-14, II-15, and II-16.

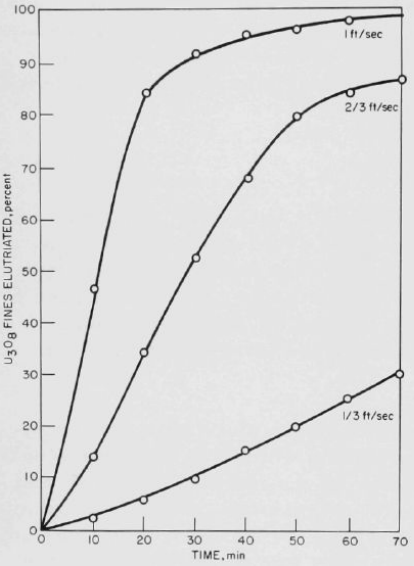

108-6533

Figure II-11

ELUTRIATION OF U_3O_8 FINES FROM A MIXTURE OF U_3O_8 FINES IN FLUIDIZED ALUNDUM AS A FUNCTION OF FLUIDIZING GAS VELOCITY

Equipment:	3-in.-diameter glass column
Bed Material:	200 g U_3O_8 (~4-μ diameter); 3100 g Type 38 Alundum (-40 +170 mesh)
Bed Height (static):	18 in.
Fluidizing Gas:	Air

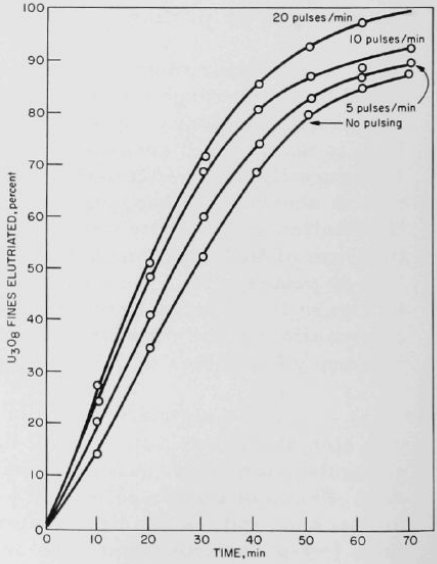

108-6534

Figure II-12

ELUTRIATION OF U_3O_8 FINES FROM A MIXTURE OF U_3O_8 FINES IN A FLUIDIZED BED OF ALUNDUM. THE EFFECT OF PULSE FREQUENCY

Equipment:	3-in.-diameter glass column
Bed Material:	200 g U_3O_8 fines (~4-μ diameter); 3100 g Type 38 Alundum (-40 +170 mesh)
Fluidizing and Pulsing Gas:	Air
Gas Pulse Manifold Pressure:	10 psig
Superficial Gas Velocity:	2/3 ft/sec
Pulse Duration:	0.3 sec

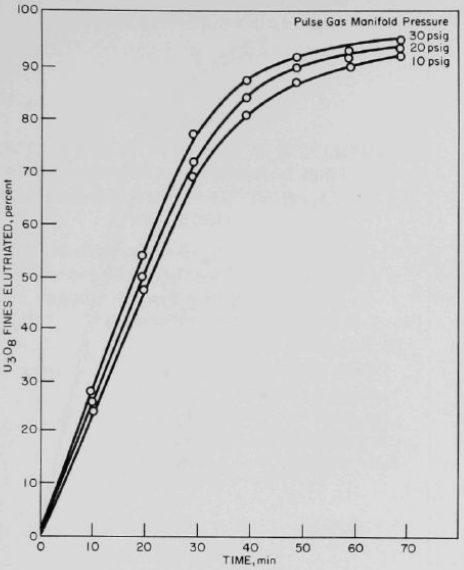

108-6535

Figure II-13

ELUTRIATION OF U_3O_8 FINES FROM A MIXTURE OF U_3O_8 FINES IN A FLUIDIZED BED OF ALUNDUM. THE EFFECT OF PULSE GAS MANIFOLD PRESSURE

Equipment:	3-in.-diameter glass column
Bed Material:	200 g U_3O_8 fines (~4-μ diameter); 3100 g Type 38 Alundum (-40 +170 mesh)
Fluidizing and Pulsing Gas:	Air
Pulse Duration:	0.3 sec
Superficial Fluidizing Gas Velocity:	2/3 ft/sec
Gas Pulse Frequency:	10 pulses/min

Figures II-14 and II-15 show that the elutriation rates for U_3O_8 fines were generally lower in those runs in which the fluidized bed was packed with a bed of uranium dioxide pellets than in those runs in which the fluidization was unhindered by the presence of the packing (uranium dioxide pellets). In the two runs made with 18-in.-deep beds of uranium dioxide pellets, the composition of the fluidized bed was the same as that used in runs with 9-in.-deep beds, but the amount of the U_3O_8-Alundum mixture was adjusted so that the fluidized-bed portion did not extend beyond the top of the pellet bed. In one of these runs, gas pulsing was not used. The rate of elutriation of fines in this run was very low. The uranium dioxide pellets appear to inhibit solids mixing and hence the transport of the U_3O_8 fines; however, it is apparent from the results of these studies that this effect can be overcome by gas pulsing of the fluidizing gas.

In the runs which investigated the elutriation rate of U_3O_8 fines from a packed fluidized bed as a function of the size of the Alundum particles, it was found that maximum elutriation rates were obtained with Alundum particles which averaged about 120 mesh (see Figure II-13). With large Alundum particles there is a lower mixing rate and, hence, less transport of the U_3O_8 fines. With the smaller Alundum particles, the internal friction of the fluidized bed is increased, which also reduces solids mixing and hence hinders the escape of fine particles.

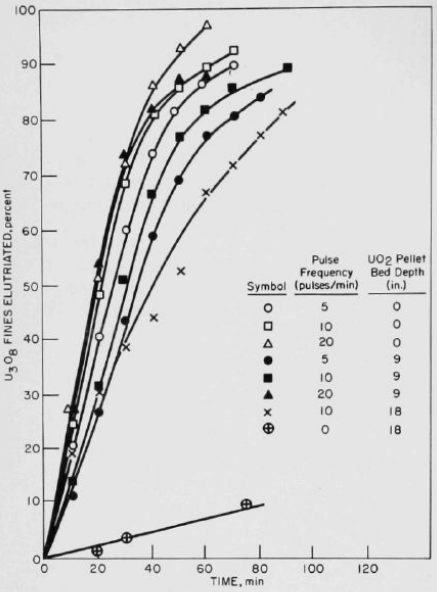

108-6536

Figure II-14

ELUTRIATION OF U_3O_8 FINES FROM A MIXTURE OF U_3O_8 FINES IN FLUIDIZED ALUNDUM. THE EFFECT OF UO_2 PELLET-BED HEIGHT AND GAS-PULSE FREQUENCY

Equipment:	3-in.-diameter glass column
Bed Material:	200 g U_3O_8 fines (~4-μ diameter); 3100 g Type 38 Alundum (-40 +170 mesh)
Fluidizing and Pulsing Gas:	Air
Superficial Fluidizing Gas Velocity:	2/3 ft/sec
Gas Pulse Pressure:	10 psig
Pulse Duration:	0.3 sec

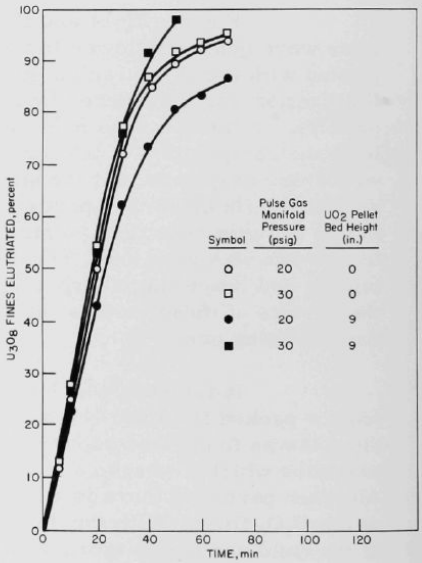

108-6537

Figure II-15

ELUTRIATION OF U_3O_8 FINES FROM A MIXTURE OF U_3O_8 FINES IN FLUIDIZED ALUNDUM. THE EFFECT OF PULSE GAS MANIFOLD PRESSURE AND UO_2 PELLET-BED HEIGHT

Equipment:	3-in.-diameter glass column
Bed Material:	200 g U_3O_8 fines (~4-μ diameter); 3100 g Type 38 Alundum (-40 +170 mesh)
Fluidizing and Pulsing Gas:	Air
Superficial Fluidizing Gas Velocity:	2/3 ft/sec
Gas Pulse Frequency:	10 pulses/min
Pulse Duration:	0.3 sec

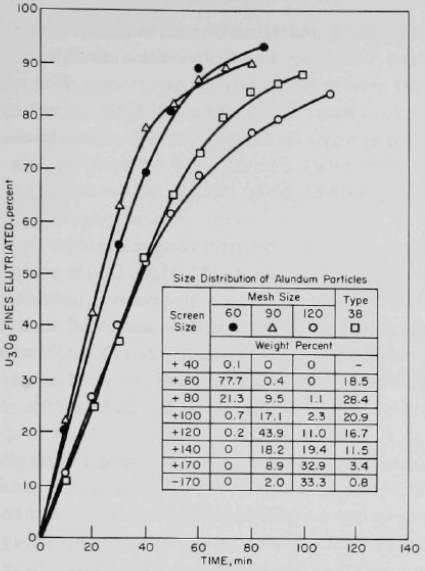

Size Distribution of Alundum Particles

Screen Size	Mesh Size 60 ●	90 △	120 ○	Type 38 □
	Weight Percent			
+ 40	0.1	0	0	-
+ 60	77.7	0.4	0	18.5
+ 80	21.3	9.5	1.1	28.4
+100	0.7	17.1	2.3	20.9
+120	0.2	43.9	11.0	16.7
+140	0	18.2	19.4	11.5
+170	0	8.9	32.9	3.4
-170	0	2.0	33.3	0.8

108-6538

Figure II-16

ELUTRIATION OF U_3O_8 FINES FROM A MIXTURE OF U_3O_8 FINES IN FLUIDIZED ALUNDUM IN A PACKED BED. EFFECT OF ALUNDUM PARTICLE SIZE

Equipment:	3-in.-diameter glass column
UO_2 Pellet-bed Height:	9 in.
Bed Material:	200 g U_3O_8 fines (~4-μ diameter); 3100 g Alundum
Fluidizing Gas:	Air
Superficial Fluidizing Gas Velocity:	2/3 ft/sec

No gas pulsing

4. Process Studies on the Recovery of Uranium from Enriched Uranium-Zirconium Alloy Fuels

(N. Levitz)

Development work on a fluid bed-volatility process for the recovery of uranium from highly enriched uranium-zirconium alloy fuels is continuing. Although current work is on zirconium-based fuel, direct application of the process to uranium-aluminum fuels will soon be started. The process involves two main reactions - hydrochlorination of the alloy while the alloy is submerged in an inert fluidized bed (the bed material serving as a heat transfer medium), and a subsequent fluorination step in the same process vessel. The hydrochlorination step effects a separation of the uranium from the zirconium, which sublimes as the volatile tetrachloride (sublimation point, 331 C at 14.7 psia); the uranium remains in the reactor assembly as particulate trichloride. Uranium and other particulate solids that might be entrained by the off-gas from the main reactor are retained in the reactor assembly by a static bed of inert granular material which serves as a high-temperature filter. During the ensuing fluorination step, the uranium is volatilized and recovered as the hexafluoride (sublimation point 56.5 C at 14.7 psia). The waste gases are treated, and the remaining inert diluent gases are discharged to the stack.

Process studies are being carried out in a bench-scale unit comprised of a $1\frac{1}{2}$-in.-diameter fluid-bed reactor section connected in series with a $1\frac{1}{2}$-in.-diameter static-bed down-flow filter section. The gases flow downward through the latter section. Granular Alundum (refractory aluminum oxide from Norton Company) is being used as the bed material in both sections. Under all the process conditions tested, it has proven satisfactory (of prime importance, it has been found to be inert).

Work to date has proved not only that the process concept is feasible, but also that one of the major objectives, overall high (~99 percent) uranium recovery, can be achieved by proper control and sequencing of reactants. The work has been evaluated primarily on the basis of the quantity of uranium lost during the process steps, although actual high uranium hexafluoride recovery has been demonstrated and uranium material balances have been good (for example, see ANL-6648, p. 156, Table 29).

Uranium is lost as particulate uranium solids passing through the packed-bed filter with the off-gas stream during hydrochlorination and as uranium remaining associated (chemically or physically) with the material (Alundum) in the fluid bed and fixed bed after the cycle is complete. Losses due to incomplete filtration have been maintained at levels of 0.2 percent or less when only hydrogen chloride was used as the chlorinating agent, although greater losses (up to several percent) have been sustained when phosgene was used in addition to hydrogen chloride (see ANL-6596, p. 150). Uranium loss due to retention by Alundum appears to be affected by changes in the chlorination and fluorination variables. Less uranium was retained when use was made of: (1) greater quantities of hydrogen chloride (in the range 4 to 25 times stoichiometric); (2) phosgene in addition to hydrogen chloride; or (3) higher final fluorination temperatures (500 C as compared with 350 C and 400 C). The residual uranium values obtained in these studies were in the range from 0.2 to 1.3 percent of the initial uranium charge.

Overall uranium losses for several process cycles carried out in succession can be reduced by re-use of the bed, since it has been found that with re-use of the bed the residual uranium concentration in the bed tends to become constant (see ANL-6543, pp. 149 to 150). When the same bed was used in five consecutive runs, the cumulative loss was 1.0 percent of the total uranium charged. Similarly, losses can be reduced if a single fluorination is used to recover the uranium accumulated in the beds from several successive hydrochlorinations. When three batches of alloy were so processed (see ANL-6648, p. 154), an overall loss of about one percent was sustained.

Current work, involving the hydrogen chloride-fluorine cycle, is directed toward obtaining information about the optimum requirements for the overall process cycle. The results of this work are to be compared

directly with the results of a previous run for which a four-reactant cycle (phosgene and hydrogen fluoride treatments, in addition to the above) was employed. In-line thermal conductivity cells continue to provide a means of following the course of both main process steps by measuring the concentration of key reaction products.

In addition to the bench-scale process studies described above, investigations of other phases of the process are being advanced. Studies are continuing in a 6-in.-diameter fluid-bed reactor on the conversion of zirconium tetrachloride to the dioxide by a pyrohydrolysis reaction with steam. This work is aimed at a method of disposal for the waste zirconium tetrachloride vapor produced during the hydrochlorination step. Currently, the feasibility of operating at higher, more practical tetrachloride feed rates than in the past is being explored. Construction work and preliminary leak-testing of a pilot-plant facility intended for demonstration of the uranium-zirconium alloy processing scheme is continuing; the installation is now about 75 percent complete.

All of the above studies will involve nonirradiated fuel material; reaction studies with highly irradiated material are planned for a bench-scale unit now in preliminary design stages.

a. Hydrochlorination and Fluorination Reaction Studies on Uranium-Zirconium Alloy Fuels and Evaluation of Fixed-bed Filters
(D. Ramaswami, D. Goeser)

Process development studies on the hydrochlorination and fluorination steps of a fluidization-volatility method for the recovery of highly enriched uranium from low uranium-zirconium alloy are in progress. These studies are being carried out in nickel apparatus consisting of a fluid-bed reactor section and a down-flow, packed-bed filter section; both sections are $1\frac{1}{2}$ in. in diameter, and both contain beds of prefluorinated Alundum (Norton Company). The fluidized bed of Alundum serves as the heat transfer medium for these highly exothermic reactions, while the packed bed of Alundum serves as a high-temperature filter for the retention of particulate solids entrained from the fluidized bed. Details of the apparatus and associated equipment and the experimental procedure are described in a previous report (ANL-6569, pp. 114 to 118).

Three 240-g batches of 5 w/o uranium-Zircaloy-2 alloy chips ($\frac{1}{8}$ to $\frac{1}{4}$ in. on a side) were processed in the current studies. The alloy was submerged in a 320-g bed of -40 +60 mesh, Type RR Alundum. The down-flow filter bed consisted of a layer (120 g) of -40 +60 mesh, Type RR Alundum sandwiched between two layers of coarser, -14 +20 mesh Type 38 Alundum (170 g above and 30 g below). The depth of each bed was about 6 in. The following run procedure was used: a single batch of alloy was charged to the reactor, and reaction with hydrogen chloride proceeded until

the major portion of the alloy was reacted (as determined by means of an in-line thermal conductivity cell which measures the hydrogen content of the off-gas stream). This routine was repeated for the second and third batches of alloy, except that reaction of the final batch was carried to completion. The uranium was then recovered by fluorination. The hydrochlorination was carried out at about 400 C. The fluorination was carried out, first, at 350 C, and then at 500 C. A summary of the run conditions and the quantities of reactants used is shown in Table II-17. As indicated, approximately four times the stoichiometric quantity of hydrogen chloride was fed during the hydrochlorination period, which lasted a total of 20.5 hr. The quantity of fluorine fed was relatively high, about 27 and 100 times stoichiometric in the two fluorination periods. Once-through flow was used for both reactants.

Table II-17

HYDROCHLORINATION AND FLUORINATION OF URANIUM-ZIRCALOY ALLOYS, RUN 35

Equipment:	$1\frac{1}{2}$-in.-diameter reactor
Alloy Charge:	3 batches (240 g each) of 5 w/o uranium-Zircaloy-2 alloy chips ($\frac{1}{8}$ to $\frac{1}{4}$ in. on a side)
Reaction Bed:	Alundum, Type RR, -40 +60 mesh, 320 g
Down-flow filter bed:	Alundum
	Top Layer: Type 38, -14 +20 mesh, 170 g
	Middle Layer: Type RR, -40 +60 mesh, 120 g
	Bottom Layer: Type 38, -14 +20 mesh, 30 g

Reactant		Temperature (C)			
Type	Quantity (X stoichiometric)	Fluid Bed	Filter Bed	Time (hr)	Remarks
HCl	0.32[a]	400 ± 25	400	4.3	First batch of alloy
HCl	0.55[a]	400 ± 25	400	3.9	Residual alloy from first batch plus second batch
HCl	3.13[a]	400 ± 25	400	12.3	Residual alloy from previous batches plus third batch.
F_2	27.3[b]	350	350	2	
F_2	98.4[b]	500	500	6[c]	

[a] Stoichiometric amounts based on original alloy charge according to the reaction $Zr + 4\ HCl \rightarrow ZrCl_4 + 2\ H_2$.

[b] Stoichiometric amount to convert the uranium in the initial charge into uranium hexafluoride.

[c] Long fluorination times are used to evaluate the effect of time on residual concentration of uranium in the Alundum of the fluid bed.

Results

The hydrogen chloride-fluorine reaction sequence as used in the current run (Run 35) appears to give about the same results as those achieved in a previous run (Run 32), where a four-reaction sequence (hydrogen chloride, phosgene, hydrogen fluoride, and fluorine) was used. In the following tabulation, the runs are compared on the basis of uranium losses:

	Weight Percent of Initial Uranium Charge	
	Run 35 (HCl, F_2 only)	Run 32 (HCl, $COCl_2$, HF, F_2)
Uranium found downstream of the filter bed after hydrochlorination	0.1	0.25
Uranium retained by the Alundum in the fluid bed and filter bed	0.5	0.4

The total uranium loss, about 0.6 w/o of the uranium charged in the three batches of alloy, is considered acceptable.

Data obtained from the analysis of samples taken from the fluid bed at half-hour intervals during fluorination tend to confirm the previous observation (see ANL-6648, p. 166) that only one hour of fluorination at 350 C and about 2 hr of fluorination at 500 C are required in order to achieve acceptable residual uranium values. The uranium associated with the Alundum particles in the fluid bed was reduced from an initial value of 1.04 w/o to 0.13 w/o during the 2-hr low-temperature fluorination period and was further reduced to 0.05 w/o during the first hour of the high-temperature fluorination period. The subsequent 5-hr, high-temperature period gave no further change in the concentration of uranium.

Discussion

Information on the progress of the hydrochlorination and the fluorination reactions is being obtained continuously by direct analyses of the off-gas streams with thermal conductivity cells (equipment is described in ANL-6569, p. 117). From this information, the rate of reaction and the efficiency of utilization of the reactant can be determined, as well as the extent of the reaction.

In the current run, in which successive hydrochlorinations of uranium-Zircaloy alloy were carried out, analysis of the thermal conductivity data indicated that (1) 70 percent of the first batch of alloy was reacted before the second batch was charged, and a total of 79 percent of

the alloy from the first two batches was reacted before the third batch was charged; (2) hydrochlorination of the alloy at rates of up to 90 g/hr was achieved, the average hydrochlorination rate during the constant-rate period being about 70 g/hr. Previously, the peak hydrochlorination rate was about 50 g/hr of alloy. Achievement of higher reaction rates was due directly to the use of higher concentrations of hydrogen chloride, made possible by an improved cooling system on the fluid-bed reactor. The improvements in the cooling system consisted primarily of a system for supplying higher rates of air coolant. A still further improvement in the cooling system is planned, namely, the use of a two-phase coolant (gas plus entrained water droplets fed into the gas stream as a fine spray). As a consequence, even higher reaction rates may be attained.

Preliminary information obtained during the fluorination step indicates that about 90 percent of the uranium charged was recovered as hexafluoride during the first 30 min of the low-temperature (350 C) fluorination period. The remainder was collected during the subsequent 1.5 hr.

Future Work

Future work includes plans to determine: (a) the effect of fuel shape on hydrochlorination rate of uranium-zirconium alloys (small plate fuel element assemblies will be used instead of chips); (b) the uranium distribution between the fluid bed and down-flow filter bed after hydrochlorination; this will be achieved by fluorinating each section separately; and (c) the effect on overall uranium behavior of the incorporation of simulated fission products into the fuel alloy.

Application of this process scheme to the recovery of uranium from uranium-aluminum alloy fuel appears straightforward; nevertheless, a program of studies is being planned to define the necessary processing conditions. An exploratory experiment with this material has already been carried through the hydrochlorination and fluorination steps without difficulty. Reporting of this experiment awaits the evaluation of the results.

b. Fluid-bed Hydrolysis of Zirconium Tetrachloride
(K. S. Sutherland, D. J. Raue)

Zirconium tetrachloride vapor, which is a waste product of the hydrochlorination step in the proposed fluidization-volatility scheme for processing uranium-zirconium alloy fuels, must be converted to a stable solid form for satisfactory disposal (storage). One of the most stable forms is the oxide, and it is proposed that conversion of the tetrachloride to the oxide be effected by using a hydrolysis reaction with steam in a fluidized bed. Previous work (see ANL-6596, pp. 154 to 156, and ANL-6648, pp. 169 to 172) has demonstrated the feasibility of carrying

out this reaction under a wide variety of operating conditions. Among the variables studied were bed temperature, initial bed material and particle size, run duration, and feed-gas composition. The zirconium tetrachloride feed rates used to date (up to about 3 kg/hr) have been lower than those contemplated for the proposed pilot plant (see ANL-6543, p. 153). Accordingly, the work being reported herein has been concerned primarily with operation at feed rates which were about two times greater than those used previously.

The major components of apparatus have been described previously (see ANL-6569, pp. 118 to 119). The equipment incorporates a vibrating screw feeder which supplies solid zirconium tetrachloride to a sublimation furnace, from which the vapor is carried in a stream of nitrogen into the fluidized bed. Equipment modifications incorporated in the current period involved (1) installation of a larger feed screw (of $\frac{3}{4}$-in. diameter instead of $\frac{1}{2}$-in. diameter) on the Vibra-Screw solids feeder in order to accommodate runs at higher tetrachloride feed rates and (2) relocating the feeder to a position directly above the sublimation furnace. The latter change was made in order to reduce the length of line through which solids had to be carried; the solid tetrachloride was entrained by the carrier nitrogen stream at a point immediately adjacent to the entry flange of the furnace, and the risk of feed line blockages is thereby reduced.

The operating conditions for the four main tests performed in the period covered by this report are given in Table II-18. As indicated, higher tetrachloride feed rates, 4.1 to 5.1 kg/hr, were used, as compared

Table II-18

FLUID-BED HYDROLYSIS OF ZIRCONIUM TETRACHLORIDE

Operating Conditions

Equipment:	6-in.-diameter fluidized-bed reactor
Initial Bed Weight:	20 kg
Bed Temperature:	350 C
Filter Blowback Pressure:	50 psig
Carrier Gas:	Nitrogen
Carrier Gas Flow Rate:	3 cu ft/min (measured at 20 C and 14 psia)

Run No.	Run Duration (hr)	$ZrCl_4$ Feed Rate (kg/hr)	Steam Rate (x stoich)	Initial Bed Material
CO-45	3	4.1	3.6	Freshly crushed sand, 83.5 percent -20 +200 mesh
CO-46	$2\frac{1}{4}$	5.1	2.9	Final bed from CO-45
CO-47	$2\frac{3}{4}$	4.4	3.5	Freshly crushed sand, 96.5 percent -100 mesh
CO-48	$5\frac{3}{4}$	4.1	3.6	Final bed from CO-47

with previous rates of 2 to 3 kg/hr. As the runs proceeded, greater proportions of fines were found in the bed, and it became apparent that at these higher feed rates, the major portion of the tetrachloride was converted to fine particulate solids instead of reacting on and adhering to the surface of the bed particles. If excessive quantities of fines were to build up in the bed during a prolonged run, gas channeling would occur. When channeling, which is associated with poor solids mixing, occurs, the near-isothermal conditions in the bed are no longer maintained and temperatures at different levels in the bed begin to deviate from their normal uniform value.

It was of interest, therefore, to determine whether beds comprised of fine material would be operable for extended periods of time. In order to simulate such a bed during the later stages of a long run, a bed of fine sand (96.5 percent passing 100 mesh, 78 percent passing 200 mesh) was prepared and used as the starting material in Run CO-47; the final bed of this run was then used for Run CO-48. For comparison, the sand used in Run CO-45 had 83.4 percent between 20 and 200 mesh and 50.6 percent between 60 and 200 mesh.

Results and Discussion

The four runs were all completed satisfactorily as indicated by:

a) no pressure increase across the exit gas filters;

b) complete conversion of the zirconium tetrachloride vapor to zirconium oxide (as indicated by the absence of zirconium in the off-gas condensate stream);

c) no caking of the bed;

d) reasonably good material balances for each run.

However, in all runs, a large proportion of the oxide produced in the reaction was fine material of less than 200 mesh. The amount appearing as fines varied between 60 and 100 percent of the weight of oxide equivalent to the tetrachloride fed to the hydrolysis reactor.

Near the end of Run CO-48, a temperature spread of up to 20 degrees developed, whereas normally the spread is only a few degrees. This is indicative of gas channeling and poor solids mixing.

The starting bed of fine sand was used for a total operating time of about $8\frac{1}{2}$ hr (both Runs CO-47 and CO-48). Thus, the expected limit of operation for a bed of fine material is about 8 hr at tetrachloride feed rates of 4 to 5 kg/hr. No such limitation in bed operating time was

indicated by the results of Runs CO-45 and CO-46, for which somewhat coarser starting material was used. The total of the operating times for these runs was about 5 hr. Subsequent efforts will therefore be devoted to a determination of the operating limits of a bed of coarser material.

The primary interest has been the successful demonstration of the process under a wide range of process conditions. Although fines production has occurred in most tests, in no case has the buildup of fines prevented the successful operation of the process; hence no special effort has been made toward finding means of preventing fines formation.

c. Process Design Work for the Fluoride Volatility Pilot Plant for Recovery of Uranium from Zirconium Alloy Fuels
(N. Levitz, J. Barghusen, J. Holmes, C. Schoffstoll, W. Kremsner)

A pilot-plant facility (see Figures II-17 and II-18) for demonstrating the fluid bed-volatility scheme for processing highly enriched uranium-zirconium alloy fuels is being installed. The installation is currently about 75 percent complete. The remaining work, concerned primarily with extension and tie-in of copper pneumatic run-outs from the panelboard to process vessels and instrumentation, will be completed during the next quarter. Leak-testing and shakedown of the equipment is being carried on concurrently with the final installation work.

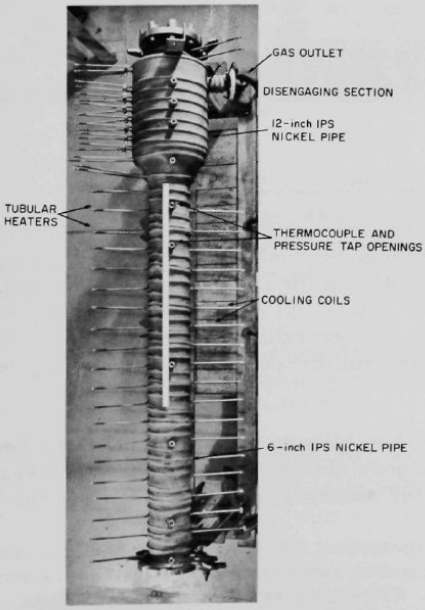

Figure II-17

PILOT-PLANT REACTOR FOR PROCESSING URANIUM-ZIRCONIUM ALLOY FUEL

Figure II-18

A SECTION OF THE PILOT-PLANT FACILITY (DURING INSTALLATION) FOR PROCESSING URANIUM-ZIRCONIUM ALLOY FUEL

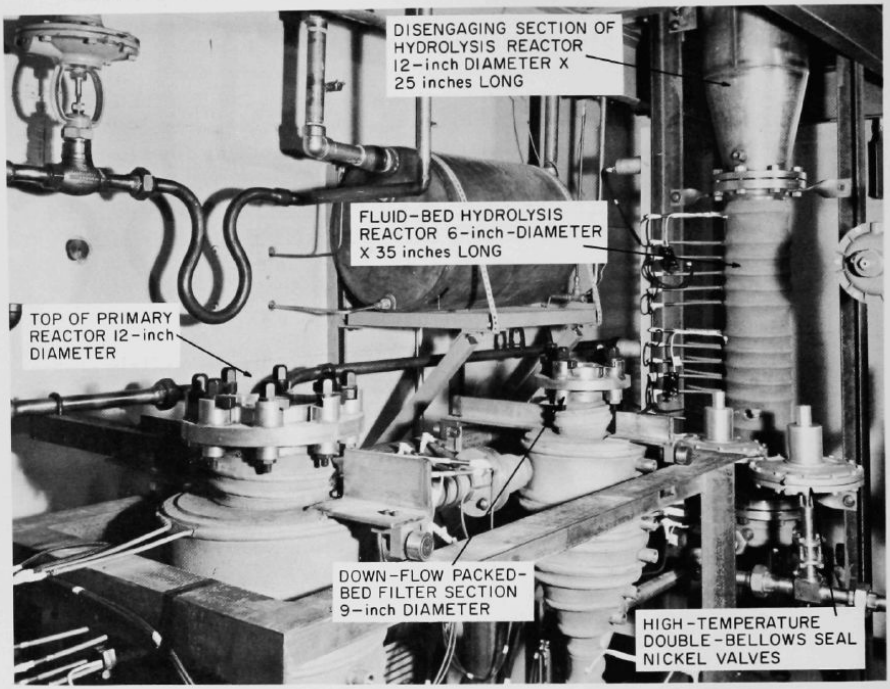

108-5836 Rev

Related Studies - Loading the Fuel

Processing of uranium-zirconium alloy fuel by the fluid bed-volatility method involves reaction of the fuel element while it is submerged in a fluidized bed of inert solids. In the current process concept, the bed will be re-used several times. Removal and reloading of the bed for successive reaction cycles will not be practicable; thus a scheme must be devised for introducing the fuel element directly into the reaction zone while the bed is present.

Initial loading of the fuel element onto the top of the bed while the bed is in a static condition does not appear difficult. An investigation has been made of a method for submerging* the element in the fluid bed.

*Since the fuel element is more dense than the fluidized bed, the element will drop through the bed by virtue of displacement of the bed particles. In contrast, a static bed will support the dense element since the packed particles cannot be displaced. If the element were allowed to drop through the fluidized bed, impact damage to the reactor might result.

The method that was conceived involves pulsing the bed with short-duration (~0.5 sec) gas pulses after the fuel element has been placed on the top of the bed while the bed is in a static condition. It was found that the element settles only while the bed is expanded (while it is momentarily fluidized); the objective, then, was to control the descent of the element by using pulses of appropriate size and frequency. In mock-up studies conducted in a 6-in.-diameter Lucite column (a prototype of the pilot-plant unit), controlled settling into beds of Alundum of a 4-ft-long fuel element weighing 15 kg was achieved. Further work is planned to establish the reliability of the method and to obtain the necessary quantitative information so that the method may be used with confidence in the pilot plant. Hopefully, such a method will be suitable in applications on a larger scale.

C. Conversion of Uranium Hexafluoride to Uranium Dioxide. Preparation of High-density Particles
(I. Knudsen, N. Levitz, M. Jones, J. Kincinas)

Process development studies were continued on a direct fluid-bed method for preparing high-density, spheroidal uranium dioxide particles from uranium hexafluoride. The process involves the simultaneous reaction of uranium hexafluoride with steam and hydrogen at temperatures of 650 to 700 C. The studies are being conducted in a 3-in.-diameter, cone-bottom Monel column described previously (see ANL-6379, p. 183). The starting bed for each run consists of uranium dioxide particles from previous runs. The operating procedure involves alternating 30-min periods of hexafluoride feed with periods of fluoride cleanup. In the cleanup period, only steam and hydrogen are fed. The uranium dioxide particles are removed semicontinuously (after each cleanup period) such that the bed weight remains approximately constant. The particles would be intended for use as coated or uncoated particles in dispersion fuels or in bulk form in packed fuel elements.

Previous work (see ANL-6596, pp. 158 to 163; ANL-6648, pp. 173 to 175) has been concerned primarily with establishing the effect on product density of a number of the process variables. Material of higher density was produced under the following conditions:

1) A higher bed temperature (700 C as opposed to 650 C). Densities of 9.7 to 9.8 g/cc and 9.3 g/cc, respectively, were obtained at these temperatures.

2) A lower hexafluoride feed rate. Typical densities were 9.5 g/cc at a feed rate of 17 g/min and of 9.1 g/cc at a feed rate of 34 g/min.

3) A deeper bed. Densities of 9.6 g/cc and 9.3 g/cc, respectively, were obtained for 18-in. and 8-in. beds.

4) Increased immersion (upward into the fluidized bed) of the hexafluoride nozzle. Material with a density of 9.5 g/cc was produced when the nozzle extended 13 in. upward into the bed, whereas a $\frac{3}{4}$-in. penetration gave material with a density of 9.0 g/cc.

Also, particles of varying density were produced when the concentration of steam in the reactant feed stream was varied. Highest densities were obtained at steam concentrations corresponding to the range 0.75 to 1.4 times the stoichiometric requirements.* A density of 9.8 g/cc was obtained in a run in which the operating conditions were a feed rate of 26 g UF_6/min, a steam concentration of 1.15 times stoichiometric, and a bed temperature of 650 C.

In contrast, changes in the hydrogen concentration alone, corresponding to the range 4 to about 20 times the stoichiometric requirements, did not appear to affect particle density. A somewhat higher residual fluoride content (650 ppm as compared with about 380 ppm) was obtained when the smaller amount of hydrogen was used.

In addition to the above studies, recent work has been directed towards the preparation of larger proportions of specific particle sizes because particular applications of dense particles might require material in several different size ranges. In the preceding report (see ANL-6648, pp. 173 to 175), the preparation of coarse particles, 22 w/o in the 16 to 20 mesh range, with densities of 8.9 g/cc (about 81 percent of theoretical), was reported. Current studies were concerned with the preparation of 80 to 100 mesh material. Also, attempts were made to prepare coarse (+20 mesh) material using a gas-pulsed fixed-bed technique instead of the regular fluid-bed method. The fixed-bed technique was evaluated as a possible alternative to the fluid-bed technique since, as the bed becomes more coarse, it becomes increasingly difficult to maintain the bed in a fluidized state and fluidizing gas requirements might very well become prohibitively high.

In the current work, the uranium hexafluoride feed rate was 25 g/min [44 lb uranium/(hr)(sq ft reactor cross section)], and the steam rate was 3.3 g/min, corresponding to 1.3 times the stoichiometric requirements. The hydrogen rate was adjusted to provide the overall desired superficial velocity of 0.5 ft/sec during the runs intended for the production of 80 to 100 mesh particles and of 1.0 ft/sec during the pulsed-bed studies. In the latter case, nitrogen gas pulses were superimposed on this steady flow.

---

*Based on the reaction $UF_6 + 2\ H_2O + H_2 \rightarrow UO_2 + 6\ HF$.

The pulse frequency ranged from 12 to 30 pulses/min and the duration of the pulses was from 0.25 to one second. The gas manifold pressure ranged from 20 to 80 psig. The reactor temperature was 650 C, and the bed weight was 6.0 kg (about 8-in. static bed height). Two runs of 11-hr total duration were made in the preparation of the 80 to 100 mesh particles. The pulsed-bed runs were of relatively short duration (1 to 4 hr), being intended only to establish the feasibility of the method.

Results

Preparation of 80 to 100 Mesh Particles. Dense oxide, primarily in the 80 to 100 mesh range, was produced from a starting bed of 100 to 140 mesh uranium dioxide particles. The product contained up to 62 percent +100 mesh particles and less than one percent +80 mesh particles. No seed particles were added in these runs so that particle growth into the +100 mesh fraction would occur.

The particle density of the final product was 9.4 g/cc (as measured by mercury displacement). This value is comparable with densities obtained in previous tests under similar conditions.

The density of the bed material actually increased during the two consecutive runs from an initial value of 8.2 g/cc to a final value of 9.4 g/cc. This increase was unusually rapid considering the fact that the quantity of new dioxide produced during each experiment was equivalent to only one displacement of the bed. Calculations indicate that such a final density would be achieved only if approximately half of the bed were to be replaced by theoretically dense oxide, and since this was not actually the case (that is, the material deposited on the particles in the bed was not of theoretical density), densification of the starting bed probably occurred by another mechanism, possibly a form of sintering. Further study of this rapid densification behavior will be made in the next series of experiments.

Pulsed-bed Work. Preliminary pulsed-bed studies showed that uniform temperatures were maintained in the bed and that the uranium hexafluoride conversion reaction could be carried out without caking of the bed; however, plugging of the uranium hexafluoride nozzle occurred after only several hours of operation. Some coarse (+20 mesh) material was produced, but particle quality was inferior to that produced under similar conditions in the fluidized bed, that is, the deposited material did not appear to adhere strongly to the base particles and many fragmented sections of the coating were found in the product. Due, apparently, to attrition of the particles, only a slight overall increase in particle size occurred. No further work on the use of this technique is planned at this time.

Future Work

In preparation for studies of the PuF_6 to PuO_2 reaction in fluidized beds, the filter vessel is being relocated directly above the reactor section so that during filter blowback, the fines produced during the reaction can be returned directly to the bed. Future work will be concerned with determining the effect on dense particle preparation of the presence of fines in the bed.

III. CALORIMETRY*

(W. N. Hubbard, H. M. Feder)

Thermodynamic data are lacking for many compounds of interest in high-temperature chemistry because of the experimental difficulties involved in making the necessary measurements. A program has been undertaken to determine some of these data.

The basic data needed are heats of formation at 25 C. Part of the program of the group consists of determinations of heats of formation by the method of oxygen bomb calorimetry. However, many of the compounds of interest are difficult to burn in oxygen and, consequently, cannot be studied by oxygen bomb calorimetry. To study compounds of interest that are difficult to burn in oxygen and thus not amenable to oxygen bomb calorimetry, the techniques of the bomb calorimetric method (a method which has been developed to a high degree of precision and accuracy) have been modified so that fluorine can be used as the oxidant.

The accumulation of basic heat of formation data for fluorides is a necessary preliminary adjunct to the general use of fluorine bomb calorimetry for the study of compounds and is a valuable program in its own merit. To date, heats of formation have been determined for magnesium fluoride, cadmium fluoride, aluminum fluoride, zinc fluoride, boron trifluoride, molybdenum hexafluoride, uranium hexafluoride, and the tetrafluorides of titanium, zirconium, hafnium, and silicon. The heats of combustion in fluorine of three compounds: boron nitride, silicon dioxide, and zirconium diboride, have been determined by fluorine bomb calorimetry. To obtain the heat of formation value for boron nitride required the use of the value obtained previously for boron trifluoride; for silicon dioxide, the value for silicon tetrafluoride was required; and for zirconium diboride, the values for boron trifluoride and zirconium tetrafluoride were required.

To determine thermodynamic properties at high temperatures, the heats of formation at 25 C from oxygen or fluorine bomb calorimetry will be combined with the change in enthalpy values measured by a high-temperature enthalpy calorimeter. This calorimetric system, which is to be used for measurements up to 1500 C, has been designed and is now being assembled and tested. Design concepts for an electron beam furnace for a drop calorimeter to operate up to 2500 C are being tested in the laboratory.

A. Combustion of Zinc in Fluorine

(E. Rudzitis and R. Terry)

Combustion techniques for burning the low-melting metals cadmium, magnesium, and aluminum have been successfully applied to combustions of zinc in fluorine. Prefluorinated zinc filings were placed on a zinc fluoride support dish and ignited by a fine fuse wire. Ignition difficulties were more

*A summary of this section is given on pages 22-23.

pronounced for zinc than for the other three elements but were overcome (1) by the use of cadmium fuse wire (which was also used in aluminum combustions) and (2) by increasing the initial fluorine pressure from 150 psi to 200 psi. The percent completeness of combustion for zinc, which ranged from 67.6 to 96.0, was generally lower than that for the other low-melting metals.

Although the support dishes were routinely exposed to fluorine prior to use, the presence of an oxide impurity in them was one of the most important sources of error in previous combustions by the fluoride dish support technique. The oxide concentration in the zinc fluoride dishes used in some of the experiments in this study was reduced below the background limit of detection by treatment of the zinc fluoride powder (before fabrication into dishes) with liquid hydrogen fluoride at temperatures up to 250 C and pressures of 1000 to 2000 psi.

The results of zinc combustions are summarized in Table III-1. In experiments 3 to 6, the support dishes were fabricated from zinc fluoride powder which had been treated with liquid hydrogen fluoride. The entries in the table are defined as follows: (1) experiment number; (2) m', the mass of sample burned; (3) Δt_c, the observed increase in calorimeter temperature, corrected for heat exchange between the calorimeter and its surroundings; (4) $\epsilon_{calor}(-\Delta t_c)$, the energy equivalent of the calorimeter multiplied by $-\Delta t_c$; (5) ΔE_{cont}, the energy absorbed by the contents of the bomb; (6) ΔE_{gas}, the correction of the bomb gases to standard state conditions; (7) ΔE_{ign}, the electrical energy introduced to ignite the sample; (8) ΔE_{fuse}, the energy evolved by the combustion of the cadmium fuse wire; (9) ΔE_{imp}, the energy evolved by fluorination of the oxide impurities in the sample and the support dishes; (10) $\Delta Ec^\circ/M$, the sum of items 4 through 9 divided by the mass of metal burned, represents the standard energy change per gram of sample at 25 C for the reaction

$$Zn(c) + F_2(g) \rightarrow ZnF_2(c)$$

Table III-1

COMBUSTION OF ZINC IN FLUORINE

(1) Experiment No.	1	2	3	4	5	6
(2) m', g	0.6874_7	0.5564_7	0.7981_4	0.8043_9	0.7939_8	0.6887_4
(3) Δt_c, C	0.54890	0.44142	0.61898	0.62552	0.61915	0.53733
(4) $\epsilon_{calor}(-\Delta t_c)$, cal	-1968.9	-1583.3	-2220.2	-2243.7	-2220.8	-1927.3
(5) ΔE_{cont}, cal	-4.1	-3.2	-4.0	-4.0	-3.9	-3.8
(6) ΔE_{gas}, cal	-0.8	-0.4	-0.6	-0.6	-0.6	-0.4
(7) ΔE_{ign}, cal	0.1	0.1	0.1	0.1	0.1	0.1
(8) ΔE_{fuse}, cal	4.5	4.4	4.5	4.5	4.5	4.0
(9) ΔE_{imp}, cal	54.2	27.5	0.4	0.4	0.4	0.4
(10) $\Delta Ec^\circ/M$, cal/g	-2785.4	-2794.2	-2781.2	-2788.8	-2796.4	-2797.9

Mean $\Delta Ec^\circ/M$ = -2790.6 cal/g

Standard Deviation of Mean = ±2.4 cal/g or ±0.06 percent

in which each reactant and product is in its standard state. Mean $\Delta Ec°/M$ is the mean standard energy of combustion per gram of sample.

Some of the more important corrections were applied as follows. The mass of metal burned, M, was obtained by subtracting the mass of the unburned metal and the mass of the impurities from the mass of the sample initially placed in the bomb. The mass of the unburned metal was determined by treatment of the residue of the combustion with hydrochloric acid and gasometric measurement of the hydrogen evolved on the assumption that the amount of unburned metal was equivalent to the amount of hydrogen evolved. The weight correction for the impurities in the sample was made on the assumption that nitrogen, hydrogen, and carbon are present in the sample as sorbed nitrogen, water, and carbon dioxide, respectively, and that oxygen and fluorine (due to prefluorination) are bound as metal oxide and fluoride, respectively.

The thermal corrections for experiments 1 and 2 were based on the results of mass spectrometric analysis of the combustion gases. The thermal corrections for the remaining runs were made on the basis of the oxygen content in the sample, which was within the limits of precision of the mass spectrographic analysis. The only gaseous component of significance in the combustion gases was oxygen. It was assumed that the amount of metal oxide fluorinated was equivalent to the net amount of oxygen found in the combustion gases. Nitrogen and small amounts of carbon dioxide and water also present in the combustion gases were assumed to have originated from desorption from the sample and the sample-support dish during the combustion process. No thermal corrections were made for the nitrogen, carbon dioxide, and water found. Small amounts of tetrafluoromethane and silicon tetrafluoride, probably originating from the fluorination of carbon dioxide and silicon dioxide, were also detected in the combustion gases. Uncertainties in the analysis and a self-compensating effect in the overall application of the oxygen correction did not warrant an application of specific thermal corrections for the small amounts of tetrafluoromethane and silicon tetrafluoride present. It is likely that a portion of the adsorbed water reacted with fluorine to form hydrogen fluoride and oxygen, although no hydrogen fluoride was detected in the combustion gases, because the analytical method used was not capable of detecting the small amount of hydrogen fluoride present. This thermal effect also was partially compensated for in the application of the oxygen correction.

The following thermodynamic constants for the formation of zinc fluoride were derived for 298.15 K in kcal/mole: $\Delta Ec° = \Delta Ef° = -182.4$, $\Delta Hf° = -183.0$ and $\Delta Gf° = -170.8$. An uncertainty interval of ± 0.4 kcal was assigned to each of the constants.

The value of $\Delta Hf^{\circ}_{298}(ZnF_2)$ determined in this work is given in Table III-2 along with the values obtained by high-temperature equilibrium measurements. The heats of reactions, ΔH°_{298}, were obtained by application of the equation $-\Delta H^{\circ}_{298}/T = R \ln K_p + \sum_{\text{Prod.-React.}} (F^{\circ}_T - H^{\circ}_{298})/T$ to the original data. The value for the heat of formation of zinc fluoride obtained in the present study agrees best with the value obtained from the study of the equilibria at various temperatures of the zinc oxide-hydrogen fluoride reaction. It is significant that the values of ΔH°_{298} for this reaction showed no significant trend with temperature. The trends in the calculated heat of reaction data for the other two equilibria, indicating systematic experimental errors, prevent assigning meaningful error limits to the derived $\Delta Hf^{\circ}_{298}(ZnF_2)$ values.

Table III-2

ESTIMATED HEATS OF FORMATION OF ZINC FLUORIDE

Equilibrium	Temperature (K)	ΔH°_{298} (kcal/mole)	$\Delta Hf^{\circ}_{298}(ZnF_2)$ (kcal/mole)
$Zn + 2HF = ZnF_2 + H_2$ [a]	873, 973, 1023	-47.1, -47.5, -48.0	-177.3
$ZnCl_2 + 2\ HF = ZnF_2 + 2\ HCl$ [b]	590, 682, 786	+4.2, +6.3, +8.8	-185.5
$ZnO + 2\ HF = ZnF_2 + H_2O$ [c]	773, 823, 873, 923	-27.6, -27.7, -27.8, -27.8	-182.9 ± 1.0
This work	298	-	-183.0 ± 0.4

[a] K. Jellinek and A. Rudat, Z. Anorg. Chem., 175, 28 (1928).
[b] K. Jellinek and R. Koop, Z. Physik, Chem., A145, 305 (1929).
[c] L. Domange, Ann. Chem., 7, 225 (1937).

B. Combustion of Niobium and Tantalum in Fluorine
(E. Greenberg and C. Natke)

The development of satisfactory combustion techniques for niobium and tantalum was reported in ANL-6333, p. 127. During the past quarter, two series of tantalum calorimetric combustions and five combustions of niobium in fluorine were completed.

Table III-3 presents preliminary data for the combustion of tantalum in fluorine. Table III-4 presents similar data for the partially completed series of niobium combustions. The quantity reported, ΔT/gram, is the corrected temperature rise of the calorimeter per gram of sample burned. The data are presented primarily to indicate the precision of the results. Experience with similar systems indicates that the precision of the results is not significantly affected by the standard-state calculations. The standard deviation of the mean for the first tantalum series is somewhat greater than

that for the second series (0.07 percent as compared with 0.01 percent) because of minor experimental difficulties. Run 6 is obviously in gross error and can be justifiably discarded by the usual statistical rules. The precision of approximately 0.01 percent for the second tantalum series and for the partially completed niobium series is considered to be quite satisfactory.

Table III-3

PRELIMINARY DATA FOR THE COMBUSTION OF TANTALUM IN FLUORINE

Run No.	ΔT/gram (C/g)	
	Series I	
1	0.7009	
2	0.7008	
3	0.7016	Mean (excluding Run 6) = 0.7012 C/g
4	0.7020	Std. Dev. of Mean = 0.0005 C/g or 0.07%
5	0.7005	
6	0.7285	
7	0.7011	
	Series II	
8	0.7014	
9	0.7009	
11	0.7013	Mean = 0.7012 C/g
12	0.7011	Std. Dev. of Mean = 0.0001 C/g or 0.01%
13	0.7009	
14	0.7018	
15	0.7013	

Table III-4

PRELIMINARY DATA FOR THE COMBUSTION OF NIOBIUM IN FLUORINE

Run No.	ΔT/gram (C/g)	
1	1.3010	
2	1.3009	Mean = 1.3010 C/g
3	1.3009	Std. Dev. of Mean = 0.0001 C/g or 0.01%
4	1.3013	
5	1.3007	

As in any calorimetric combustion work, it is necessary adequately to characterize the initial and final states and compositions of the materials used in these combustions in order to evaluate properly the calorimetric data. As applied to this work, a most important part of this characterization is proof that all the niobium or tantalum consumed during combustion has been burned to the respective pentafluorides with no trace of lower fluorides. (If lower fluorides are formed, the amount of such side products must be accurately determined so that suitable thermal corrections can be applied.) Conventional analytical procedures are inadequate for demonstrating the absence of side products to a level which is comparable with the precision obtained in the combustion data. X-ray diffraction analysis will identify only the major product. Minor phases present in amounts smaller than a few percent cannot usually be detected. Elemental analysis for metal and fluorine is not sensitive enough to reveal small amounts of lower fluorides. It was therefore highly desirable to devise some method for accurately demonstrating the purity of the combustion products.

A solution to the problem was sought by taking advantage of the difference in vapor pressures of the trifluorides and pentafluorides of niobium and tantalum. The pentafluorides are much more volatile and can be sublimed in vacuum at temperatures well below that required for volatilization of the trifluorides. An apparatus was prepared for volatilizing in vacuum a weighed sample of the combustion product. Because the pentafluorides of niobium and tantalum hydrolyze rapidly in the atmosphere, provision was made for weighing the sample and loading the apparatus in a dry box. Preliminary experiments with the tantalum combustion product revealed nonvolatile residues to the extent of 1 percent of the original sample. It was strongly suspected that the dry box atmosphere was not adequate for handling tantalum pentafluoride and that the residue was not a lower fluoride but rather a nonvolatile hydrolysis product which had formed during handling of the sample in the dry box.

This experiment was repeated with the niobium combustion product, using a dry box with a highly inert atmosphere. This time, quantitative volatilization of the combustion product sample was effected, demonstrating that no significant quantities of lower fluorides were formed during combustion. This experiment adds considerable confidence to the calorimetric data and will be performed again with the tantalum combustion product, using the highly purified inert atmosphere box. It is anticipated that this approach will become a generally useful analytical method that will be applicable to other metal-fluorine systems to be studied by fluorine bomb calorimetry in the future.

In the absence of X-ray data for niobium pentafluoride and tantalum pentafluoride in the literature, the solid combustion products were identified by the similarity of their X-ray patterns to each other and to that of

molybdenum pentafluoride.[1] Infrared analysis indicated that carbon and silicon impurities in the system were burned to the respective tetrafluorides.

C. Combustion of Ruthenium
(H. A. Porte, E. Greenberg, C. Natke)

Six calorimetric combustions of ruthenium in fluorine have been completed, and the detailed calculations are in progress. The sample arrangement and combustion technique were very similar to that described[2] for the combustion of zirconium in fluorine.

Table III-5 presents preliminary data for the combustion of ruthenium in fluorine. The entries in the table are: (1) experiment number; (2) the mass in vacuo of the ruthenium reacted, which was determined by subtracting the mass of unburned metal recovered after combustion from the mass of sample originally introduced into the bomb; (3) the observed increase in the calorimeter temperature, corrected for heat exchange between the calorimeter and its surroundings; (4) the energy equivalent of the calorimetric system, multiplied by $-\Delta t_c$; (5) the energy evolved by combustion of the molybdenum fuse wire; and (6) the energy change per gram of ruthenium burned for the reaction

$$Ru(c) + 2\tfrac{1}{2}\, F_2(g) \rightarrow RuF_5(s) \quad .$$

Table III-5

PRELIMINARY DATA FOR THE COMBUSTION OF RUTHENIUM IN FLUORINE

(1) Experiment No.	1	2	3	4	5	6
(2) m', g	2.21302	2.36571	2.30697	2.63447	2.24638	2.27031
(3) Δt_c, C	1.31456	1.39981	1.36703	1.56054	1.32878	1.34577
(4) $\epsilon_{calor.}$ $(-\Delta t_c)$, cal	-4655.96	-4957.90	-4841.80	-5527.18	-4706.33	-4766.50
(5) ΔE_{fuse}, cal	1.44	1.59	1.53	1.76	1.63	1.48
(6) $\Delta Ec^0/M$ (ruthenium), cal/g	-2103.24	-2095.06	-2098.11	-2097.36	-2094.35	-2098.84

Mean $\Delta Ec^0/M$ = -2097.8 cal/g

Standard Deviation of Mean = ±1.3 cal/g or ±0.06 percent

It was necessary to demonstrate that the combustion of ruthenium results in the formation of ruthenium pentafluoride uncontaminated by lower fluorides. Several experiments were carried out in an attempt to volatilize completely a sample of the ruthenium combustion product. Even

---

[1] LaValle, D. E. (ORNL), Private Communication to L. Stein (ANL), May 22, 1959.

[2] Greenberg, E., Settle, J. L., Feder, H. M., and Hubbard, W. N., J. Phys. Chem., 65, 1168 (1961).

in the most successful experiment, a nonvolatile residue of 0.4 percent of the sample weight was obtained. This experiment was carried out using the high-purity inert-atmosphere box. In earlier experiments, in which a glove box of poorer atmosphere was used, the weight of the residue was greater by an order of magnitude. Ruthenium pentafluoride reacts readily with moisture, and there were visible signs of reaction even when the high-purity inert-atmosphere box was used. The evidence obtained, while not as conclusive as in the case of niobium, suggests that the nonvolatile residue is formed by hydrolysis of ruthenium pentafluoride. No additional volatilization experiments are being planned.

D. Exploratory Combustions of Carbon in Fluorine
(E. Greenberg)

The heat of formation of carbon tetrafluoride has been the subject of five separate modern thermochemical studies:

(1) Kirkbride and Davidson[3] studied the displacement reaction between carbon tetrafluoride and potassium to give potassium fluoride and carbon, obtaining a value of ΔHf°_{298} (CF_4, g) = -218 kcal/mole.

(2) The value -220.4 kcal/mole was obtained by Jessup, McCosky, and Nelson[4] by the combustion of carbon tetrafluoride in fluorine.

(3) The value -218.3 kcal/mole was obtained by Scott, Good, and Waddington[5] by combustion of mixtures of Teflon and a hydrocarbon oil in which the reaction products were CF_4 and HF.

(4) The value -212.7 kcal/mole was obtained by Duus[6] by the hydrogenation of C_2F_4 to C and HF and the decomposition of C_2F_4 to C and CF_4.

(5) The value -217.2 kcal/mole was obtained by Neugebauer and Margrave[7] by reactions similar to those used by Duus.

Because the literature values for the heat of formation of tetrafluoromethane vary over a range of several kilocalories, it is desirable to attempt resolution of this discrepancy by direct combustion of carbon in fluorine. The heat of transformation between graphite and diamond is

---

[3]F. W. Kirkbride and F. G. Davidson, Nature 174, 79 (1954).

[4]R. S. Jessup, R. E. McCosky, and R. A. Nelson, J. Am. Chem. Soc. 77, 244 (1955).

[5]D. W. Scott, W. D. Good, and G. Waddington, J. Am. Chem. Soc. 77, 245 (1955).

[6]H. C. Duus, Ind. Eng. Chem. 47, 1445 (1955).

[7]C. A. Neugebauer and J. L. Margrave, J. Phys. Chem. 60, 1318 (1956).

well known from oxygen bomb calorimetry (both varieties have been burned to carbon dioxide); therefore, either form of carbon is satisfactory for fluorine combustion studies. Initial experiments in a glass bomb indicated that the combustion technique used for zirconium (vertically supported rods, ignited at the top) was quite promising. Graphite rods $\frac{1}{8}$ in. in diameter were employed as sample material.

Successful ignition of graphite rods was achieved with use of a carbon filament fuse and a small piece of graphite cloth; such an all-graphite sample is completely analogous to the system employed for zirconium. However, there was some indication that the use of graphite cloth led to incompletely burned products. Attention is therefore being directed to the use of metal wire and foil (such as molybdenum) to ignite the carbon rod.

Preliminary analytical work indicated that a small amount (about 0.1 to 1 percent) of hexafluoroethane side product was formed, in addition to the main product, tetrafluoromethane. A gas chromatographic method for the determination of small amounts of hexafluoromethane in tetrafluoromethane was developed by M. Runner of Chemical Research Services, Addison, Illinois. This method has been used to analyze the gaseous products of several combustions which were carried out in glass bombs, and has been found to be satisfactory.

Trial combustions are now being carried out in a nickel calorimetric combustion vessel in order to avoid the contaminants introduced when using the glass bomb. Since the volumes and thermal characteristics of the two vessels are quite different, it is necessary to use a somewhat different fluorine pressure in order to obtain successful combustions. Current experimental work is being directed towards finding the optimum conditions for burning graphite rods (using molybdenum foil and fuse wire) in a nickel bomb. The combustion products will be analyzed to demonstrate that the amount of hexafluoroethane is not excessive.

E. Exploratory Combustions of Silicon Carbide in Fluorine (E. Greenberg)

About a year ago, work in this laboratory resolved a discrepancy in the heat of formation of silica as determined by oxygen bomb calorimetry[8] and by equilibrium studies.[9] Recently, Chipman[10] has pointed out similar discrepancies between literature values for the heat of formation of silicon carbide. The values were found to range from about -12 to -20 kcal/mole. The heat of formation of silicon tetrafluoride has already been determined, and the heat of formation of tetrafluoromethane is currently under study.

[8]Humphrey, G. L., and King, E. G., J. Am. Chem. Soc., 74, 2041 (1952).

[9]Chipman, J., J. Am. Chem. Soc., 83, 1762 (1961).

[10]Rein, R. H., and Chipman, J., J. Phys. Chem., 67, 839 (1963).

Consequently, it may be possible to resolve the discrepancies by determining the heat of combustion of silicon carbide in fluorine.

At a pressure of 10 atm of fluorine, silicon carbide does not appear to react significantly with fluorine. At the same pressure of fluorine, however, silicon carbide can be ignited by using either a small amount of sulfur, which ignites spontaneously in fluorine, or a molybdenum fuse wire in close proximity to the powdered sample. The latter method is preferred. The use of sulfur has the disadvantage that the combustion is more violent, thereby sweeping sample material out of the sample container to a greater extent.

Both nickel and silica have been tried as sample-support materials. Silica used as a $\frac{1}{16}$-in.-thick dish ignited easily and burned extensively. It is possible that a relatively massive silica dish which does not have exposed edges near the combustion zone would be satisfactory. Nickel, on the other hand, shows very little surface reaction when used as a support for combustions of silicon carbide. One-half-gram samples of silicon carbide have been burned on rather heavy nickel dishes without severe attack on the dish. Ignitions were achieved with a molybdenum fuse wire, and some scattering of the sample was evident. Combustion was about 50 to 65 percent complete, and the unburned silicon carbide appears visually to have undergone no change or reaction.

Future development of the combustion technique will include analysis of the gaseous combustion products.

F. Thermochemistry of the Uranium-Sulfur System
(J. Settle)

In various fields of high-temperature work, including nuclear reactor technology, there is considerable interest in the properties of the uranium sulfides, particularly the monosulfide. A knowledge of the enthalpies of formation of these compounds and of their high-temperature heat capacities and entropies would allow more accurate estimates to be made of their chemical behavior at elevated temperatures.

A search of the literature revealed that five binary compounds of uranium and sulfur have been identified.[11-15] These are US, U_2S_3, U_3S_5, US_2, and US_3. Three crystalline forms have been reported for US_2.[15,16]

---

[11] Shotzer, E. F., Schneider, O., and Bilt, W., Z. anorg. u. allgem. Chem., 243, 307 (1940).

[12] Zumbush, M., Z. anorg. u. allgem. Chem., 243, 322 (1940).

[13] Eastman, E. D., Brewer, L., Bromley, L. A., Gilles, P. W., and Lofgren, N. L., J. Am. Chem. Soc., 72, 4019 (1950).

[14] Zachariasen, W. H., Acta Cryst., 2, 291 (1949).

[15] Picon, M., and Flahaut, J., Bull. Soc. Chim. France, 1958, 776 (1958).

[16] Mooney, R. C. L., CP-1507 (1944).

Thermodynamic data on the uranium sulfides are very scanty. Westrum and Grønvold[17] and Westrum[18] have measured the low-temperature heat capacities and entropies of uranium monosulfide, beta uranium disulfide, and uranium trisulfide. Cater,[19,20] studied the vaporization of uranium monosulfide by the effusion method over the temperature range from 1840 to 2770 K. The composition of the vapor was studied by means of a time-of-flight mass spectrometer in the temperature range from 2100 to 2400 K. Combination of the data obtained from these experiments enabled Cater to calculate the heats for the following reactions:

$$US(s) = US(g) \qquad \Delta H^{\circ}_{2300} = 150.3 \pm 2.1 \text{ kcal/mole} \quad ; \quad (2)$$

$$US(s) = U(g) + S(g) \qquad \Delta H^{\circ}_{2300} = 271.2 \pm 4.0 \text{ kcal/mole} \quad . \quad (3)$$

Cater estimated the enthalpy of formation of uranium monosulfide from rhombic sulfur and solid uranium at room temperature to be $\Delta Hf^{\circ}_{298}(US, s) = -99$ kcal/mole or -90 kcal/mole, depending upon whether 3.6 or 4.4 ev was used for the dissociation energy of gaseous S_2. Rand and Kubaschewski[21] have estimated the enthalpies of formation at 298 K of US, U_2S_3, US_2, and US_3 to be -93 ± 5, -224 ± 8, -120 ± 10, and -127 ± 10 kcal/mole, respectively. Rand and Kubaschewski made their estimates by analogy to similar thermochemical systems for which some experimental data are available. Therefore, it appears that an experimental determination (at room temperature) of the enthalpies of formation of some of these uranium-sulfur compounds would be desirable. Fluorine bomb calorimetry apparently is suitable for this purpose. A good value for the standard enthalpy of formation of sulfur hexafluoride is necessary if fluorine bomb calorimetry is to be used. Gross, Hayman, and Levi[22] have determined that $\Delta Hf^{\circ}_{298.15}(SF_6, g) = -288.5 \pm 0.7$ kcal/mole. This value may not be of adequate accuracy. Therefore, it may be necessary for this group to redetermine it.

---

[17] Westrum, E. F., Jr., and Grønvold, F., Symposium on the Thermodynamics of Nuclear Materials, p. 3, International Atomic Energy Agency, Vienna (1962).

[18] Westrum, E. F., Jr., Low Temperature Chemical Thermodynamics Project, TID-11188 (Nov. 25, 1960).

[19] Cater, E. D., The Vaporization Thermodynamics, and Phase Behavior of Uranium Monosulfide, ANL-6140 (1960).

[20] Cater, E. D., Gilles, P. W., and Thorn, R. J., J. Chem. Phys., 35, 608 (1961).

[21] Rand, M. H., and Kubaschewski, O., The Thermochemical Properties of Uranium Compounds, Interscience Publishers, New York (1963).

[22] Gross, P., Hayman, C., and Levi, D. L., XVIIth Int. Congr. Pure and Applied Chem., Abstracts 1, 405 (1959).

Uranium monosulfide is the first to be studied. Preliminary studies of its combustion characteristics in fluorine are now in progress. Variables being considered are: the weight of sample, the particle size of the sample, the initial fluorine pressure, and various methods of supporting the reacting sample. It appears that a 1.5- to 2.5-g sample of uranium monosulfide supported on a massive zirconium dish and under 10 to 20 atm fluorine pressure can be successfully converted to uranium heaxfluoride and sulfur hexafluoride. The best conversion achieved thus far (in a series of five exploratory combustions) was about 95 percent complete, but it is expected that this can be significantly improved by adjusting the variables mentioned above.

G. High-temperature (1500 C) Enthalpy Calorimeter
(D. R. Fredrickson, R. L. Nuttall, and R. Kleb)

During the past quarter, work has continued on the furnace component of the calorimetric system (see Chemical Engineering Division Summary for October, November, December, 1961, ANL-6477, p. 164) which will be used to measure changes in enthalpy up to 1500 C. Furnace temperature controls (which are described in ANL-6648, p. 182) were modified slightly, and the furnace was again tested, being controlled at 277 C and 1004 C. A platinum capsule with thermocouples on the top and bottom was suspended in the hot zone of the furnace to check for temperature gradients. The control circuitry was modified (see ANL-6648, p. 185) to include a standard Barber Colman Series 620 silicon-controlled rectifier unit for the control of the main shield heater. All three heaters now employ silicon-controlled rectifiers. A maximum variation of 0.1 C in the main shield temperature for a period of 16 hr was observed at 1004 C. This variation was shown on a recorder with full scale representing 5 C.

In the tests of the furnace, a platinum capsule containing platinum, platinum-10 percent rhodium thermocouples was suspended in the hot zone of the furnace. The cylindrical capsule was approximately 1 x 4 cm and contained powdered Al_2O_3 to position the thermocouples and give a uniform temperature. The capsule contained thermocouples at the top and bottom, with provisions for reading the differential temperature as well. Thermocouple leads were taken out through a "tee" at the bottom of the furnace, through a slotted rubber stopper. At a furnace temperature of 1004 C, the maximum variation in temperature from top to bottom of the capsule was 0.18 C, as read on a K-3 potentiometer.

In an effort to make optical pyrometer measurements of the furnace temperature, a temporary glass window and prism was placed at the bottom of the furnace prior to furnace heatup. It was observed that soon after heating began, a deposit started to form on this window; within a short time, the window was completely covered with the deposit. Upon being exposed to air, the deposit changed from a dull yellow dry substance to a black sticky substance. Spectrographic and spectrochemical analyses

of the deposited material indicated the absence of heavy metals such as tungsten and molybdenum. (These might be expected to be deposited if oxidation of the furnace core had occurred.) Spectrochemical analysis did indicate sodium to be present in large quantity in the deposit, along with the following elements: potassium and zinc, 1 percent; aluminum, 2 percent; cadmium, 3 percent; lead, 0.6 percent; and magnesium, 0.4 percent.

Increasing difficulty has been encountered in the control of the furnace temperature with each heatup. Two absolute thermocouples (one in the floating shield and the other in the bottom shield) showed an open circuit after several initial heatups. The outer-shield main-shield differential thermocouple readings have been very erratic. Varying the power to the outer-shield heater affected the absolute main shield-control thermocouple, showing a ground loop of undetermined nature. In an effort to evaluate these control problems, an extended period (2 weeks) of heating is planned at a temperature near 1000 C. Heating over an extended period of time should show whether or not the deposit which forms affects the furnace windings and thermocouples. Opening of the furnace for repairs and changes may be necessary.

H. High-temperature (2500 C) Enthalpy Calorimeter (R. L. Nuttall)

As part of the Calorimetry Group program to determine the thermal properties of material at high temperature, a calorimetric system for measuring enthalpy changes between 25 C and 2500 C is being constructed. Like the 1500 C calorimetric system, the 2500 C system is a drop type. (A sample is brought to temperature equilibrium in a furnace and then dropped into a calorimeter for measurement of the enthalpy change as the sample cools.)

The cylindrical furnace core which will contain the sample during heatup is to be heated by electron bombardment from two diametrically opposed electron guns. Longitudinal temperature uniformity will be obtained by sweeping the electron beams along the length of the furnace core by a suitable program. Circumferential temperature uniformity will be obtained by rotating the furnace core around its axis.

The electron guns and the power supply assembly for operating them have been purchased. The power supply assembly was damaged in transit, but because the damage appears to be slight, it was agreed that the necessary repairs will be made here as the assembly is tested. A vacuum chamber on which the electron guns can be mounted for testing of the power supply assembly has been built, and testing and repair of the damages has been started.

The furnace has been designed, and detailed drawings are being made.

The calorimeter is to be an adiabatic type similar to one previously designed here for use with the lower-temperature drop calorimeter. The calorimeter has been designed, and detailed drawings have been completed. Shop construction should start in the near future.

A "drop mechanism" is being designed. This mechanism will accelerate the sample to several times gravitational acceleration to minimize the time the sample spends in the cold region between the furnace and calorimeter.

IV. REACTOR SAFETY*

The oxidation, ignition, and combustion processes of metals and compounds used in nuclear technology are being studied to provide information to aid in minimizing the hazards associated with handling these materials.

A. Metal-Oxidation and Ignition Kinetics
(L. Baker)

1. Isothermal Oxidation of Uranium in Air at 500 C and Higher
(R. Wilson, L. Baker, R. Koonz)

The air oxidation of uranium at temperatures above 500 C is being studied in order to determine the nature and degree of protectiveness of oxide films formed at high temperatures. An important part of this study will be assessment of the role of nitrogen in the oxidation reaction.

Previous studies of the oxidation of uranium were carried out in oxygen in the temperature ranges from 125 to 295 C[1,2,3] and from 300 to 625 C.[4] Studies of the ignition behavior of uranium[5] and its alloys[6] and studies of the temperature[7] and propagation[8] of burning along wires and foils of uranium have indicated that protective oxide films are formed at temperatures above 450 C. Experimental arrangements used in the previous studies of oxidation, ignition, and burning were not satisfactory for oxidation studies in the high-temperature range because of excessive self-heating. For this reason, a new experimental procedure was devised.

---

*A summary of this section is given on pages 23 to 25.

[1]Leibowitz, L., Schnizlein, J. G., Mishler, L. W., and Vogel, R. C., J. Electrochem. Soc. 108, 1153 (1961).

[2]Leibowitz, L., Schnizlein, J. G., Bingle, J. D., and Vogel, R. C., J. Electrochem. Soc. 108, 1155 (1961).

[3]Schnizlein, J. G., Bingle, J. D., and Leibowitz, L., J. Electrochem. Soc. 108, 1166 (1961).

[4]Baker, L., Jr. and Bingle, J. D., The Kinetics of Oxidation of Uranium between 300 and 625 C, in preparation (see also ANL-6543, p. 168 and ANL-6569, p. 136).

[5]Baker, L., Jr., Schnizlein, J. G., and Bingle, J. D., The Ignition of Uranium, in preparation.

[6]Schnizlein, J. G., Baker, L., Jr., and Bingle, J. D., The Ignition of Binary Alloys of Uranium, in preparation.

[7]Mouradian, E. M. and Baker, L., Jr., Nuclear Sci. Eng. 15, 388 (1963).

[8]Leibowitz, L., Baker, L., Jr., Schnizlein, J. G., Mishler, L. W. and Bingle, J. D., Nuclear Sci. Eng. 15, 395 (1963).

a. Apparatus and Procedure

A schematic diagram of the apparatus is shown in Figure IV-1. The sample, a nominal one-cm cube of uranium,* was supported on a stainless steel-clad thermocouple and contained within a quartz reaction cell. The oxidizing gas was dried air which contained about 6 v/o argon. The argon served as an internal standard for the analytical procedure. The mixture was prepared by equilibrating a tank of air and a tank of argon, which resulted in a single high-pressure cylinder containing the desired mixture. During a run, the premixed gas passed through a double-stage pressure regulator, was dried in Molecular Sieve, and subsequently passed through a low-pressure regulating valve. The gas then passed through a micrometer-head needle valve which was used to regulate the flow rate. Flowmeters were located at the inlet and at the outlet of the reaction cell.

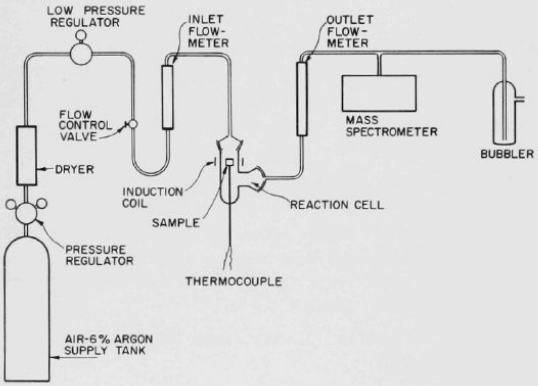

Figure IV-1
APPARATUS USED FOR THE ISOTHERMAL OXIDATION OF URANIUM IN AIR AT 600 C AND ABOVE

Samples were heated by induction to 500 C, 600 C, 700 C, 800 C, 900 C, and 1000 C. A single-turn induction coil, which was external to the reaction cell, was used. Specimens were heated from room temperature to the test temperature in about one minute. An isothermal temperature was maintained by manual adjustment of the power of the induction generator. In this way, it was possible to compensate for heat generated by the oxidation reaction. The quantity of oxygen and nitrogen removed from the stream was determined by a small mass spectrometer** which was programmed to sweep across the spectrum from m/e 14 to m/e 40 at 2-min-intervals. Gas was fed into the mass spectrometer through a small bleed line on the main flow stream (see Figure IV-1).

*The total impurity content of the uranium is about 250 ppm. A detailed analysis of the metal may be found in J. G. Schnizlein, et al., Ignition Behavior and Kinetics of Oxidation of the Reactor Metals, Uranium, Zirconium, Plutonium, and Thorium, and Binary Alloys of Each. A Status Report, ANL-5974 (April 1959), p. 146.

**Type 21-611, Consolidated Electrodynamics Corporation, Pasadena, California.

The gas flow rate during a run was adjusted so that between 10 and 20 percent of the oxygen in the gas stream was consumed. At this oxidation rate, an accurate computation of the quantity of oxygen and nitrogen which reacted could be made from the results of the mass spectrometric analyses. The argon in the air stream served as an internal standard. At no time was the air stream allowed to become excessively depleted in oxygen.

b. Results

The upper temperature limit of the experiment was found to be 1000 C. At 1100 C, the corners of the specimen cubes began to melt during the period of rapid heating. The results of typical experiments at each of the experimental temperatures are shown in Figure IV-2 and a compilation of the data is given in Table IV-1. The oxidations at 500 and 600 C occurred generally in two linear stages. The reactions at 700 and 800 C followed a single linear rate law. The reaction rates at 900 and 1000 C were initially parabolic and subsequently became linear. The mass spectrometric analyses of the exit gas showed no change in the ratio of nitrogen to argon, indicating that there was no measurable reaction of nitrogen with the samples at any of the temperatures studied.

Figure IV-2

TYPICAL RESULTS FROM STUDY OF THE URANIUM-AIR REACTION

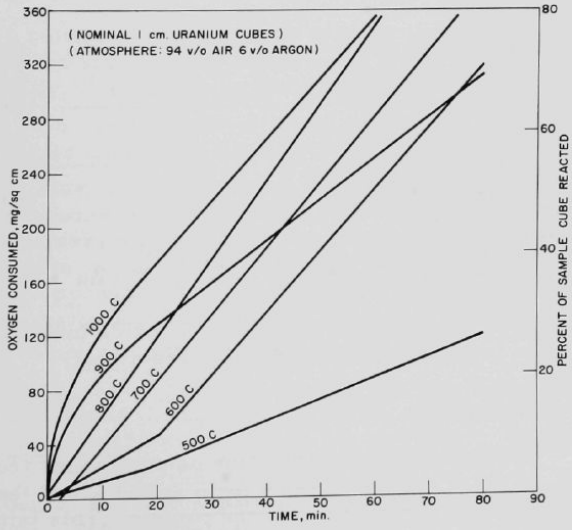

108-6540

Table IV-1

ISOTHERMAL RATE CONSTANTS FOR THE URANIUM-AIR REACTION

(Nominal one-cm uranium cube specimens)
(Atmosphere: 94 v/o air-6 v/o argon)

Temperature (C)	Reaction Rate Law and Rate Constant		
	First Stage	Transition Time (min)	Second Stage
500	Linear 1.1[a]	18	Linear 1.7
500	Linear 1.4	35	Linear 1.5
500	Linear 2.3	24	Linear 3.4
600	Linear 1.8	-	-
600	Linear 2.3	20	Linear 4.4
600	Linear 2.2	30	Linear 3.8
600	Linear 3.9	-	-
600	Linear 4.4	-	-
700	Linear 4.9	-	-
700	Linear 7.4	-	-
700	Linear 7.6	-	-
700	Linear 8.8	-	-
800	Linear 5.8	-	-
800	Linear 7.7	-	-
900	Parabolic 676[b]	27	Linear 2.1
900	Parabolic 856	18	Linear 3.0
900	Parabolic 1053	20	Linear 3.0
1000	Parabolic 1060	38	Linear 2.7
1000	Parabolic 1270	40	Linear 2.7
1000	Parabolic 1640	16	Linear 4.5

[a]Linear rate constants in mg O_2/(sq cm)(min)
[b]Parabolic rate constants in (mg O_2/sq cm)^2/min

X-ray diffraction studies of the oxide indicated that U_3O_8 was the only oxide formed after considerable reaction.

c. Discussion

The results showed that the oxide changes from a non-protective form at 800 C to a protective form at 900 C and that no significant quantity of nitrogen is absorbed by the sample. This latter finding makes it possible to seek a simpler and more rapid method of measuring the rate of oxidation. A method involving the continuous measurement of pressure decrease in a closed system is presently under development.

The linear reaction at 600 C in air differs somewhat from the slightly decelerating reaction noted in previous studies with pure oxygen at 600 C (see ANL-6543, p. 168). Whether this difference is due to a catalytic effect of the nitrogen or whether it is a result of different experimental conditions will be determined in future studies. In particular, it is necessary to study the initial stages of the air-uranium reaction in greater detail because of the importance of the initial reaction in ignition and burning processes.

2. Isothermal Oxidation of Plutonium
(J. G. Schnizlein, D. F. Fischer)

In order to test whether the ignition behavior of plutonium is strictly thermal in nature, it is necessary to have adequate oxidation rate data. Early studies at Los Alamos[9] and in Great Britain,[10] conducted in air at temperatures below 100 C, demonstrated a marked increase of oxidation in the presence of moisture. Waber[11,12] and Sachmann[13] have reported that in humid air for extended periods of time, oxidation rates of plutonium follow logarithmic, parabolic, linear, and accelerating rate laws. In dry air, parabolic behavior is usually observed. Sachmann[13] observed that oxidation in dry air at 100 C followed a succession of parabolic-shaped curves. The first parabolic rate continued 9 days during which period the weight gain was 2.4 mg/sq cm. This would correspond to a film of plutonium oxide less than 20 μ thick. It was thought that the rate of oxidation is limited by diffusion of oxygen ions through a thin film of PuO or Pu_2O_3. The oxide observed after completion of the experiment was PuO_2.

In studies of the oxidation of plutonium at higher temperature, Waber[12] observed accelerating oxidation in oxygen at 345 C and 400 C; Dempsey and Kay,[14] using air as the oxidant, observed two-stage linear

[9] Covert, K. S., and Kolodney, M., Protection of Plutonium Against Atmospheric Oxidation, LA-314 (June 1945).

[10] Dean, D., Kay, A. E., Lowthian, B. W., Powell, R. F., and Dempsey, E., Unpublished data communicated by E. Dempsey to Physical Society Conference on "Materials for Nuclear Engineering," July 11, 1957 (Bagley, K. Q., Nuclear Eng. 2, 461(Nov 1957).

[11] Waber, J. T., The Corrosion Behaviors of Plutonium and Uranium, Proceedings of the Second UN International Conference on Peaceful Uses of Atomic Energy, Geneva 6, 204 (1958).

[12] Waber, J. T., and Wright, E. S., The Corrosion of Plutonium, Presented AEC-ASM Conf., Chicago (1957). Also Chapter XVIII The Metal Plutonium (Coffinberry, A. S., and Miner, W. N., Eds.), The Univ. of Chicago Press, Chicago, Ill., 194 (1961).

[13] Sachmann, J. F., The Atmospheric Oxidation of Plutonium Metal, Plutonium, 1960 International Conference on the Metallurgy of Plutonium, Grenoble, Cleaver Hume, Ltd., London, 222 (1961).

[14] Dempsey, E., and Kay, A. E., J. Inst. Metals 86, 379 (1958).

oxidation rates at 205 C, linear oxidation at 303 C, parabolic at 416 C, and initially parabolic at 487 C (accelerating to ignition after 300 min). The protective nature of the oxide film at 416 C, when the metal has a delta-phase structure, results in a lower oxidation rate than at lower temperatures. Notley[15] later demonstrated that the oxidation rate passes through a minimum in the vicinity at 416 C. Since both porous oxide and an adherent oxide were observed and since the amount of adherent oxide increased when the temperature was increased from 400 to 450 C, it was proposed that the minimum oxidation rate could be a net result of the increased thickness of adherent oxide and the simultaneous increase of the rate of oxygen diffusion with increased temperature. X-ray diffraction studies showed the readily removable oxide to be PuO_2 and the adherent interfacial oxide to include both cubic and hexagonal Pu_2O_3. Properties and phase relationships of the oxides in the plutonium-oxygen system were reported earlier by Holley et al.[16] and recently by Chikalla et al.[17]

Current studies of the oxidation of plutonium are designed to develop a more thorough understanding of the reaction. It is anticipated that important conclusions concerning the ignition behavior of plutonium can be deduced from the isothermal kinetics when sufficient data at temperatures through 500 C are acquired.

a. Experimental

Special plutonium samples of high purity were obtained from Hanford* in the form of cubes. Concentrations of metallic impurities totalled less than 1000 ppm. Analytical data on impurities in the plutonium are presented in Table IV-2.

Oxygen and air from cylinders were used without further purification. To avoid use of contaminated gas, each gas was sampled and analyzed by mass spectrography prior to use. Typical analyses, expressed in volume percent, were as follows: oxygen: 99.7 O_2, 0.3 N_2, 0.01 Ar, 0.03 H_2O; air: 20.7 O_2, 78.5 N_2, 0.92 Ar, 0.1 H_2O.

---

[15]Notley, M. J. F., Hodkin, E. N., and Davidson, J. A. C., The Oxidation of Plutonium and Certain Plutonium Alloys in Air and Carbon Dioxide, UKAEA-AERE-R 4070 (1962). See also D. M. Poole et al., Properties of Some Plutonium Fuels, Proc. 1960 Intnl. Conf. Metallurgy of Plutonium, Grenoble, France, pp. 627-649 (Published by Cleaver Hume Ltd.).

[16]Holley, C. E., Jr., Mulford, R. N. R., Huber, E. J., Jr., Head, E. L., Ellinger, F. H., and Bjorklund, C. W., Thermodynamics and Phase Relationships for Plutonium Oxides, Proceedings of the Second UN International Conference on Peaceful Uses of Atomic Energy, Geneva, 6, 215 (1958).

[17]Chikalla, T. D., McNeilly, C. E., and Skavdahl, R. E., The Plutonium-Oxygen System, HW-74802 (1962).

*Prepared under the supervision of O. J. Wick, R. W. Stewart, T. Nelson, P. G. Pallmer, and R. R. King of Hanford Atomic Products Operation, General Electric Co., Richland, Washington.

Table IV-2

IMPURITIES IN THE PLUTONIUM INGOT USED TO PREPARE CUBES

Metallic element concentrations were obtained by three separate spectrographic analyses, carbon by combustion, and hydrogen, oxygen, and nitrogen by gas analysis. The analyses were performed by Hanford Atomic Products Operation.

	ppm				ppm		
Mg	423	180	220	Si	2	2	14
Fe	190	198	178	Cr	5	5	5
Ca	-	100	100	Sn	5	3	7
Cu	200	50	50	C	260		
Pb	50	50	50	O_2	110		
Ni	5	23	38	N_2	105		
Mn	5	20	20	H_2	3		
Ag	0.1	10	10				

The glovebox facility and associated equipment used for these experiments have been previously described (see Chemical Engineering Division Summary for July, August, September, 1961, ANL-6413, p. 168).

The course of oxidation was followed by changes in weight of a sample. A recording balance which automatically adds weights was equipped with a temperature transducer to permit continuous measurement of the sample temperature without interfering with the operation of the balance. The movable portion consists of a coil in series with a precision resistor and a thermocouple which provides the thermoelectric output to cause a current in the coil. The movable coil is interlocked with a toroidal magnetic amplifier which provides to a recording potentiometer (exterior to the box) a potential proportional to the temperature. Calibration has demonstrated a precision of two degrees.

b. Results and Discussion

Oxidation experiments have been performed at temperatures of 140 through 480 C in oxygen. In general, the observation of somewhat different behavior in each of the temperature ranges of different phases (see Chemical Engineering Division Summary for January, February, March, 1962, ANL-6543, p. 180) is consistent with that reported by Dempsey and Kay.[14] In the range of the beta phase (120-220 C), a three-stage oxidation is observed. The third stage shows a linear rate of 20 $\mu g/(sq\ cm)(min)$ which does not appear to be temperature-dependent. In the range of the gamma phase (220-320 C), an apparently linear rate is observed, ranging

from 80 to 200 μg/(sq cm)(min). In the range of the delta phase (320-450 C), the oxide film becomes more protective.

By careful examination of the initial portion of each oxidation run, it was possible to show an initial fit to the parabolic rate law for varying periods of time. The subsequent linear rate might then be controlled by diffusion of oxygen ions through an adherent layer of compact oxide of essentially constant thickness. During the parabolic portion of oxidation in the temperature range of beta-phase plutonium (120-220 C), the thickness of this layer is calculated to be approximately one micron. The thickness of the adherent layer increases to approximately 50 μ as the temperature is increased through the temperature range of the gamma phase (220-320 C).

An Arrhenius plot of the parabolic rate constants is presented in Figure IV-3. It is apparent that the same initial rate-control process is in effect over the temperature range from 140 to 320 C. The activation energy for this process is 32 kcal/mole. The oxide producing the protective film has not yet been identified, but the activation energy is a reasonable value for solid-state diffusion of oxygen ions. Above 300 C, the parabolic rate constant decreases to a minimum at approximately 400 C.

The linear rate constants for the oxidation subsequent to the formation of a film having an essentially constant thickness are presented in an Arrhenius plot in Figure IV-4. The activation energy for this overall process from 140 through 300 C is 16 kcal/mole. Above 300 C, a different process occurs, which is associated with the increased protectiveness of the oxide film and the occurrence of a minimum rate in the vicinity of 400 C.

In the temperature range in which the beta phase is stable (120 to 220 C), a paralinear rate law is followed to a weight gain of approximately 400 μg/sq cm, after which a faster rate of approximately 20 μg/(sq cm)(min) is observed. The oxide produced is green instead of gray and is a loose powder. The third-stage rate does not appear to have any temperature dependence.

Oxidation experiments were also performed in air at selected temperatures. In each case, the oxidation was essentially identical to that observed in oxygen.

c. Conclusions

It appears that the complexity of the metallurgy of plutonium metal, i.e., the existence of six stable phases at temperatures under 600 C, is reflected in its oxidation kinetics. However, the early oxidation behavior between 140 and 300 C can be satisfactorily explained in terms of a single paralinear rate law. The initially formed oxide is protective until a

Figure IV-3

PARABOLIC OXIDATION DATA FOR PLUTONIUM

(Initial stage of oxidation)

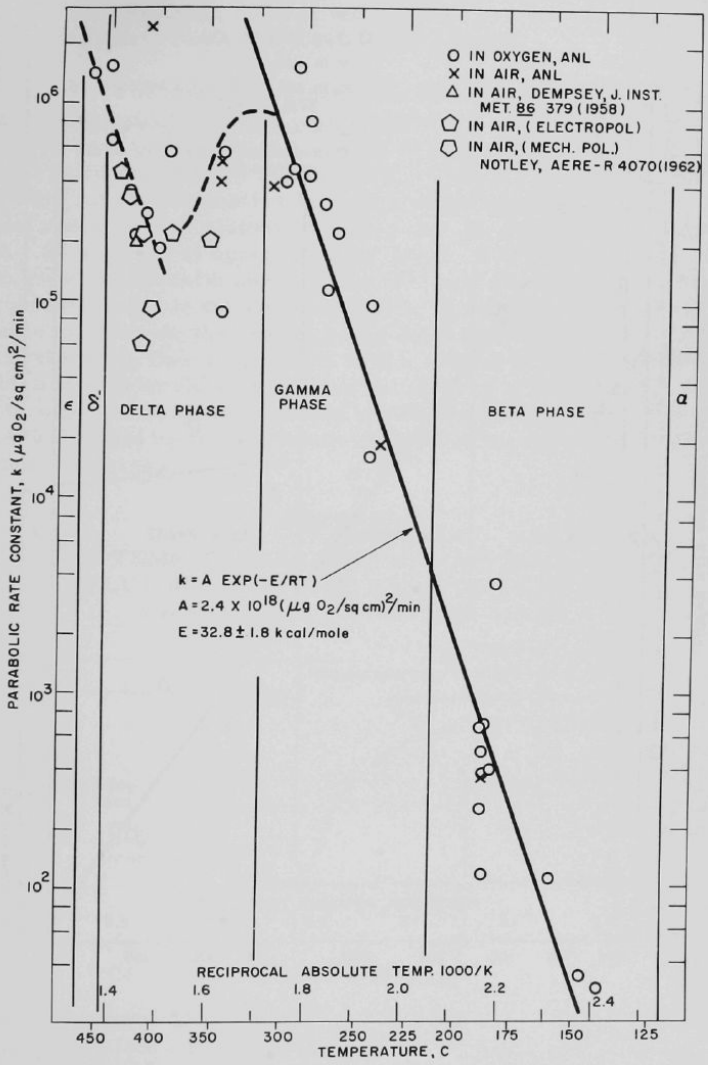

108-6541

Figuve IV-4

LINEAR OXIDATION DATA FOR PLUTONIUM

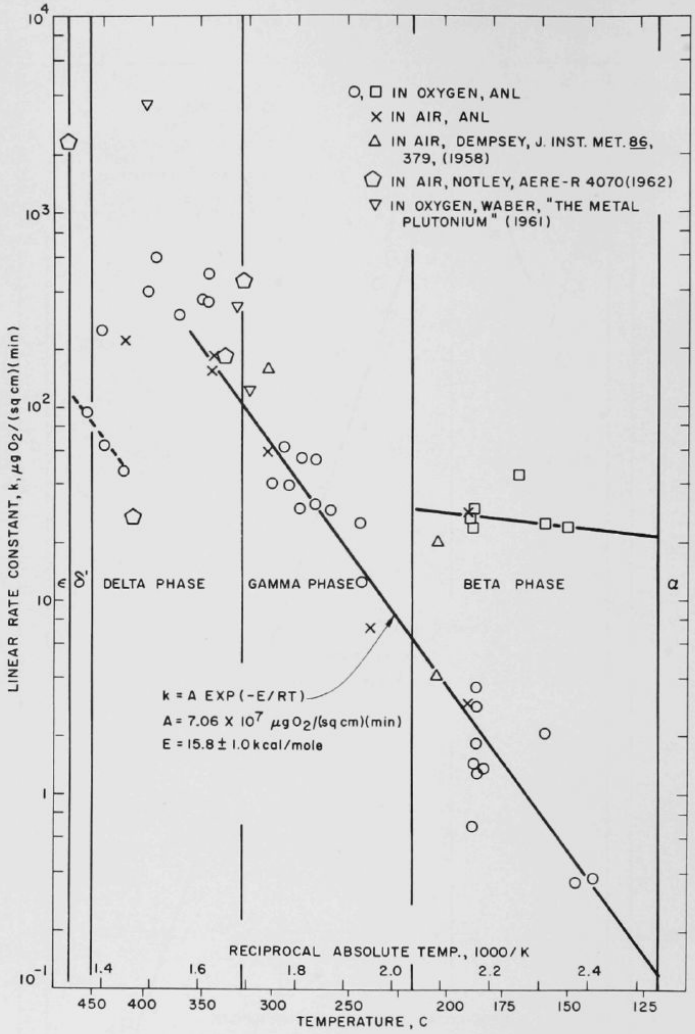

108-6542

thickness of approximately one micron is developed. This layer remains compact and adherent as subsequent oxidation proceeds at an essentially linear rate. The activation energy of 32 kcal/mole for the initial parabolic oxidation process is a reasonable value for solid-state diffusion of oxygen through the compact oxide. Although the compact oxide may be PuO, the presence of beta Pu_2O_3 on most of the oxidized samples examined by Notley[15] makes beta Pu_2O_3 the most likely possibility.

The change in kinetics in the vicinity of 300 C, which results in the low oxidation rates with a minimum near 400 C, might be attributed to an effect of the delta phase of plutonium, which is stable in the temperature range from 320 to 450 C. Chikalla et al.[17] and McNeilly[18] have pointed out discontinuities in values of the thermal expansion and electrical resistivity of plutonium oxides with an oxygen to plutonium ratio between 1.64 and 1.98 at approximately 300 C. The plutonium-oxygen phase diagram given by Chikalla and associates[17] and shown in Figure IV-5 indicates a phase change in the oxide at 300 C. It would therefore appear more reasonable to attribute the change in the oxidation kinetics near 300 C to a change in the oxide than to attribute it to a change in the metal structure. The oxidation data would be explained in terms of a low diffusion rate of oxygen through the oxide phases that are stable above 300 C. The minimum rate at 400 C would be the net result of this and the increasing diffusion at higher temperatures.

Figure IV-5

LOW TEMPERATURE-HIGH OXYGEN PORTION OF PLUTONIUM-OXYGEN PHASE DIAGRAM BY CHIKALLA, T. D., HW-74802 (1962)

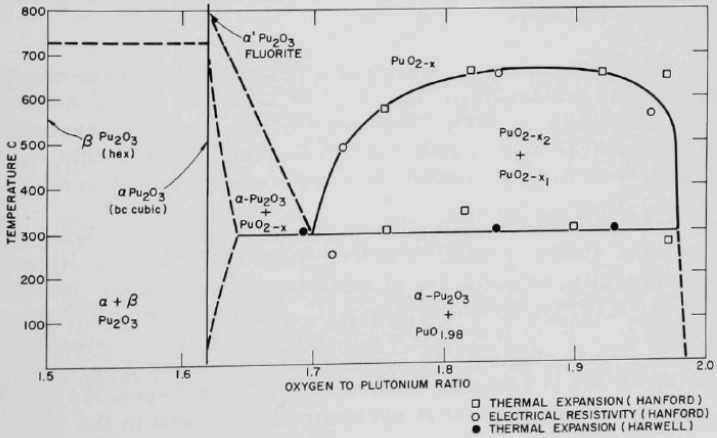

108-6543

[18]McNeilly, C. E., Electrical Properties of Plutonium Oxides, HW-75120 (1962).

Oxidation studies above 300 C will be continued. Because of high oxidation rates, it is probable that a heat sink apparatus will be needed to maintain isothermal conditions.

B. Metal-Water Reactions
(L. Baker)

1. Studies of the Stainless Steel-Water Reaction by the Condenser-discharge Method
(L. Baker, Jr., R. Warchal)

The condenser-discharge experiment is an attempt to obtain fundamental rate data under experimental conditions similar to those that would be encountered during a serious accident in a nuclear reactor. Either a nuclear runaway or a sudden loss of coolant during operation of a water-cooled reactor could result in contact of very hot fuel and cladding metals with water or steam and might involve fine particles. The condenser-discharge experiment simulates the limiting case of a nuclear incident, in that the heating time is very short and very fine metal particles are produced.

In the condenser-discharge experiment, samples in the form of metal wires are rapidly melted and dispersed in a water-filled cell by a surge current from a bank of condensers. The energy input to the wires is used to calculate the initial reaction temperature. The transient pressures are measured and used to indicate reaction rate. The amount of hydrogen generated gives the extent of reaction, and the particle size of the residue indicates the surface area exposed to reaction. Analysis of results is based on one of the usual laws of metal oxidation and on the laws of gaseous diffusion and heat transfer.

Experiments with stainless steel-316 wires were carried out in water at room temperature, 100 C, 200 C, and 315 C (see ANL-6596, p. 186 and ANL-6648, p. 194). The extent of metal-water reaction was found to be identical in 100, 200, and 315 C water and was only slightly greater than the extent of reaction in room-temperature water.

During the present quarter, stainless steel-302 wires (of 30-mil diameter) were studied briefly to determine if there are significant differences in results with an alloy of slightly altered composition. Stainless steel-316 has a nominal composition of 17 percent chromium, 12 percent nickel, and 2 to 3 percent molybdenum, whereas stainless steel-302 is a simpler alloy containing only 18 percent chromium and 8 percent nickel. Stainless steel-302 is identical in composition with Types 304 and 304 L except that the carbon content is not controlled as well in the 302 alloy.

In Figure IV-6, results of runs with stainless steel-302 wires in water at room temperature and 200 C are compared with previous results for stainless steel-316. Results with the two alloys were identical except that in the region of high initial metal temperatures in heated water, there was somewhat greater metal-water reaction in two runs with the 302 alloy than with the 316 alloy. The greater reaction may have resulted from the formation of smaller particles by the 302 alloy, since no tendency was noted toward the increased reaction in room-temperature water which would be expected if the increase were a result of differences in reaction kinetics. Particle size measurements for the runs with stainless steel-302 have not been completed. Measurements of the reaction rate by means of a pressure transducer were generally unsatisfactory because of the small amount of gas generation and electrical interference from the discharging condensers.

Figure IV-6

STAINLESS STEEL-WATER REACTION BY THE CONDENSER-DISCHARGE METHOD

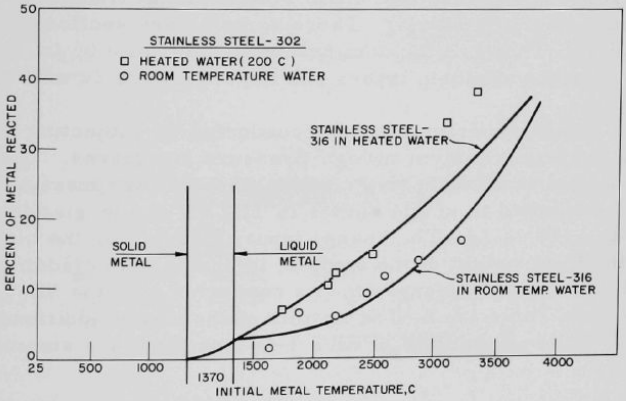

108-6544

2. Studies of the Aluminum-Water Reaction in TREAT
(R. O. Ivins, F. J. Testa, P. Krause)

The use of the TREAT (Transient REActor Test facility) reactor at the NRTS, Idaho, to study the reaction of various metals with water is continuing. The technique consists of subjecting fuel specimens immersed in water to a transient nuclear burst. The objectives of this program are:

1. to determine the extent of reaction between the metal and water;
2. to determine the fuel temperature and pressure history during the excursion;
3. to determine the physical damage that occurs as a result of the transient; this includes metallographic and particle size evaluations

Eleven 81 w/o aluminum-17 w/o uranium (fully enriched)-2 w/o nickel plates have been subjected to destructive transients in TREAT while immersed in room-temperature water. This material is of the same composition as the fuel (uranium-loaded) section of the fuel plates which comprised the core of the SL-1 reactor. The samples tested had the nominal dimensions of 0.2 in. by 0.5 in. by 0.5 in.

A series of nine experiments with aluminum-clad, 77 w/o aluminum-23 w/o fully enriched uranium plates was reported in the previous quarterly report (ANL-6648, p. 201). An additional transient was performed with a sample of this material. These samples are sections of a SPERT 1-D type plate. They had the nominal dimensions of 0.06 in. by 0.5 in. by 1.4 in. Both of the cladding layers and the core were 20 mils thick.

These experiments were conducted by subjecting the sample plates to a nuclear transient in high-pressure autoclaves. The samples were submerged in 45 cc of water with a 20-psia overpressure of helium. They were subjected to single bursts in TREAT of energies increasing from 288 cal/g to 1378 cal/g. The energy input reported for the clad material is based on the total weight of the sample, including both cladding and core. The results of the eleven experiments conducted with the SL-1 material are summarized in Table IV-3. The results of the single additional experiment conducted with the sample of SPERT 1-D-type plate are summarized in Table IV-4.

Chromel-alumel thermocouples were used to measure surface and center plate temperatures; however, contact was lost at the melting point of the material, limiting the reliable temperature measurements to those below the melting point of aluminum (660 C). Pressure transducers were used in the experiments conducted at the higher reactor energies to record the pressure history during the transient. The unbonded strain-gage-type transducers used were sensitive to radiation, limiting the usefulness of the pressure traces obtained; however, no significantly large or rapid pressure rises were noted.

Table IV-3

SUMMARY OF RESULTS OF TREAT TRANSIENTS CONDUCTED ON UNCLAD ALUMINUM-URANIUM ALLOY (SL-1) PLATES

(81 w/o Aluminum - 17 w/o Uranium-2 w/o Nickel)
(0.2 in. x 0.5 in. x 0.5 in.)

Calc Energy Input (cal/g)	TREAT Experiment CEN No.	Fuel Wt (g)	Reactor Characteristics		Peak Temp, Adiabatic (C)	Appearance of Fuel after Transient	Avg Particle Size, d_{sv} (mils)	Extent of Reaction (%)
			Period (ms)	Int. Power (Mw-sec)				
288	114	2.6061	112	174	900	Melted and bulged, retaining original shape	~500[a]	0.1
398	97	2.6030	79	240	1320	Melted into one globule	~500[a]	2.8
473	121	2.5915	79	285	1590	Melted into one "semi-circular" globule	~500[a]	4.5
530	122	2.4170	79	320	1820	Melted into one spherical globule	~500[a]	7.2
530	123	2.3784	79	320	1820	Melted into one spherical globule	~500[a]	14.2
580	115	2.6257	77	350	2020	Melted and fragmented	110	16.4
672	116	2.5711	62	405	2330	Melted and fragmented	42	19.7
739	98	2.5450	51	445	2330	Melted and dispersed particles welded to inner surfaces of autoclave	-	22.2
880	137	2.4910	54	530	2330	Melted and fragmented	61.3	27.4
1023	99	2.5050	50	616	2330	Melted and dispersed particles welded to inner surfaces of autoclave	-	54.2
1378	138	2.7102	41	830	2330	Melted and fragmented	11.9	43.2

[a]Estimated

Table IV-4

SUMMARY OF RESULTS OF TREAT TRANSIENTS CONDUCTED ON ALUMINUM-CLAD ALUMINUM-URANIUM ALLOY (SPERT 1-D) PLATE

Calc Energy Input (cal/g)	TREAT Experiment CEN No.	Fuel Wt (g)	Reactor Characteristics		Peak Temp, Adiabatic (C)	Appearance of Fuel after Transient	Avg Particle Size, d_{sv} (mils)	Extent of Reaction (%)
			Period (ms)	Int. Power (Mw-sec)				
855	136	1.9262	41	830	2330	Melted - Fragments welded to stainless steel crucible and support arm	82.7	20.0

The appearance of the samples after irradiation showed the effects of the increasingly destructive inputs of nuclear energy. The residues were sized with standard sieve screens, and an average particle size diameter was calculated as the Sauter mean diameter d_{sv}.* These are tabulated in Tables IV-3 and -4. Figures IV-7, -8, and -9 contain photographs of three of the samples and photomicrographs of metallurgically mounted and polished portions of two of the samples of SL-1 material tested at various energies.

*The Sauter mean diameter, $d_{sv} = \frac{\Sigma N_i d_i^3}{\Sigma N_i d_i^2}$

where N_i = number of particles in the i^{th} group;
d_i = average diameter of the i^{th} group.

Figure IV-7

UNCLAD URANIUM-ALUMINUM FUEL PLATE (SL-1)
AFTER TREAT TRANSIENT CEN-114 - 288 cal/g
Photograph of Plate before and after Transient

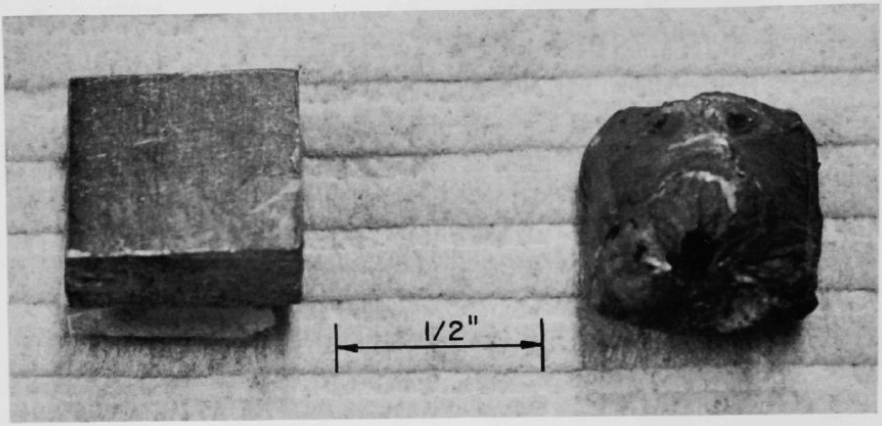

108-5582 Rev.

Figure IV-10 is a photomicrograph of a sample of the original material before testing. There are two phases, which were probably intermetallic compounds of uranium and aluminum (UAl_4 and possibly UAl_3), in an aluminum matrix.

The differences in metallographic appearance of the samples subjected to various reactor energies is similar to that reported in the previous quarterly (ANL-6648, p. 201). Slab-like crystals were formed between nuclear energy inputs of 530 and 800 cal/g (see Figure IV-8). No eutectic was found, however, at the higher energies with the SL-1 material. The photomicrographs in Figure IV-9 are typical of the appearance of the SL-1 material subjected to energies greater than 790 cal/g. The formation of what appeared to be a typical eutectic was previously reported for the SPERT material at an energy input of 794 cal/g. The porosity of the samples was found to increase with increasing energy input for both materials.

X-ray diffraction analysis of the residue of various runs indicated the presence of alpha alumina as the product of the aluminum-water reaction. The extent of reaction was determined from the hydrogen analysis of samples of the gas phase in the autoclaves. Figure IV-11 is a plot of the amount of plate reacted versus the nuclear energy input for both materials tested and includes previous data for the SPERT material. The extent of reaction increased markedly above an energy of 530 cal/g. Below this region, the largest extent of reaction was 2.8 percent. At energies

above 530 cal/g, the amount of material reacted increased to values in the order of 10 to 20 percent. The unclad plates reacted to a slightly greater extent than the clad plates (see Figure IV-11). The differences in the extent of reaction were probably due to the lower surface to volume ratio of the SL-1 specimens, which resulted in lowered heat losses and greater metal-water reaction. At an energy above ~800 cal/g, a third region of very extensive reaction (30 to 50 percent) occurs.

Figure IV-8

UNCLAD URANIUM-ALUMINUM FUEL PLATE (SL-1)
AFTER TREAT TRANSIENT CEN-115 - 580 cal/g

Fuel Plate after Transient

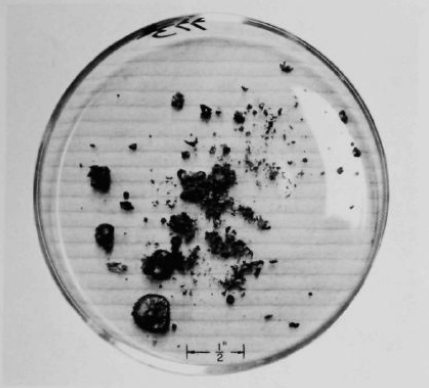

Particle Size Distribution

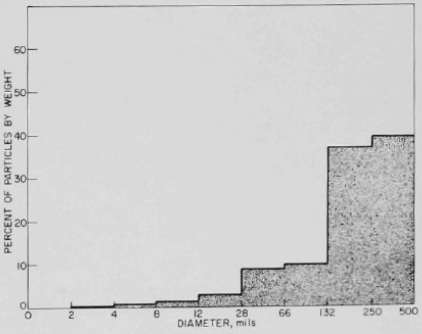

Cross-section of Large Particle

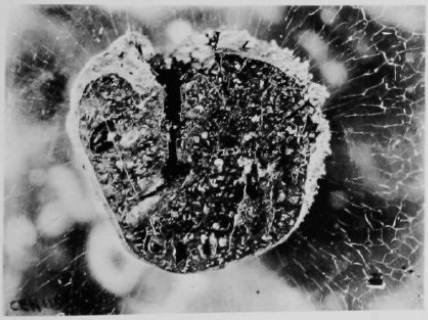

4.6X

Photomicrograph

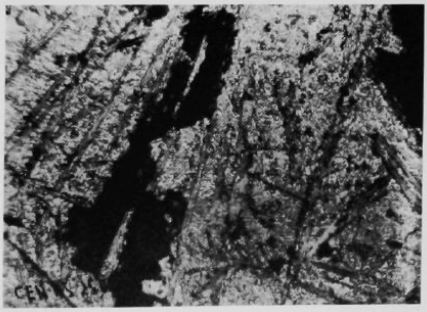

115X

108-6546

Figure IV-9

UNCLAD URANIUM-ALUMINUM ALLOY FUEL PLATE (SL-1)
AFTER TRANSIENT CEN-138 - 1378 cal/g

Photograph

Particle Size Distribution

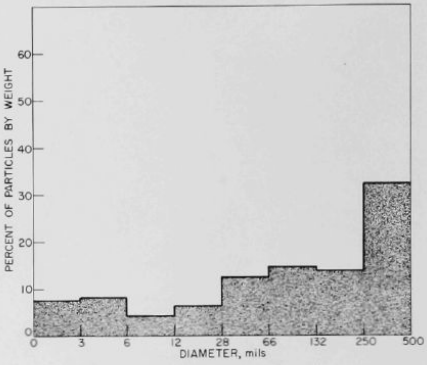

Photomicrograph

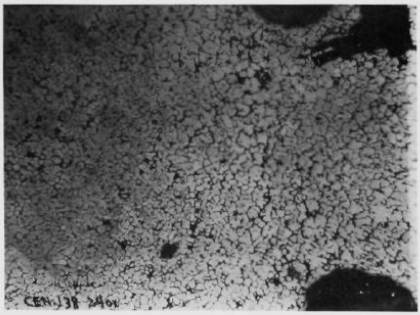

110X

Photomicrograph

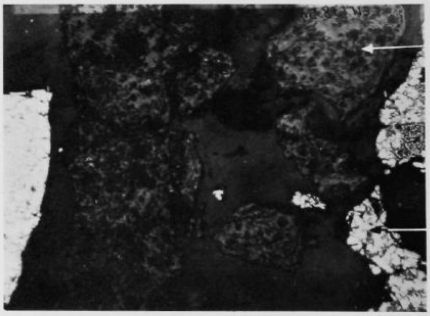

110X

108-6547

Figure IV-10

PHOTOMICROGRAPH OF ALUMINUM-URANIUM ALLOY FUEL PLATE (SL-1) BEFORE IRRADIATION

108-6548

250X

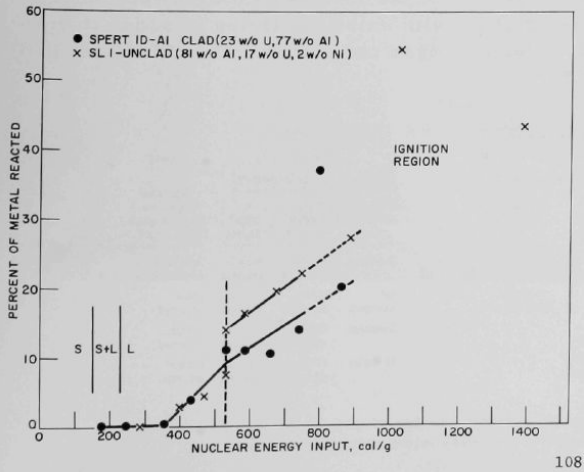

108-6549

Figure IV-11

RESULTS OF TREAT MELTDOWN TESTS WITH ALUMINUM-URANIUM ALLOY SPECIMENS

The data appear to correlate well with the results of isothermal studies of aluminum by the levitation method reported in the previous quarterly (ANL-6648, p. 196). Slow oxidation of aluminum in steam, occurring at 1300 C and below and obeying a cubic rate law, would account for the lack of significant reaction in the in-pile studies below an energy input of 530 cal/g. The vigorous oxidation of aluminum in steam, which is reported to occur between 1400 and 1750 C and which follows a linear rate law, might then be associated with the in-pile samples that received energy inputs between 530 and ~800 cal/g. The vapor-phase ignitions occurring at temperatures above 1750 C would then account for the large amount of reaction occurring during the most vigorous transients of the series. The boundaries for the regions of reaction are somewhat vague, since the in-pile experiments are more complex than the laboratory studies. They are nonsteady-state phenomena and require information concerning the temperature history of individual particles to allow a description of the reaction. It is expected that a more rigorous correlation between the results of the two experimental methods can be achieved by a computer study of the type previously developed to describe the zirconium-water reaction (see L. Baker, Jr., and L. C. Just, Studies of Metal-Water Reactions at High Temperatures. III. Experimental and Theoretical Studies of the Zirconium-Water Reaction, ANL-6548, May 1962).

3. Status of Metal-Water Reaction Studies (L. Baker)

The long-range objective of the metal-water reactions program is to provide a practical means for estimating the rate and extent of reaction that will occur during postulated reactor accidents. The program has been divided into three separate phases, as indicated in Table IV-5. The first phase involves the experimental determination of the isothermal rate laws and rate constants. The second phase involves experimental observation of the nonisothermal reaction with small particles in order to simulate accidental situations under idealized conditions. The third and final

Table IV-5

STATUS OF RESEARCH PROGRAM ON METAL-WATER REACTIONS

	Phase I: Determination of Isothermal Reaction Rate Law				Phase II: Study of Nonisothermal Reactions			Phase III
Metal	Pressure Pulse Method	Volumetric Method	Levitation Melting Method	Other Institution	Condenser-discharge Method	Laser Heating Method[a]	TREAT Studies	Theoretical Calculation of Rate and Extent of Reaction[b]
Zirconium	-	-	-	Available 1000-1850 C	Completed	Will be attempted	Work in progress	Some work successfully done
Aluminum	Completed 800-1200 C	-	Completed 1200-1800 C	-	Not applicable	Will be attempted	Work in progress	Will be attempted
Stainless Steel	-	Work in progress[c]	-	-	Completed	Will be attempted	Work in progress	Will be attempted
Uranium	-	Completed 400-1600 C	-	-	Completed	Will be attempted	Work in progress	Work in progress

[a] In initial stage of development.

[b] It is planned to extend these calculations to cases of full-scale reactor accidents.

[c] Volumetric method not completely satisfactory and further method development work may be necessary.

phase of the program is the development of a mathematical model of metal-water reactions that will combine isothermal rate laws with equations of heat and mass transfer so that the course of the reaction can be computed under any set of initial conditions. An important function of the noniso-thermal experiments is to provide a check on computed results and also to detect physical limitations to the reaction rate that would not be apparent in isothermal experiments. In the TREAT experiments, there is a more direct simulation of reactor excursion accidents in which the nature and degree of fragmentation of representative fuel element specimens is determined.

It has recently become apparent from the analysis of the SL-1 incident and the SPERT-1 meltdown that an important source of disruptive energy may result from rapid contact of hot, dispersed material with water. The relative contribution of a rapid steam-formation process and a chemical reaction process is presently unknown. Studies by the laser method and the TREAT method will be oriented toward an examination of steam-formation rates as well as chemical reaction rates.

V. ENERGY CONVERSION*

Two methods of directly converting nuclear energy into electricity are being studied. One method involves the use of regenerative cells; the other concerns itself with studies of the thermocouple effect.

A. Regenerative Emf Cell

(C. E. Crouthamel, M. Foster, C. E. Johnson, R. Heinrich, R. Eppley, J. Allen, G. McCloud)

The application of a regenerative emf cell in a closed cycle to convert heat to electricity continues to be an attractive possibility for future applications. The current program is concerned with devising regenerative cell systems which will be suitable for coupling to a reactor heat source in a closed cyclic operation. The program also includes the study of the chemical and physical properties of selected systems for the purpose of obtaining data needed for the design of a practical cell. The program to date has not progressed to engineering activities.

Work has been centered around the lithium-bismuth bimetallic cell and the lithium hydride cell. Experiments with alkali molten metals and fused salts are difficult inorganic experiments to execute successfully. Therefore, the first phase of this experimental program was mainly learning to cope with the problems of handling molten lithium and other alkali metals, and has led to the design and fabrication of a basic research tool - the very high-purity inert-atmosphere box with its associated high-temperature furnace wells (see M. S. Foster et al., Helium-purification Unit for High-purity Inert-atmosphere Boxes, ANL-6652, Dec. 1962). A familiarity with the limitations of construction materials for the galvanic cell and a knowledge of the behavior of the fused salt electrolytes in the cell in the presence of molten alkali metals and other more noble metals such as bismuth, tin and tellurium are being acquired. The basic studies of the thermodynamics of the lithium-bismuth cells are approaching completion. Studies on the lithium hydride cell have been concerned with the delineation of the lithium hydride-lithium chloride phase diagram and with the operation of a hydrogen diffusion electrode.

The basic studies are now being extended to the regeneration cycle by high temperature cell operations. Detailed studies of a second bimetallic cell are also being planned.

1. Bimetallic Cells

(M. S. Foster and R. Eppley)

Lithium-Bismuth Cell

Systematic studies to evaluate the thermodynamic properties of the lithium-bismuth cell in terms of emf-temperature-composition data are now approaching completion. Preliminary experiments with other bimetallic

*A summary of this section is given on pages 25 and 26.

cells in which lithium was used as an anode and which led to the selection of the lithium-bismuth cell for detailed study are reported in Chemical Engineering Division Summary Reports ANL-6477, p. 209, and ANL-6543, p. 200.

A number of cells have been operated which may be represented by one of the following types:

1. $\mathrm{Li}\ (\ell) \left| \begin{matrix} \mathrm{LiCl} \\ \mathrm{KCl} \end{matrix} \right| \mathrm{Li\ in\ Bi}\ (\ell)\ (x_{Li} = \text{atom fraction Li})$

2. $\mathrm{Li}\ (\ell) \left| \begin{matrix} \mathrm{LiCl} \\ \mathrm{KCl} \end{matrix} \right| \begin{matrix} \mathrm{Li_3Bi\ (s)\ saturated\ Bi}\ (\ell) \\ (x_{Li} = \text{overall atom fraction Li} = 0.60) \end{matrix}$

3. $\mathrm{Li}\ (\ell) \left| \begin{matrix} \mathrm{LiCl} \\ \mathrm{LiF} \end{matrix} \right| \begin{matrix} \mathrm{Li_3Bi\ (s)\ saturated\ Bi}\ (\ell) \\ (x_{Li} = \text{overall atom fraction Li} = 0.60) \end{matrix}$

4. $\mathrm{Li}\ (\ell) \left| \begin{matrix} \mathrm{LiCl} \\ \mathrm{LiF} \end{matrix} \right| \mathrm{Li\ in\ Bi}\ (\ell)\ (x_{Li} = \text{atom fraction Li})$

5. $\begin{matrix} \mathrm{Li_3Bi\ (s)\ saturated\ Bi}\ (\ell) \\ (x_{Li} = \text{overall atom fraction Li} = 0.60) \end{matrix} \left| \begin{matrix} \mathrm{LiCl} \\ \mathrm{LiF} \end{matrix} \right| \begin{matrix} \mathrm{Li\ in\ Bi}\ (\ell) \\ (x_{Li} = \text{atom fraction Li}) \end{matrix}$

In cells of type 1 and type 2, the electrolyte consisted of the purified eutectic (mp 352 C) of composition 41 m/o potassium chloride and 59 m/o lithium chloride (see Chemical Engineering Division Summary Report for April, May, June, 1961, ANL-6379, p. 233, for method of purification with chlorine gas). In cells of types 3, 4, and 5, the electrolyte consisted of the eutectic (mp 500 C) of composition 30 m/o lithium fluoride and 70 m/o lithium chloride. This eutectic was purified in the same manner as the other. The lithium and bismuth alloys were prepared by weighing and alloying pure lithium metal and bismuth metal in a helium-atmosphere dry box to yield appropriate compositions.

The first two cells studied were of type 1, with $x_{Li} = 0.05$. Considerable difficulty was experienced in obtaining stable cell voltages, especially at temperatures above 500 C, and no useful thermodynamic data were obtained. Two causes of this voltage instability have been found. The first is the reduction of potassium chloride by the lithium metal, and the second is the irreversible transfer of lithium metal from the pure lithium metal anode to the cathode. These sources of instability will be discussed below.

Two cells of type 2 were operated with a bismuth cathode saturated with the intermetallic compound Li_3Bi. At an overall composition of 60 a/o lithium in bismuth, solid Li_3Bi is in equilibrium with a liquid alloy phase over the temperature range from 415 to 775 C. Above 775 C, the alloy becomes a single liquid phase. The irreversible transfer of lithium to this cathode at temperatures below 775 C should not affect the cathode

potential, since the transfer would only result in further precipitation of solid Li_3Bi without changing the concentration of lithium in the liquid phase at any given temperature between 415 and 775 C. However, the cell voltages of the type-2 cells were found to fluctuate markedly when the operating temperature was increased to above 500 C. This instability of cell voltage is attributed to the instability of the lithium anode in its electrolyte environment. At temperatures above 500 C, the lithium reduces the potassium chloride to potassium metal. The potassium is partially distilled, as evidenced by the condensation of potassium metal on the cooler sections of the electrode leads in the upper part of the cell. The remaining potassium metal, which is immiscible with lithium, forms a second liquid metal phase at the anode. Thus two liquid metal phases are in contact with each other and with the electrolyte that contains ions of the two metal phases. The resulting anode potential is, therefore, a composite of the individual metal| metal ion potentials (in this case, a composite of the $Li|Li^+$ and $K|K^+$ potentials) and is less positive, with respect to the cathode potential, than the single $Li|Li^+$ potential. It is expected, therefore, that the emf of a type-3 cell, in which the possibility of obtaining a composite anodic potential is removed by substituting lithium fluoride for potassium chloride in the electrolyte, will be greater than that of a type-2 cell at a given temperature above 500 C.

The rate of reduction of potassium chloride in a type-2 cell should increase with an increase in temperature. Thus, the difference in emf's of cells of types 2 and 3 should also increase with operating temperature. This behavior is exemplified in Figure V-1. It was possible to operate cells with a lithium chloride-lithium fluoride electrolyte at much higher temperatures than cells with a lithium chloride-potassium chloride electrolyte. Each curve shown in Figure V-1 was obtained by the least-squares method from two individual experiments. The upper curve, for the type-3 cell, corresponds to the equation

$$\epsilon\ (v) = 0.5264 + 7.3958 \times 10^{-4}\ T - 6.4317 \times 10^{-7}\ T^2 \quad . \qquad (1)$$

The standard deviation of the data from this curve is 3.4 mv.

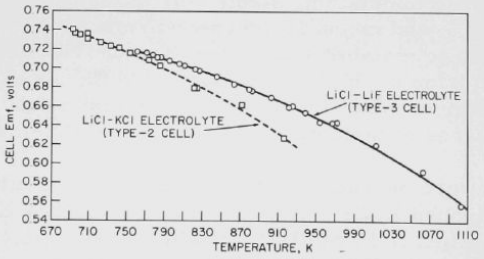

Figure V-1

EMF VS TEMPERATURE FOR THE LITHIUM-BISMUTH CELL

Type-2 Cell: Lithium (ℓ) | LiCl / KCl | Bismuth (ℓ) Satd. with Li_3Bi(s)

Type-3 Cell: Lithium (ℓ) | LiCl / LiF | Bismuth (ℓ) Satd. with Li_3Bi(s)

108-6550

In the case of the type-4 cell, which has an unsaturated lithium-bismuth cathode, the second source of voltage instability remained, namely, the solubility of lithium metal in the electrolyte and its irreversible transfer to the cathode. The voltages of cells of this type were found to drop rapidly with time and temperature cycling. A solution to this problem was necessary before complete emf-temperature-composition data could be obtained. Since stable emf-temperature data had been obtained with type-3 cells (see Figure V-1), it was possible to use the bismuth electrode saturated with Li_3Bi as a secondary reference anode for the emf measurements of more dilute lithium-bismuth cathodes in cells of type 5. In these experiments, the concentration of lithium in the electrolyte was reduced many fold by the reduced activity of lithium in the anode. Thus, in type-5 cells, the lithium composition of the cathode remained stable. The performance of these cells was very satisfactory; the voltages were stable and reproducible. Figure V-2 shows the complete emf-temperature-composition data for type-4 cells. The data were derived from measurements made with type-3 and type-5 cells, except for the data pertaining to the cell in which a 60 a/o lithium-bismuth cathode was used against a pure lithium anode. The data for this cell were obtained by direct measurement.

Figure V-2

LITHIUM - BISMUTH CELL CHARACTERISTICS

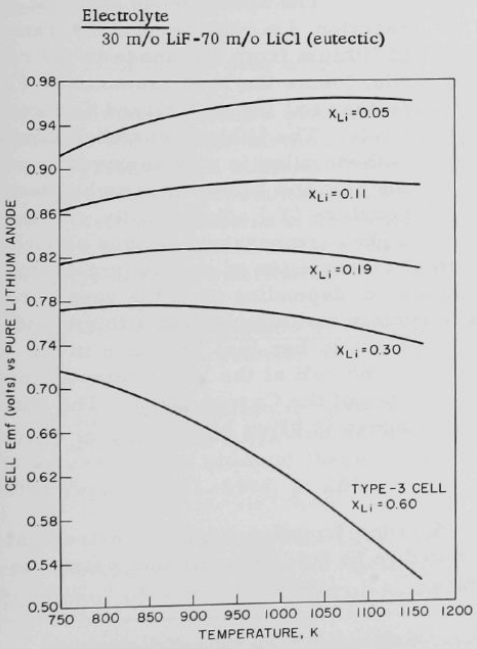

108-6551

Lithium-Bismuth-Uranium Cell

If bimetallic cells are thermally regenerable, it is necessary to add heat to the alloy formed in the cell cathode. A novel approach to the problem of adding heat might be to dissolve a small amount of enriched uranium in the alloy. The configuration of the cathode material in the cell would be noncritical to avoid heat generation in the galvanic cell, but in the region of the regenerator, it would be critical or approach criticality. If, due to solubility or cell practice limitations, the amount of uranium was insufficient to achieve criticality in the regenerator, additional neutrons might be supplied from an external source. The heat necessary for regeneration would thus be generated directly in the alloy from fission energy.

In order to determine whether the addition of a small quantity of uranium to the lithium-bismuth cathode of a cell would seriously affect its voltage, a cell was assembled in which the anode was pure lithium and the cathode was an alloy of lithium, bismuth, and uranium (normal) in which the atomic ratio of the elements Li:Bi:U was 0.610:0.384:0.006. The data obtained with this cell together with data obtained with cells (type 3) without uranium are shown in Figure V-3. The curve (solid line) was obtained by applying the least-squares method to the experimental data. Considerable scatter of the data from the curve is evident.

Figure V-3

TEMPERATURE VARIATION OF EMF IN THE LITHIUM-BISMUTH-URANIUM CELL

Cell: Li | LiCl-LiF | Li (61 a/o), Bi (38.4 a/o), U (0.6 a/o)

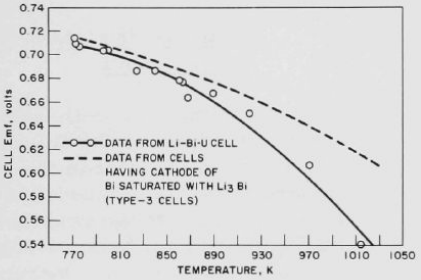

108-6552

The data presented in Figure V-3 indicate that the addition of a small amount of uranium does not seriously affect the cell voltage at anticipated cell temperatures (450 to 550 C) and to this extent are consistent with the suggested use of uranium as a heat source in the thermal regeneration of the lithium-bismuth cell.

Thermal Regeneration

The spontaneous galvanic cell reaction, i.e., the reversible transfer of lithium from the anode to the cathode, forms the low-temperature (T_1) isothermal leg of a closed Carnot Cycle. The lithium-enriched liquid cathode alloy is now removed from the cell and raised to a higher temperature (T_2) adiabatically. At this higher temperature heat is absorbed isothermally by the alloy. The thermal dissociation of the lithium-bismuth alloy may be wholly or partially completed, depending upon the vapor pressure of lithium above the alloy. The lithium and bismuth (or lithium and lithium-bismuth alloy of lower lithium content than that produced in the galvanic cell) are separately returned to the cell at the lower temperature T_1. This last step forms the final adiabatic leg of the Carnot Cycle. The maximum overall efficiency of the cyclic process is given by

$$(T_2 - T_1)/T_2 \quad .$$

If one assumes that the data for Equation 1 may be extrapolated to 1273 K, the cell voltage is calculated to be 0.4256 v. At this point, the entire cathode would be molten; thus,

$$\ln \gamma_{Li} X_{Li} = - \frac{F\epsilon}{RT} \quad ; \quad X_{Li} = 60 \text{ a/o} \quad ,$$

or

$$\ln a(\text{Li in Bi}) = -3.8796$$

and

$$a(\text{Li in Bi}) = 2.07 \times 10^{-2} \quad .$$

If it is desired to calculate the vapor pressure of lithium over this alloy at equilibrium, the following relationship may be used:

$$a(\text{Li in Bi}) = a(\text{Li in gas over alloy}) \quad .$$

Further, from data on pure lithium,[1]

$$^{v}p_{\text{Li, pure}} \text{ at } 1273 \text{ K} = 40 \text{ mm} \quad .$$

If we assume

$$a(\text{Li in gas over alloy}) = \frac{^{v}p_{\text{Li in gas over alloy}}}{^{v}p_{\text{Li, pure}}}$$

then

$$^{v}p_{\text{Li in gas over alloy}} = 2.07 \times 10^{-2} \times 40 = 0.8 \text{ mm} \quad .$$

This estimated value is quite low, indicating that it may be difficult to regenerate the lithium-bismuth cell by straightforward thermal means. However, systems with bismuth which involve other alkali metals may be expected to have substantially higher vapor pressures of the alkali metals above their solutions in bismuth in view of the higher vapor pressures of the pure alkali metals and the lower melting points (indicative of lower stability) of their intermetallic compounds with bismuth.

2. Phase Studies by Heating and Cooling Curves
(C. E. Johnson and J. Allen)

Information is needed on the various salt systems that may have utility in the lithium hydride or bimetallic fuel cells. The apparatus that is being used in the study of these systems was discussed in a previous quarterly report (ANL-6596, p. 203).

Phase diagrams have been used by several investigators to derive thermodynamic data for binary salt mixtures. Haendler,[2] Flood,[3] and Buesman[4] have reported thermodynamic data calculated on the basis of

---

[1] Handbook of Chemistry and Physics, 43rd ed. Chem. Rubber Publishing Co. Cleveland, Ohio, 1961-62.
[2] Haendler, H., Sennet, P., and Wheeler, C., J. Electrochem. Soc. 106, 264 (1959).
[3] Flood, H., Fykse, O., and Urnes, S., Z. Electrochem 59, 364 (1955).
[4] Buesman, C., ORNL-2323 (1957).

phase diagrams of binary halide salt mixtures. Utilizing the method suggested by Wagner,[5] thermodynamic data have been calculated for the binary lithium hydride-lithium chloride system.

In the analysis of this phase diagram only the heterogeneous equilibrium between pure solid and a binary liquid mixture is considered. With no evidence for solid solution, it can be concluded that only pure solid is present. For such a system the relative partial molar free energy of component 1 in the liquid mixture is

$$\bar{F}_1^{m(\ell)}(\chi_2^{(\ell)}, Te) = \Delta H_f\left(\frac{Te - Tm_1}{Tm_1}\right) + Te\int_{Tm_1}^{Te}\frac{dT}{T^2}\int_{Tm_1}^{T} Cp_1^{(\ell)} - Cp_1^{(s)}\, dT$$

when the mixture is in equilibrium with the pure solid of component 1. Here Te is the liquidus-solidus equilibrium temperature of the system at composition χ_2 (mole fraction of component 2), ΔH_f the heat of fusion of one mole of component 1 at Tm_1 (the normal freezing point of component 1), and $Cp_1^{(\ell)}$ and $Cp_1^{(s)}$ are the molar heat capacities of pure component 1 in the liquid and solid state. The standard state for the liquid phase is taken as the pure supercooled liquid and that of the solid phase is the pure solid at the equilibrium temperature.

It is advantageous to express the derived quantities in terms of the excess partial molar free energy:

$$\bar{F}_1^{E(\ell)}(\chi_2) = \bar{F}_1^{m(\ell)} - RTe\ln\left(1-\chi_2^{(\ell)}\right) \quad ;$$

$$\bar{F}_2^{E(\ell)}(\chi_2) = \bar{F}_2^{m(\ell)} - RTe\ln\chi_2 \quad .$$

If the activity coefficients of each component are desired, they are readily obtainable from

$$\bar{F}_1^{E(\ell)}(\chi_2) = RT\ln\gamma_1 \quad ; \quad \bar{F}_2^{E(\ell)}(\chi_2) = RT\ln\gamma_2 \quad .$$

According to Wagner,[5] values for the activity coefficient may be difficult to interpret. In ideal solutions the activity of each component is unity. Numerous real systems deviate from ideal behavior to a large extent and hence activity coefficients represent a most convenient method of comparing these deviations.

The phase diagram for the system lithium hydride-lithium chloride is shown in Figure V-4. With the use of these data and the above equations, calculations have been made of the free energy of mixing and the

[5] Wagner, C., Thermodynamics of Alloys, Addison Wesley Press, Cambridge, Mass. (1952) Chap 4, pp. 67-75.

activity coefficient for each component over the composition ranges in which the components precipitate from solution. These data are given in Tables V-1 and -2. In these calculations, it was assumed that C_p is independent of temperature. The value for the heat of fusion of lithium hydride was taken from the estimated value of Gibb and Messer.[6] The activity coefficients, which are near unity, indicate that the system closely approximates an ideal solution.

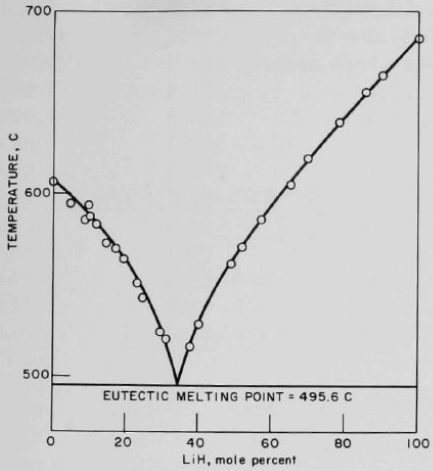

Figure V-4

LiH-LiCl PHASE DIAGRAM

108-6553

Table V-1

THERMODYNAMIC DATA FOR LiH IN LiH-LiCl SYSTEM

LiH (Mole Fraction)	Te [a] (K)	$\bar{F}^m$ [b] (cal/mole)	$\bar{F}^E$ [c] (cal/mole)	γ [d]
0.340[e]	768.8	-1561	86.7	1.058
0.382	796.4	-1331	193.1	1.130
0.401	802.3	-1281	176.5	1.117
0.451	825.6	-1086	219.6	1.143
0.495	834.8	-1010	156.1	1.099
0.522	845.5	-921.3	169.8	1.106
0.576	859.0	-810.1	131.7	1.080
0.654	889.1	-563.7	186.1	1.111
0.698	892.9	-532.0	105.4	1.061
0.786	912.7	-371.6	64.0	1.036
0.852	929.1	-238.2	57.7	1.032
0.901	938.3	-165.7	28.5	1.015
1.0	959.0	-	-	1.0

[a] Te = Liquidus-solidus equilibrium temperature

[b] $\bar{F}^m$ = Relative partial molar free energy.

[c] $\bar{F}^E$ = Excess partial molar free energy.

[d] γ = Activity coefficient

[e] Eutectic composition

[6] Gibb, T. R. P., Jr., and Messer, C. E., NYO-3957 (1957) p. 16.

Table V-2

THERMODYNAMIC DATA FOR LiCl IN LiH-LiCl SYSTEM

LiCl (Mole Fraction)	Te[a] (K)	$\bar{F}m$[b] (cal/mole)	$\bar{F}E$[c] (cal/mole)	γ[d]
0.660[e]	768.8	-59.7	44.3	1.029
0.689	795.3	-451.3	138.6	1.092
0.706	802.4	-414.1	144.4	1.093
0.750	820.7	-317.2	151.9	1.098
0.765	826.5	-286.3	153.6	1.098
0.802	837.3	-228.5	139.3	1.087
0.825	842.0	-203.6	118.9	1.074
0.850	846.2	-181.0	92.4	1.056
0.853	848.0	-171.6	96.9	1.059
0.880	856.1	-127.7	90.1	1.054
0.902	860.1	-106.5	69.4	1.041
0.939	867.6	-66.1	41.9	1.025
0.950	870.2	-52.0	36.0	1.021
1.0	879.9	-	-	1.00

[a] Te = Liquidus-solidus equilibrium temperature.

[b] $\bar{F}m$ = Relative partial molar free energy.

[c] $\bar{F}E$ = Excess partial molar free energy.

[d] γ = Activity coefficient.

[e] Eutectic composition.

3. Hydrogen Diffusion Electrode
(R. Heinrich and G. McCloud)

The study of various materials for possible use as diaphragms in a hydrogen gas electrode was continued. Two diaphragms, one a 0.0055-in-thick, 10 w/o molybdenum-iron alloy and the other a 0.0055-in.-thick, 5 w/o molybdenum-iron alloy, were received from Battelle Memorial Institute. These alloy compositions were chosen for study because the solubility of hydrogen in molybdenum-iron alloys reaches a maximum at about 8 w/o molybdenum.[7,8] Since hydrogen solubility is usually related to the rate of hydrogen permeation of an alloy, it was anticipated that hydrogen solubility would prove to be a good criterion for the selection of the alloys.

[7] Barrer, R. M., Diffusion in and through Solids, Cambridge University Press (1951) p. 158.

[8] Sieverts, A., and Bruning, K., Arch. Eisenhuttenw., 1, 641-5 (1934).

After welding the alloy specimens to suitable holders by means of an electron beam, the rate of permeation of hydrogen through the alloys was measured over the range from 350 to 800 C. The data for the two alloys (calculated for a 0.010-in. thickness based on measurements made with 0.0055-in.-thick specimens) are given in Table V-3, along with data for a 0.010-in.-thick pure (Armco) iron diaphragm similarly welded to a suitable holder. The data indicate that the permeation rates for the BMI alloys were slightly lower than those for pure iron below about 650 C and were slightly higher above about 700 C. It was concluded that these alloys would not be suitable for cell application since only low current densities could result from their use.

Table V-3

PERMEATION RATES OF HYDROGEN THROUGH 10-MIL-THICK IRON AND IRON-MOLYBDENUM ALLOYS

Temp (C)	Armco Fe (cc/min/sq cm) x 10^2	Battelle 5 w/o Mo-Fe[a] (cc/min/sq cm)	Battelle 10 w/o Mo-Fe[a] (cc/min/sq cm)
350	-	4.26×10^{-3}	4.96×10^{-3}
400	1.07	6.71×10^{-3}	7.66×10^{-3}
450	1.93	1.29×10^{-2}	1.24×10^{-2}
500	2.80	2.32×10^{-2}	1.98×10^{-2}
550	4.43	3.40×10^{-2}	2.76×10^{-2}
600	6.61	4.78×10^{-2}	4.47×10^{-2}
650	8.74	6.44×10^{-2}	5.30×10^{-2}
700	1.17	8.42×10^{-2}	7.46×10^{-2}
750	1.58	1.05×10^{-1}	9.26×10^{-2}
800	-	1.28×10^{-1}	1.17×10^{-1}

[a] Calculated values for a 10-mil-thick diaphragm based on measurements made with a 5.5-mil-thick specimen.

Vanadium

Because of an inability to obtain reliable welds of vanadium to stainless steel, the welded-type diaphragm could not be used in determining hydrogen permeation rates through vanadium. Instead, a swage-type seal[9] was employed. The first data recorded with a pure, 0.010-in.-thick vanadium diaphragm at 500 C yielded the very high permeation rate of 7.42 cc/min/sq cm. The experiment which yielded this high permeation rate lasted 80 sec. After purging with hydrogen gas for 20 min, the experiment was repeated. However, the new permeation rate was much lower than the initial rate, and subsequent attempts to reproduce this rate were unsuccessful. The most consistent data obtained are recorded in Table V-4. However, even these

[9] Brymner, R., and Steckelmacher, W., J. Sci. Inst. 36, 278 (1959).

data could not be reproduced several days later. It is concluded that, although hydrogen purified by diffusion through silver-palladium was used throughout the experiment, the amounts of trace impurities of nitrogen and oxygen in the system were sufficient to restrict permeation of hydrogen through vanadium at the temperatures of the tests (500 to 575 C). Inconsistent operation of a hydrogen gas diffusion electrode was also apparent in experiments with niobium diaphragms at Thompson Ramo Wooldridge.[10] Some method of protecting the metal surface of any of the reactive metals needs to be devised before reliable operation of the diaphragm can be assured.

Table V-4

PERMEABILITY OF HYDROGEN THROUGH 10-MIL-THICK PURE VANADIUM DIAPHRAGMS

Temp (C)	Permeation Rate [cc(STP)/min/sq cm[a]]	Current Density Calculated at 100% Electrode Efficiency (ma/sq cm)
500	3.64	520
525	4.58	657
550	6.38	914
575	8.69	1240

[a] 0.699 cm^3/min/sq cm is equivalent to 100 ma/sq cm at one hundred percent cell efficiency.

B. Thermoelectricity Research
(R. K. Edwards)

Studies in thermoelectricity are underway in an effort to contribute to the future technological development of direct conversion of nuclear reactor heat energy into electrical power by means of the thermocouple effect.

Two limited materials areas have been selected as of special interest. Liquid thermocouple materials are under investigation. Refractory solid thermocouple systems form the other major area since they are considered to be of particular interest in reactor energy conversion.

The personnel associated with thermoelectricity research are undertaking additional research in the area of high-temperature materials. A program of high-temperature chemistry centered about likely high-performance refractory fuels for nuclear reactors in their operating environments is being undertaken. Currently, planning and acquisition of equipment is in progress. Studies of refractory materials are planned as follows:

[10] ASD-TDR-62-241, Electrode Development Program, TAPCO Division of Thompson Ramo Wooldridge, Inc. (Jan 23, 1962).

(a) effusion and mass spectrometric studies of the gaseous decomposition products of the refractory nuclear fuels, (b) gaseous transport studies, and (c) phase-diagram studies.

1. Liquid Systems
(R. K. Edwards, P. Danielson)

The studies of Seebeck coefficients in liquid systems were deferred during this report period. It is intended to complete these studies by measurement of Seebeck coefficients in the liquid indium-bismuth system at 750 C, so that the coefficients of the three related systems: indium-bismuth, indium-antimony, and antimony-bismuth, may be compared at the same temperature, and to measure the electrical conductivities of these systems. Equipment revision for this purpose is in progress.

2. Refractory Solid Thermocouple Systems
(M. Tetenbaum, F. Mrazek)

Materials possessing high melting points and low vapor pressures are desirable for use as energy-conversion devices at high temperatures, such as might be encountered in possible nuclear reactor systems. The lanthanide and actinide sulfide systems are highly refractory, and have phases with carrier concentrations in the semiconducting range. The uranium and thorium sulfide systems and their solid soutions have been selected for study.

Experimental

Measurements of the Seebeck coefficient as a function of temperature have been made with sintered specimens (~85 percent of theoretical density) of uranium monosulfide (US)-thorium monosulfide (ThS) solid solutions* of composition (expressed in mole percent) 75 US-25 ThS and 25 US-75 ThS. The results are shown in Figure V-5, along with previously reported thermoelectric power measurements in the US-ThS system (see ANL-6648, p. 227).

The results obtained with these solid solutions are consistent with previous observations, namely, that (1) thermoelectric power shows only a weak dependence on temperature and (2) the Seebeck coefficient decreases with increasing ThS content.

The trend in Seebeck coefficient values with composition appears to reflect the increased metallic character of the US-ThS system with increasing ThS content, and is also consistent with the behavior of room-temperature resistivity values** obtained with these specimens, namely,

* We are indebted to P. Shalek, Metallurgy Division, for preparing these specimens.

** A similar trend in room-temperature resistivity values has been obtained by P. Shalek of the Metallurgy Division.

that a decrease in resistivity occurs with increasing ThS content, as shown in Table V-5. The initial resistivity rise when ThS is added to US can be attributed to lattice disorder.

Figure V-5

ABSOLUTE SEEBECK COEFFICIENT VS TEMPERATURE FOR URANIUM MONOSULFIDE, THORIUM MONOSULFIDE, AND URANIUM MONOSULFIDE-THORIUM MONOSULFIDE SOLID SOLUTIONS

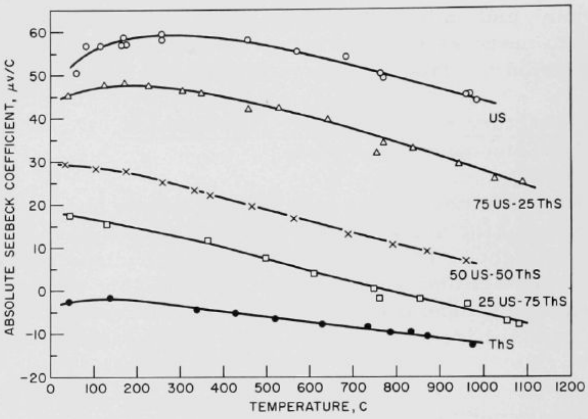

108-6554

Table V-5

APPROXIMATE ROOM-TEMPERATURE RESISTIVITY VALUES AS A FUNCTION OF COMPOSITION FOR THE US-ThS SYSTEM

Composition[a]	Resistivity (μ ohm-cm)
US	290
75 US-25 ThS	365
50 US-50 ThS	270
25 US-75 ThS	175
ThS	70

[a] Sintered specimens ~85% theoretical density.

Theory

The temperature dependence of the thermoelectric power of uranium monosulfide has been calculated by means of simplified semiconductor theory.

The general expression for the Seebeck coefficient for a given current carrier of one sign is given by

$$\alpha = \pm \frac{k}{e}\left[\frac{r+2}{r+1}\,\frac{F_{r+1}(\eta^*)}{F_r(\eta^*)} - \eta^*\right] \quad , \tag{1}$$

where α is the Seebeck coefficient or thermoelectric power, k the Boltzmann constant, e the carrier charge, $\eta^* = E^*/kT$ is the reduced chemical potential, E^* the chemical potential of the carriers, r the scattering index, and $F_r(\eta^*)$, $F_{r+1}(\eta^*)$ denote Fermi-Dirac integrals defined by

$$F_m(\eta^*) = \int_0^\infty \frac{\eta^m \, d\eta}{1 + \exp(\eta - \eta^*)} \quad , \tag{2}$$

where $\eta = E/kT$ is the reduced energy, the value of E being the energy of the hole relative to the top of the valence band.

For atomic lattices where $r = 0$ (scattering due to acoustic vibrations), we have

$$\alpha = \frac{k}{e}\left[\frac{2F_1(\eta^*)}{F_0(\eta^*)} - \eta^*\right] \quad . \tag{3}$$

For the case of an ionic lattice where $r = 1$ (scattering due to polar vibrations), we have

$$\alpha = \frac{k}{e}\left[\frac{3}{2} \times \frac{F_2(\eta^*)}{F_1(\eta^*)} - \eta^*\right] \quad .$$

Assuming that the carrier concentration n in uranium monosulfide is independent of temperature, we can estimate η^* by means of the following expression:

$$n = 4\pi \,\frac{(2m^* kT)^{3/2}}{h^3}\, F_{1/2}(\eta^*) \quad , \tag{4}$$

where h is Planck's constant, and m^* is the effective mass of the carrier.

Using $n \cong 10^{21}$, obtained from Hall coefficient measurements,† and assuming $m^* = m_0$ = free electron mass, the curves shown in Figure V-6 were calculated by means of the above equations. It is apparent that the agreement between the calculated and experimental values is quite poor.

Figure V-6

COMPARISON OF CALCULATED AND EXPERIMENTAL SEEBECK COEFFICIENTS FOR URANIUM MONOSULFIDE FOR DIFFERENT SCATTERING MECHANISMS

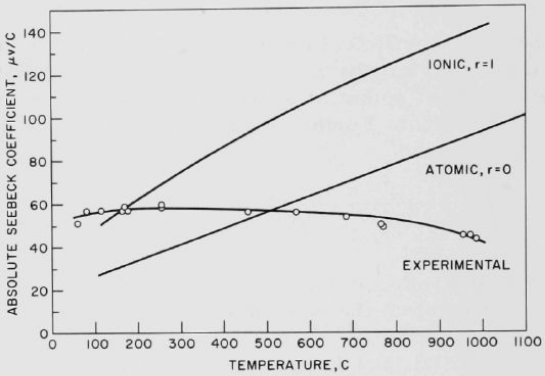

108-6555

The discrepancy between the calculated and experimental Seebeck values can be attributed to a temperature-dependent effective mass term, or perhaps, although less likely since the system is degenerate, to an appreciable change in carrier concentration with temperature. By use of the experimental Seebeck coefficient values and the above equations, the effective mass values have been estimated for the temperature range studied. The results are summarized in Table V-6. The spread in effective mass values with temperature is too large. It is apparent that the above treatment does not account satisfactorily for the temperature dependence of the thermoelectric power of uranium monosulfide.

Table V-6

EFFECTIVE MASS VALUES REQUIRED TO FIT DATA

Temp (C)	Seebeck Coefficient (mv/C)	$\frac{m^*}{m_0}$ Ionic	$\frac{m^*}{m_0}$ Metallic	Temp (C)	Seebeck Coefficient (mv/C)	$\frac{m^*}{m_0}$ Ionic	$\frac{m^*}{m_0}$ Metallic
25	50	1.3	2.3	400	59	0.7	1.2
50	52	1.2	2.2	600	55	0.5	0.9
100	56	1.2	2.0	800	50	0.4	0.7
200	59	1.0	1.8	1000	44	0.3	0.5

†Measurements obtained by M. Kanter and C. Kazmierowicz, Solid State Science Division, Argonne National Laboratory.

VI. ROUTINE OPERATIONS
(H. G. Swope)

High-level Gamma Irradiation Facility
(H. G. Swope, G. Teats, R. Juvinall, V. Lemke and J. Stange)

A summary of irradiations performed in Rack M-1 for January through March, 1963 is given in Table VI-1.

Table VI-1

SUMMARY OF IRRADIATIONS PERFORMED IN RACK M-1 DURING JANUARY THROUGH MARCH, 1963

Month	No. of Samples[a]	No. of Special Dosimetry Samples	Total Urn Units[b]	
			Day[c]	Night
January	47	10	256	999
February	55	10	375	1179
March	79	24	410	1529
Totals	181	44	1041	3707

[a]Equivalent to a No. 2 size can.

[b]One urn unit equals 2×10^6 rad.

[c]Includes loadings and re-immersions.